0-315-01031-2

National Library
of Canada

Canadian Theses Division

Ottawa, Canada
K1A 0N4

Bibliothèque nationale
du Canada

Division des thèses canadiennes

48889

PERMISSION TO MICROFILM — AUTORISATION DE MICROFILMER

- Please print or type — Écrire en lettres moulées ou dactylographier

Full Name of Author — Nom complet de l'auteur
DEBORAH JANE BARNES

Date of Birth — Date de naissance
SEPT. 12, 1956

Country of Birth — Lieu de naissance
CANADA

Permanent Address — Résidence fixe
#204 - 7615 - 105 STREET
EDMONTON, ALBERTA
T6E 4G9

Title of Thesis — Titre de la thèse
MICRO-FABRIC AND STRENGTH STUDIES OF OIL SANDS

University — Université
UNIVERSITY OF ALBERTA

Degree for which thesis was presented — Grade pour lequel cette thèse fut présentée
MASTER OF SCIENCE IN CIVIL ENGINEERING

Year this degree conferred — Année d'obtention de ce grade
1980

Name of Supervisor — Nom du directeur de thèse
MAURICE B. DUSSEAULT

Permission is hereby granted to the NATIONAL LIBRARY OF CANADA to microfilm this thesis and to lend or sell copies of the film.

The author reserves other publication rights, and neither the thesis nor extensive extracts from it may be printed or otherwise reproduced without the author's written permission.

L'autorisation est, par la présente, accordée à la BIBLIOTHÈQUE NATIONALE DU CANADA de microfilmer cette thèse et de prêter ou de vendre des exemplaires du film.

L'auteur se réserve les autres droits de publication; ni la thèse ni de longs extraits de celle-ci ne doivent être imprimés ou autrement reproduits sans l'autorisation écrite de l'auteur.

Date
JULY 24, 1980

Signature
Deborah Barnes

NL-91 (4/77)

National Library of Canada

Cataloguing Branch
Canadian Theses Division

Ottawa, Canada
K1A 0N4

NOTICE

The quality of this microfiche is heavily dependent upon the quality of the original thesis submitted for microfilming. Every effort has been made to ensure the highest quality of reproduction possible.

If pages are missing, contact the university which granted the degree.

Some pages may have indistinct print especially if the original pages were typed with a poor typewriter ribbon or if the university sent us a poor photocopy.

Previously copyrighted materials (journal articles, published tests, etc.) are not filmed.

Reproduction in full or in part of this film is governed by the Canadian Copyright Act, R.S.C. 1970, c. C-30. Please read the authorization forms which accompany this thesis.

THIS DISSERTATION
HAS BEEN MICROFILMED
EXACTLY AS RECEIVED

Bibliothèque nationale du Canada

Direction du catalogage
Division des thèses canadiennes

AVIS

La qualité de cette microfiche dépend grandement de la qualité de la thèse soumise au microfilmage. Nous avons tout fait pour assurer une qualité supérieure de reproduction.

S'il manque des pages, veuillez communiquer avec l'université qui a conféré le grade.

La qualité d'impression de certaines pages peut laisser à désirer, surtout si les pages originales ont été dactylographiées à l'aide d'un ruban usé ou si l'université nous a fait parvenir une photocopie de mauvaise qualité.

Les documents qui font déjà l'objet d'un droit d'auteur (articles de revue, examens publiés, etc.) ne sont pas microfilmés.

La reproduction, même partielle, de ce microfilm est soumise à la Loi canadienne sur le droit d'auteur, SRC 1970, c. C-30. Veuillez prendre connaissance des formules d'autorisation qui accompagnent cette thèse.

LA THÈSE A ÉTÉ
MICROFILMÉE TELLE QUE
NOUS L'AVONS REÇUE

NL-339 (3/77)

THE UNIVERSITY OF ALBERTA

MICRO-FABRIC AND STRENGTH STUDIES OF OIL SANDS

by

© DEBORAH J. BARNES

A THESIS
SUBMITTED TO THE FACULTY OF GRADUATE STUDIES AND RESEARCH
IN PARTIAL FULFILMENT OF THE REQUIREMENTS FOR THE DEGREE
OF MASTER OF SCIENCE

DEPARTMENT OF CIVIL ENGINEERING

EDMONTON, ALBERTA
FALL, 1980

THE UNIVERSITY OF ALBERTA

FACULTY OF GRADUATE STUDIES AND RESEARCH

The undersigned certify that they have read, and recommend to the Faculty of Graduate Studies and Research, for acceptance, a thesis entitled MICRO-FABRIC AND STRENGTH STUDIES OF OIL SANDS submitted by DEBORAH J. BARNES in partial fulfilment of the requirements for the degree of MASTER OF SCIENCE.

....

Supervisor

....

Dave Sego

Fred J. Longstaffe

Date June 26, 1980

ABSTRACT

Diagenetic alteration has decreased the porosity of oil sand materials and increased their strength and competency. The diagenetic processes of pressure solution and authigenic crystal overgrowth are examined in terms of the environmental conditions related to their occurrence and the grain fabric alterations they produce. The influence of these processes on oil sand materials is demonstrated by reference to scanning electron and optical micrographs of intact samples of the McMurray and Grand Rapids Formations. The grain fabric of a number of comparative materials is examined to aid in delineation of sandstone fabric.

Previous investigations of the strength of granular materials are reviewed, together with several models for the strength of granular materials and rocks. The curvilinear failure envelope obtained in oil sand materials is discussed, and a curve-fitting technique for analysis of oil sand strength is examined.

Block samples of oil-free McMurray and Grand Rapids Formations were obtained from river valley outcrops in the Fort McMurray area. The specimens were tested in the direct shear apparatus to delineate Mohr-Coulomb failure criteria and dilatent behaviour. In addition, oedometer tests were conducted to determine the compressibility of the materials. Index data were collected to aid analysis of grain fabric.

The results of the strength and index tests are examined in terms of the factors which influence the strength of a locked sand. A qualitative classification for the effect of diagenesis on strength is proposed based on the porosity reduction resulting from diagenesis.

PREFACE

Further documentation of the diagenetic alteration of the materials examined may be found by reference to a report submitted to the Alberta Oil Sands Technology and Research Authority, Agreement Number 56, File Number 8869G, May, 1980.

ACKNOWLEDGEMENTS

The financial support of the Alberta Oil Sands Technology and Research Authority for the research work herein is gratefully acknowledged. The research was carried out under the auspices of the Department of Civil Engineering, and was supervised by Dr. Maurice B. Dusseault, who provided invaluable direction and assistance.

Technical assistance has been provided by Gerry Cyre, Don Fushtey, Hal Soderberg, Al Muir, and Scotty Rogers. Assistance with computer work was given by Ray Howells. The valuable assistance of George Braybrook with the scanning electron microscope work is acknowledged.

Assistance with the field sampling program was provided by Hilton Barnes, Maurice Dusseault, Sean Maloney, and Howard Plewes. Advice on sampling locations from John Kramers and Grant Mossop of the Alberta Research Council was much appreciated.

Many thanks are due to the staff and students of the Civil Engineering Department for the fellowship and guidance they provided throughout the writer's period of study.

The writer would like to express sincere appreciation for the patience, assistance, and moral support provided by her husband Hilton.

TABLE OF CONTENTS

Chapter Page

1. INTRODUCTION 1

2. DIAGENETIC PROCESSES 8

2.1 Introduction 8

2.2 Geochemical Properties of Silica 9

2.3 Pressure Solution 12

2.3.1 Definition 12

2.3.2 Mechanism of Pressure Solution 12

2.3.3 Factors Affecting Pressure Solution 17

2.3.4 Grain Surface and Contact Features 22

2.4 Authigenic Overgrowths 24

2.4.1 Definition 24

2.4.2 Development of Overgrowths 24

2.4.3 Grain Surface and Contact Features 29

2.5 Summary 30

3. INFLUENCE OF DIAGENESIS ON OIL SAND MATERIALS 44

3.1 Introduction 44

3.2 Sampling Procedures and Specimen Preparation 45

3.3 Grain Fabric of the McMurray Formation 45

3.3.1 Location and Geological Origin of Specimens 45

3.3.2 Photomicrographs of the McMurray Formation 47

3.4 Grain Fabric of the Grand Rapids Formation 48

3.4.1 Location and Geological Origin of Specimens 48

3.4.2 Photomicrographs of the Grand Rapids Formation ..49

3.5 Fabric of Comparative Materials 50

3.5.1 Itacolumites 50

3.5.2 Cemented and Bituminous Sands 52

3.6 Summary 53

4. STRENGTH OF GRANULAR AND INTERLOCKING MATERIALS 72

4.1 Introduction 72

4.2 Strength Investigations 72

4.3 Analysis of Strength Properties 75

4.4 Strength Analysis of Oil Sands 78

4.5 Summary 79

5. EXPERIMENTAL INVESTIGATION 86

5.1 Introduction 86

5.2 Testing Program 86

5.2.1 Materials Tested 86

5.2.2 Index Tests 87

5.2.3 Oedometer Tests 88

5.2.4 Direct Shear Tests 88

5.3 Experimental Results 89

5.3.1 Index Data 89

5.3.1.1 Grain Size Data 89

5.3.1.2 Density and Water Content Tests Results 91

5.3.1.3 Density Index Test Results 93

5.3.2 Oedometer Test Results 94

5.3.3 Direct Shear Test Results 95

5.4 Discussion and Analysis of Test Results 100

5.4.1 Factors Influencing Shear Strength 100

5.4.2 Diagenetic Classification by Porosity Reduction 103

5.5 Practical Implications of Oil Sands Behaviour 106

6. CONCLUSION 130

Bibliography 133

Appendix A List of Symbols 140

Appendix B Sample Preparation and Test Methods 142

B.1 Direct Shear Tests 142

B.2 Compressibility Tests 144

B.3 Grain Size Distribution 145

B.4 Density Tests 146

B.5 Density Index Tests 147

Appendix C Test Results 149

C.1 Direct Shear Test Results 149

C.1.1 Summary Tables of Direct Shear Test Results 150

C.1.2 Summary Plots of Direct Shear Test Results 156

C.1.3 Plots for Individual Direct Shear Test Results 172

C.2 Compressibility Test Results 222

C.3 Grain Size Analysis 232

C.3.1 Grain Size Distribution Curves for Original Samples 233

C.3.2 Data Summary for Analysis of Sheared Samples 239

LIST OF TABLES

Table Page

5.1 Grain size data for original samples 108

5.2 Grain size data for sheared samples of Grand Rapids Formation 109

5.3 Density, porosity, and water content test results 110

5.4 Density index test results 111

5.5 Compressibility test results 112

5.6 Curve-fit correlation parameters, relationship between shear stress and normal stress 113

5.7 Estimate of porosity reduction resulting from diagenesis 114

5.8 Classification of diagenetic alteration in sandstones 115

LIST OF FIGURES

Figure Page

1.1 Location of Alberta's four major heavy oil deposits 5

1.2 Correlation chart for Alberta's heavy oil deposits 6

1.3 Stratigraphy and depositional environments of the Athabasca Oil Sands 7

2.1 Solubility vs. temperature for amorphous silica and quartz 32

2.2 Solubility vs. pH for amorphous silica 33

2.3 Bathurst mechanism for pressure solution 34

2.4 Weyl mechanism for pressure solution 35

2.5 Relative solubility increase caused by external load 36

2.6 Effect of constant differential stress and pore pressure on porosity 37

2.7 Cement generated vs. porosity loss due to solution for different packing arrangements of perfect spheres 38

2.8 Cement generated vs. porosity loss due to solution for actual sandstones 39

2.9 Types of grain contacts 40

2.10 Stages of development of a crystal overgrowth 41

2.11 Porosity loss and cement precipitated with time 42

2.12 Theoretical overgrowth development stages 43

3.1 Overgrowth features in the McMurray Formation 55
3.2 Solution pitting in the McMurray Formation 56
3.3 Long and concavo-convex grain contacts in the McMurray Formation 57
3.4 Stereo pairs of grain fabric in the McMurray Formation 58
3.5 Optical micrographs of the McMurray Formation 59
3.6 Overgrowth features in Grand Rapids Formation A 60
3.7 Grain features in Grand Rapids Formation A 61
3.8 Long and concavo-convex grain contacts, Grand Rapids Formation C 62
3.9 Closely-packed structure, Grand Rapids Formation C 63
3.10 Photomicrographs of Indian itacolumite 64
3.11 Optical micrographs of Indian itacolumite 65
3.12 Interlocking structure of micaceous itacolumite, sample 1 66
3.13 Optical micrographs of micaceous itacolumite, sample 1 67
3.14 Interlocking structure of micaceous itacolumite, sample 2 68
3.15 Cemented sandstone and talus fragment of McMurray Formation 69
3.16 Bituminous sands from California and Utah 70
3.17 Dense post-glacial sand 71
4.1 Mohr envelope for granulated marble 81
4.2 Bimodal failure criterion 82

4.3 Empirical relationship between principal stresses at failure in a rock mass 83

4.4 Curve-fitting technique for strength of oil sands 84

4.5 Comparison of Mohr-Coulomb envelopes for dense, locked, and cemented sands 85

5.1 Grain size distribution for all test materials 116

5.2 Void ratio vs. stress curve for oedometer test FG-C2-79 117

5.3 Shear test results, fine-grained McMurray Formation, normal stress=250 kPa 118

5.4 Shear test results, fine-grained McMurray Formation, normal stress=4000 kPa 119

5.5 Shear test results, Grand Rapids Formation A, normal stress=250 kPa 120

5.6 Shear test results, Grand Rapids Formation A, normal stress=4000 kPa 121

5.7 Shear stress vs. normal stress for all test materials 122

5.8 Shear stress vs. normal stress, fine-grained McMurray Formation 123

5.9 Shear stress vs. normal stress, medium-grained McMurray Formation 124

5.10 Shear stress vs. normal stress, coarse-grained McMurray Formation 125

5.11 Shear stress vs. normal stress, Grand Rapids Formation A 126

5.12 Shear stress vs. normal stress, Grand Rapids Formation C 127

5.13 Dilatency rate at failure vs. normal stress, coarse-grained McMurray Formation 128

5.14 Relationship between shear strength correlation parameters and median grain size 129

1. INTRODUCTION

Development of Alberta's heavy oil deposits by surface mining and *in situ* production techniques requires a knowledge of the geological and engineering properties of the oil sand materials. The locations of Alberta's four major heavy oil deposits are shown in Figure 1.1. The primary resource recovery taking place at present is the surface mining operations in the Athabasca deposit. This deposit is the only one of the four areas which contains locations where overburden thickness is low enough to permit surface mining. Pilot projects for *in situ* recovery are also in operation in the different areas.

The concern of this study is an examination of the micro-fabric and strength properties of oil sands. Samples of oil-free McMurray and Grand Rapids Formations from the Athabasca area were used to investigate the influence of micro-fabric on the engineering properties of strength and compressibility.

Figure 1.2 is an illustration of the stratigraphy of the oil sands deposits and the zones of oil saturation at each location. A more detailed description of the stratigraphy and depositional environments of the Athabasca deposit is given in Figure 1.3.

The primary zone of oil saturation in the Athabasca deposit is in the McMurray Formation, a quartzose sand of early Cretaceous age. Carrigy (1959) proposed a threefold division of the McMurray Formation as follows:

1. Upper Member: fine-grained horizontally-bedded quartz sands;
2. Middle Member: medium-grained cross-bedded sands with lenticular beds of silt, shale, clay, and ironstone;
3. Lower Member: poorly-sorted fine- to coarse-grained sands, together with a basal clay stratum.

Grain size analysis shows a fining-upwards trend through the formation. The depositional environments associated with these strata are shown in Figure 1.3 (Mossop,1978).

The Grand Rapids Formation consists of three major sandstone units with shaley sequences (Kramers, 1974). The deposit is a quartz-feldspar sandstone with a variable clay content. The Grand Rapids Formation is the primary zone of oil saturation in the Wabasca and Cold Lake oil sands deposits.

Examination of grain surface features and grain contacts in oil sands by use of the scanning electron microscope (SEM) demonstrates that the materials have been diagenetically altered by processes of pressure solution and authigenic crystal overgrowth, resulting in an interlocking fabric. This fabric is characterized by high strength and dilatency at low normal stress, and a gradual suppression of dilatency with increasing normal stress. The result of this behaviour is a Mohr-Coulomb failure envelope with extreme curvature. This type of material has been designated as a "locked sand" (Dusseault and Morgenstern, 1979).

The primary concern of traditional analyses of diagenetic alteration in sandstones is an evaluation of the porosity reduction and its influence on the reservoir characteristics of the mass. The development of surface mining in oil sands and the possibility of future resource exploitation by mine-assisted *in situ* processing has added a new dimension to the analysis of diagenesis in terms of its influence on the engineering behaviour of the material.

The difficulties of obtaining undisturbed samples in oil sands have been described by Dusseault (1977). Exsolution of gas from the pore fluid phase on removal of overburden pressure causes gross disturbance of the soil skeleton, and attempts to control this process have resulted in only limited success. The results of laboratory tests for measurement of density and strength are thus not representative of the *in situ* properties of the material. Density test results obtained in the laboratory are generally lower than the values obtained by geophysical logging techniques. Therefore a correlation between diagenetic fabric (with corresponding porosity) and strength would be a valuable tool in assessing the engineering behaviour of oil sands.

The diagenetic processes of pressure solution and authigenic crystal overgrowth are described in Chapter 2 in terms of the environmental conditions associated with their occurrence and the surface and contact features which they produce. In Chapter 3 the influence of these diagenetic processes on the grain fabric of oil sands is demonstrated by reference to scanning electron and optical photomicrographs of undisturbed block specimens.

In Chapter 4 the various strength relationships which have been proposed for granular materials and rocks are examined, and past experiments on interlocking materials are reviewed. The curvilinear Mohr-Coulomb envelope obtained for oil sands is analyzed.

The results of strength, compressibility, and index tests on oil-free samples of the McMurray and Grand Rapids Formations are presented in Chapter 5. The influence of diagenesis on the engineering properties of oil sand materials is discussed, together with some of the practical implications of these properties.

Chapter 6 summarizes the conclusions drawn from the experimental work.

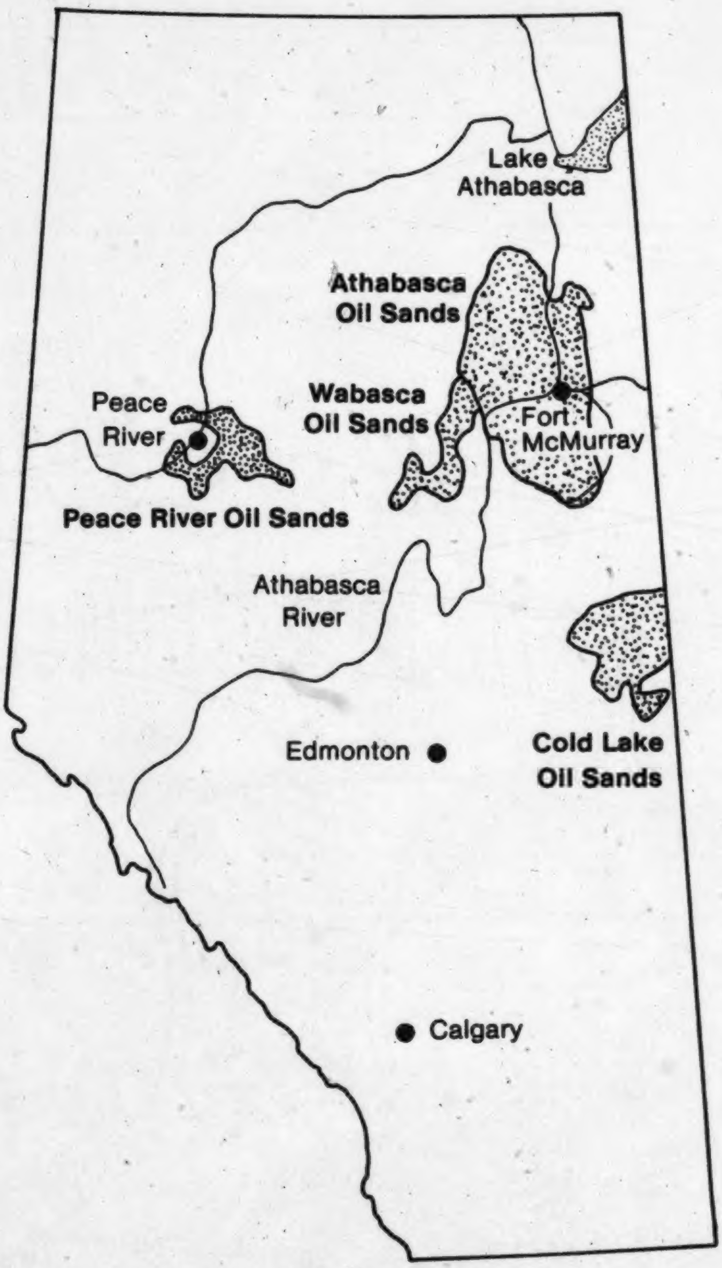
Lake
Athabasca
Athabasca
Oil Sands
Wabasca
Oil Sands
Peace
River
Fort
McMurray
Peace River Oil Sands
Athabasca
River
Edmonton
Cold Lake
Oil Sands
Calgary

Figure 1.1 : Location of Alberta's four major heavy oil deposits.

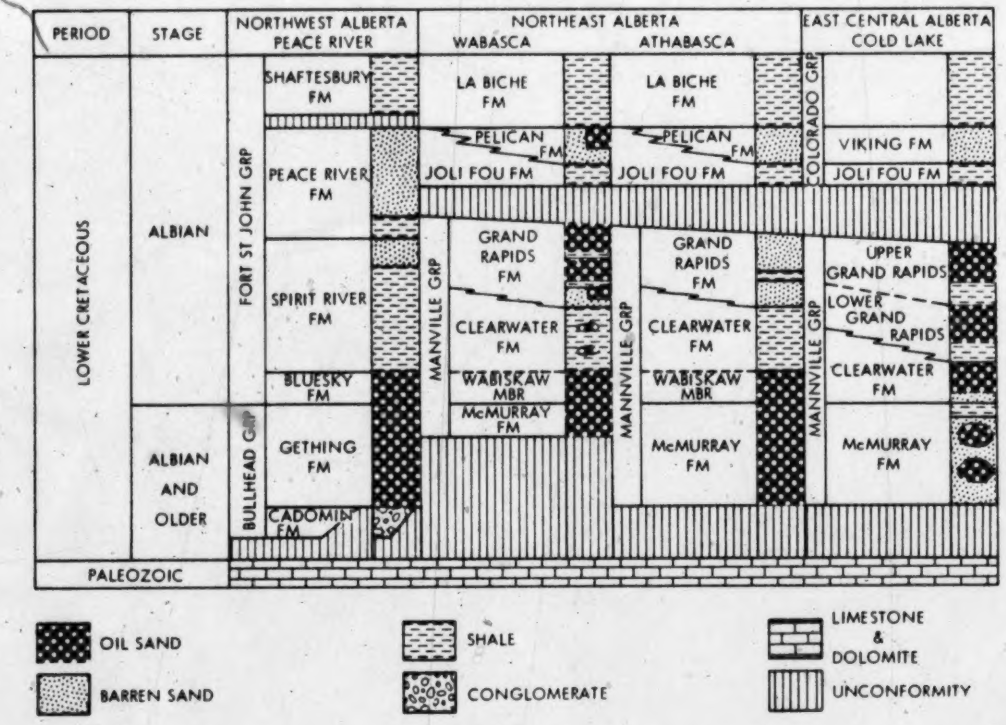
PERIOD
STAGE
NORTHWEST ALBERTA PEACE RIVER
NORTHEAST ALBERTA
WABASCA
ATHABASCA
EAST CENTRAL ALBERTA COLD LAKE
LOWER CRETACEOUS
ALBIAN
ALBIAN AND OLDER
PALEOZOIC
FORT ST JOHN GRP
BULLHEAD GRP
SHAFTESBURY FM
PEACE RIVER FM
SPIRIT RIVER FM
BLUESKY FM
GETHING FM
CADOMIN FM
LA BICHE FM
PELICAN FM
JOLI FOU FM
MANVILLE GRP
GRAND RAPIDS FM
CLEARWATER FM
WABISKAW MBR
McMURRAY FM
LA BICHE FM
PELICAN FM
JOLI FOU FM
MANNVILLE GRP
GRAND RAPIDS FM
CLEARWATER FM
WABISKAW MBR
McMURRAY FM
COLORADO GRP
VIKING FM
JOLI FOU FM
MANNVILLE GRP
UPPER GRAND RAPIDS
LOWER GRAND RAPIDS
CLEARWATER FM
McMURRAY FM
OIL SAND
BARREN SAND
SHALE
CONGLOMERATE
LIMESTONE & DOLOMITE
UNCONFORMITY

Figure 1.2 : Correlation chart for Alberta's heavy oil deposits (after Singh, 1971).

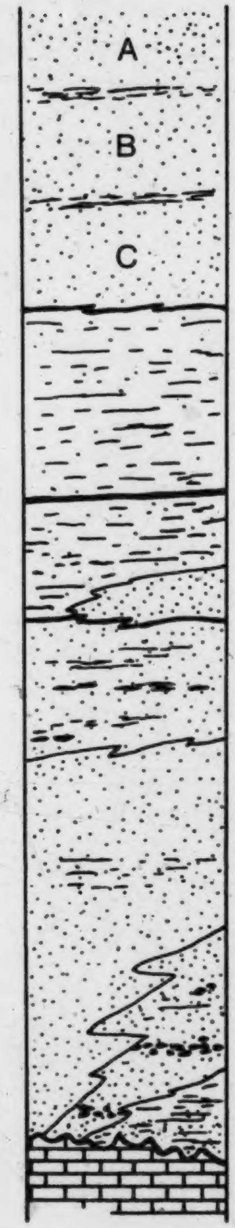

Grand Rapids Formation
Three major sandstone units (non-marine) with shaley sequences (shallow marine); quartz-feldspar sandstone.

Clearwater Formation
Marine clay shales (70%), fine-grained sands and silts (25%), concretions and cemented bands (5%), shallow marine sequence.

Wabiskaw Member
Glauconitic shallow marine sand; barrier bar facies.

Upper McMurray Formation
Fine-grained horizontally-bedded quartz sands to clayey silts; tidal flat regime.

Middle McMurray Formation
Medium-grained quartz sands, lenses of siltstone, shale coal, ironstone and cemented sandstone; fluvial-estuarine accretion plain facies.

Lower McMurray Formation
Poorly sorted fine-to-coarse-grained quartz sands with pebble conglomerate; channel lag deposits in a continental stream regime.

Basal Clays
Clay-shales of paludo-lacustrine origin.

Devonian Limestones
Competent jointed limestones.

Figure 1.3 : Stratigraphy and depositional environments of the Athabasca Oil Sands.

2. DIAGENETIC PROCESSES

2.1 Introduction

Diagenesis is the process of physical and chemical change which occurs in a sediment after deposition. In general, diagenetic processes are defined as those which take place at low temperature and pressure, and as such are the lower end of the metamorphic spectrum. Thus diagenetic changes grade into metamorphism as the environmental conditions progress from those associated with low depths of burial to greater depths. These changes affect the characteristics of the mass both as a reservoir rock and as an engineering material.

There are three basic methods of pore space filling (Taylor, 1950): simple pore filling or cementation, pressure solution, and recrystallization of material on free grain surfaces (authigenic overgrowth). Only the latter two processes are of importance in the oil sand materials studied herein.

In this chapter the geochemical properties of silica are reviewed to provide a background for discussion of diagenesis. The processes of pressure solution and authigenic overgrowth are examined in terms of the conditions necessary for their occurrence and the mechanisms which control them. The effect of these processes on the grain fabric and grain contacts of sandstones is described.

2.2 Geochemical Properties of Silica

Silica exists in a number of different forms in sediments (Siever, 1957). Crystalline alpha-quartz, stable at low temperatures and pressures, and beta-quartz, stable at higher temperatures and pressures, are the most common forms. Other forms are chert, which is composed primarily of microcrystalline quartz, and amorphous silica, which has only transitory crystalline order.

Silica in solution can exist in one of two forms, either molecularly dispersed, or as a colloidal material when the concentration of molecularly dispersed silica exceeds the solubility. This colloidal solution is the first stage of precipitation.

The fundamental property of silica which controls the development of pressure solution and authigenic overgrowth is its solubility. This is dependent on a number of factors:

1. Form of silica: A difference in solubility between the various forms of silica exists because of the different surface energies caused by ordered and disordered states. Amorphous silica is thus more soluble than crystalline quartz (Figure 2.1). Krauskopf (1959) indicated that the solubility of amorphous silica at 25°C is about 140 ppm, whereas the solubility of quartz for similar temperature ranges is approximately 6 to 14 ppm.
2. Temperature: Both the solubility of silica and the rate of attainment of solution equilibrium are increased by

an increase in temperature (Figure 2.1).

3. Pressure: An increase in stress will cause an increase in the solubility of silica (Kennedy, 1950; de Boer, 1977a, b). This will be discussed further under the topic of pressure solution.
4. pH: The solubility of silica is largely independent of pH for values below nine, and then rises abruptly with increasing alkalinity (Figure 2.2).
5. Presence of other solids: Okamoto *et al*. (1957) found that the presence of aluminum will assist the formation of colloidal silica and thus aid silica precipitation. Other materials may also affect silica solubility.

Considerable time is required for the silica solubility reaction to approach equilibrium. Precipitation of amorphous silica takes place when the solution becomes supersaturated, and the amorphous precipitate is then converted to quartz over long periods of time. For the development of pressure solution and crystal overgrowths in the laboratory, high temperatures must be used to shorten the duration of the experiments to a reasonable time period. This may not be an adequate representation of the silica solubility reaction over long time periods.

The degree of silica saturation of natural waters has been discussed by Siever (1962), Milligan (1976), and Davis (1964). Davis conducted a review of published data on silica concentration in natural waters. The median silica concentration in groundwater was found to be 17 ppm with a variation in median between regions of 9 to 85 ppm. The median concentration in stream water was found to be 14 ppm. Concentrations of less than three ppm were found only in ocean and lake water, where the silica is removed by the biological action of siliceous organisms such as diatoms.

Water recently derived from rain or snow also has a lower silica concentration. There is evidence that the silica concentration of this water reaches equilibrium fairly rapidly, in spite of the slow rate of the silica solubility reaction. Davis has presented possible reasons for this phenomenon. Particles suspended in runoff expose a larger surface area, and consequently more silica is dissolved. Also, the turbulence of the runoff streams will cause fracturing of quartz grains and thus increase silica solubility. If the runoff passes through the upper soil profile, this will constitute an additional source of silica.

The two primary influences on the silica concentration in natural waters are the type of material through which the water flows and the temperature. The increased temperature of thermal spring waters results in a high concentration of dissolved silica, up to 4000 ppm (Davis, 1964).

Sources of silica in solution were examined by Siever (1957). The primary source was found to be weathering of silicate minerals. Other sources include weathering of clays, thermal springs, and biochemical dissolution of siliceous organisms.

2.3 Pressure Solution

2.3.1 Definition

Pressure solution is the process whereby grains are dissolved at their points of contact due to the effective intergranular stress. This results in a decrease in porosity and an increase in strength.

A number of different mechanisms have been proposed for pressure solution, and these will be discussed below. On the basis of nonhydrostatic thermodynamics the most logical mechanism has been determined. With this understanding of how pressure solution occurs, the factors which influence its development are discussed.

2.3.2 Mechanism of Pressure Solution

Bathurst (1958) proposed a mechanism for pressure solution which states that there is direct contact (no intervening solution film) between the grain surfaces of adjoining particles, and thus solution can only take place where the pore fluid meets the grain contact (at the edges of the contact). The solubility at these locations will be increased by high shear stresses associated with the stress transfer across the grain boundaries. As the edges of the contact gradually dissolve, the contact area will be reduced until collapse occurs and the contact area is restored. The process then repeats itself (Figure 2.3).

Weyl (1959) postulated the existence of a thin fluid film between the grain contacts which allows diffusion of dissolved material through the film and into free pore space. The activating force for pressure solution would thus be the effective normal stress across the grain contact. The solution film is adsorbed on the surface of the grain, and, if there is no significant direct contact between the grains, must be able to support shear stress (Figure 2.4). The concept of a bound water layer does not, however, preclude the possibility that some portion of the grains may be in direct contact.

As reported by de Boer (1977a), the existence and properties of this adsorbed solution film have been investigated (Every *et al*., 1961; Kenichi, 1968) and the results support Weyl's assumption. It was found that the adsorbed water layer was capable of withstanding considerable pressures. No measurements of silica diffusion through such a layer have been reported.

Thomson (1959) proposed a pressure solution mechanism based on silica diffusion within the mass. He observed that the presence of clay, in this case illite, promoted pressure solution along grain boundaries, and postulated that the exchange of calcium and magnesium for the potassium in illite creates an alkaline environment and increases the silica solubility. The silica then dissolves and migrates to areas of low pH at free grain surfaces where it is deposited.

Lerbekmo and Platt (1962) also observed that pressure solution was promoted by clay, and postulated the following mechanism: ferric oxide is reduced to form iron carbonate and iron sulphide, and the consequent release of hydroxyl ions increases the pH locally and thus increases the silica solubility. This reaction requires a source of sulphur, which was postulated to be sulphur-bearing organic material.

Neither of the latter two mechanisms constitutes an adequate explanation for the occurrence of pressure solution, as solution has been observed to occur without the presence of clay. The validity of the proposals of Weyl and Bathurst must thus be examined.

Weyl's mechanism is the only one which accounts for the phenomenon of "force of crystallization" (Becker and Day, 1916; Taber, 1916). When a crystal placed between two boundaries is fed with the appropriate supersaturated solution it will grow until it comes into contact with the boundaries, and will then exert a force to push them apart, even if it is free to grow in other directions. This process is the reverse of pressure solution. Only Weyl's mechanism is reversible, thus taking this phenomenon into consideration.

In order to analyze the validity of the Bathurst and Weyl mechanisms, a nonhydrostatic thermodynamic analysis of the change in solubility with pressure has been undertaken by several researchers (de Boer, 1977a, b; Rutter, 1976; Paterson, 1973). The results of these analyses indicate that at a "free" surface exposed only to the pore fluid the solubility increase with stress is negligible, whereas the solubility is significantly increased at a face subjected to compressive loading in addition to the fluid pressure, ie. at a grain boundary (Figure 2.5). This tendency for the solubility to increase with normal stress far outweighs the effect of dissolution along a preferred lattice orientation. Since the stresses are almost completely concentrated within the contact area, the solubility is not significantly increased at the edges of the contact, thus Bathurst's mechanism is not adequate to account for the occurrence of pressure solution. This conclusion supports the validity of Weyl's mechanism. There will be a small zone very close to the contact area where the solubility will be slightly increased, but the pressure solution process will be dominated by the solution which takes place within the contact area.

The analysis described above indicates that it is the portion of the normal stress above the fluid pressure which causes the significant increase in solubility. Thus it is the effective stress which activates pressure solution. This concept has been experimentally verified by Sprunt and Nur (1976). Their experiments were conducted on samples of St. Peter sandstone at elevated temperatures, using distilled water as the pore fluid. The tests were of two-week duration. It was found that samples subjected to hydrostatic pressure experienced almost no reduction in porosity, while in those subjected to nonhydrostatic stress the porosity was reduced to as little as 55 percent of its original value.

Kennedy (1950), on the basis of experiment, stated that temperature has a greater influence than stress on silica solubility. His experiments were conducted under hydrostatic conditions, and this accounts for the small solubility increase encountered with increased stress. Weyl (1959) developed thermodynamic solubility equations for a hydrostatic stress system, and these equations predict a much lower solubility increase than the nonhydrostatic analysis.

On the basis of Weyl's mechanism, pressure solution can be considered as a process involving three steps: the material is dissolved from the solid phase into the intergranular film; it is then diffused through the film into free pore space in response to a chemical potential gradient; and finally it is precipitated as secondary overgrowths on free grain surfaces, or transported out of the system. The slowest portion of this process, and therefore the one which controls the rate of pressure solution, is the diffusion through the solution film.

Rutter (1978) has developed an expression relating the rate of displacement (rate of solution) to the stress, temperature, diffusion characteristics and thickness of the intergranular film. While the behaviour of the solution film is not well understood, it is evident that the most sensitive parameter is the diffusion coefficient for the film and its dependence on the intergranular stress. It becomes apparent from his analysis that pressure solution can take place over a wide range of temperature and pressure conditions if the time scale is sufficiently large for the reaction to take place. There is thus no direct correlation between degree of pressure solution and the age of the formation, as the environmental conditions may be continually fluctuating. The occurrence of pressure solution is not limited to materials which have been buried to a certain depth.

The presence of pore water has been found to be necessary for the development of pressure solution, but the concentration of ions in the fluid does not appear to influence solution. De Boer (1977b) conducted a series of experiments in which the concentration of sodium chloride in the pore fluid was varied in samples placed under a constant stress and temperature. The results for all tests were nearly identical, indicating that the concentration of ions in the pore fluid has no effect on pressure solution. This conclusion supports the validity of Weyl's mechanism.

2.3.3 Factors Affecting Pressure Solution

The environmental and material factors which influence pressure solution are:

1. Stress: The stresses within the material are influenced by a number of factors: deposition and original packing of the grains, grain size and shape, the depth of burial (weight of overburden), the fluid pressure in the pores, and the degree of structural deformation,

due either to differential compaction or tectonic activity. Because of the variety of factors which influence pressure solution, no universal relationship can be found between the degree of solution and depth of burial, though some correlations have been done for individual locations (Taylor, 1950; Maxwell, 1964; Phillip *et al.*, 1963; Selley, 1978). Siever (1959) noted that in two locations within a sandstone mass which were subjected to similar overburden pressures, increased structural deformation in one location had increased the amount of pressure solution which had taken place. He stated that the effects of structural deformation appeared to outweigh the influence of burial depth.

In the experiments of Sprunt and Nur (1976) discussed above, a series of tests were conducted on hollow cylinder specimens with a pore pressure applied to the inside diameter and a confining pressure applied outside, thus creating a stress differential (effective stress) in the specimen. One set of tests was conducted under a constant stress differential for a series of pore pressures, and it was found that for an experiment of two-week duration the porosity reduction due to solution increased with increasing pore pressure. A second set of tests was performed with constant pore pressure, and the confining pressure was varied. The results indicate that the porosity reduction did not depend on confining pressure (Figure 2.6). It was concluded that although a stress differential is required to activate pressure solution, the rate of solution is controlled by the pore pressure. It was not possible to determine whether the final equilibrium porosity depended on the effective stress, as the experiments were not carried to equilibrium.

2. Temperature: An increase in temperature will cause an increase in solubility and will therefore promote pressure solution. The heat induced by tectonic activity (folding, faulting) may thus enhance the intensity of pressure solution.
3. Clay coatings: As previously mentioned, clay coatings can enhance pressure solution (Cecil and Heald, 1971; Taylor, 1978a). A dramatic illustration of this is given by Heald (1956). Two samples located two inches from each other in a sandstone mass were examined. In the clay-free sample little pressure solution had occurred, whereas in the second sample, in which the particles were covered by a thin clay coating, extensive pressure solution had taken place. De Boer (1977b) makes reference to a study by Novelli and Mattavelli (1967) which concluded that increased grain interpenetration in a sandstone was caused by illite clay coatings. For clay contents greater than five percent, however, they found that interpenetration was almost absent.

On the basis of Weyl's mechanism for pressure solution, it becomes apparent that the clay layer enhances pressure solution by holding water within the grain boundary and allowing easier diffusion of dissolved material. Too much clay may result in a "cushioning effect" (Siever, 1959), whereby the clay is embedded in the grains and equalization of pressure occurs.

It has been postulated that the clay acts as a catalyst in the silica-diffusion reaction (Thomson, 1959; Lerbekmo and Platt, 1962). De Boer (1977b) stated that this is not likely to contribute significantly to the promotion of pressure solution.

4. Grain size: The theory developed by Weyl predicts that a decrease in grain size will increase the porosity reduction due to pressure solution, and this has been supported by observations of actual materials (Renton *et al.*, 1969). The porosity reduction will also increase with increasing angularity of the grains. This indicates that a higher specific surface area will increase the influence of pressure solution. According to Trurnit (1967), grains with lower radii of curvature will penetrate into those with higher radii of curvature, all other conditions being equal.
5. Organic impurities: Pressure solution has been found to be inhibited by the presence of organic impurities such as oil, gas, or other hydrocarbons (Phillip *et al.*,

1963). Siever (1962) found that the solubility of silica is significantly reduced in peat waters.

Rittenhouse (1971) has calculated the porosity loss resulting from solution of grains at contact points for various packing arrangements of ideal spherical and ellipsoidal particles. Figure 2.7 shows the relation between the porosity loss due to pressure solution and the amount of cement generated for four packing arrangements. Because of the close packing of the grains, orthorhombic packing rotated 30 degrees is considered to represent the maximum amount of cement which could be generated from a given porosity loss for any sandstone. In a real sandstone the cement generated would be less than this due to the effects of angularity, poor sorting, and three-dimensional stress conditions. This indicates that the process of cement production from pressure solution is comparatively inefficient in reducing sandstone porosity, although solution itself causes a significant porosity reduction.

Sibley and Blatt (1976) conducted a thin-section study of sandstones in which they estimated the amount of detrital and authigenic quartz, clay minerals, and pore space in fourteen sandstones from various locations. The amount of porosity loss due to pressure solution was also estimated. The results of this analysis have been plotted on a diagram of cement generated from pressure solution versus the porosity loss due to solution, assuming all the dissolved silica from pressure solution becomes authigenic quartz

(Figure 2.8). The horizontal axis also shows the equivalent minus-cement porosity, assuming an initial porosity of 40 percent for comparison. The theoretical relationships for orthorhombic packing rotated 30 degrees under one- and three-dimensional strain have also been plotted. This data supports Rittenhouse's conclusion that orthorhombic packing rotated 30 degrees represents the maximum amount of cement which could be generated for a given porosity loss.

2.3.4 Grain Surface and Contact Features

Diagenesis results in increased interlocking of grain contacts. Unaltered materials usually have tangential contacts, and these will gradually be changed to long, concavo-convex, and sutured contacts (Figure 2.9). Trurnit (1967) developed a classification system for the geometry of pressure solution contacts in terms of the influence of the radii of curvature and the relative solubility of the grains. He stated that grains possessing different solubilities will tend to develop smooth contacts, whereas those with equal solubility will initially develop smooth contacts, which will progress to sutured (stylolitic) contacts.

Stylolites are a special form of pressure solution feature. They are irregular sutured boundaries composed of a series of interdigitated columns. Stylolites usually occur in limestones, and also develop in sandstones. These features originate from pressure solution followed by immediate local redeposition of the dissolved material. They are characterized by irregular seams which often contain a clay residue. Stylolites create a local reduction in porosity and increase in competency of the formation (Heald, 1955). Sutured contacts between individual grains in sandstone have been described by Sloss and Feray (1948) as "microstylolites".

With the aid of the scanning electron microscope, numerous studies of the surface features of sand grains have been undertaken (for example, Krinsley and Donahue, 1968; Krinsley and Doornkamp, 1973). Two basic types of features associated with pressure solution have been documented. The first of these is a wavy, etched pattern which appears to initiate in existing surface depressions, and may spread over the grain surface. The second is a worn, low-relief solution surface, often seen as fields of aligned solution pits, the crystallographic orientation of the grain controlling their development.

The surface of individual sand grains may show deep depressions or flattened areas where pressure solution has caused interpenetration of the grains. Initially, the grain will have surface features caused by its origin and depositional environment (abrasion features, fracture surfaces), but increasing diagenesis will eventually obliterate all traces of the original surface features.

2.4 Authigenic Overgrowths

2.4.1 Definition

Authigenic overgrowths are formed by the precipitation of material from a supersaturated solution, and crystallization of the material on free grain surfaces. The most common form of overgrowth in sandstones, and the one which occurs in the McMurray Formation, is the development of secondary quartz crystals on the surface of the detrital grains. This results in an increase in the interlock between the grains, and a consequent reduction in porosity and permeability and increase in the strength of the formation.

The silica may be deposited either in crystallographic order as quartz, or under higher supersaturations as amorphous silica, which will be converted to quartz over a long time period. In the experiments conducted by de Boer *et al*. (1977) a sample of sandstone was diagenetically altered by pressure solution and authigenic overgrowth. The precipitated material was found to be composed of both quartz and amorphous silica.

2.4.2 Development of Overgrowths

There are two stages of development in crystal overgrowth (Ernst and Blatt, 1964; Waugh, 1970; Pittman, 1972). The first is the formation of small crystals across the surface of the grain. In the second stage these growths will develop into large crystals with well-defined faces (Figure 2.10). The final appearance of a well-developed overgrowth is a pyramidal structure with planar faces. If conditions for growth are maintained, the overgrowth will develop into the pore space until it meets a detrital grain or another overgrowth. The two faces will then conform to each other with either a linear or sutured boundary, depending on their relative crystal orientations and growth rates.

As the development of overgrowths proceeds, the porosity and permeability of the material will be gradually reduced, consequently the amount of silica precipitated will decrease with time due to the decreased mobility of the formation water (Figure 2.11). The environmental conditions of pressure, temperature, pH, and silica supply will affect the nature of the above relationship, as well as the initial properties of the material.

The overgrowths develop in optical continuity with the host grain. The influence of the crystal order of the underlying grain is indicated by the fact that overgrowths will not nucleate on chert grains, as the grains are composed of varied crystal orientations (Sloss and Feray, 1948). Also, overgrowths will nucleate on either side of a lineage boundary (flaw in the crystal order) but will not meet across it, though one crystal may eventually grow over top of the boundary (Figure 2.12). The overgrowths have the same crystal orientation as the host grain, and the lineage boundary is thus extended into the overgrowth. Ernst and Blatt (1964) found that the greater the strain in a quartz particle, the less was the probability of overgrowths nucleating on the surface. Again, this is a function of the higher surface energy resulting from the distortion of the crystal orientation.

A thermodynamic analysis has been performed by Paterson (1973) to determine the preferred orientation of crystal development for several materials. He found that for alpha-quartz under homogeneous stress conditions, the direction of preferred crystal development was along the c-axis of the crystal (Figure 2.12). However, the fact that the pore fluid will not transmit shear stress creates local stress heterogeneities, and this will cause deviations from the preferred development. The subject of crystal overgrowth under pressure is discussed below. Further deviations in crystal development will be caused by the initial shape of the grains.

Pressure solution may not be sufficient to account for the overgrowths present in a material (Sibley and Blatt, 1976). As previously shown, Rittenhouse (1971) has shed doubt on the efficiency of cementation generated by pressure solution. The silica required for overgrowth development may originate from pressure solution or local clay diagenesis, or may be introduced from an external source by moving formation waters and precipitated by a change in equilibrium conditions (for instance, a decrease in temperature). If grains of chert or strained quartz are present, they may constitute an added source of silica as their solubility is greater than that of unstrained quartz.

The stress conditions, temperature, and pH of the formation water will all influence the solubility of silica and therefore the development of overgrowths. Another important factor is the amount of silica being supplied to the system, either from pressure solution or moving formation waters. However, it is difficult to specify the exact environmental conditions which will favour overgrowth development.

There are three physical possibilities for the solubility condition in a silica-water system (Durney, 1976). The system can be in local equilibrium, with the concentration of dissolved silica equal to the saturation value for the given pressure, temperature and pH conditions. Alternatively, the water may be undersaturated with respect to the equilibrium condition, in which case solution will occur, or it may be supersaturated, in which case precipitation will occur. Thus silica precipitation could take place over a wide range of temperature, pressure, and pH conditions, depending on the amount of silica in solution. It is the departure from the equilibrium conditions dictated by the environment which will cause solution or precipitation to occur.

This analysis indicates that overgrowth development could begin anywhere on a grain, even within a contact area (which is the phenomenon of "force of crystallization"), provided the saturation is greater than the equilibrium value. However, the stress conditions within the mass make grain contacts (subjected to fluid pressure and an additional effective stress) preferred sites for solution, and free surfaces (subjected to fluid pressure only) preferred sites for overgrowth development.

Numerous studies of overgrowth development in sandstones have revealed that although the presence of clay coatings on the grains promotes pressure solution, it inhibits the development of overgrowths (Cecil and Heald, 1971; Hawkins, 1978; Taylor, 1978a). Heald and Larese (1974) analyzed the influence of clay coatings by observing the number of overgrowth-grain versus overgrowth-overgrowth contacts in clay-free and clay-containing sandstone. The sandstone which contained clay exhibited a greater number of overgrowth-grain contacts, indicative of uneven overgrowth development. The presence of clay prevented the nucleation of overgrowths on the grain surfaces. The samples were taken from the same mass and had been subjected to the same environmental conditions. Heald (1956) observed that secondary quartz appeared to have replaced thin clay coatings in a sandstone, but in locations where the clay coating was thick no overgrowths had nucleated. These growths nucleated in small breaks in the clay coating. After commencement, the growth may spread over the grain surface leaving the clay as an inclusion or "dust line".

The grain size of the material will influence the effect of overgrowth development on the porosity. Heald and

Renton (1966) produced quartz overgrowths in samples of fine- and coarse-grained well-sorted sandstones by using an elevated temperature. When the pore fluid was allowed to circulate freely, the coarse-grained sample cemented more quickly than the fine-grained one, as its greater permeability allowed greater influx of cement. When the flow was regulated to the same value in both cases, the fine-grained sample cemented more quickly. They also observed that the cementation rate was faster in more angular materials. As in the case of pressure solution, the rate of overgrowth development is a function of the specific surface area of the grains. The more angular the material is, the greater will be the surface area available for overgrowth nucleation.

2.4.3 Grain Surface and Contact Features

Examination of overgrowths in thin section usually reveals a "dust line" between the detrital grain and the overgrowth. This small gap may consist of void space or may be infilled by impurities. The dust line may originate as a thin coating on the surface of the detrital grain, or as a liquid inclusion, and may be infilled with secondary quartz at a later date. Dust lines are a diagnostic feature for recognizing overgrowth development in thin section. The presence of overgrowths is revealed in the scanning electron microscope by smooth planar surfaces or pyramidal structures on the grain surface. The initial stage of overgrowth development will appear as small projections on the grain.

2.5 Summary

The diagenetic processes of cementation, pressure solution, and authigenic overgrowth act to reduce the porosity of a sand and increase its competency. The extent to which diagenesis has modified the grain fabric of the material will determine its strength and its engineering behaviour.

The manner in which diagenesis influences the fabric of the material will be determined by the sequence of diagenetic events in its history. For instance, early cementation in a sandstone will prevent the occurrence of pressure solution, and this will fundamentally affect the material properties. Also of importance is the length of time during which conditions suitable for the occurrence of diagenesis exist. The fabric will be altered to a greater or lesser degree depending on fluctuations in the environmental conditions.

Both pressure solution and authigenic crystal overgrowth cause a reduction in the porosity of oil sands. The general effect of diagenesis is to increase the contact area between individual particles and create long, concavo-convex, or sutured contacts as opposed to the tangential contacts normally encountered in unaltered sands. The strength and stiffness of the materials is increased by this interlocked fabric, as the altered structure will sustain higher stresses with lower deformations. The effect of this diagenetic change on the engineering behaviour of oil sands will be described in the following chapters.

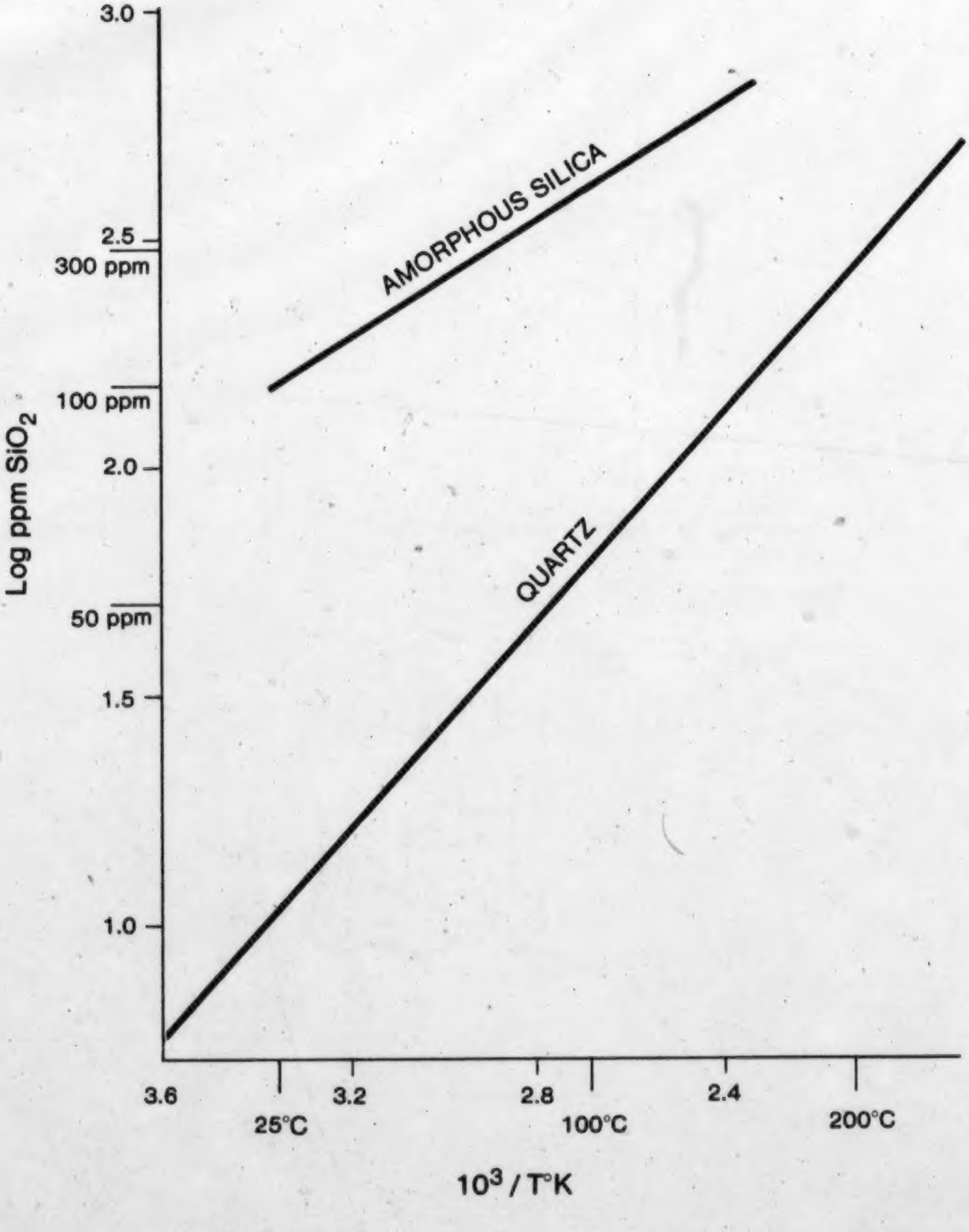

Figure 2.1 : Solubility vs. temperature for amorphous silica and quartz (after Siever, 1962).

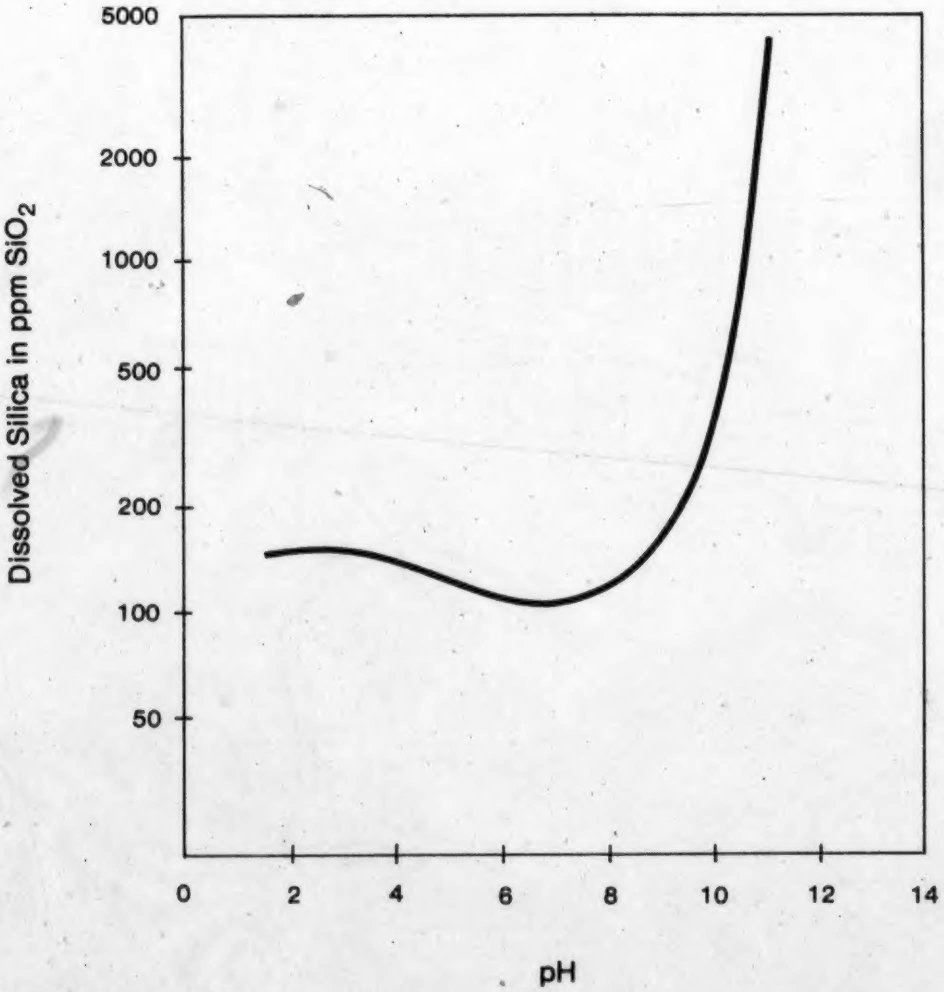

Figure 2.2 : Solubility vs. pH for amorphous silica (after Krauskopf, 1959).

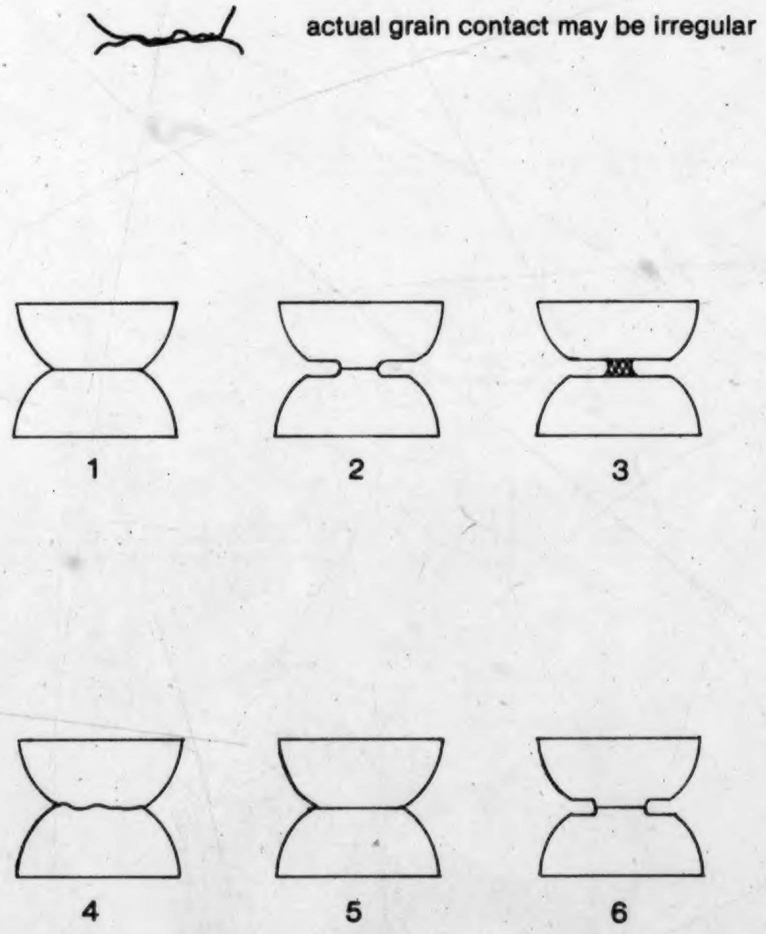
actual grain contact may be irregular
1
2
3
4
5
6

Figure 2.3 : Bathurst mechanism for pressure solution (after Weyl, 1959).

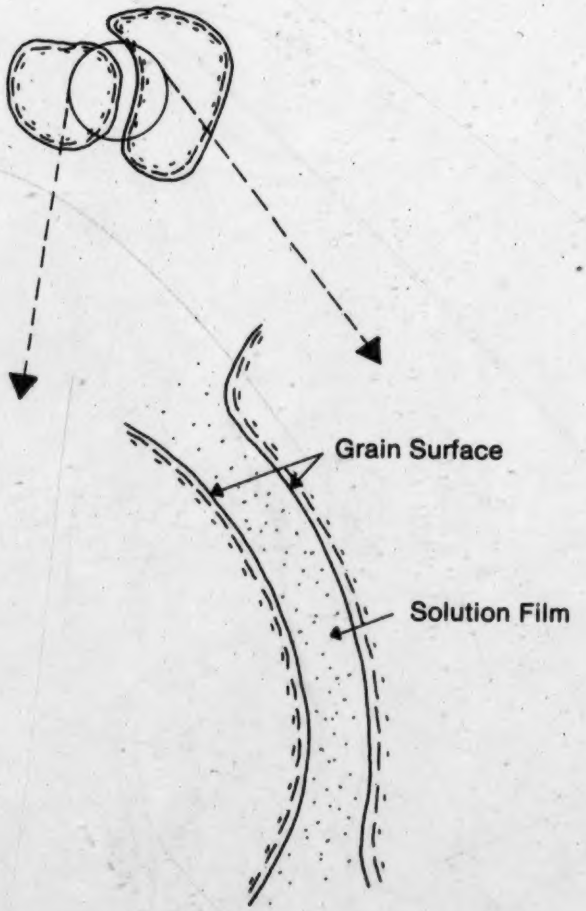
Grain Surface
Solution Film

Figure 2.4 : Weyl mechanism for pressure solution.

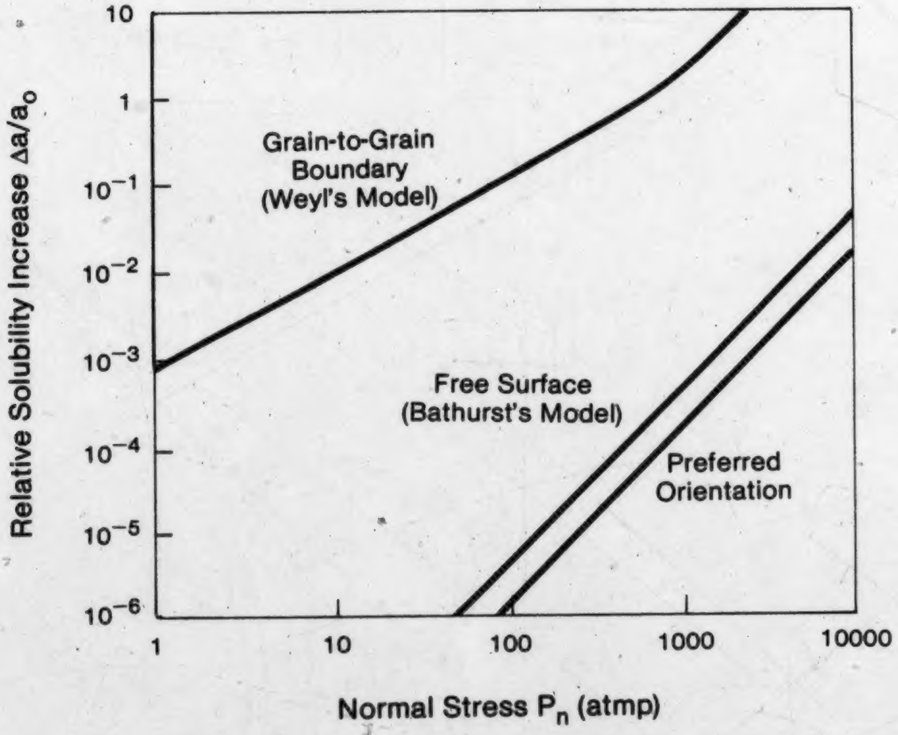

a_o = Solubility Under Hydrostatic Load

Figure 2.5 : Relative solubility increase caused by external load for "free" surface, grain-to-grain boundaries and preferred orientation (temperature = 300°K, molar volume = 22.7 cm^3/mol), (after de Boer, 1977a).

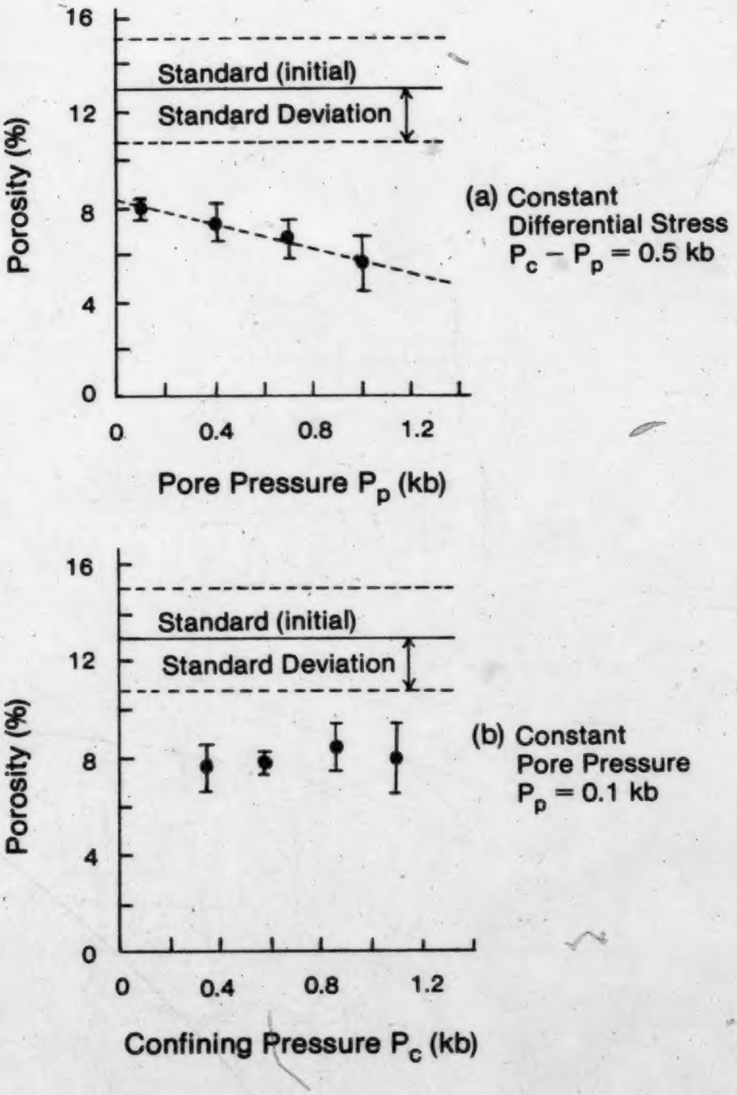

Error Bar with Mean for
Porosity Measurements

Figure 2.6 : (a) Effect of constant differential stress on porosity, duration is two weeks.
(b) Effect of constant pore pressure on porosity, duration is two weeks.
(after Sprunt and Nur, 1976).

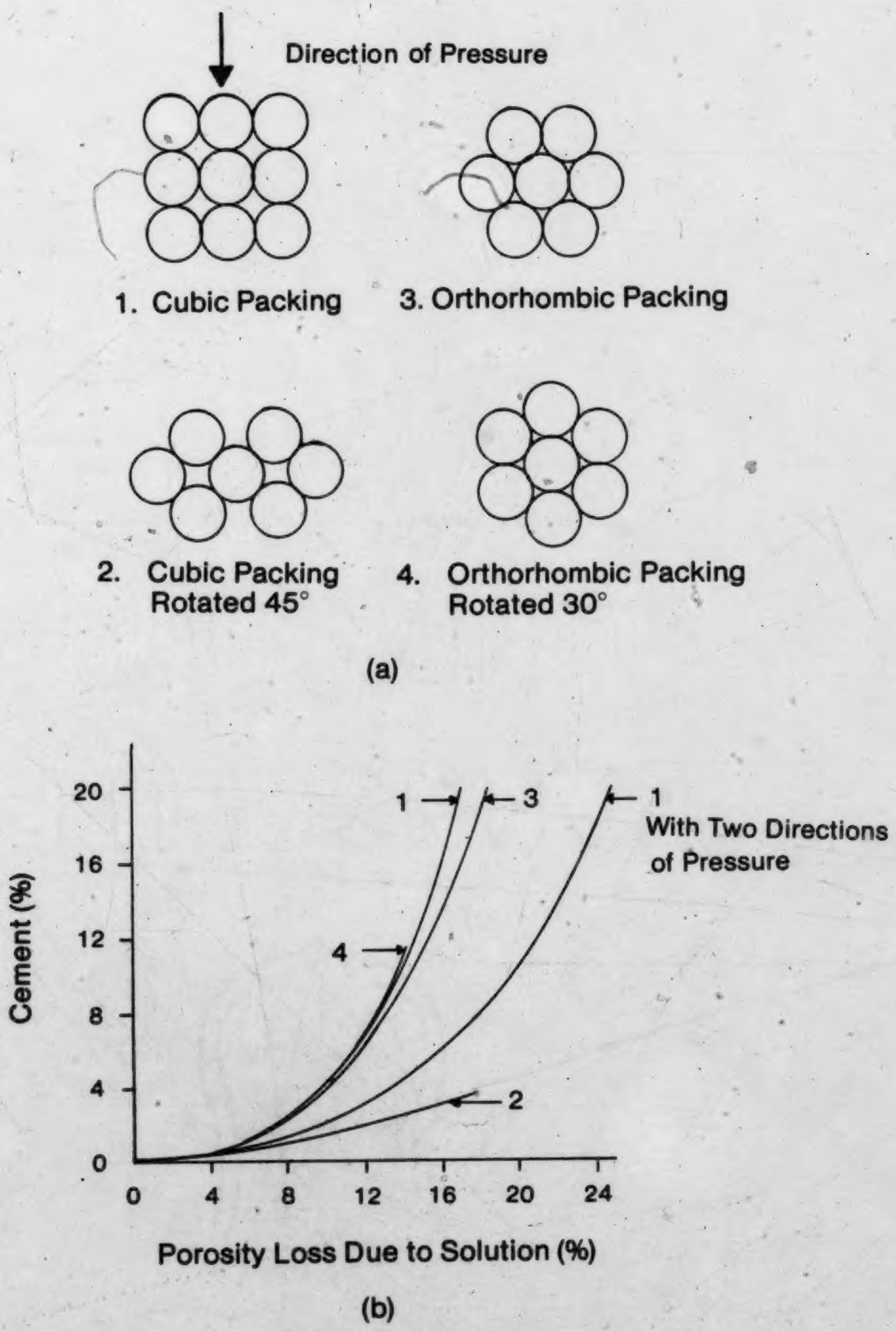

Figure 2.7 : (a) Packing arrangements for perfect spheres.
(b) Cement generated vs. porosity loss due to solution.
(after Rittenhouse, 1971).

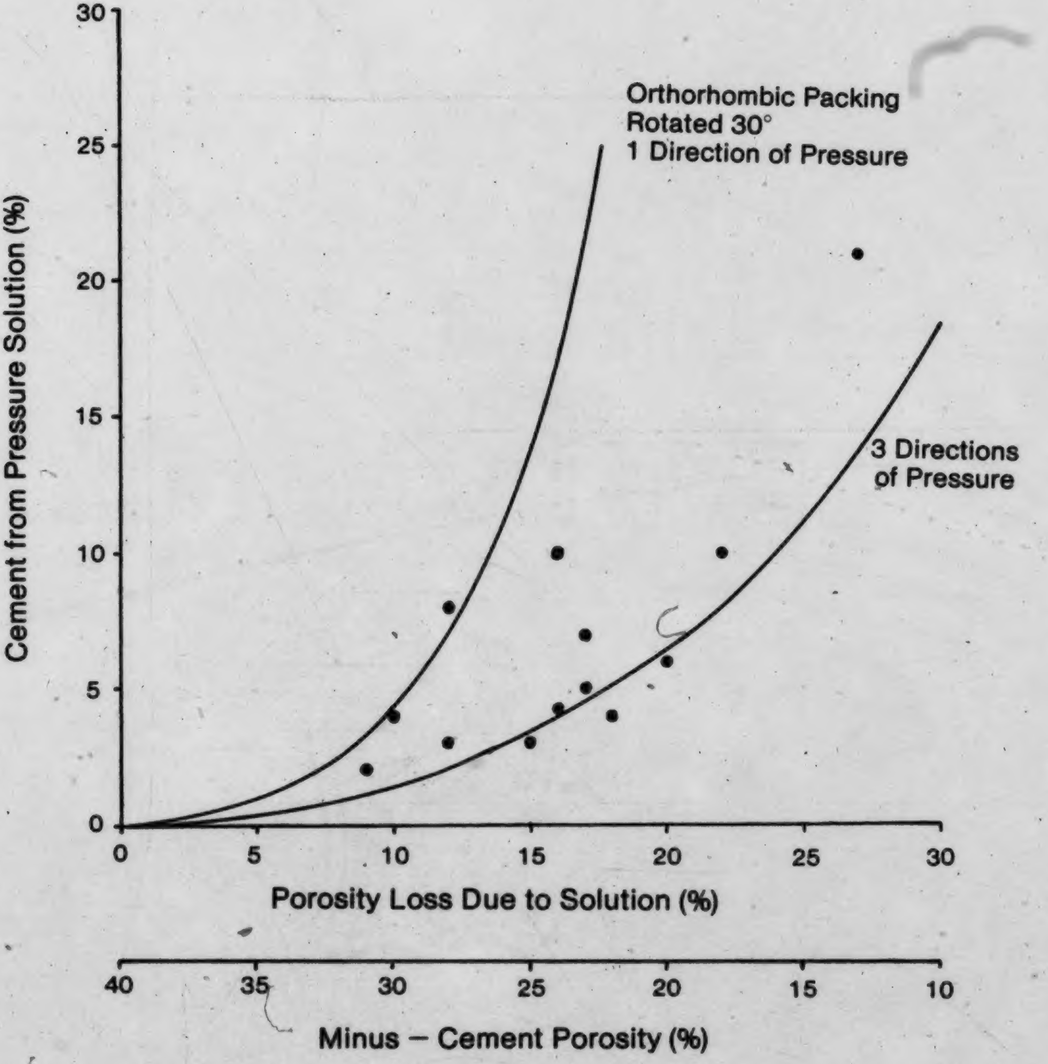

Figure 2.8 : Cement generated vs. porosity loss due to solution for actual sandstones (Sibley and Blatt, 1976).

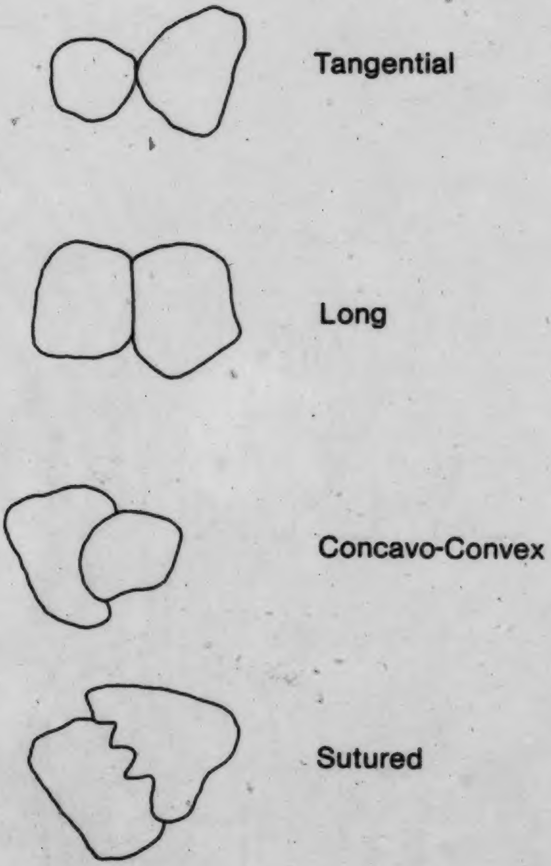
Tangential
Long
Concavo-Convex
Sutured

Figure 2.9 : Types of grain contacts (after Taylor, 1950).

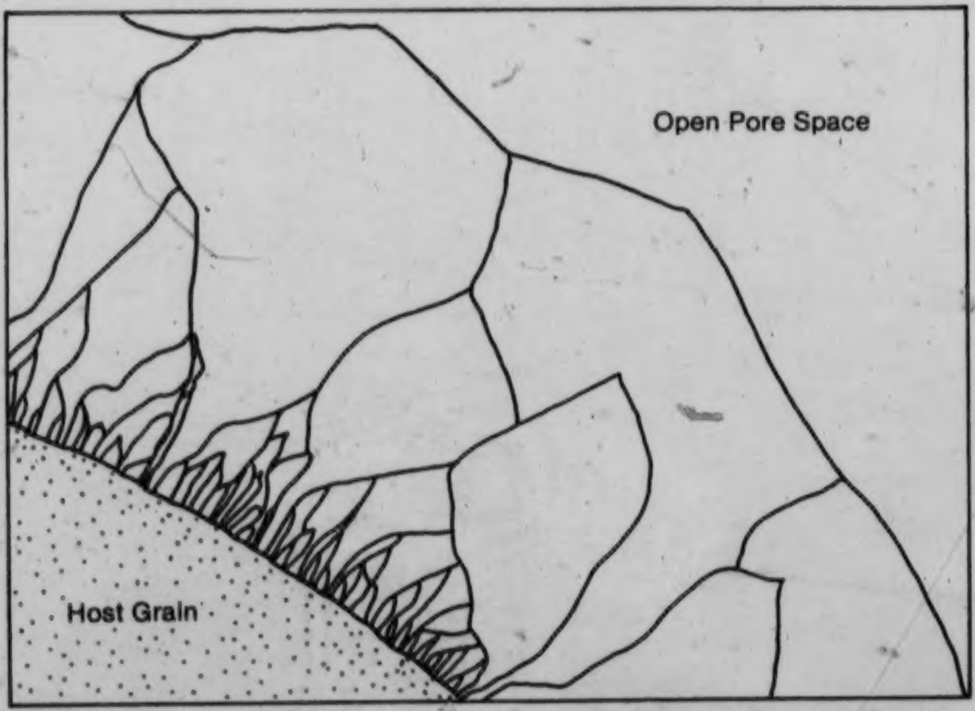
Open Pore Space
Host Grain

Figure 2.10 : Stages of development of a crystal overgrowth (after Pettijohn et al., 1972).

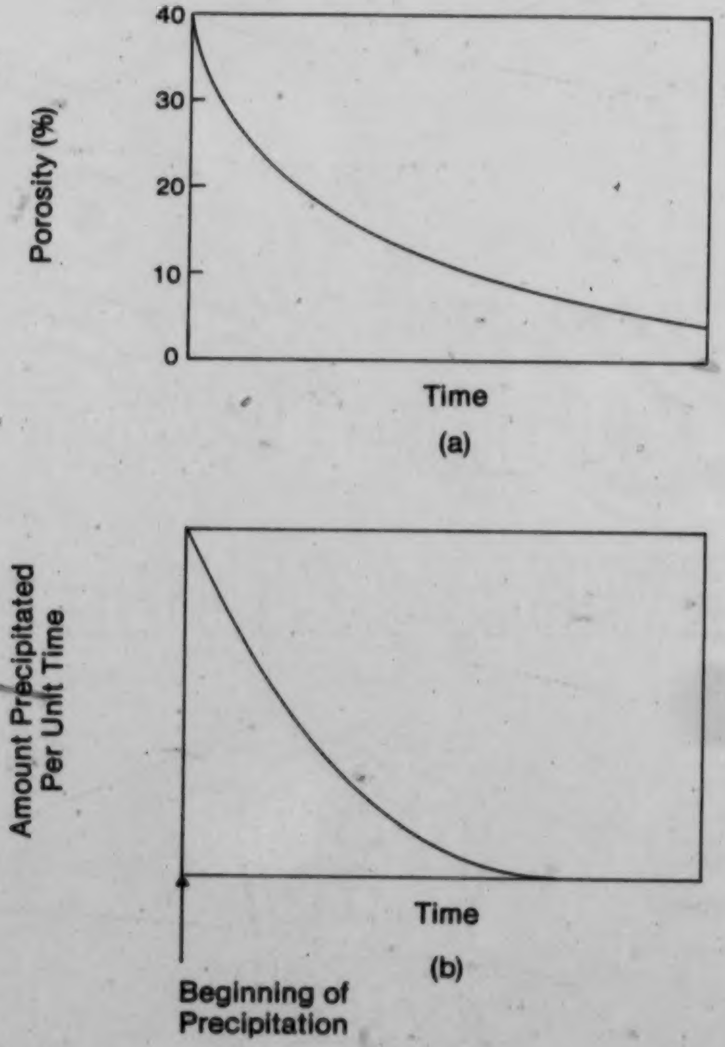

Figure 2.11 : (a) Porosity loss with time as cementation proceeds.
(b) Amount of cement precipitated vs. time.
(after Pettijohn et al., 1972).

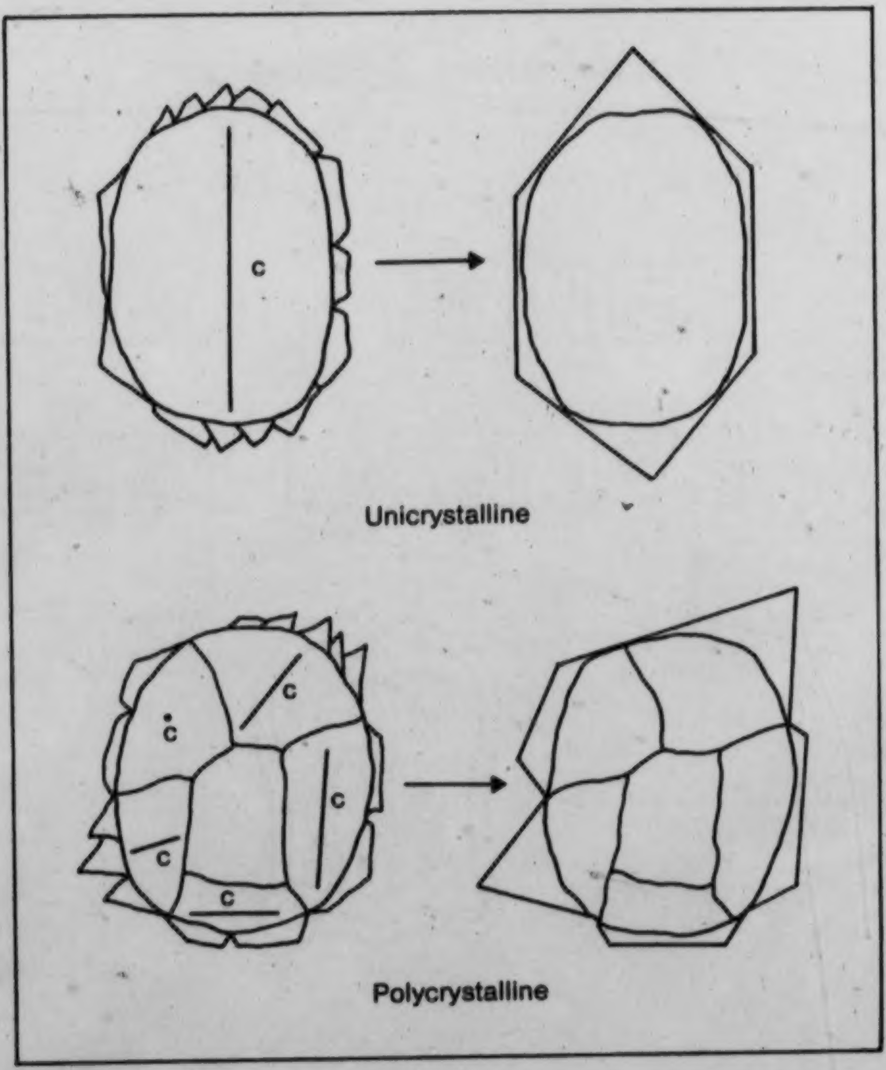
c
Unicrystalline
c
c
c
c
c
Polycrystalline

Figure 2.12 : Theoretical overgrowth development stages for unicrystalline and polycrystalline quartz; orientation of c-axis shown.
(after Waugh, 1970).

3. INFLUENCE OF DIAGENESIS ON OIL SAND MATERIALS

3.1 Introduction

Oil-free specimens of the McMurray and Grand Rapids Formations from the Athabasca area were examined in the scanning electron and optical microscopes to evaluate the influence of diagenesis on the grain fabric of oil sands. The use of oil-free specimens enabled clear examination of the grain surface and contact features, which would be obscured by the presence of bitumen. The samples were also free from the disturbance normally caused by exsolution of gas from the interstitial bitumen on removal of overburden pressure. All specimens examined were found to have undergone some degree of diagenetic alteration.

The types of oil sand specimens used for microscope observation and strength testing are enumerated below, and the location and geological origin of the samples is given. The diagenetic fabric alteration of the samples is delineated by examination of the grain surface and contact features present in the materials.

Several comparative materials were examined to aid in the delineation of sandstone fabric. Among these samples are two flexible quartzose sandstones (itacolumites), a cemented sandstone, and two bituminous sandstones from the United States.

3.2 Sampling Procedures and Specimen Preparation

The oil sand specimens used for laboratory testing and micrograph analysis were obtained from river valley outcrops in the vicinity of Fort McMurray. Block specimens of the materials were cut from the outcrop face, placed in plastic bags, and wrapped with fiberglass tape to provide confining pressure. The samples were extremely delicate when not confined, but stayed intact well when all-round external pressure was applied by use of the tape.

Intact specimens of oil sand and comparative materials for scanning electron microscope examination were prepared by mounting a small block on an aluminum stub and breaking the sample in tension to expose an undisturbed surface. In addition, grain mounts of certain grain size fractions of the McMurray Formation were prepared. The intact specimens were mounted to examine the nature of the grain contacts in the material, whereas the grain mounts were prepared to study the grain shapes and surface features.

Standard thin sections of the McMurray Formation and several comparative materials were prepared for optical microscope analysis. Plane-polarized light was used for the optical photomicrographs.

3.3 Grain Fabric of the McMurray Formation

3.3.1 Location and Geological Origin of Specimens

For the purpose of analyzing the grain fabric and strength characteristics of the Athabasca Oil Sands, intact oil-free samples of the McMurray Formation were obtained from an outcrop on the High Hill River, approximately 40 kilometers upstream from Fort McMurray along the Clearwater River. A description of the morphology of this slope has been given by Dusseault (1977). Block samples were taken from three locations in the slope.

1. Coarse-grained sand (Lower Member): This material was sampled from the lower portion of the slope. It contains pebbles two to three millimeters in diameter in a matrix of fine- and medium-grained quartz sand. The material is well-graded, with a median grain diameter of approximately 0.62 mm. Concentrated beds of coarse- or fine-grained sand were observed in the samples in a cross-stratified pattern.
2. Medium-grained sand (Middle Member): This sand was sampled at a location approximately five meters above the coarse-grained specimens. It consists of an extremely uniform sand with a median grain diameter of approximately 0.43 mm. Horizontal stratification was observed in the samples. The material contained occasional coal specks, but these were infrequent and did not influence the tests conducted.
3. Fine-grained sand (Middle Member): The material was obtained from a location approximately ten meters above the medium-grained specimens, and consists of a horizontally-stratified, very uniform sand with a median grain diameter of 0.20 mm.

The sample locations were chosen to illustrate the three major lithologies of the Athabasca oil sands deposit. All samples were clean, almost purely quartzose sands with a pronounced lack of cement. The terms fine-, medium-, and coarse-grained McMurray Formation will be used to refer to the three materials.

3.3.2 Photomicrographs of the McMurray Formation

The fabric of the McMurray Formation has been altered by the processes of pressure solution and authigenic crystal overgrowth. The resultant structure is illustrated by the use of scanning electron and optical micrographs.

Figure 3.1 illustrates a number of quartz overgrowths. The intermediate stage of development, smooth planar faces, is shown in Figure 3.1(a), while 3.1(b) and (c) illustrate well-developed pyramidal overgrowths. Figure 3.1(d) shows an inverted pyramidal overgrowth with a pitted surface.

The effect of solution on the grain surfaces is shown in Figure 3.2. Fields of oriented solution pits such as those illustrated in the figure are a common occurrence in the McMurray Formation.

Solution and overgrowth result in interlocking contacts between grains. Figure 3.3 shows a number of interpenetrative grain contacts resulting from diagenesis. Pressure solution appears to dominate porosity reduction processes in this material.

Figure 3.4 shows two stereo pairs of the McMurray

Formation. Two optical micrographs of the material are shown in Figure 3.5, demonstrating the interlock between grains. The fabric is composed of tangential, long, and concavo-convex contacts. The McMurray Formation has undergone comparatively mild diagenetic alteration.

3.4 Grain Fabric of the Grand Rapids Formation

3.4.1 Location and Geological Origin of Specimens

Intact oil-free specimens of the Grand Rapids Formation were obtained from the Grand Rapids outcrop on the Athabasca River, approximately 80 km southwest of Fort McMurray. This location borders on the Wabasca oil sands deposit. The Grand Rapids Formation is an oil-bearing stratum about 50 km southwest of the outcrops.

The Grand Rapids Formation consists of three major quartz-feldspar sandstone units separated by shaley sequences, as described in Chapter 1. Two separate parts of the deposit were sampled: the lower 'C' sand and the upper 'A' sand (Kramers,1974).

The Grand Rapids A material is an extremely uniform fine-grained sand with a median grain diameter of 0.10 mm. Grain size analysis indicates that approximately four percent of the material is finer than 0.074 mm.

The Grand Rapids C material is only slightly more well-graded than the A sand, and coarser-grained, with a median grain diameter of 0.23 mm. Grain size analysis indicates that ten percent of the material is finer than

0.074 mm. This fine-grained material is partly smectitic (montmorillonitic) clay coatings on the grains (Kramers, 1974). This clay coating is absent in the Grand Rapids A sand. The manner in which the clay coating influences the diagenetic alteration of these two materials will be described below.

3.4.2 Photomicrographs of the Grand Rapids Formation

Figures 3.6 and 3.7 are scanning electron micrographs of the Grand Rapids Formation A. Both pressure solution features and quartz and feldspar overgrowths are observed. The feldspar overgrowths are identified by crystal face intersection angles of close to 90° as opposed to the more pyramidal shape of quartz crystals. The feldspar overgrowths also exhibit cleavage planes. The overgrowths are more influential in the porosity reduction of this material than in the McMurray Formation. The grain surfaces are fairly clean.

Figure 3.6 shows both quartz and feldspar overgrowths. Small crystal projections which are the initial stage of overgrowth development are shown in Figure 3.7(a). Figure 3.7(b) is an illustration of a field of solution pits on a grain surface. Figures 3.7(c) and (d) show interpenetrative contacts resulting from pressure solution.

As stated above, the presence of a thin clay coating on the grains can enhance pressure solution by holding pore fluid within the contact area and allowing easier diffusion of dissolved material. This process appears to have been operative in the Grand Rapids Formation C. The montmorillonitic clay coating on the grains has inhibited the development of overgrowths (they are almost totally absent), and the porosity reduction is dominated by pressure solution. Figures 3.8 and 3.9 show long and concavo-convex contacts in the Grand Rapids Formation C which have resulted from pressure solution. Even though the porosities of the A and C sands are almost identical, two different processes have altered them.

The difference in mineralogy between the Grand Rapids and McMurray Formations will influence their engineering behaviour. This topic is discussed in Chapter 5.

3.5 Fabric of Comparative Materials

3.5.1 Itacolumites

Photomicrographs of two flexible quartzose sandstones or itacolumites are shown in Figures 3.10 through 3.14 for comparison with the oil sand materials. Itacolumites have an extremely well-developed diagenetic structure. The interdigitation of the grains results from crystal overgrowth (Carozzi, 1960). Because of the narrow uniform gap between the grains, a slab of the material visibly flexes when held in the hand.

Figures 3.10 and 3.11 are scanning electron and optical micrographs of an itacolumite from India. Scanning electron microscope specimens were prepared oriented along three orthogonal axes. This material appears to be isotropic and is composed of very angular quartz grains. The grains interlock very closely and have extremely smooth, well-developed crystal surfaces with no evidence of solution pitting. Crystal overgrowth is thus the dominant mode of porosity reduction. Planar and pyramidal overgrowth features are visible.

There is no chemical cementation between adjoining grains. The material does possess a cohesion at zero confining stress, but this results from the three-dimensionality of the interlocking grain fabric.

The material contains a small percentage of non-quartz grains which are kaolinite crystals in an unusual tubular form (lower right of Figure 3.10) as identified by X-ray diffraction analysis. The grains are probably the result of feldspar decomposition. These crystals cover the surface of occasional grains (for example, the small grain in the center of Figure 3.10, upper left). These grains are not the cause of the flexibility of the material, but may aid in the delineation of its diagenetic history.

Figure 3.12 illustrates the grain fabric of a micaceous itacolumite from the United States. The material contains visible mica flakes oriented along foliation planes. Micrographs taken parallel to three orthogonal axes are shown, the z-axis being the one which faces on the mica planes. This material shows distinct anisotropy, with the quartz grains elongated in the direction of the foliation planes. The mica does not appear to be of authigenic origin, as the crystal faces are not well-developed and planar.

Figure 3.13 contains two optical micrographs of the micaceous itacolumite. The anisotropy of the material is demonstrated together with the closely interlocked grain structure.

Figure 3.14 shows micrographs of a second sample of the above itacolumite. This second specimen was observed to have much less flexibility than the first. Examination in the scanning electron microscope indicates that the size of the gap between the grains is less in the second sample. Also, the micrographs taken along the z-axis indicate a greater interlocking between the grains. In some locations overgrowths overlap the boundaries between grains.

3.5.2 Cemented and Bituminous Sands

As mentioned above, the manner in which diagenesis influences the properties of a material will be dependent on the sequence of diagenetic events in its history. Figure 3.15 shows two photomicrographs of a cemented sandstone from Colorado. There is direct chemical bonding between the grains, a phenomenon which is almost totally absent in the McMurray and Grand Rapids Formations. Differences in structure will influence the material behaviour significantly. This topic is discussed in Chapter 4.

Photomicrographs of an oil-rich talus fragment of the McMurray Formation are also shown in Figure 3.15. These micrographs illustrate the manner in which the bitumen obscures the grain contacts and surfaces. This indicates the advantage in using oil-free specimens for micrograph analysis.

Photomicrographs of two bituminous sands from California and Utah are shown in Figure 3.16. Although the grain features are somewhat obscured by bitumen, the California tar sand appears to have undergone diagenetic alteration: a number of crystal overgrowths are visible on the grain surfaces. As opposed to the McMurray and Grand Rapids Formations, these materials appear to have been partially cemented as they are very hard. These diagenetic processes will influence not only the oil content and distribution but the ease with which it can be recovered.

Figure 3.17 shows a dense post-glacial sand sampled near the town of Fort McMurray. This material illustrates the difference between a closely-packed dense sand and one which has undergone diagenetic alteration. The grain contacts are largely tangential, with the occasional long contact which is a function of packing rather than diagenesis. Interpenetration between grains is absent.

3.6 Summary

From examination of the micrographs of the oil sand and comparative materials it can be seen that there is a wide range of degrees and types of diagenetic alteration. A cemented sandstone and a non-cemented locked sand might have approximately the same porosity, but the behaviour of the two materials will be different.

The McMurray and Grand Rapids Formations have been altered by the processes of pressure solution and authigenic overgrowth. Long and concave-convex grain contacts have been formed, and the porosity of the materials has been reduced. Chemical cementation is almost totally absent. The influence of this interlocking non-cemented fabric on the engineering behaviour of oil sands will be discussed in the following chapters.

(a) (b)

(c) (d)

Figure 3.1 : Overgrowth features in the McMurray Formation.
(a) planar crystal faces, fine-grained sample.
(b) truncated pyramid, fine-grained sample.
(c) well-developed pyramid, coarse-grained sample.
(d) inverted pyramid with pitted surface, fine-grained sample.

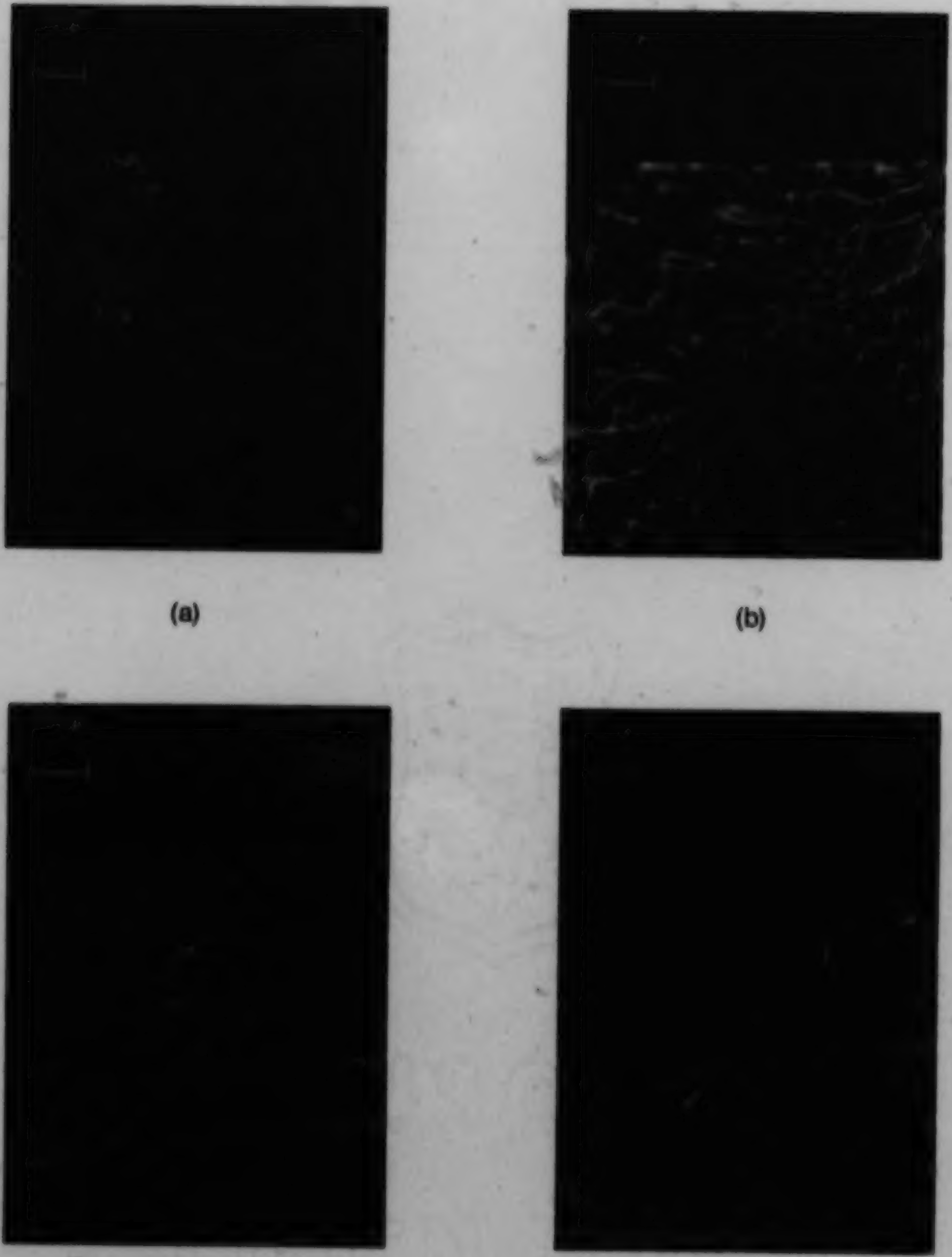

(a)

(b)

(c)

(d)

Figure 3.2 : Solution pitting in the McMurray Formation.
(a) pitted grain surface, fine-grained sample.
(b) close-up of pitted surface, coarse-grained sample.
(c) field of oriented pits, fine-grained sample.
(d) pitted grain surface, medium-grained sample.

Figure 3.3 : Long and concavo-convex grain contacts in the McMurray Formation, fine-grained sample.

Figure 3.4 : Stereo pairs of grain fabric, fine-grained McMurray Formation.

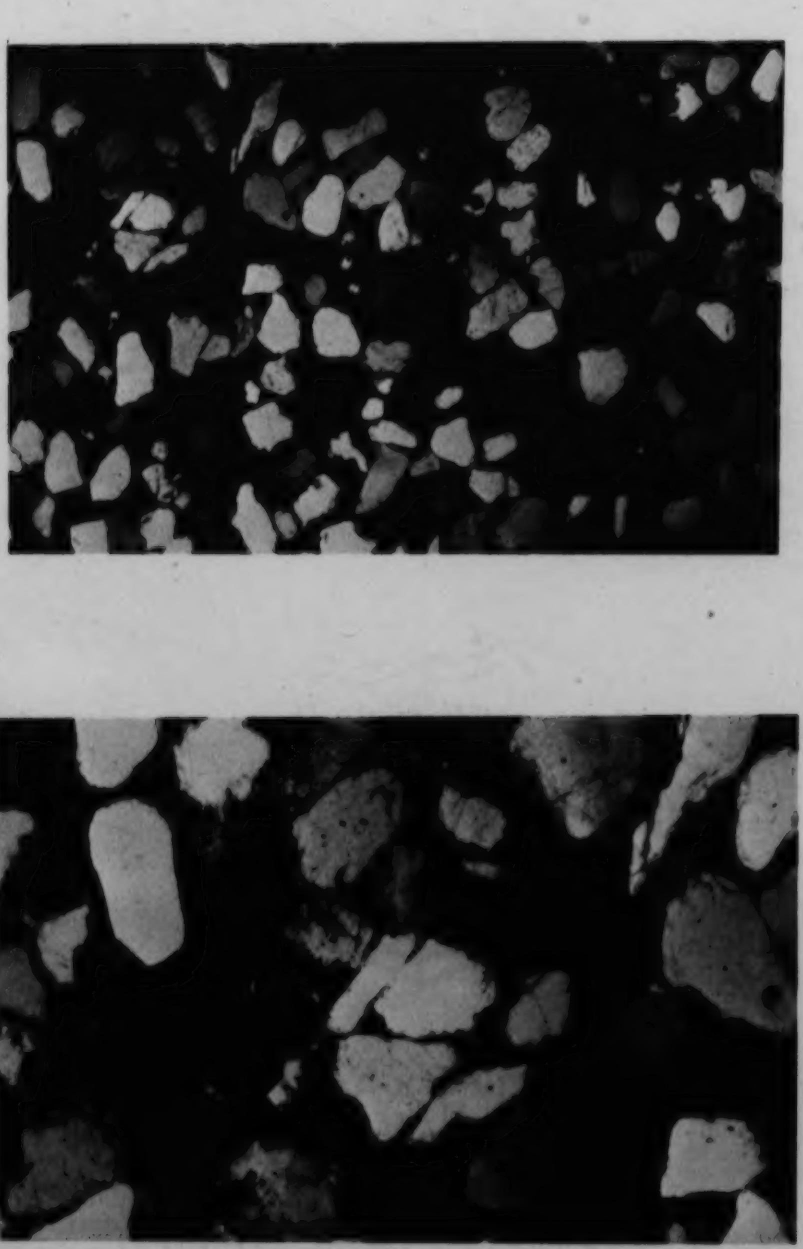

Figure 3.5: Optical micrographs of the McMurray Formation.
Top : fine-grained sample, x 10.
Bottom : fine-grained sample, x 25.

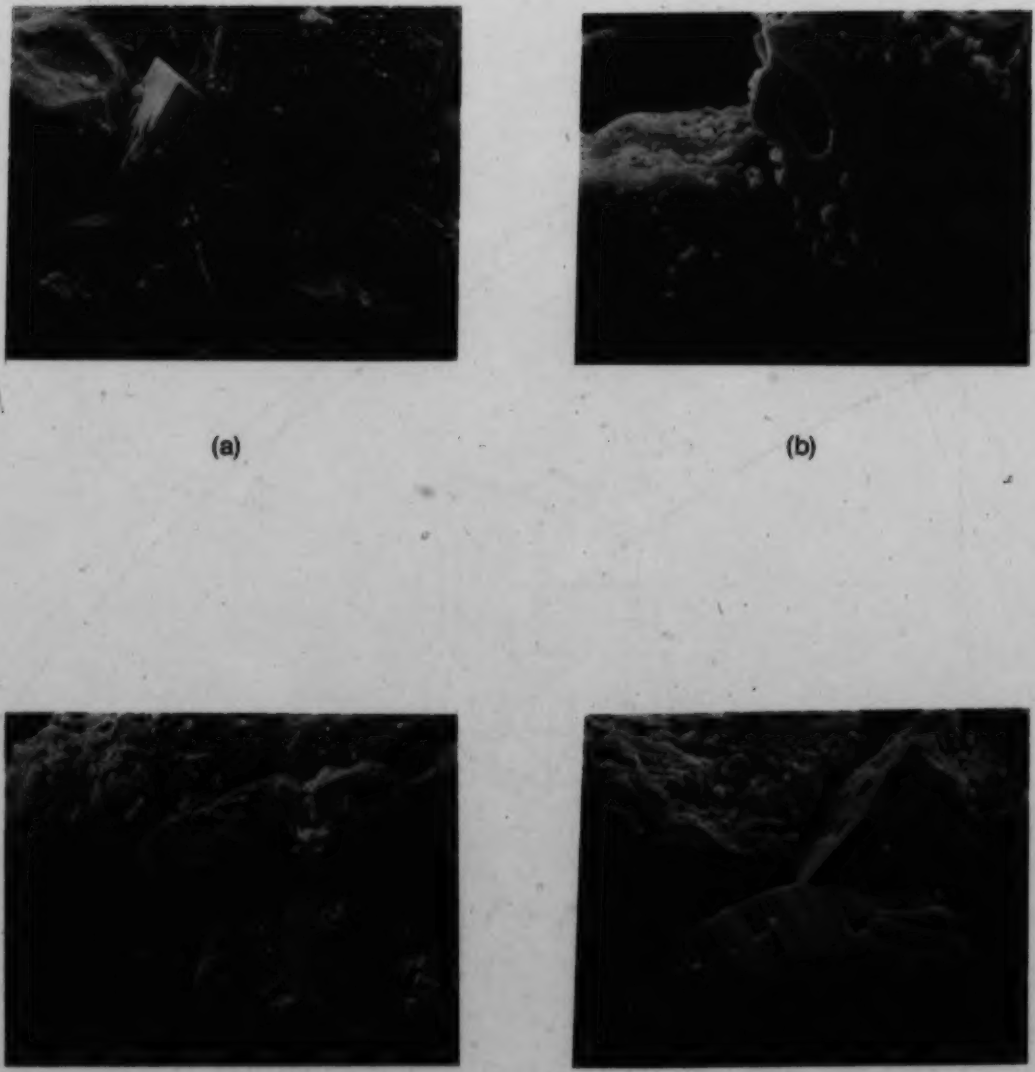

(a) (b)

(c) (d)

Figure 3.6 : Overgrowth features in Grand Rapids Formation A.
(a) feldspar overgrowth.
(b) quartz overgrowth.
(c) grain modified by solution and overgrowth.
(d) overlapping of crystal overgrowths.

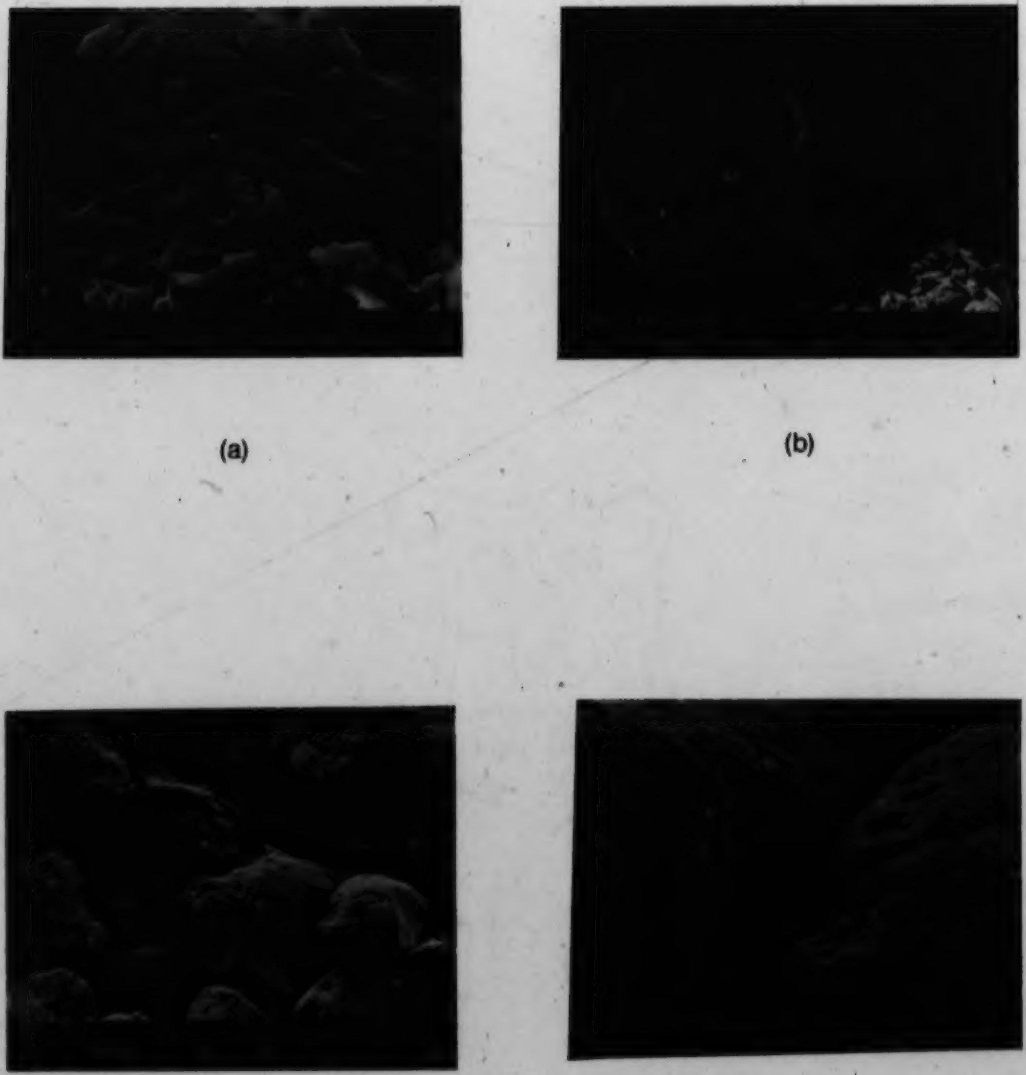

(a)

(b)

(c)

(d)

Figure 3.7 : Grain features in Grand Rapids Formation A.
(a) small overgrowth crystals.
(b) pitted grain surface.
(c) interpenetrative grain contact resulting from solution.
(d) close-up of contact shown in (c).

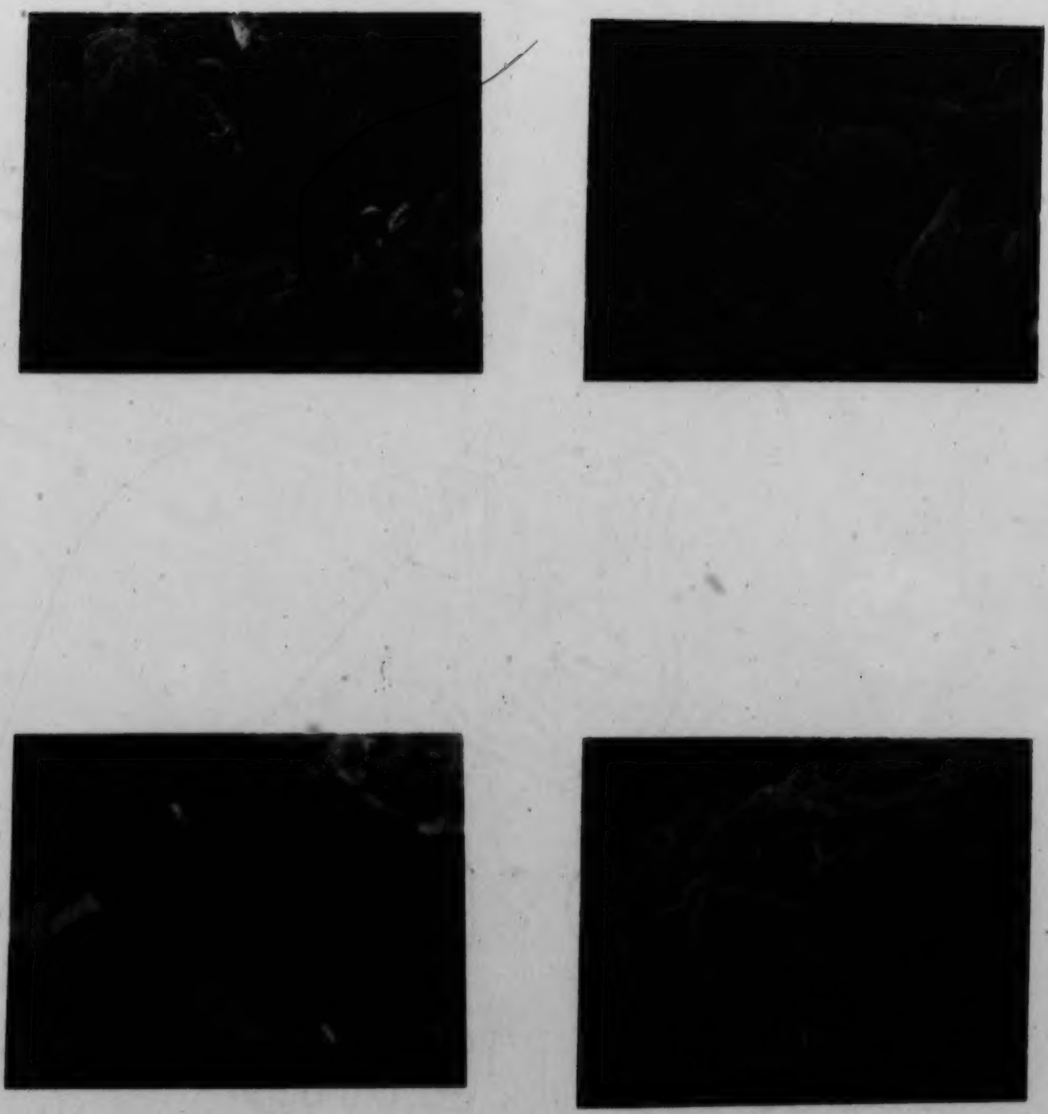

Figure 3.8 : Long and concavo-convex grain contacts in Grand Rapids Formation C; note clay covering on grain surfaces.

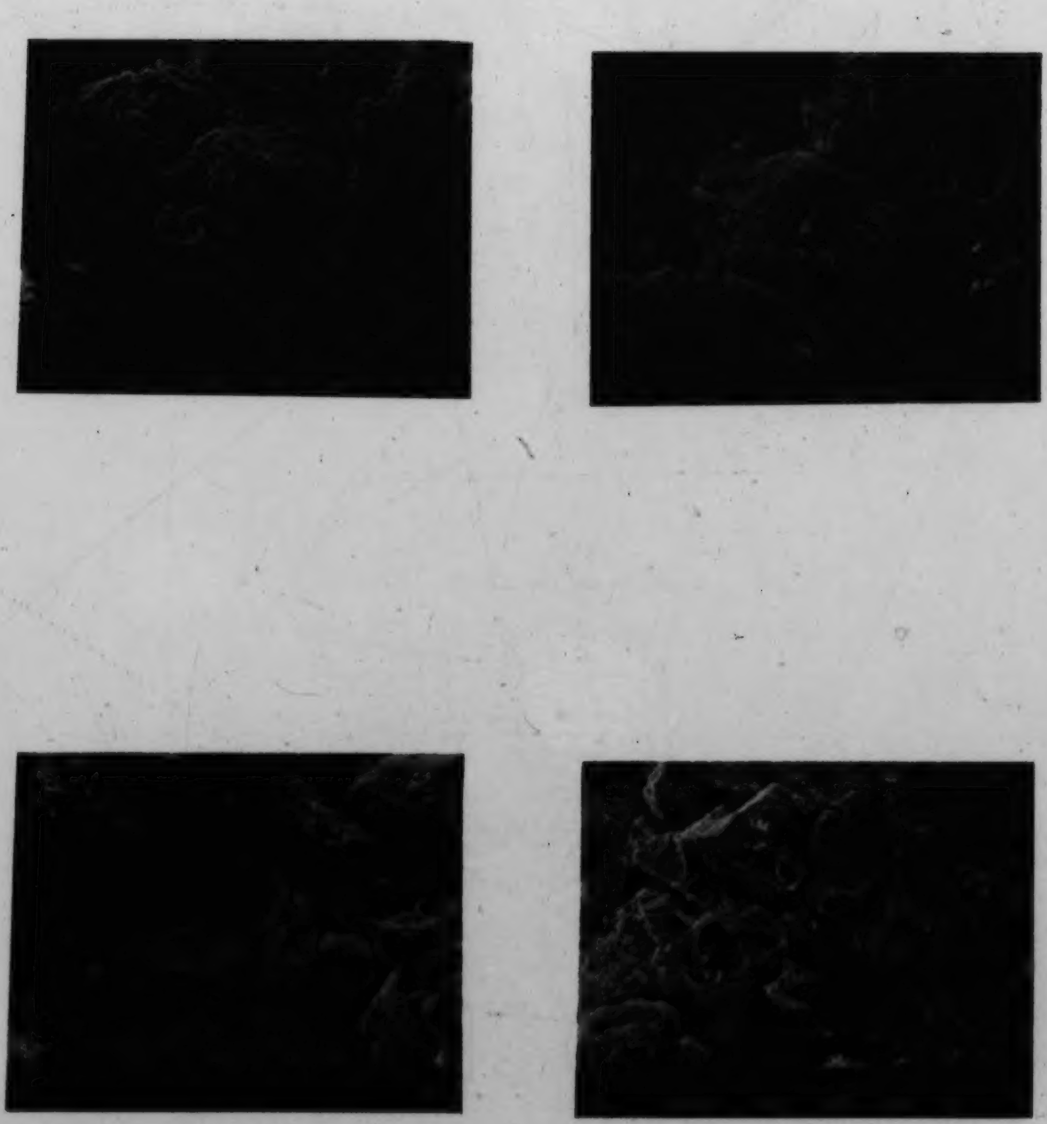

Figure 3.9 : Closely-packed diagenetic structure in Grand Rapids Formation C ; note clay covering on grain surfaces.

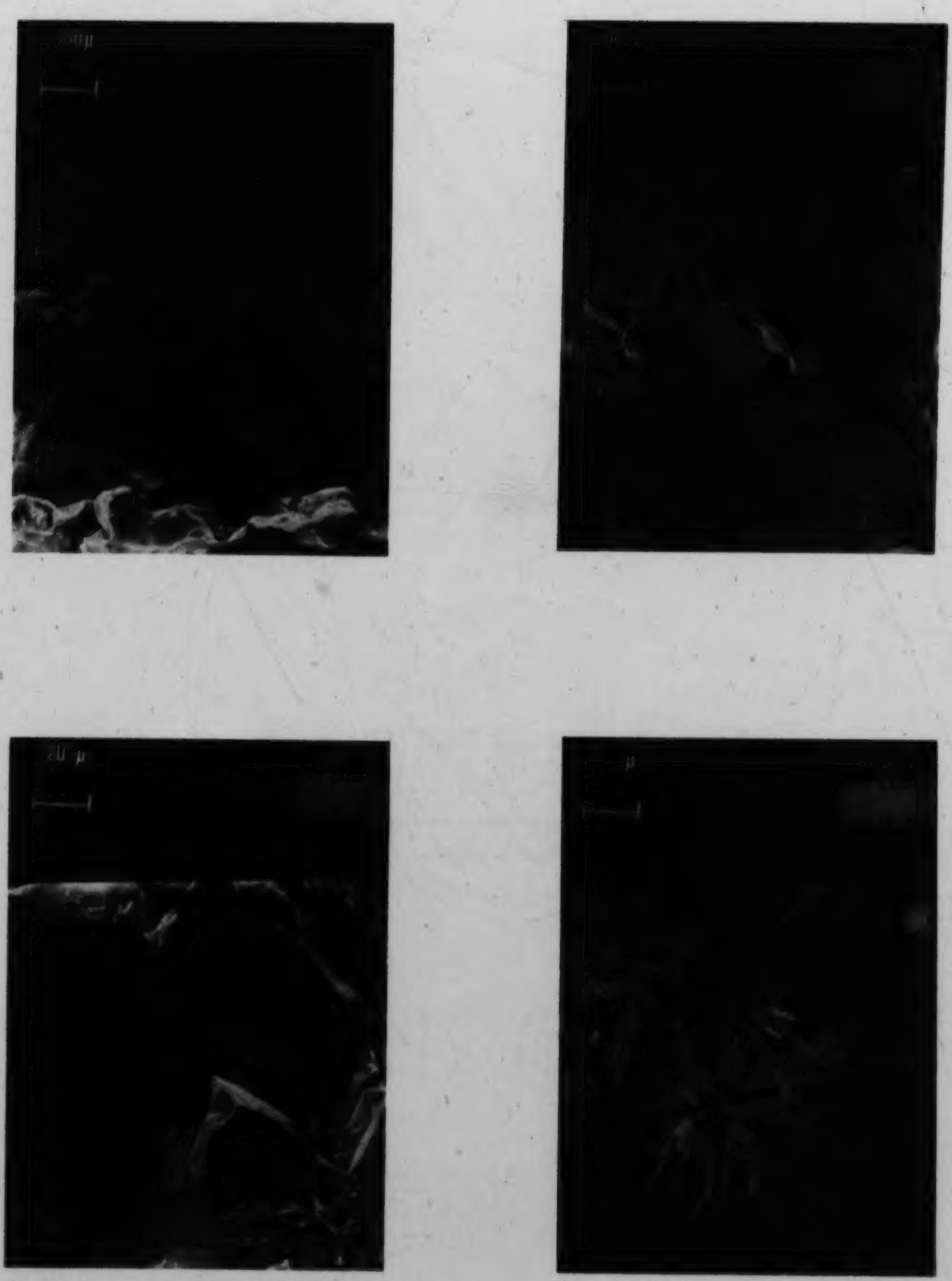

Figure 3.10 : Photomicrographs of Indian itacolumite showing extensive grain interlock and crystal overgrowth; tubular mineral on grain surfaces is kaolinite.

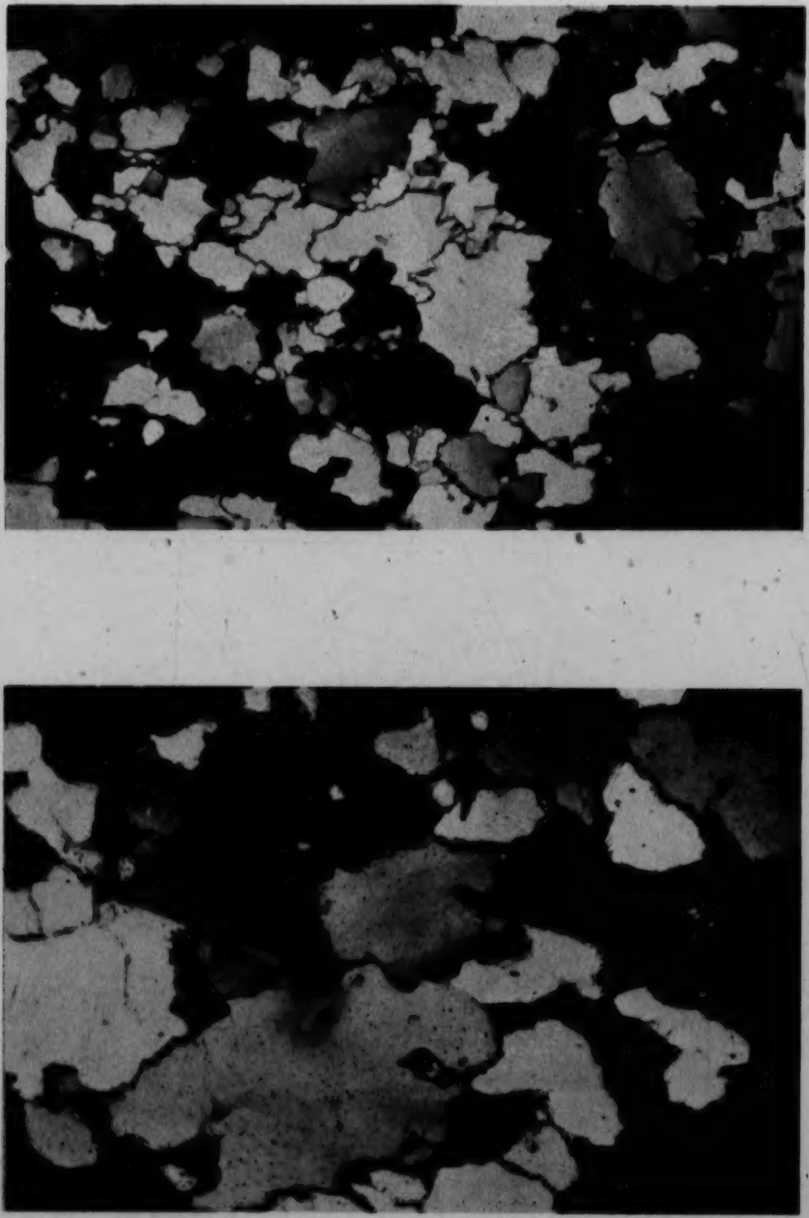

Figure 3.11 : Optical micrographs of Indian itacolumite showing interlocking grain structure.
Top : x 10.
Bottom : x 25.

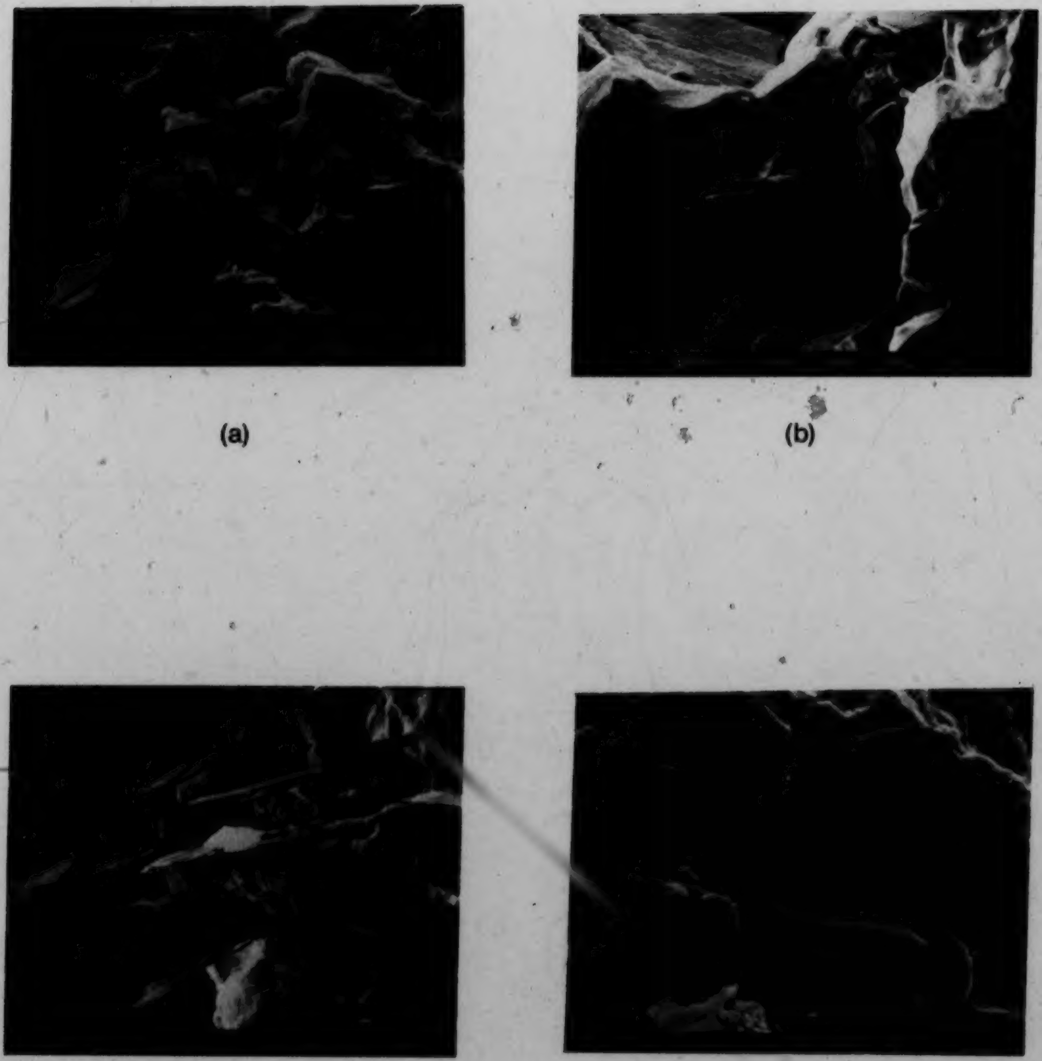

(a) (b)

(c) (d)

Figure 3.12 : Interlocking grain structure of micaceous itacolumite from the United States, sample 1.
(a) x – axis; perpendicular to mica planes.
(b) y – axis; perpendicular to mica planes.
(c) y – axis; perpendicular to mica planes.
(d) z – axis; facing on mica planes.

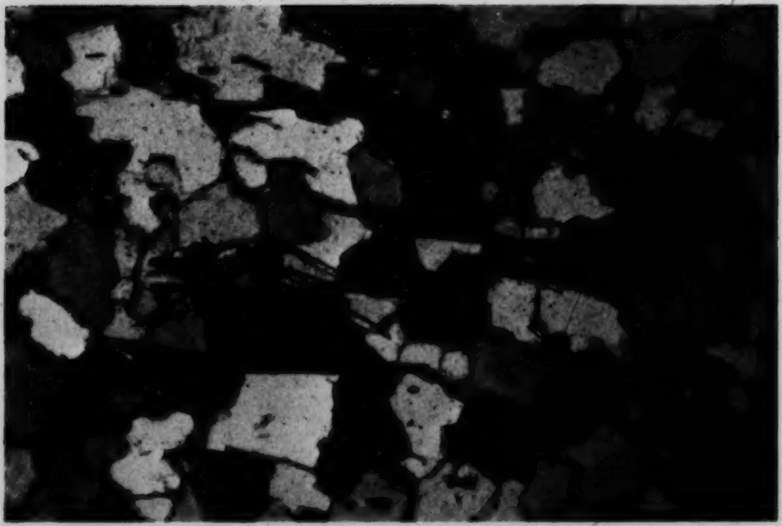

Figure 3.13 : Optical micrographs of micaceous itacolumite from the United States, sample 1.
Top : x – axis, × 25.
Bottom : z – axis, × 10.

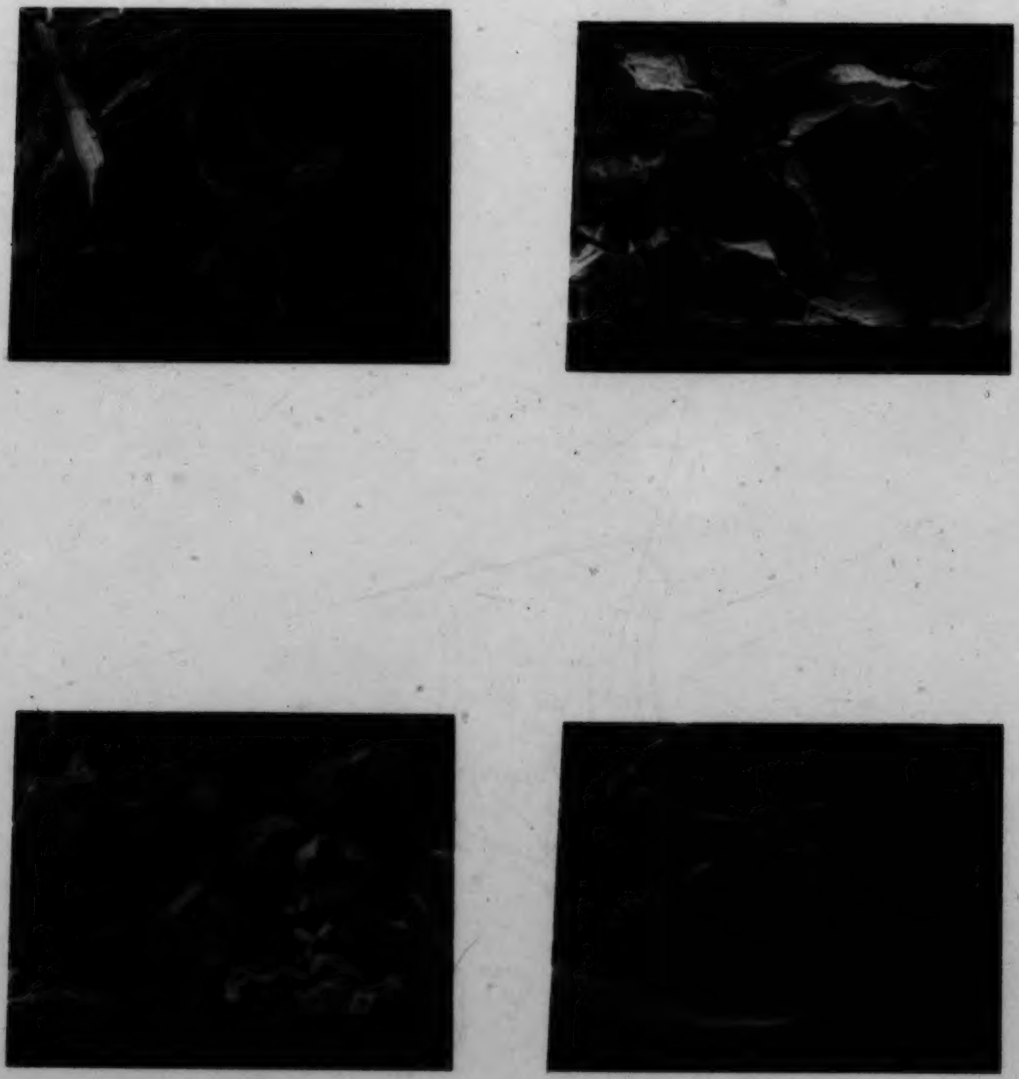

Figure 3.14 : Closely interlocking structure of micaceous itacolumite from the United States, sample 2, less flexible material than sample 1.

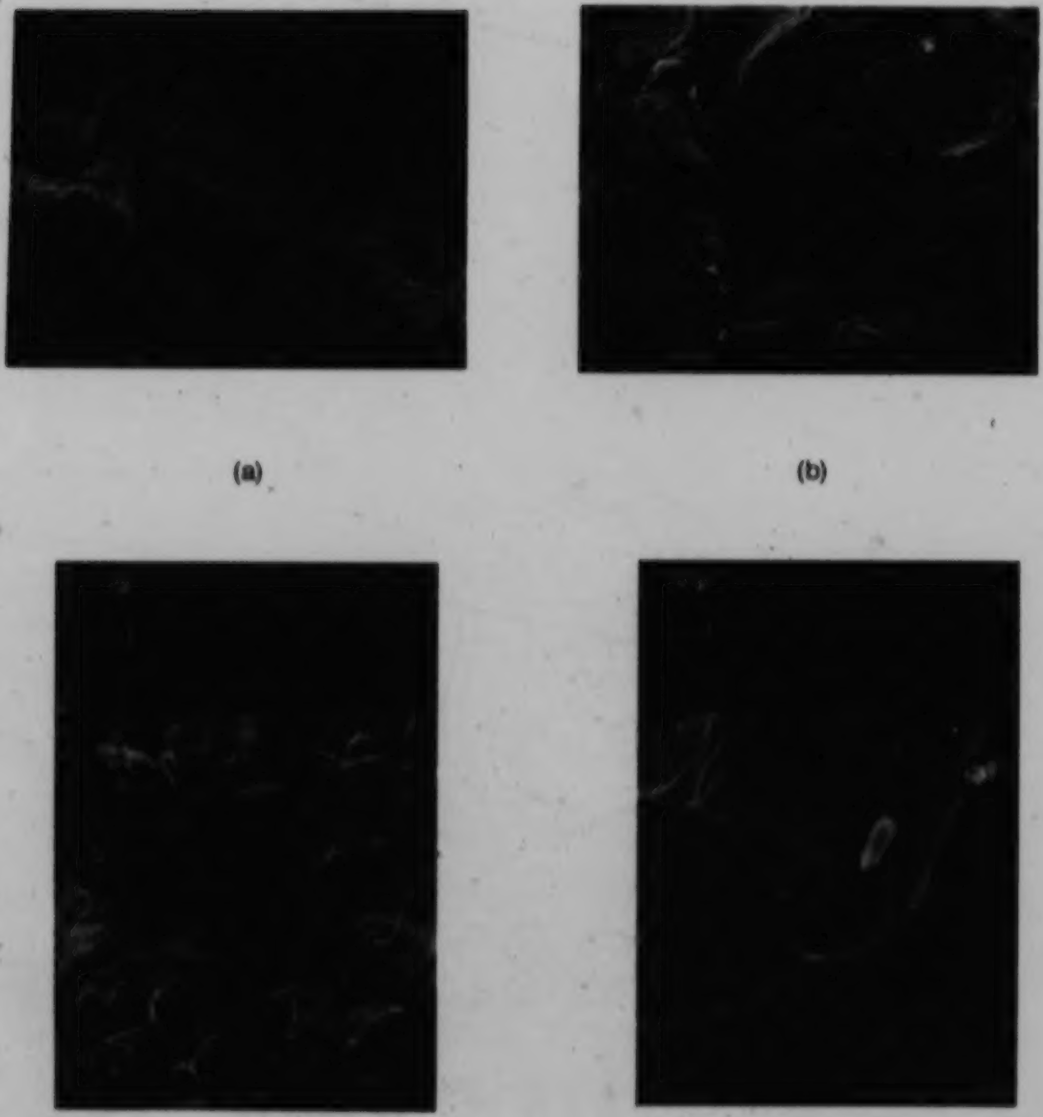

(a) (b)

(c) (d)

Figure 3.15 : (a) Cemented sandstone from Colorado.
(b) Cemented sandstone from Colorado.
(c) Talus fragment of McMurray Formation.
(d) Talus fragment of McMurray Formation.

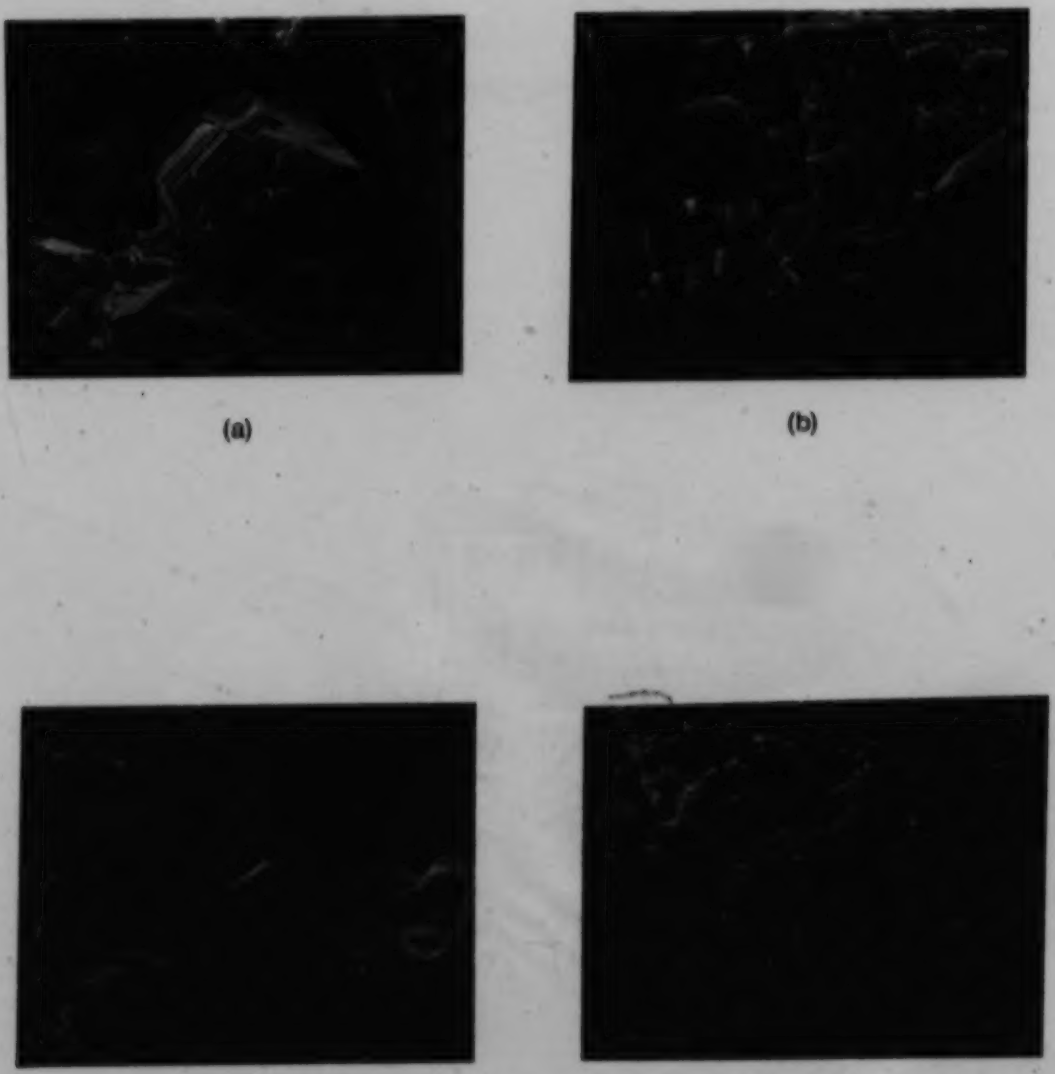

(a)

(b)

(c)

(d)

Figure 3.16 : (a) Bituminous sandstone from California.
(b) Bituminous sandstone from California
(c) Bituminous sandstone from California.
(d) Bituminous sandstone from Utah.

Figure 3.17 : Dense post-glacial sand from Fort McMurray area.

4. STRENGTH OF GRANULAR AND INTERLOCKING MATERIALS

4.1 Introduction

The behaviour of granular materials during shear has been the subject of extensive research. This chapter discusses some of the experimental work which has been performed on granular and interlocking materials. Several of the strength models which have been proposed will be reviewed, and strength analysis of oil sands will be discussed. A comparison will be made between the shear behaviour of dense, cemented, and locked sands.

4.2 Strength Investigations

The traditional soil mechanics interpretation of the strength of granular materials is a linear Mohr-Coulomb failure envelope. The slight curvature present in experimentally-determined envelopes is generally ignored as being unimportant, and the angle of shearing resistance is approximated as constant with variation in normal stress. Investigations have shown, however, that even in conventional loose and dense sands a change in normal stress does affect the angle of shearing resistance.

A series of triaxial tests were performed by Vesic and Clough (1968) on loose and dense samples of a medium-grained uniform quartz sand. The results show a slight curvature in the Mohr envelope in the normal stress range up to approximately 100 kg/cm². At very low stresses, grain crushing is minimal and dilatency effects dominate the material strength. As the normal stress increases, grain crushing increases until the "breakdown" stress is reached (the point at which all effects of initial void ratio are eliminated). Beyond this stress level the angle of shearing resistance is constant and equal to the angle of interparticle friction.

For granular materials with tangential grain contacts, the linear approximation for the failure criterion is adequate for most purposes. However, in oil sand materials and other locked sands, the interlocking of the grains causes a greater curvature of the failure envelope, and this must be taken into consideration. Drawing a straight-line envelope through a series of oil sand test data points would indicate that the material possesses a cohesive strength at zero normal stress, which is in fact not the case.

Barton (1974) has studied the structure of sandstones of the Eocene strata in England. Only 90 percent of the in-situ density of these materials can be recovered by compacting a disturbed sample, indicating that some diagenetic alteration has taken place. The material possesses some cohesion, and will stand with a vertical face. Barton postulates that the source of the cohesion is clay mineral bridges between the particles, as revealed by scanning electron microscopy. Test results show that the unconfined compressive strength of the sandstone decreases rapidly with moisture contents greater than one percent.

This is attributed to swelling of the clay mineral bridges. A series of multi-stage triaxial tests were conducted, and the results were interpreted as a linear Mohr envelope. The shear stress versus normal stress relationship is not given, but it seems likely that the interlocking nature of the material as evidenced by the scanning electron micrographs would cause some envelope curvature.

A more complete study of an interlocking granular material was undertaken by Rosengren and Jaeger (1968). Samples of coarse-grained marble were heated to 600°C, causing separation of the grains along the boundaries. The material resulting from this procedure had an interlocking granular structure and a porosity of approximately four percent. A series of triaxial compression tests were conducted on this material, and the resulting Mohr envelope is shown in Figure 4.1. The results indicate high friction angles at low normal stress, and a decrease in secant angle of shearing resistance which reflects a gradual suppression of dilatency with increasing normal stress. This behaviour is very similar to that of oil sand materials, but over a larger range of normal stress.

A model study of an interlocking aggregate was undertaken by Milligan (1976). Glass beads were placed in a direct shear box, and dissolution of the beads at contact points was effected by the use of a hydrofluoric acid solution. The result of this process was a set of shear specimens of an interlocking aggregate. The direct shear test results show a definite curvature in the Mohr envelope, and a definite increase in strength above that obtained for undissolved beads. This strength increase resulted from the creation of interlocking grain contacts, which were in turn caused by the dissolution process.

Extensive strength testing of oil sands has been performed by Dusseault (1977). Samples of McMurray Formation oil sand were obtained in such a manner as to minimize disturbance due to exsolution of gas from the pore fluid (freezing of samples immediately after coring). The results indicate that the Mohr-Coulomb envelope is curved and the strength is increased to a value substantially higher than that of a conventional dense sand, even though the samples did undergo some disturbance.

4.3 Analysis of Strength Properties

A number of different strength criteria have been proposed for rocks and granular materials. The criteria discussed below are based on either experimental data, empirical laws, energy relationships, or curve-fitting techniques.

One attempt to quantify the effects of dilatency on strength characteristics is the bimodal failure criterion for interlocking discontinuities in rock developed by Patton (1966). Patton's experiments were conducted on artificial rock specimens which were fabricated to set dimensions and tested in a direct shear apparatus. He found that at low normal stresses the total angle of shearing resistance was equal to the angle of frictional sliding resistance plus the angle of the asperities (Figure 4.2). At a certain normal stress level, the internal cohesive strength of the discontinuities becomes equal to the strength due to sliding resistance, and at this point shearing of the asperities takes place. The angle of shearing resistance is then reduced to approximately the residual value.

Since Patton's experiments were performed on very uniform samples it was possible to approximate the envelope by two straight lines, and to identify the breakdown stress at which shearing of asperities takes place. The actual failure envelope for a rock mass with irregular discontinuities or for an interlocking granular material is curved, and crushing takes place over a range of normal stress values. Thus the mode of failure is gradually changing from dilatency to crushing with increasing normal stress.

Other failure criteria have been developed for rock masses on the basis of energy considerations. One of these was developed by Ladanyi and Archambault (1969), who defined the shearing resistance as the sum of four components, due respectively to external work done in dilating against the external force, additional internal work in friction due to dilatency, work done in internal friction if the sample does not change volume in shear, and energy dissipation due to shear across irregularities. These components are defined in terms of the frictional shearing resistance angle, the dilative rate at failure, and the area across which shear of asperities takes place. Although this model aids the understanding of the process of shear, it is of little practical value for actual analysis, as the parameters needed are difficult to evaluate.

Hoek and Brown (1980) have proposed an empirical relationship between the principal stresses at failure in a rock mass as follows(Figure 4.3):

$$\sigma_1 = \sigma_3 + \sqrt{m\sigma_c\sigma_3 + s\sigma_c^2}$$

where σ_1 is the major principal stress at failure, σ_3 is the minor principal stress at failure, σ_c is the uniaixial compressive strength of the intact rock, and m and s are constants which depend on rock properties and on the extent to which the rock is broken up before being subjected to the principal stresses. If the constant s is equal to unity, the rock is intact; if s is equal to zero, the rock is completely broken up.

A curve-fitting technique for modeling the strength of oil sands has been proposed by Dusseault (1977). The curve-fit relationship is of the following form:

$$\tau_p = a\sigma_n^b$$

where τ_p is the peak shear stress, σ_n is the normal stress, and a and b are constants to be evaluated by curve fitting. The value of the constants a and b will be dependent on the units used for stress.

The component of strength above the residual value can be divided into a portion due to dilatency and due to shear of grains by taking a tangent to the curve at a given normal stress (Figure 4.4). The value τ_t which is obtained is an apparent cohesion intercept due to the interlocking fabric of the grains. From this analysis, it can be seen that the dilatency component is suppressed and the fabric cohesion component dominates with increasing normal stress. This topic will be discussed further in Chapter 5

4.4 Strength Analysis of Oil Sands

When sheared at low normal stress, dense and locked sands exhibit a strain-weakening peak-to-residual behaviour. The closely-packed or interlocked structure causes the soil skeleton to push apart during shear. The energy required to shear the soil is thus the sum of a frictional and a dilatent component. As normal stress increases, the dilatency of the soil structure is suppressed, and shearing of grains takes place.

Figure 4.5 is a comparison of the Mohr-Coulomb envelopes for several different types of granular materials. The failure envelope for a dense sand with largely tangential grain contacts will be very close to linear, with only a slight curvature.

The long and concavo-convex grain contacts present in a locked sand will cause a substantial curvature of the Mohr-Coulomb envelope. The increase in strength above that of a dense sand will be related to the degree of diagenetic alteration. The secant angle of shearing resistance will be high at low normal stress. As normal stress increases the effects of the structure will be suppressed. According to Vesic and Clough (1968) there will be a certain stress level above which the shear behaviour is independent of the initial soil structure.

The failure criterion for jointed rock masses developed by Patton (1966) is also shown in Figure 4.5. This criterion clearly delineates the transition point between the dilatent and crushing failure modes.

The envelope shown in Figure 4.5 for locked sands is typical of oil sands as these materials possess zero cohesion at zero normal stress. This is due to the lack of chemical cementing agents and the fact that the grains are only slightly interlocked. For itacolumites such as the ones discussed in Chapter 3 the envelope would show a high cohesion value at zero normal stress. This results from fabric interlock rather than chemical cementation.

The Mohr-Coulomb envelope for a chemically cemented sandstone is shown in Figure 4.5. The cohesion intercept in this material results from actual physical bonding between the grains.

4.5 Summary

The behaviour of locked sands during shear is different from that of either dense or cemented sands. Diagenetic alteration creates a curvature of the Mohr-Coulomb failure envelope, and the strength increase will be related to the degree of fabric alteration.

Locked sands are characterized by a lack of cementitious cohesion. The interlocking grain fabric is responsible for the high angles of shearing resistance encountered at low normal stress values.

The energy-based failure criteria discussed above are not practically applicable to design problems in oil sands as the parameters needed for analysis are difficult to evaluate. The use of a curve-fitting technique on actual test data may be the approach which is most amenable to analysis.

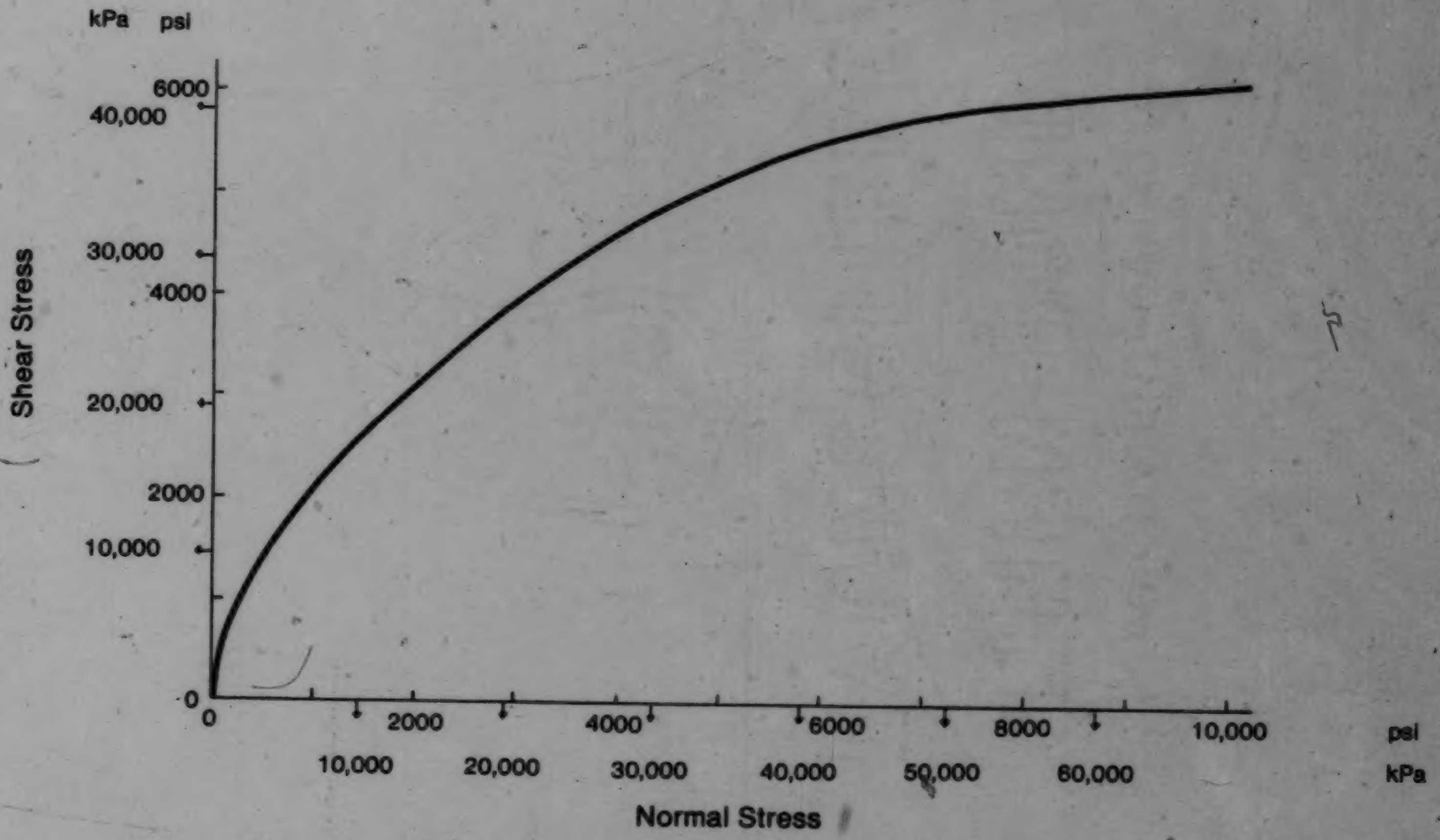

Figure 4.1 : Mohr envelope for granulated marble
(after Rosengren and Jaeger, 1968).

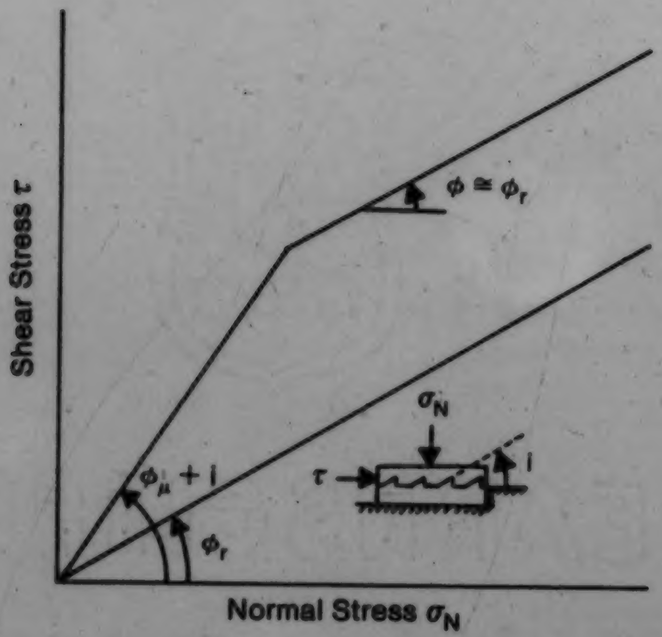
Shear Stress τ
$\phi \cong \phi_r$
σ_N
τ
i
$\phi_\mu + i$
ϕ_r
Normal Stress σ_N

ϕ_μ = angle of frictional sliding resistance
ϕ_r = residual angle of friction
i = angle of inclination of asperities

Figure 4.2 : Bimodal failure criterion
(after Patton, 1966).

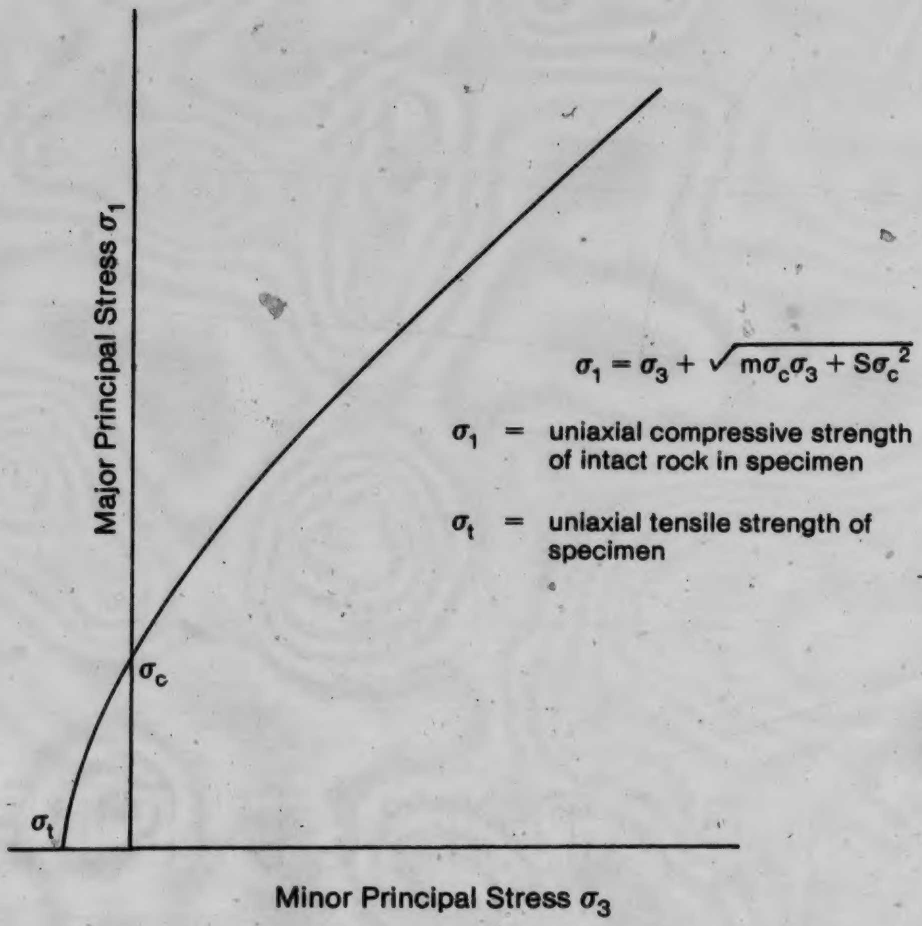

$$\sigma_1 = \sigma_3 + \sqrt{m\sigma_c\sigma_3 + S\sigma_c^2}$$

σ_1 = uniaxial compressive strength of intact rock in specimen

σ_t = uniaxial tensile strength of specimen

Figure 4.3 : Empirical relationship between principal stresses at failure in a rock mass (after Hoek and Brown, 1980).

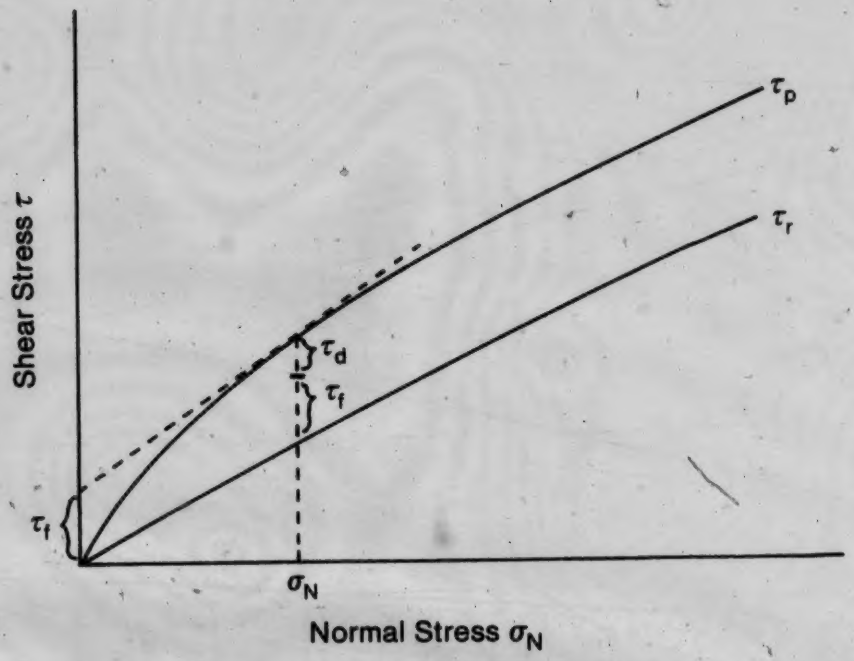

τ_p = peak shear stress
= $a\sigma_N{}^b$
τ_f = component due to shear of grains
= $(1-b)\, a\sigma_N{}^b$
τ_d = component due to dilatency
= $ab\sigma_N{}^b - \tau_r$
τ_r = residual shear stress
= $d\sigma_N{}^e$
τ_p = $\tau_f + \tau_d + \tau_r$

Figure 4.4 : Curve-fitting technique for strength of oil sands (after Dusseault, 1977).

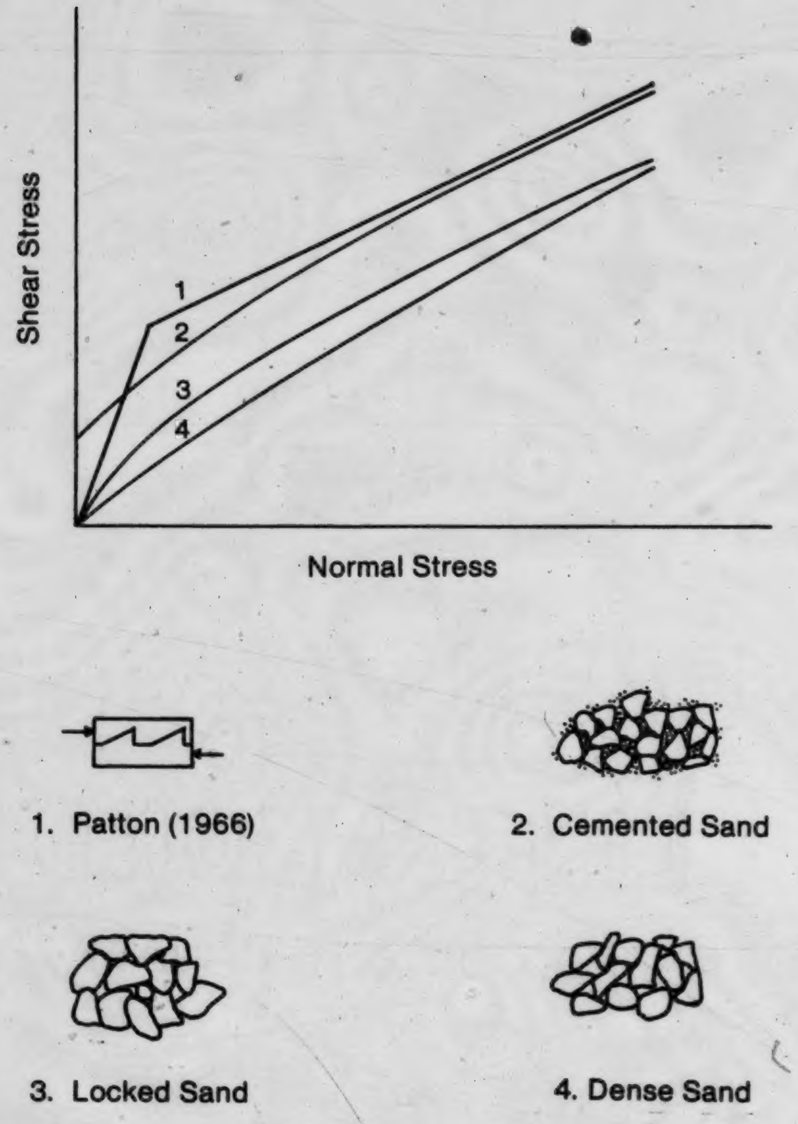

Figure 4.5 : Comparison of Mohr-Coulomb envelopes for dense, locked, and cemented sands.

5. EXPERIMENTAL INVESTIGATION

5.1 Introduction

A laboratory testing program was performed on samples of oil-free McMurray and Grand Rapids Formations. Index data were collected to aid in examination of the grain fabric of oil sands. The compressibility of the materials was measured by oedometer testing, and direct shear tests were conducted to evaluate strength and dilatency characteristics.

The results of these tests are examined in the context of diagenetic alteration and its influence on sandstone fabric. Some of the practical implications of this behaviour for open-pit mining and *in situ* production are discussed.

5.2 Testing Program

5.2.1 Materials Tested

Five main sample groups of oil-free materials were examined in the testing program: fine-, medium-, and coarse-grained McMurray Formation, and Grand Rapids Formation A and C. The sampling locations and geological origin of these specimens are discussed in Chapter 3. These samples were also used for microscope examination.

As discussed above, all specimens were obtained from river valley outcrops in the Fort McMurray area. The use of oil-free materials eliminated the problems of sample disturbance caused by exsolution of gas from the interstitial bitumen.

The behaviour of oil-free samples may not be identical with that of oil-rich material; however, the behavioural characterisitics during shear may very well be similar. Any effects of interstitial bitumen on material behaviour can only be evaluated when high-quality oil-rich specimens are obtained. The data collected for oil-free samples will provide a valuable comparison should such specimens become available.

5.2.2 Index Tests

A number of standard index tests were conducted on the five main sample groups: grain size distribution, density (porosity), water content, and density index (relative density).

The grain size of the materials was evaluated by washing the samples through the number 200 U.S. sieve (0.074 mm. diameter). The samples were then oven-dried and a sieve analysis was performed to determine the grain size distribution. The analysis was conducted on the original samples as well as on the direct shear test samples after shearing. The latter tests were performed to evaluate grain crushing during shear.

The density of the materials was determined by immersing a small intact block of each material in hot wax and subsequently measuring the volume by mercury displacement. The porosity, void ratio, and saturated density of the materials were then calculated.

Density index tests were performed to compare the *in situ* density with the density which can be achieved by compaction. The minimum density of the samples was measured by pouring the dry material through a funnel into a standard Proctor mold. The maximum density was determined by vibratory compaction of the dry material. The density index was calculated as follows:

$$I_D = \frac{e_{max} - e}{e_{max} - e_{min}}$$

where e_{max} is the maximum void ratio, e_{min} is the minimum void ratio, and e is the *in situ* void ratio.

5.2.3 Oedometer Tests

Oedometer tests were conducted on the five sample types to determine the compressibility of the materials. The testing apparatus consisted of a dead loading frame with a lever arm. The load placed on the sample by the weight of the loading frame was approximately 3 MPa. Because this load was seated before measurement of vertical displacement could begin, the exact void ratio under the initial load could not be measured. The modulus of compressibility a_v was detemined by finding the slope of the void ratio-stress curve. The coefficient of compressibility m_v could not be calculated as the initial void ratio was not known exactly.

5.2.4 Direct Shear Tests

Strength tests were conducted in a standard direct shear testing frame. The tests were conducted over a normal stress range of 50 to 5000 kPa (7 to 725 psi). Measurements of shear stress, horizontal displacement, and vertical displacement were recorded during each test. Plots of shear stress versus horizontal displacement were used to examine the shear behaviour before and after peak shear stress. The vertical displacement was used as a measure of the dilatency of the soil structure during shear.

Residual strength tests were conducted on the samples of Grand Rapids Formation A and C, and on the samples of McMurray Formation above a normal stress of 2000 kPa.

Plots of shear stress versus normal stress were constructed for each set of shear specimens to examine the change in shear behaviour which takes place with increasing normal stress. Plots of dilatency rate at failure versus normal stress were used to demonstrate the suppression of dilatency with increasing normal stress. The dilatency rate at failure was calculated as the volume change of the sample divided by the horizontal displacement.

5.3 Experimental Results

5.3.1 Index Data

5.3.1.1 Grain Size Data

The grain size distribution curves for all five main sample groups are presented in Figure 5.1. The only material which contains a significant amount of clay-size particles is the Grand Rapids Formation C. As discussed above, this fine material is in the form of montmorillonitic clay coatings on the grain surfaces. The influence of this clay on the compressibility of the material is discussed below.

Table 5.1 is a summary of the grain size data for the materials. The values of coefficient of uniformity for fine- and medium-grained McMurray Formation and Grand Rapids Formation A (c_u less than two) indicate that these materials are extremely uniform. The coefficient of uniformity of the Grand Rapids Formation C material is slightly higher than that of the above materials. This higher value results from the presence of approximately ten percent clay, and the sand portion of the material is quite uniform. The coarse-grained McMurray Formation is the only material which is well-graded, having a coefficient of uniformity of 5.93.

The three samples of McMurray Formation have median grain diameters of 0.200, 0.430, and 0.620 mm, whereas the samples of Grand Rapids Formation A and C have median grain diameters of 0.100 and 0.230 mm respectively. The use of this variety of materials will aid in delineating the influence of mineralogy, grain size, and gradation on the strength of the material.

The extent of grain crushing during shear was evaluated by grain size analysis of the direct shear samples after shearing. Table 5.2 contains grain size data for sheared samples of Grand Rapids Formation over a range of normal stress levels. Although residual tests were conducted on the Grand Rapids Formation samples at higher stress levels, the results presented in Table 5.2 are the only ones which are comparable, as the same number of residual cycles were conducted for each. The table shows a significant increase in the percentage of material washed through the number 200 sieve, indicating that grain crushing has occurred. No significant change was observed in the samples of McMurray Formation.

The grain crushing in the Grand Rapids Formation results from the presence of feldspar grains, which have cleavage planes and are therefore weaker than quartz grains. Little change was observed in the McMurray Formation as it is almost totally quartzose. Quartz has no significant plane of weakness along which preferential cleavage can take place.

The crushing of grains during shear will influence the observed residual behaviour of the materials. This topic is discussed below.

5.3.1.2 Density and Water Content Tests Results

The results of density and water content analyses are presented in Table 5.3. The saturated density of each material was calculated so that there is a direct comparison with results of geophysical logs and bitumen-saturated samples. The density results are presented as an average saturated density value with a measurement error. The porosity of each of the materials was also calculated. The density values obtained range from 2.06 to 2.27 g/cm³. These results show an increase in density above that of a dense sand (usually less than 2.0 g/cm³). This high density has resulted from diagenetic alteration.

The density of the coarse-grained McMurray Formation was found to be 2.27 g/cm³. This high density results from the presence of large grains and the relatively well-graded nature of the material. Of the samples of McMurray Formation, the fine-grained material appears to have been affected the most by diagenesis. It is a very uniform material with a density of 2.11 g/cm³.

If the assumption is made that approximately the same environmental forces (stress, temperature, pH, rate of fluid flow) were operative in the three sampling locations of the McMurray Formation, then approximately the same magnitude of grain interpenetration would have taken place in each location. This assumption is fairly logical, as the sampling locations were within 35 m of each other. A given amount of grain interpenetration would have a much more significant effect (greater porosity reduction) on the fine-grained material than on the coarse-grained material, as the ratio of grain interpenetration to grain diameter is much higher. In the same manner, if the rate of influx of pore fluid was approximately the same in each location, the fine-grained material would undergo faster overgrowth development (Heald and Renton, 1966), as the relative surface area available for overgrowth nucleation is larger in a fine-grained material. Thus it is logical that for the fine- and medium-grained McMurray Formation, which are both of a similar uniform gradation, the fine-grained material should have undergone more significant alteration. The influence of this factor on shear strength is discussed below.

The water content test results presented in Table 5.3 are an average of measurements taken on the direct shear sample trimmings. The water content of the McMurray Formation and the Grand Rapids Formation A materials was found to be very low, ranging from one to six percent. The water content of the Grand Rapids Formation C is higher, ranging from 13 to 20 percent. This increased value results from the presence of water in the clay coating on the grains. As discussed above, the clay layer appears to have enhanced pressure solution by holding water within the contact areas and allowing easier diffusion of dissolved material into free pore space. The materials have been saturated for most of their history, so pressure solution would probably have taken place without the clay, but its presence would enhance the solution process.

5.3.1.3 Density Index Test Results

The results from the density index tests are presented in Table 5.4. The density index values are all greater than 100 percent, indicating that the materials cannot be recompacted without grain crushing to their *in situ* densities. The results indicate that the fine-grained McMurray Formation has been affected the most by diagenesis and the coarse-grained material the least. The Grand Rapids materials appear to have been substantially altered by diagenetic processes.

5.3.2 Oedometer Test Results

The results of the oedometer or one-dimensional consolidation tests performed on the five main test materials are presented in Table 5.5. For the samples of McMurray Formation and Grand Rapids Formation A, the first-cycle modulus of compressibility ranges from 0.80×10^{-6} to 2.15×10^{-6} kPa^{-1}. The compressibility for these materials stabilizes quickly over successive loading cycles to a value ranging from 0.17×10^{-6} to 0.52×10^{-6} kPa^{-1}. The medium- and coarse-grained samples of the McMurray Formation are slightly more compressible than the fine-grained material.

These results compare with a compressibility of 20×10^{-6} kPa^{-1} for a dense sand (Mitchell, 1976). The effect of diagenesis is to make the materials less compressible and more competent. The increased grain contact area and the densified structure result in a lower compressibility value. As the grain contacts are altered from tangential to long and concavo-convex, the compressibility of the material will decrease, as stresses are distributed over a larger area and grain crushing is decreased.

The first-cycle modulus of compressibility for the Grand Rapids Formation C is approximately 6.1×10^{-6} kPa^{-1}, which is higher than for the other materials. This increased value results from the compression of the thin montmorillonitic clay coatings during the initial loading cycle. In succeeding cycles, the effect of the clay content is eliminated by displacement of the clay, and the compressibility stabilizes to approximately the same value as for the other materials.

A typical void ratio versus stress curve is presented in Figure 5.2. This curve is the test result for a sample of fine-grained McMurray Formation. The first-cycle modulus of compressibility is approximately $0.7X10^{-6}$ kPa^{-1}, while for succeeding cycles the value quickly stabilizes at approximately $0.2X10^{-6}$ kPa^{-1}. This behaviour is typical of all materials tested. It is interesting to note that the test results plot as a straight line on a linear-axis plot over the stress range used in testing.

It is possible that the cyclic compressibility value may be more typical of the *in situ* compressibility value at depth than the first-cycle compressibility. The materials sampled have undergone stress relief and are slightly disturbed compared with material at depth. The overburden pressure in most areas of the oil sands deposits is much higher than the stress levels used in testing. It seems logical, therefore, that the cyclic compressibility would be more representative of the *in situ* material.

5.3.3 Direct Shear Test Results

Several example plots of shear stress vs. horizontal displacement and vertical displacement vs. horizontal displacement for the direct shear tests conducted are presented in Figures 5.3 through 5.6. Figure 5.3 shows the shear behaviour of fine-grained McMurray Formation at low normal stress. The shear stress drops off sharply after peak stress is reached. Associated with the high strength and strain-weakening behaviour is a high dilatency during shear. Figure 5.4 illustrates the shear behaviour of this material under high normal stress. The drop from peak to residual stress is less prominent, and the dilatency of the soil structure has been largely suppressed.

The shear behaviour of the Grand Rapids Formation A sand is illustrated in Figure 5.5 for a normal stress of 250 kPa. The material undergoes dilatency during shear, and the strain-weakening behaviour is prominent. With subsequent shearing cycles the stress quickly levels off to a constant residual or ultimate strength value. Figure 5.6 illustrates the shear behaviour of the Grand Rapids Formation A at a normal stress of 4000 kPa. The dilatency of the soil is suppressed, but the stress does not decrease to a residual value; rather it increases until peak stress is exceeded.

For samples of Grand Rapids Formation A and C tested at a normal stress of 2000 kPa and above, the ultimate shear strength was observed to increase with each successive shearing cycle. When the samples were removed from the shear box, the shear plane was observed to be noticably hardened. The presence of the weaker feldspar grains, which have cleavage planes, caused grain crushing to occur, the result being that with each cycle the shear plane densified and the stress increased. In some samples, where five or six residual cycles were conducted, the shear plane was observed after testing and found to be concave upwards. The hardening of the shear plane thus caused the material to shear along an alternative path, creating an expansion of the sheared zone. The residual strength test results for the Grand Rapids Formation A and C at high stress levels are thus upper bound estimates of the residual strength.

No difficulties were encountered in measuring the residual strength of the fine-grained McMurray Formation. However, for both the medium- and coarse-grained materials the stress was observed to increase sharply with successive cycles. This did not appear to result from grain crushing, as little change was observed in the grain size analysis after shearing. The problem was caused by the jamming of the large grains in the confined space between the two halves of the shear box.

The behaviour of locked sands during shear is characterized by a strain-weakening peak-to-residual behaviour and a high dilatency at low normal stress. At low normal stress, the energy required to push the soil skeleton apart is high, and consequently the shear strength is high. As normal stress is increased, grain crushing begins to occur and the dilatency of the structure is suppressed. This behaviour is characterized by a curvilinear Mohr-Coulomb envelope.

The measured shear stress in the direct shear tests was observed to increase to approximately half its peak value before any vertical displacement occurred. The horizontal displacement to this point (approximately 0.1 cm) is taken up by elastic compression of the grains.

The shear test results for the five main sample groups are presented in Figures 5.7 through 5.12. The peak strength curves plotted on the Mohr-Coulomb envelopes are linear log-log statistical best-fit curves of the form

$$\tau_p = a\sigma_N{}^b$$

as described in Chapter 4 (τ_p = peak shear stress in kPa; σ_N = normal stress in kPa). The values of the correlation parameters a and b are calculated based on units of kPa for stresses. Figure 5.7 is a comparison of the curve-fit relationships for all five materials.

Figure 5.8 shows the shear stress vs. normal stress relationship for fine-grained McMurray Formation. The residual test results are plotted, and an approximate residual envelope has been shown. This envelope does not result from curve-fitting; it is an approximate projection through the points.

Extensive strength testing of oil sands (Dusseault, 1977) has indicated that the residual envelope for the McMurray Formation approximates a straight line over a low range of normal stress (0 to 1000 kPa) and that the residual angle of shearing resistance is approximately 33°. These results are consistent; consequently no residual testing of the McMurray Formation at low stress levels was performed.

Figure 5.9 and 5.10 contain the Mohr-Coulomb envelopes for the samples of medium- and coarse-grained McMurray Formation respectively. As discussed above, the residual shearing resistance could not be properly measured, thus the residual test results for these materials are not plotted.

The peak and residual Mohr-Coulomb envelopes for Grand Rapids Formation A and C are shown in Figures 5.11 and 5.12. As indicated by the grain size analyses, grain crushing in these materials increased with increasing normal stress. For the samples of Grand Rapids Formation above a normal stress level of 2000 kPa, no credence is given to the residual measurements as the shear zone compacted and stress increased with each successive residual cycle. The residual envelopes shown are approximate projections through the data points and are not curve-fit relationships.

Each Mohr-Coulomb envelope shows the values of the correlation parameters a and b. Table 5.6 is a summary of the correlation parameters and correlation coefficients for all materials.

For each sample tested, the dilatency rate at failure was calculated as the volume change of the sample (as measured by vertical displacement) divided by the horizontal displacement. The dilatency rate was found to be a maximum at and immediately before peak shear stress, as indicated by the slope of the vertical displacement vs. horizontal displacement plot. Figure 5.13 is a plot of dilatency rate at failure vs. normal stress for the samples of coarse-grained McMurray Formation. This plot shows the suppression of dilatency by increasing normal stress. A similar plot was obtained for all sample groups.

5.4 Discussion and Analysis of Test Results

5.4.1 Factors Influencing Shear Strength

The strength of granular materials is governed by a number of different factors. These factors have been categorized as follows.

1. deposition of material: original density or packing
2. relating to mineralogy:
    a. internal strength of grains
    b. presence of relatively weaker grains
3. relating to grain size:
    a. grain size
    b. gradation
    c. grain shape
4. relating to diagenetic alteration:
    a. nature of interparticle contacts (tangential, long, concavo-convex, or sutured)
    b. microscopic nature of grain contacts
    c. density of the material (porosity)
    d. degree of porosity reduction caused by diagenetic processes

All these factors are interrelated in a complex manner. The points listed under one to three will determine, together with the environmental conditions of stress, temperature, and pore fluid flow, the extent to which diagenetic processes modify a sediment. Thus the influence of a specific factor on the strength of the material is difficult to determine.

Table 5.6 contains a summary of the correlation parameters for the shear stress vs. normal stress relationship for the five main test materials. The parameters a and b are plotted in Figure 5.14 against the median grain size of the samples. Although no quantitative conclusions can be drawn from this plot, the general trend shows that the b value decreases with increasing median grain size, and the a value increases with increasing median grain size. The mineralogy is also obviously influential. The quartz-feldspar Grand Rapids Formation has lower b values and higher a values than the quartzose McMurray Formation.

The influence of the various factors listed above on the strehgth of the materials will be discussed using the parameters a and b as a measure of shear behaviour.

The components of shear strength above residual due to dilatency and fabric cohesion (shear of grains) are presented in Figure 4.4. The fabric cohesion is determined by taking a tangent to the Mohr-Coulomb envelope at a given normal stress, and projecting this tangent back to zero normal stress. On the basis of this analysis, the components are defined as follows:

$$\begin{aligned}
\tau_f &= \text{component due to shear of grains} \\
&= (1-b)a\sigma_N{}^b \\
&= (1-b)\tau_p \\
\tau_f/\tau_p &= (1-b)
\end{aligned}$$

$$\begin{aligned}
\tau_d &= \text{component due to dilatency} \\
&= ab\sigma_N{}^b - \tau_r \\
&= b\tau_p - \tau_r \\
\tau_d/\tau_p &= b - \tau_r/\tau_p
\end{aligned}$$

From the equations it can be seen that a and b together define the magnitude of the peak shear stress, and b is a measure of the portion of shearing resistance above residual due to dilatency and to shearing of grains.

For equal values of the parameter a, a lower b value implies a greater curvature of the failure envelope and increased suppression of dilatency with increasing normal stress. As would be expected, the b values for the Grand Rapids Formation are lower than for the McMurray Formation, and the envelope curvature is greater. This greater suppression of dilatency results from shearing of the weaker feldspar grains present in the Grand Rapids Formation. The higher value of the parameter a combined with the lower b value gives the Grand Rapids materials a strength at low normal stress (0 to 700 kPa) which is slightly higher than that of the McMurray Formation samples. The samples of Grand Rapids Formation examined in the scanning electron microscope were observed to have a greater number of interlocking grain contacts than the McMurray Formation samples, which supports the observation of higher strength at low normal stress.

As stated above, the value of b obtained is observed to increase with decreasing median grain size. This implies that the more fine-grained the material is, the greater will be the portion of strength due to dilatency. It has been demonstrated that an equal amount of diagenetic alteration will have a greater effect (more porosity reduction) on a fine-grained material. If this fine-grained material has undergone greater porosity reduction and consequently has greater grain interlock, it is logical that dilatency will have a larger influence on strength.

A coarse-grained material will be influenced less by diagenetic processes, thus the change in dilatency characteristics would be smaller. The fabric cohesion or shearing of grains would be a more dominant part of the shear strength.

5.4.2 Diagenetic Classification by Porosity Reduction

Beard and Weyl (1973) conducted a series of experiments to measure the original packing of sands. Material was selected from two different alluvial systems and samples were prepared to represent different grain sizes and gradations. The porosity of the samples was determined under dry-loose and wet-packed conditions. The maximum porosity of the samples was measured by placing dry material in as loose a state as possible. This dry material was then wetted and tamped in such a manner as to avoid grain crushing, and the "packed" porosity of the materials was determined. The data will be used, together with the density index test results, to estimate the degree of diagenetic alteration (porosity reduction) of the oil sand materials tested.

The five main test materials were classified by grain size and gradation according to the system proposed by Beard and Weyl. Table 5.7 contains the *in situ* porosities of the materials, together with the porosity which can be achieved by wet-packing according to Beard and Weyl. The estimated porosity reduction is calculated on this basis. Table 5.7 also contains the minimum porosity values from the density index test results (dry vibration method), and the porosity reduction by diagenesis is also estimated using these results.

The minimum porosity results from the density index tests on the Grand Rapids Formation materials are much higher than the porosities achieved by Beard and Weyl for samples of similar grain size and gradation. This results partly from the difference in method of compaction (dry vibration as opposed to wet tamping) and also from differences in the sphericity and angularity of the particles. The grains in the Grand Rapids Formation are very angular and have indented surfaces which would result in looser packing.

On the basis of the approximate data presented in Table 5.7 and the observation of comparative materials (for example, itacolumites) a qualitative classification of degree of diagenetic alteration has been developed. The classification is given in Table 5.8.

Category 1 describes unaltered and only slightly altered sands. The curvature of the Mohr-Coulomb envelope is slight, and tangential grain contacts predominate.

The oil sand materials examined encompass categories 2 and 3. The grain contacts have been altered to long and concavo-convex, and the failure envelope has a substantial curvature.

The itacolumites examined fit into category 5. They possess substantial cohesion at zero normal stress, and the grain contacts are concavo-convex. Grain interlock in these materials is extensive, and the materials are difficult to disaggregate.

The divisions between the groups are an arbitrary and approximate method of delineating the degree of diagenetic alteration. This classification serves as a broad categorization of the effect of diagenesis on strength. Porosity reduction is not the only essential factor in diagenetic alteration, but it appears to be a good indicator for the materials examined. The classification does not apply to materials which have actual chemical bonding between grains (cementation); it is applicable only to locked sands which have been altered by the processes of pressure solution and/or crystal overgrowth.

The possibility of course exists that a quartz material may have undergone diagenetic alteration before introduction of cementitious material (calcite, siderite). In this case the classification system is applicable to the minus-cement porosity of the material. In addition to the cementitious cohesion at zero normal stress, the Mohr-Coulomb failure envelope of such a material may have substantial curvature, depending on the degree of diagenetic alteration before cementation.

5.5 Practical Implications of Oil Sands Behaviour

The interlocking structure and dilatent behaviour of oil sand materials has important implications for resource recovery by both surface mining and *in situ* processes. The following factors related to structure and strength will influence oil recovery schemes in oil sands:

1. the lack of cementitious cohesion
2. the interlocking grain structure which causes:
    a. a high-strength curvilinear failure envelope
    b. high dilatency during shear at low normal stress
    c. high density
    d. strain-weakening behaviour

Natural slope angles of 60 and 70 degrees have been observed in river valley outcrops in oil sands in the Fort McMurray area. The extensive grain interlock gives oil sand materials excellent stability under low normal stress such as encountered in river valley outcrops and in pit walls of surface mining operations. This is of extreme economic importance in surface mining. The angle at which the pit walls may be cut will be limited by geologic details and pore fluid behaviour, such as clay seams unfavourably oriented with respect to the pit wall, or exsolving gas maintaining pore pressures, rather than by the strength of the oil sand itself.

In tunnelling or shafting operations the cohesionless, strain-weakening behaviour of oil sands will create a need for immediate excavation support. The dense interlocking nature of the material will create stress arching around the opening. However, the zone of shear failure around the tunnel or shaft will be loosened, weak material which no longer possesses fabric interlock and will thus ravel rapidly after excavation. Due to the interlocking fabric of the oil sand materials, a relatively small amount of immediate support would be required if the material were a clean locked sand. However, the effect of the dissolved gas in the bitumen phase must also be considered as a possible factor in tunnel ravelling.

The hydraulic fracturing process in oil sands will be affected by the strain-weakening behaviour. A zone of shear failure is created around the fracture tip, and the fluid injection properties will be influenced by the dilatent behaviour. The propagation of a hydraulic fracture by shear failure in oil sands requires a disruption of the interlocking grain structure. This disruption may require high energy input (fluid injection pressure), which correlates with the high shear strength of the material.

Table 5.1: Grain size data for original samples.

Material	D_{60} (mm)	D_{50} (mm)	D_{10} (mm)	$c_u = \frac{D_{60}}{D_{10}}$	% passing no. 200 sieve
Fine-grained McMurray Formation	0.210	0.200	0.160	1.31	0.4
Medium-grained McMurray Formation	0.480	0.430	0.280	1.71	1.4
Coarse-grained McMurray Formation	0.890	0.620	0.150	5.93	1.1
Grand Rapids Formation A	0.110	0.100	0.076	1.45	3.9
Grand Rapids Formation C	0.250	0.230	0.070	3.57	10.7

Table 5.2: Grain size data for sheared samples of Grand Rapids Formation.

Direct Shear Test Sample	Normal Stress (kPa)	% passing no. 200 sieve
GRA-2-79	250	6.6
GRA-3-79	400	6.7
GRA-4-79	700	7.6
GRA-5-79	1000	9.0
GRA-6-79	2000	11.8
GRC-1-79	100	11.5
GRC-2-79	250	12.3
GRC-3-79	400	15.5
GRC-4-79	700	19.0
GRC-5-79	1000	15.8
GRC-6-79	2000	19.7

Table 5.3: Density, porosity, and water content test results.

Material	γ_{sat} (g/cc)	n (%)	w (%)
Fine-grained McMurray Formation	2.11±.04	32.7	5.9
Medium-grained McMurray Formation	2.07±.04	35.2	1.4
Coarse-grained McMurray Formation	2.27±.04	23.0	1.6
Grand Rapids Formation A	2.06±.01	36.1	5.2
Grand Rapids Formation C	2.06±.03	37.6	17.5

Table 5.4: Density index test results.

Material	e_{max}	e_{min}	e	I_D(%)
Fine-grained McMurray Formation	0.9261	0.6891	0.4865	185.5
Medium-grained McMurray Formation	0.8575	0.6097	0.5421	127.3
Coarse-grained McMurray Formation	0.5851	0.3316	0.2992	112.8
Grand Rapids Formation A	1.2037	0.8580	0.5660	184.5
Grand Rapids Formation C	1.6255	1.0105	0.6038	166.1

Table 5.5: Compressibility test results.

Material	Modulus of Compressibility a_v (kPa^{-1})X10^{-6}			
	load	unload	reload	unload
Fine-grained McMurray Formation	0.80	0.33	0.35	0.28
Medium-grained McMurray Formation	2.15	0.28	0.30	0.25
Coarse-grained McMurray Formation	2.05	0.17	0.52	0.20
Grand Rapids Formation A	0.96	0.32	0.28	0.27
Grand Rapids Formation C	6.13	0.17	0.51	0.17

Table 5.6: Curve-fit correlation parameters, relationship between shear stress and normal stress.

Material	a	b	correlation coefficient
Fine-grained McMurray Formation	2.4711	0.8607	0.9983
Medium-grained McMurray Formation	2.8672	0.8089	0.9966
Coarse-grained McMurray Formation	3.9115	0.7891	0.9972
Grand Rapids Formation A	4.8135	0.7667	0.9957
Grand Rapids Formation C	10.2264	0.6496	0.9805

Table 5.7: Estimate of porosity reduction resulting from diagenesis.

Material	n (%)	from Beard and Weyl, 1973		from density index test results	
		n_p achieved by wet packing (%)	porosity reduction $n - n_p$ (%)	n_{min} achieved by vibration (%)	porosity reduction $n - n_{min}$ (%)
Fine-grained McMurray Formation	32.7	39.8	7.1	40.8	8.1
Medium-grained McMurray Formation	35.2	38.1	2.9	37.9	2.7
Coarse-grained McMurray Formation	23.0	29.8	6.8	24.9	1.9
Grand Rapids Formation A	36.1	40.2	4.1	46.2	10.1
Grand Rapids Formation C	37.6	39.1	1.5	50.3	12.7

Table 5.8: Classification of diagenetic alteration in sandstones.

Category	Porosity Decrease (%)	Nature of Grain Contacts	Effect on Strength
1	0 - 2	tangential	-very small to no alteration -small strength increase with only slight failure envelope curvature -zero fabric cohesion at zero normal stress
2	2 - 6	tangential, long, and concavo-convex	-small degree of alteration -failure envelope is noticeably curved -very small fabric cohesion at zero normal stress; material will stand unsupported but is very easily disturbed
3	6 - 10	predominantly long and concavo-convex	-medium alteration -failure envelope is curved; substantial strength increase at low normal stress -very small fabric cohesion at zero normal stress; material will stand unsupported but is easily disturbed
4	10 - 15	predominantly concavo-convex	-high degree of alteration -failure envelope is markedly curved -moderate fabric cohesion at zero normal stress; material can still be broken up
5	>15	highly interlocked concavo-convex	-extreme degree of alteration -high curvature of failure envelope -substantial fabric cohesion at zero normal stress; material is difficult to disaggregate

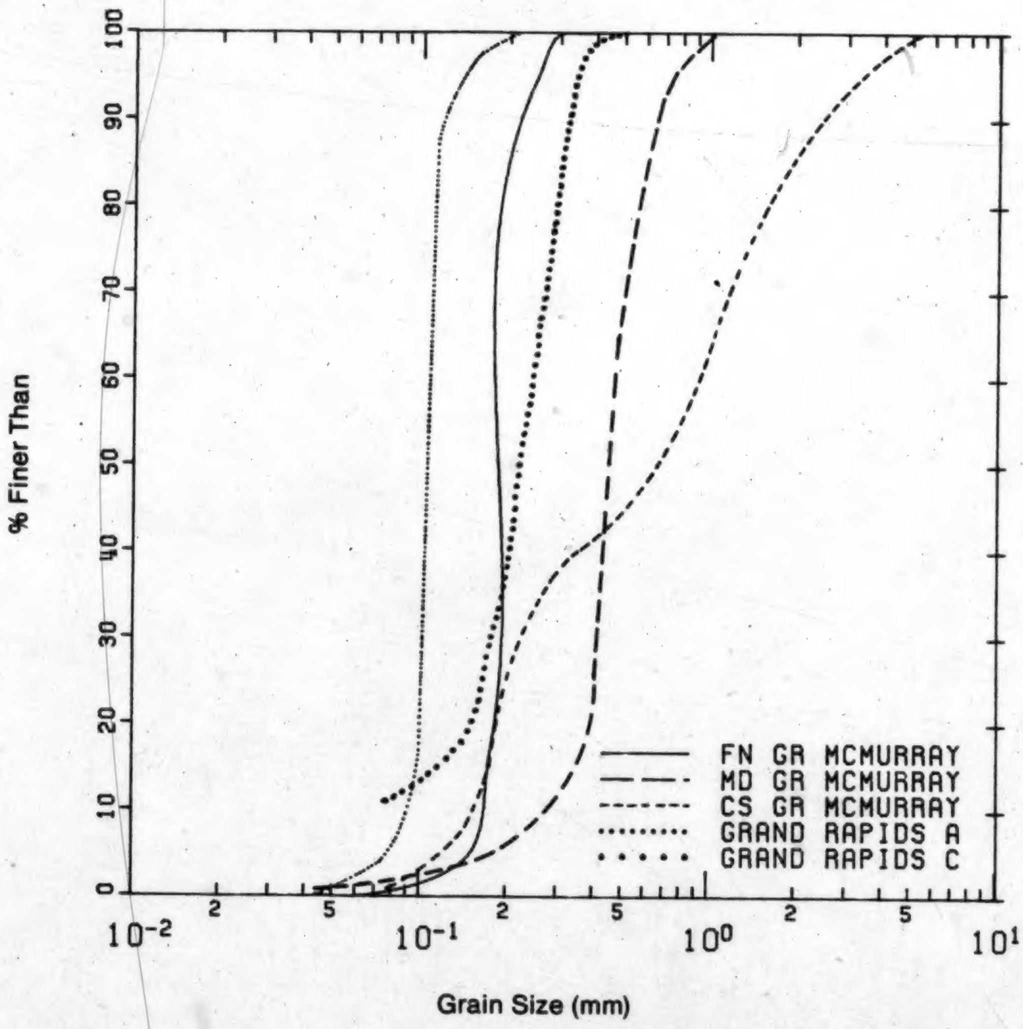

Figure 5.1 : Grain size distribution for all test materials.

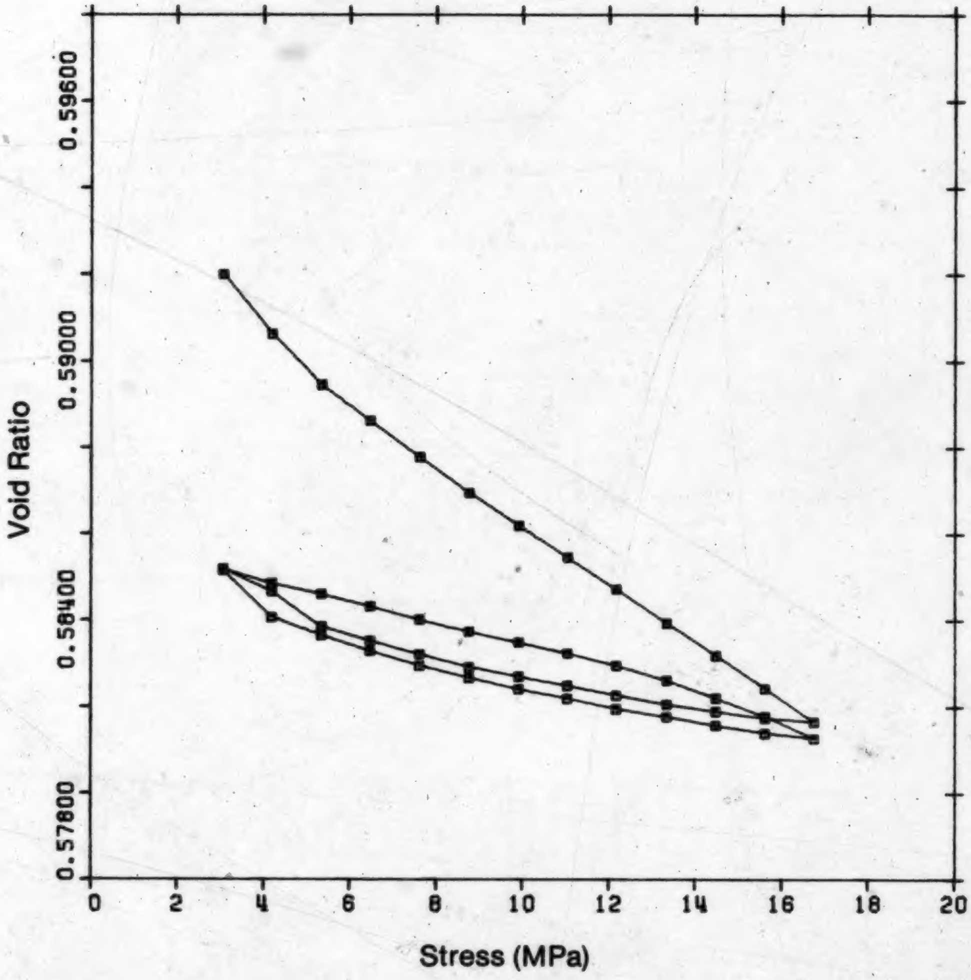

Figure 5.2 : Void ratio vs. stress curve for oedometer test FG - C2 - 79 on fine-grained McMurray Formation.

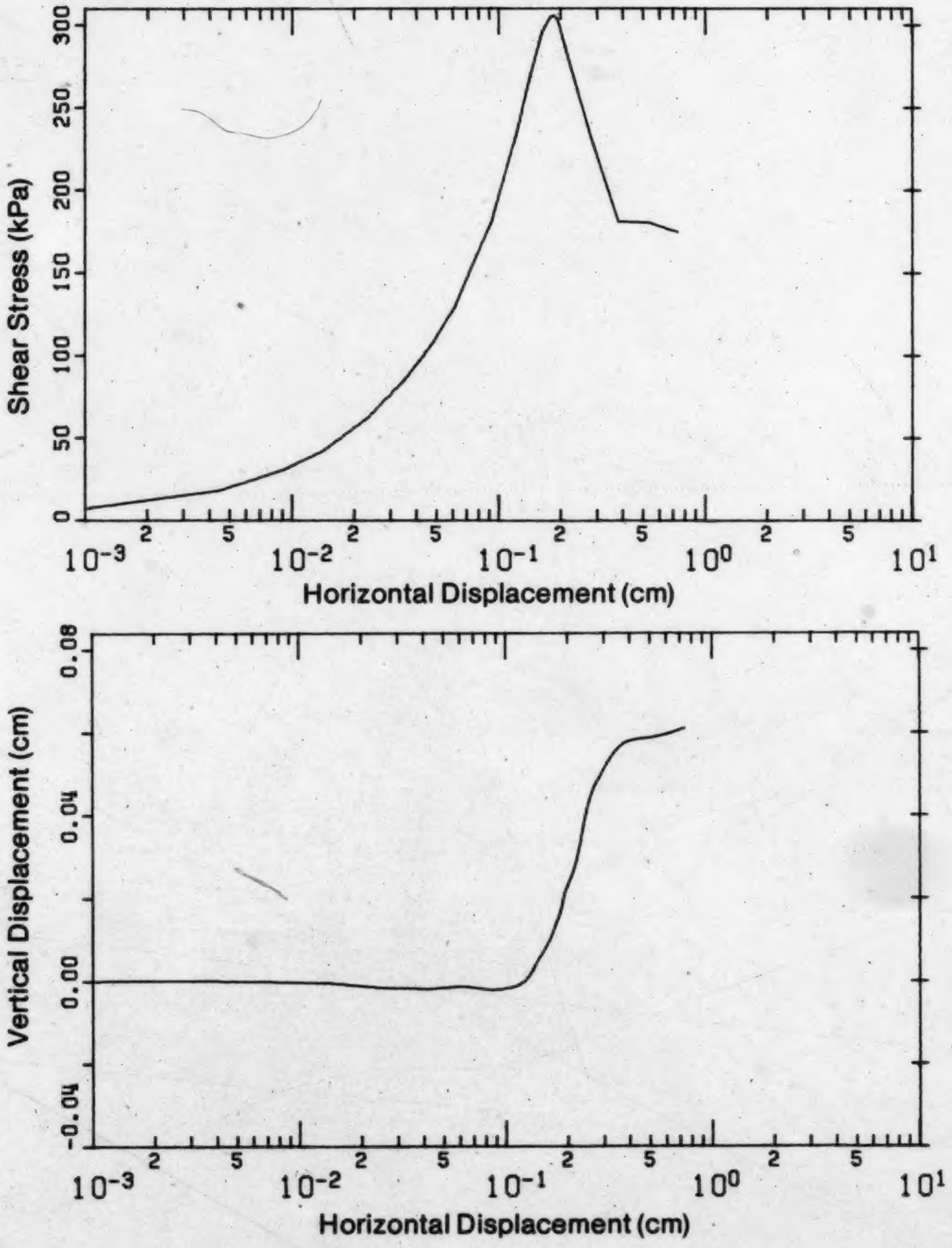

Figure 5.3 : Shear test results, fine-grained McMurray Formation, normal stress = 250 kPa.

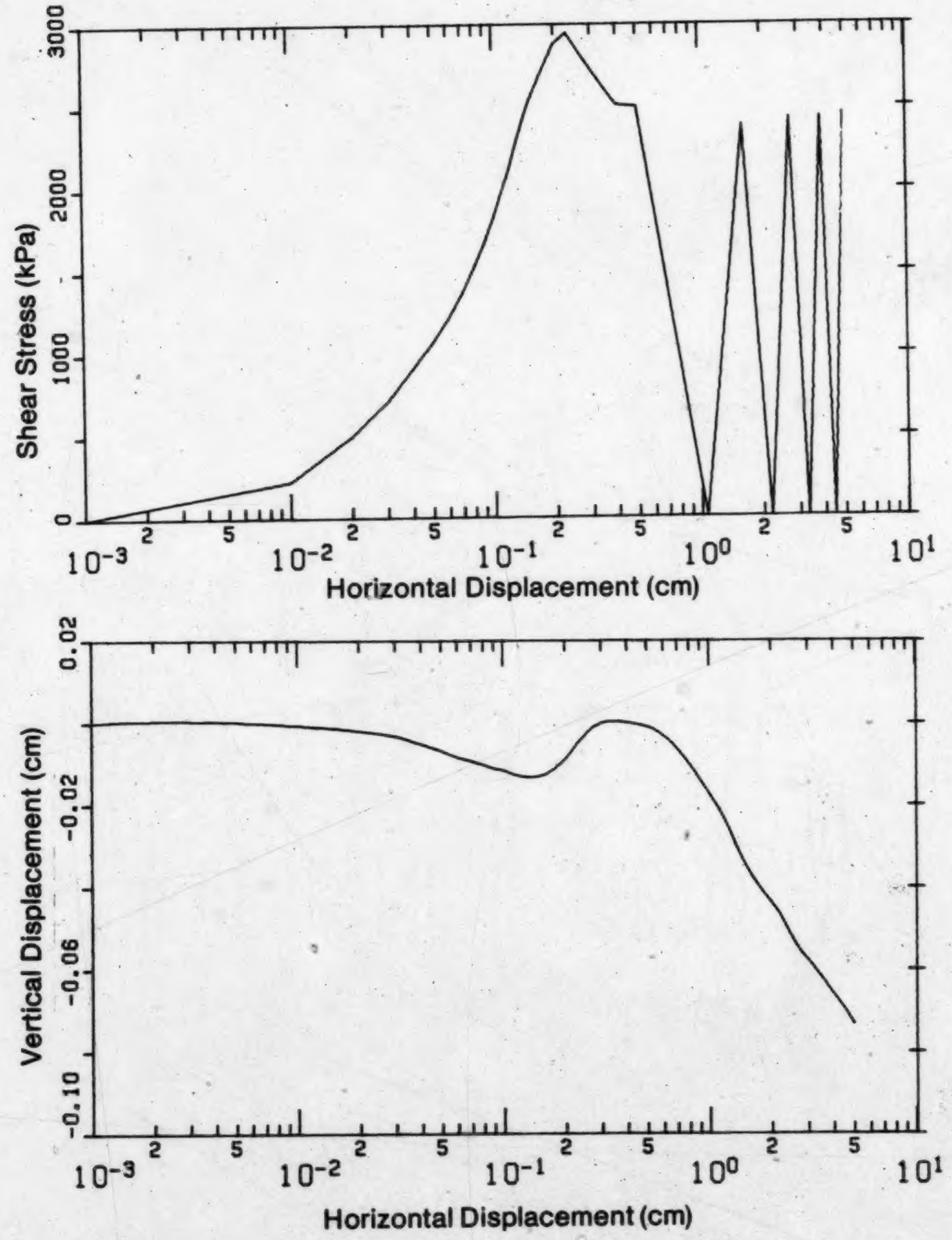

Figure 5.4 : Shear test results, fine-grained McMurray Formation, normal stress = 4000 kPa.

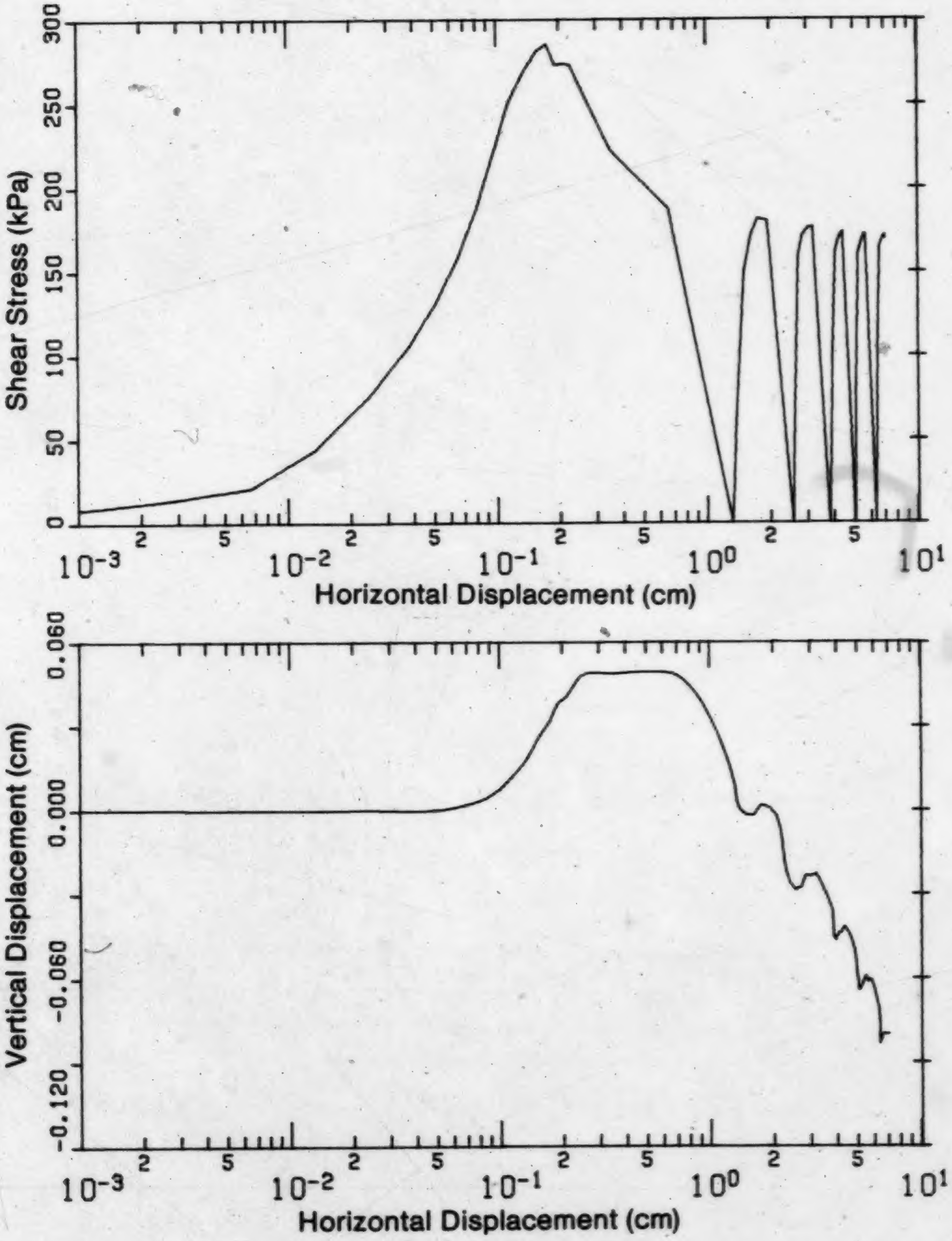

Figure 5.5 : Shear test results, Grand Rapids Formation A, normal stress = 250 kPa.

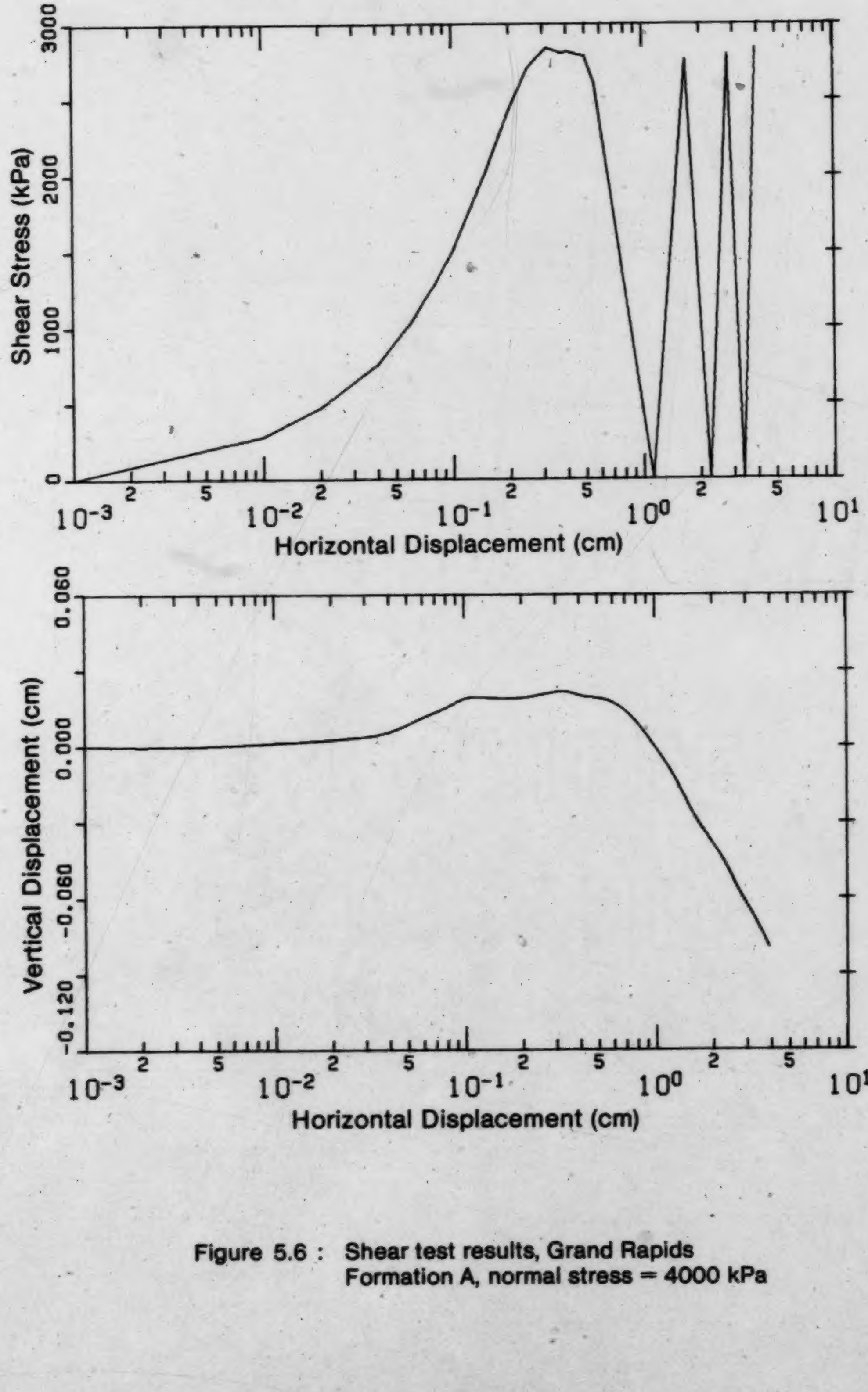

Figure 5.6 : Shear test results, Grand Rapids Formation A, normal stress = 4000 kPa

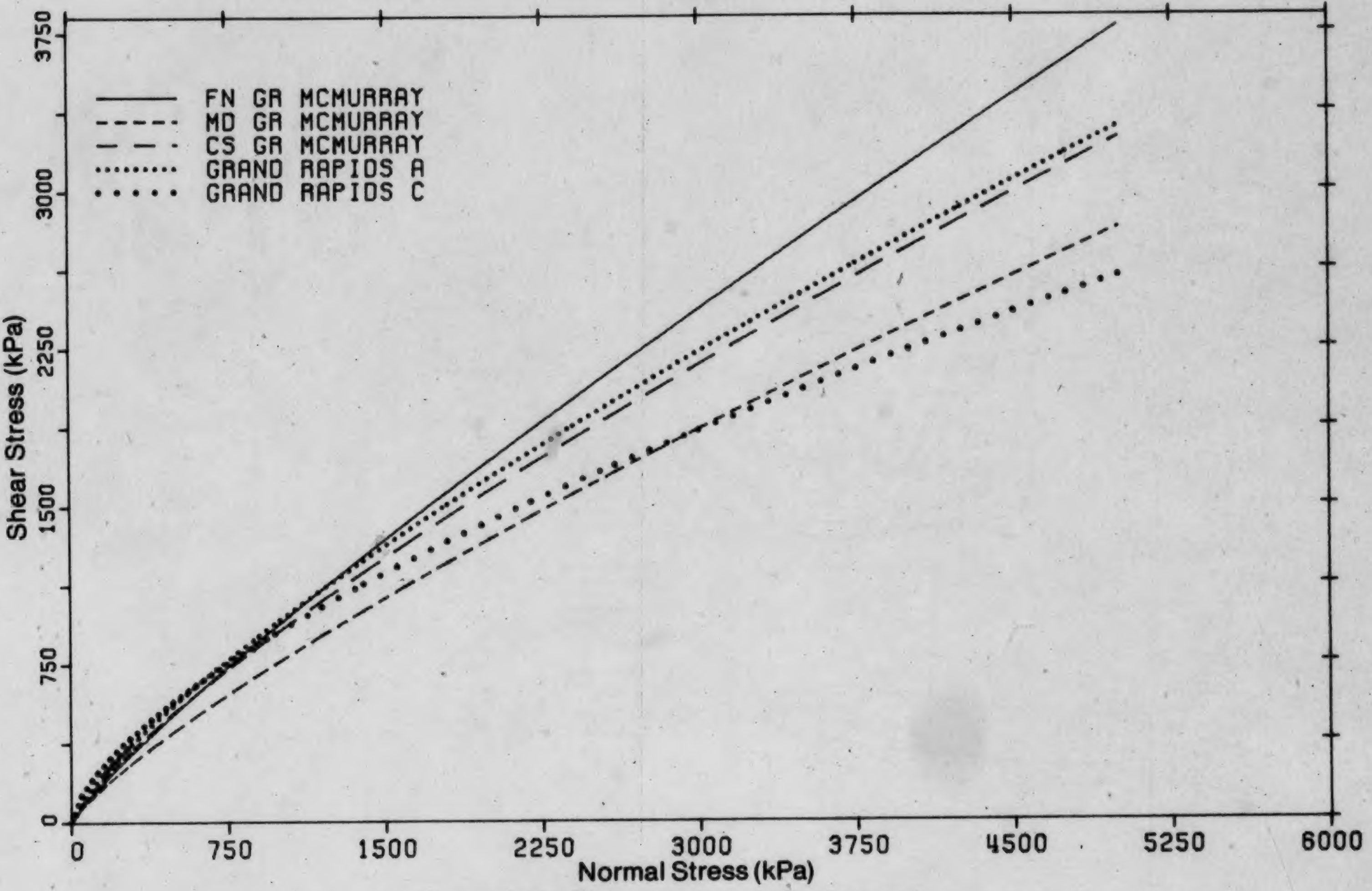

Figure 5.7 : Shear stress vs. normal stress for all test materials.

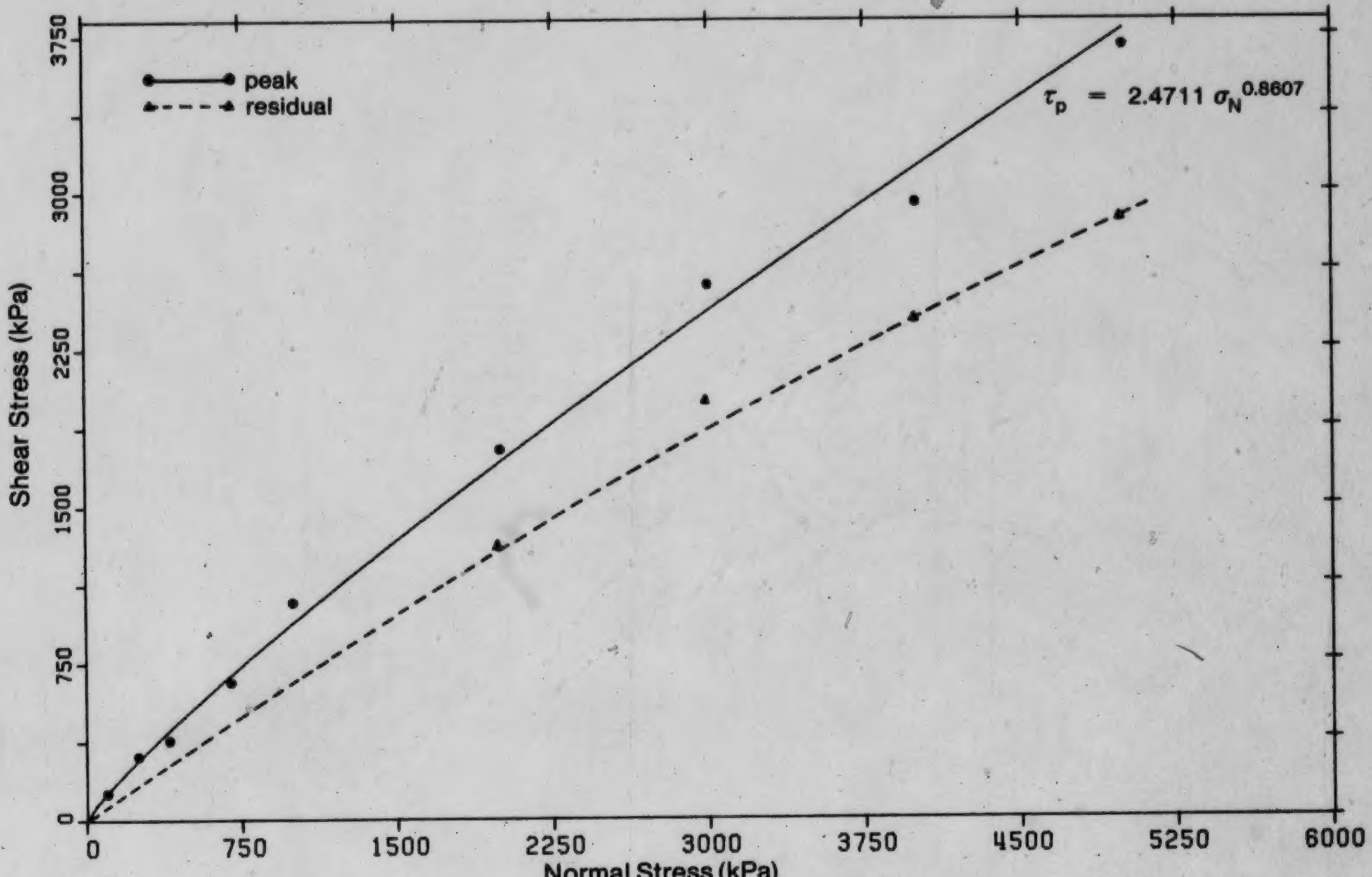

Figure 5.8 : Shear stress vs. normal stress, fine-grained McMurray Formation.

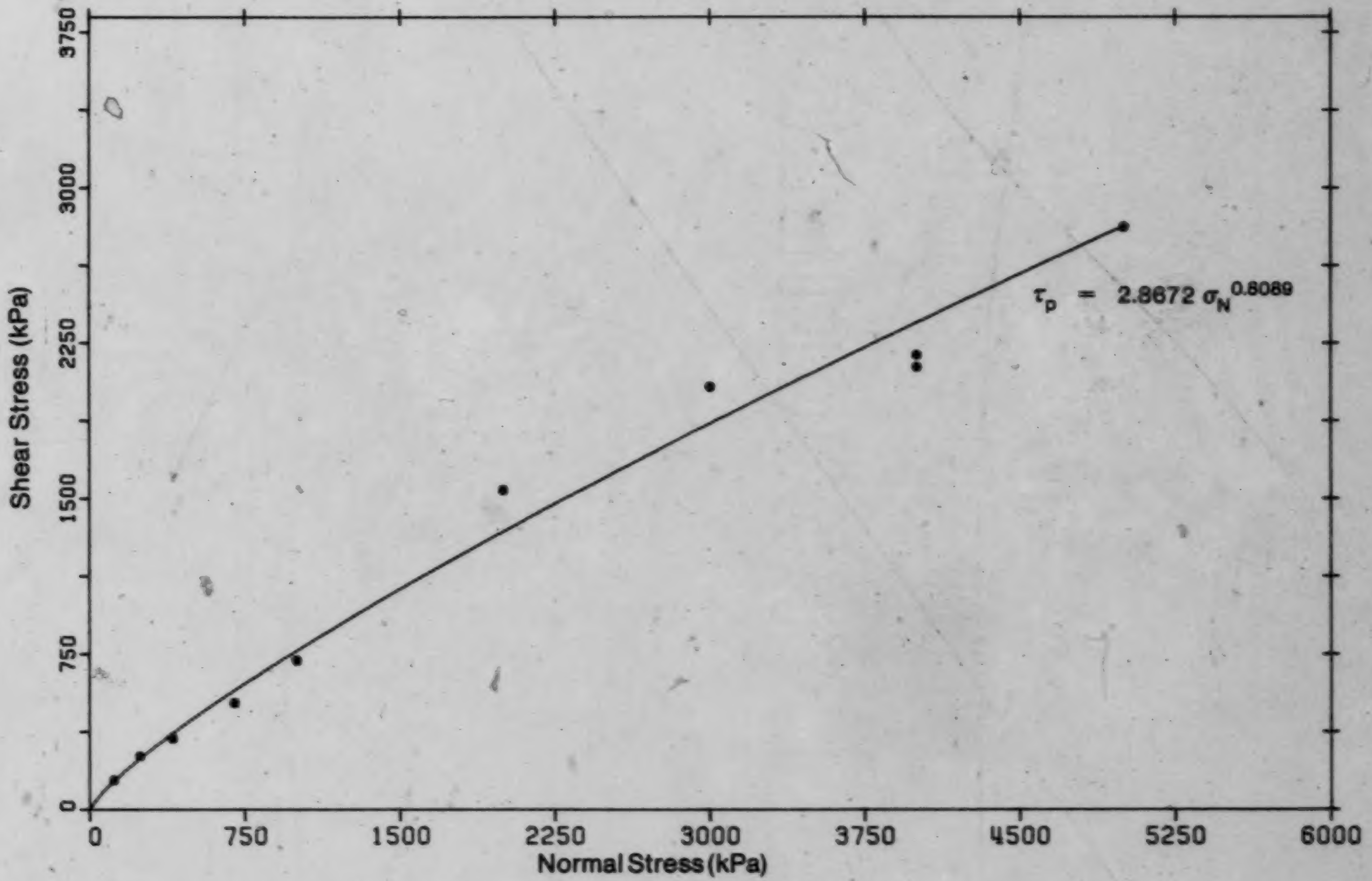

Figure 5.9 : Shear stress vs. normal stress, medium-grained McMurray Formation.

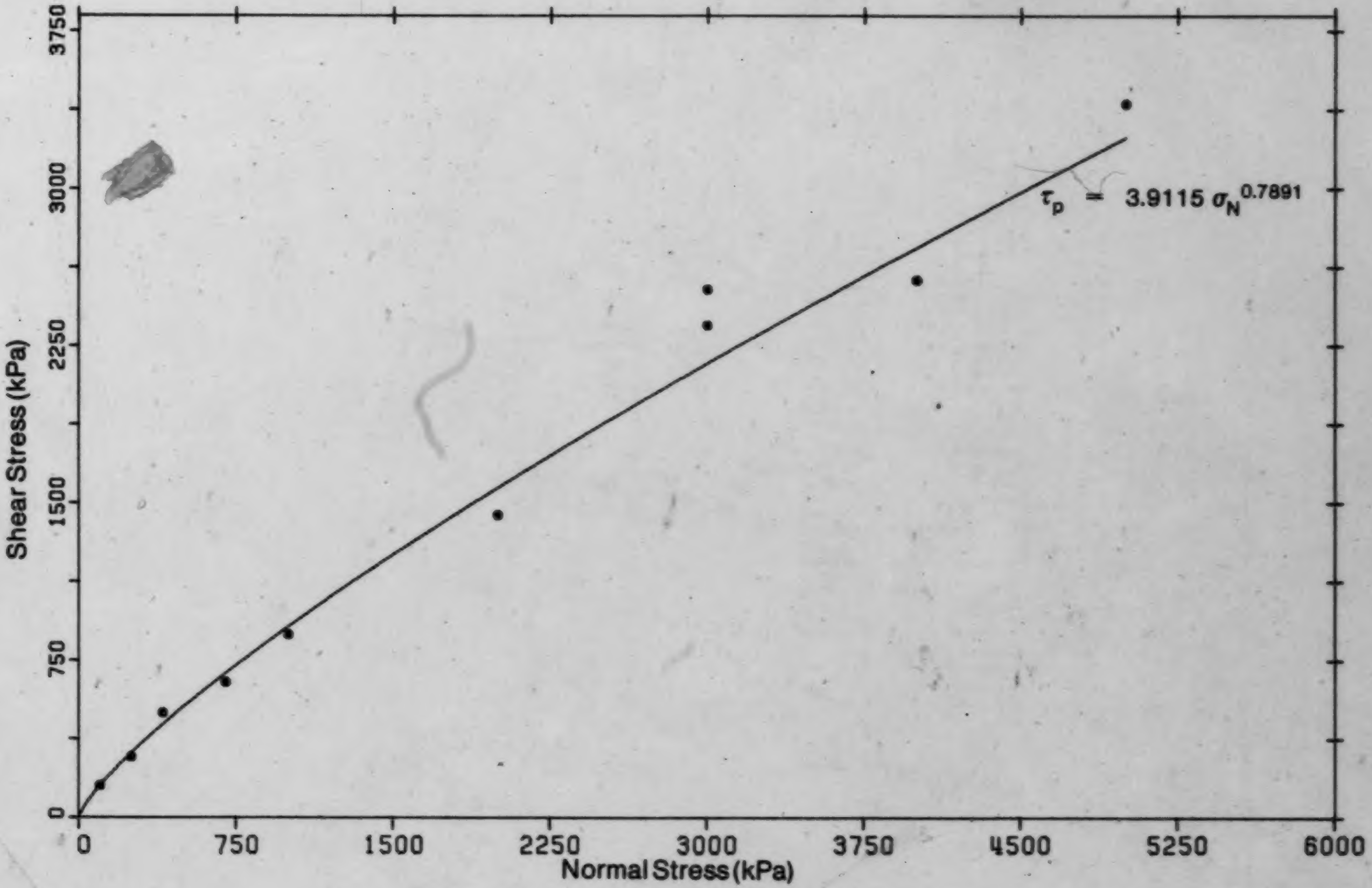

Figure 5.10 : Shear stress vs. normal stress, coarse-grained McMurray Formation.

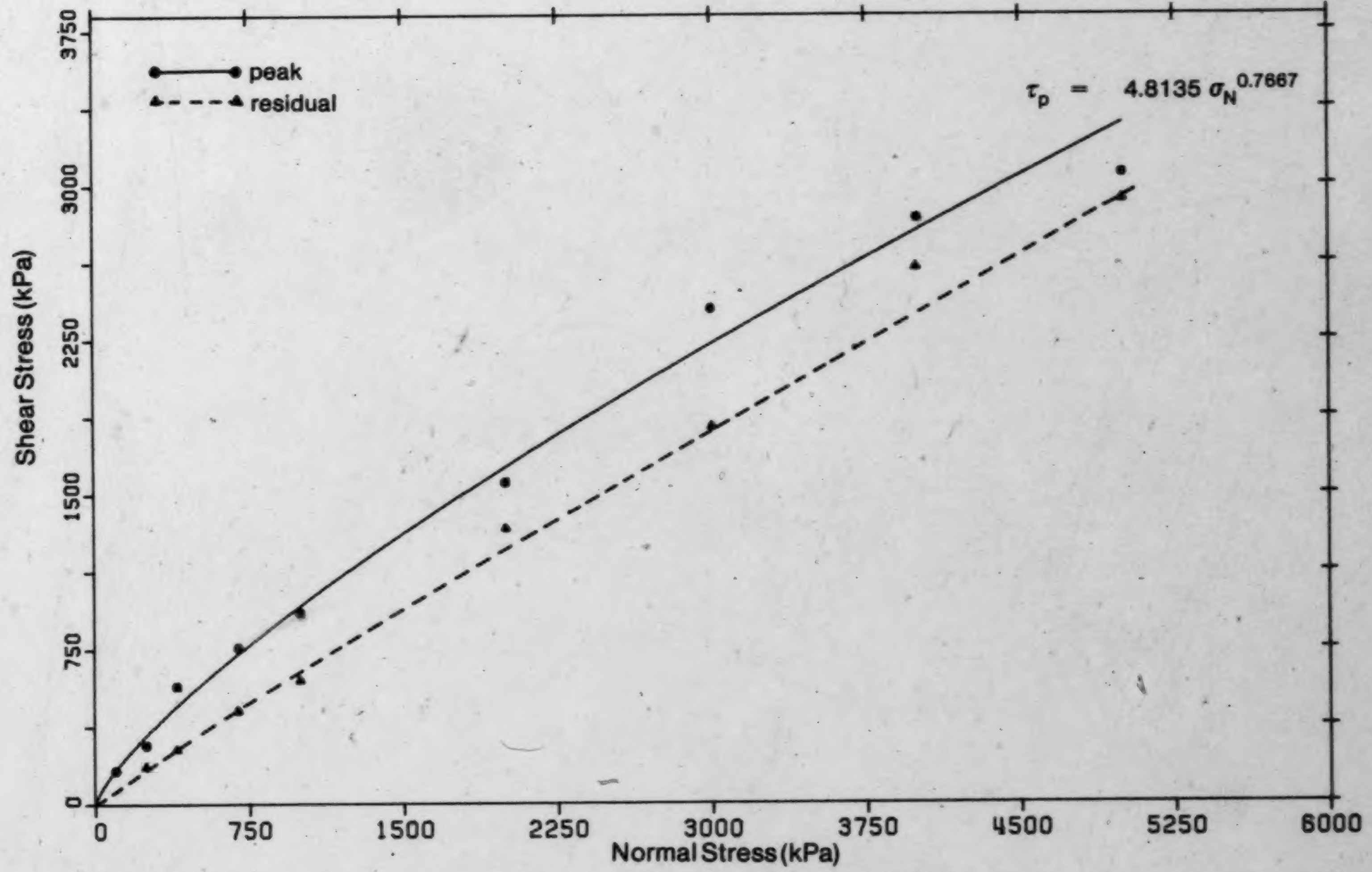

Figure 5.11 : Shear stress vs. normal stress, Grand Rapids Formation A.

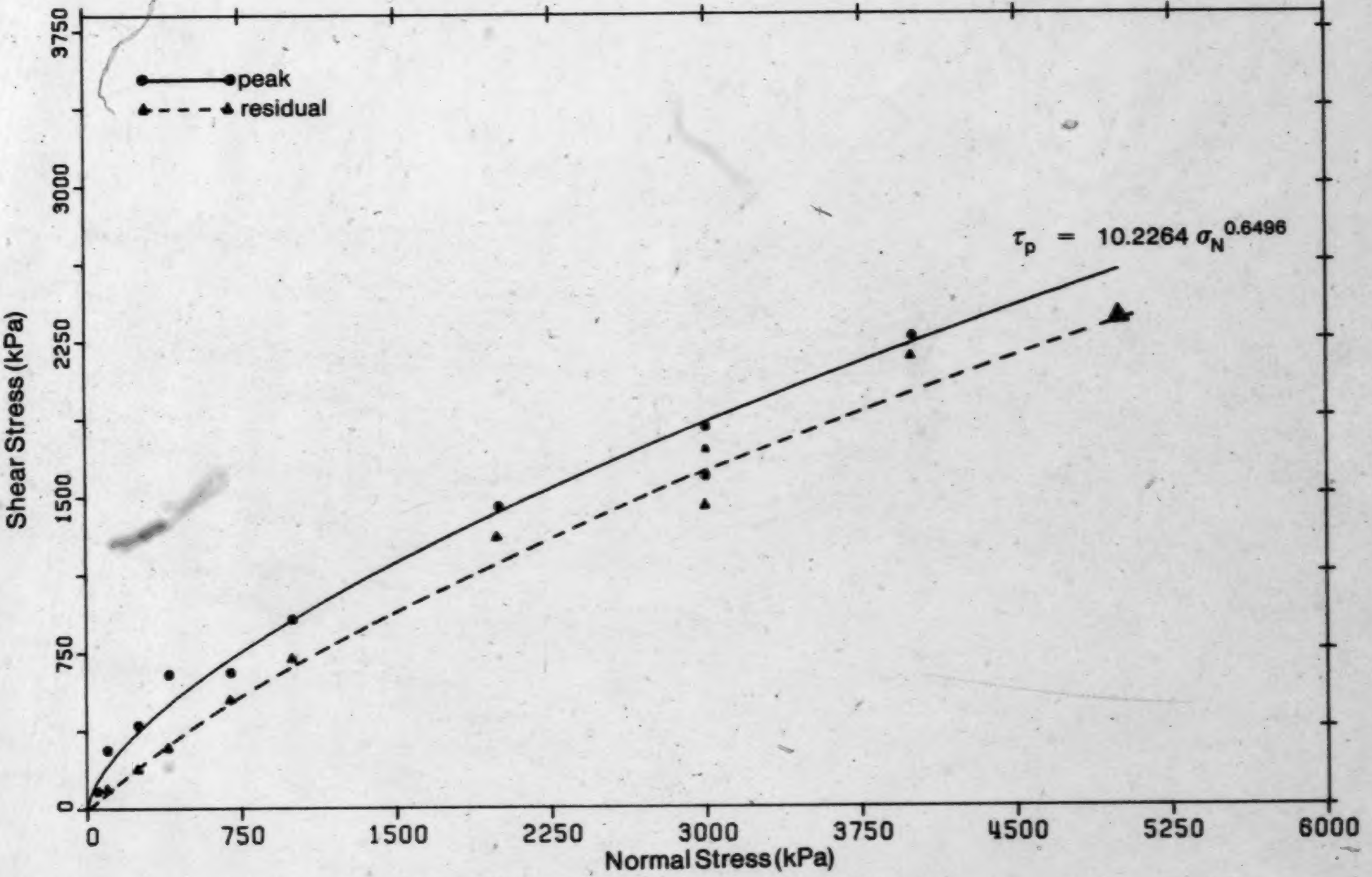

Figure 5.12 : Shear stress vs. normal stress, Grand Rapids Formation C.

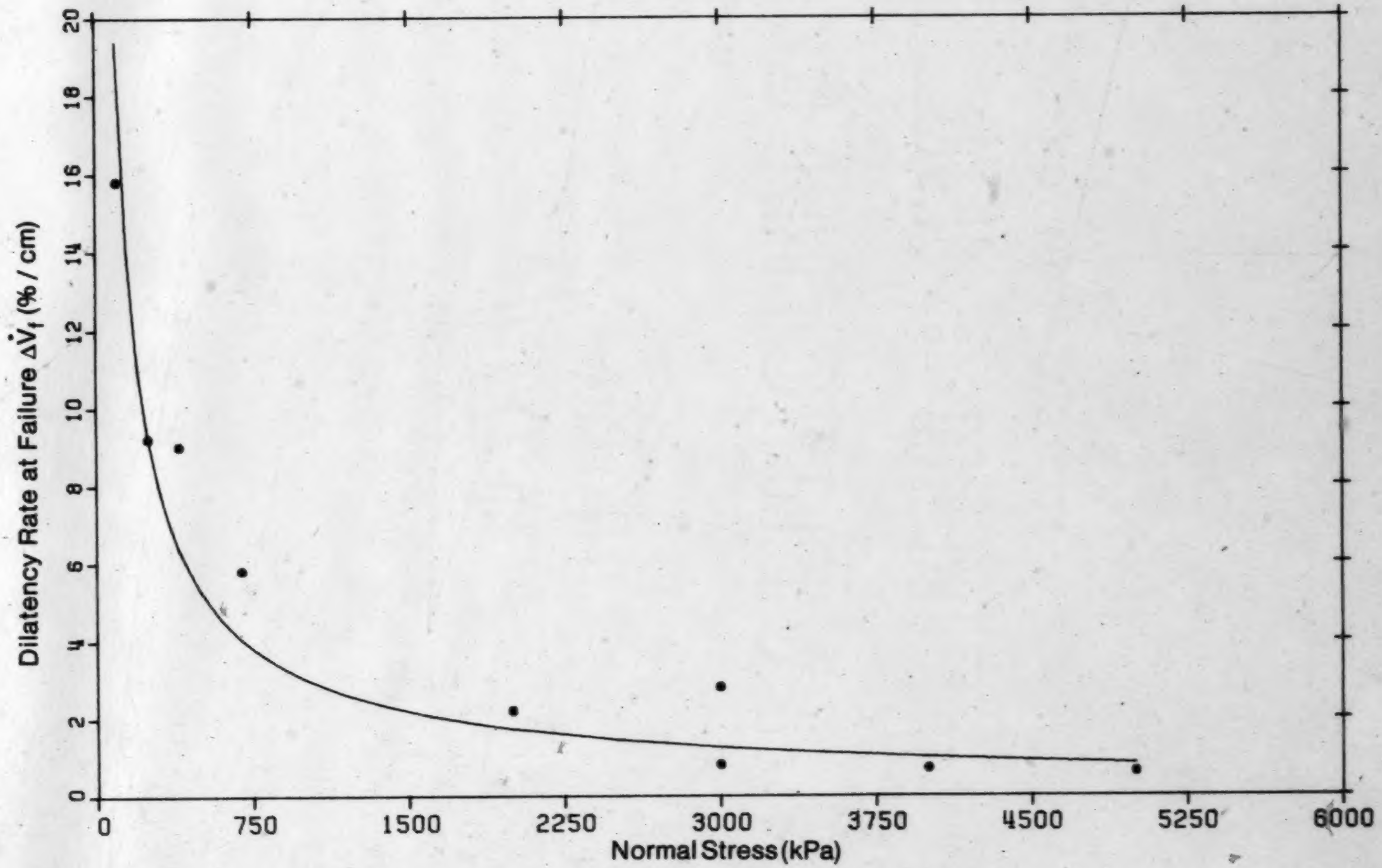

Figure 5.13 : Dilatency rate at failure vs. normal stress coarse-grained McMurray Formation.

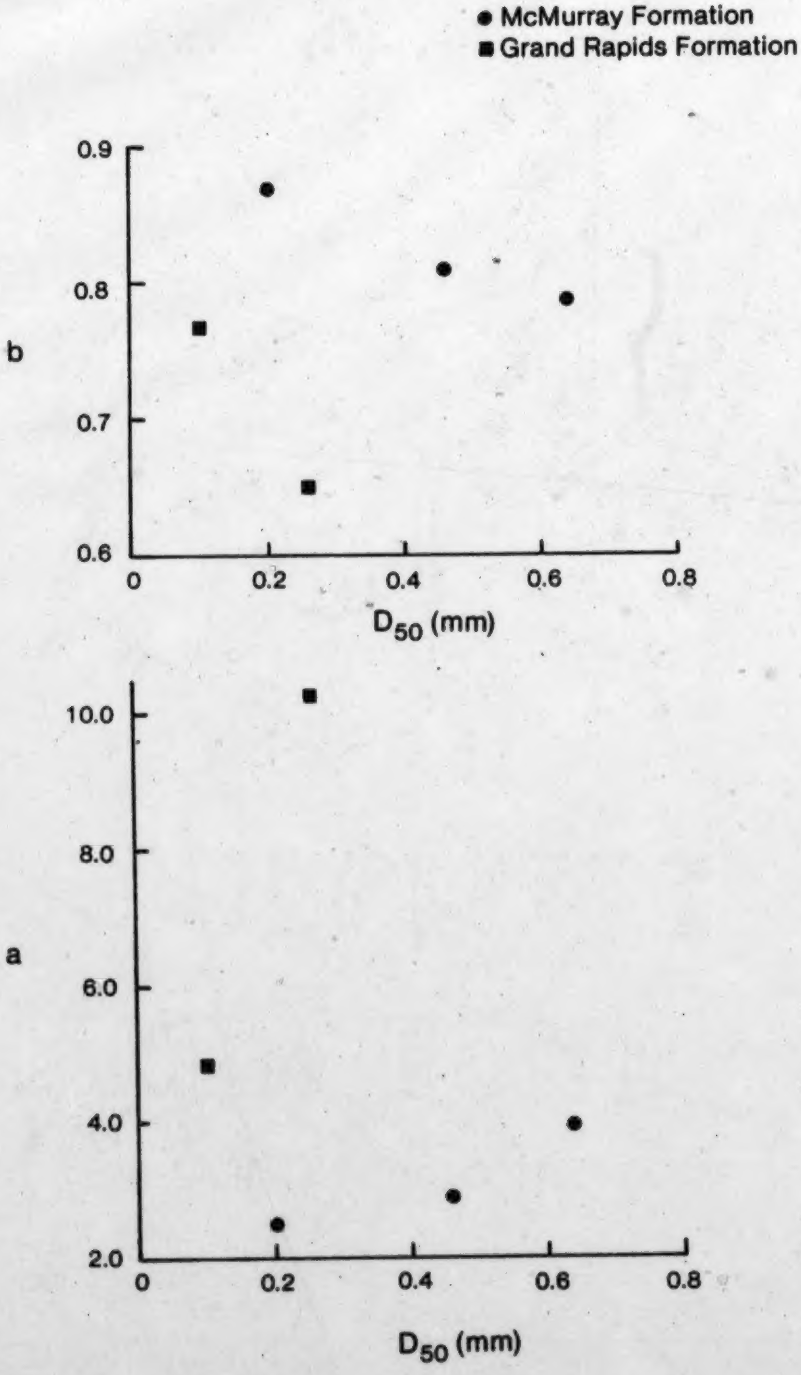

Figure 5.14 : Relationship between shear strength correlation parameters and median grain size.

6. CONCLUSION

An examination of oil sands in the scanning electron and optical microscopes reveals that the diagenetic processes of pressure solution and authigenic crystal overgrowth have altered the materials. The materials have an interlocking grain fabric with many long and concavo-convex grain contacts.

The processes of pressure solution and authigenic crystal overgrowth have been reviewed, with special attention paid to the environmental conditions necessary for their occurrence and the grain surface and contact features which they produce.

A number of theoretical analyses for the strength of granular materials and rocks have been examined, together with experimental data on the strength of rocks and interlocking aggregates. A curvilinear curve-fitting model for the strength of oil sand has been examined.

The results of direct shear tests on oil-free block samples of the McMurray and Grand Rapids Formations show that these locked sands have curvilinear Mohr-Coulomb failure envelopes with negligible fabric cohesion at zero normal stress. The dilatency during shear and the strain-weakening peak-to-residual behaviour result from the grain interlock. The materials have high strength and very low compressibility.

The factors which relate to structure and strength of oil sand which will influence oil recovery schemes are:

1. the lack of cementitious cohesion
2. the interlocking grain structure which causes:
   a. a high-strength curvilinear failure envelope
   b. high dilatency during shear at low normal stress
   c. high density
   d. strain-weakening behaviour

These characteristics have many important implications for the design of structures and processes in oil sands (slope stability in open-pit mines, tunnelling and shafting operations, hydraulic fractures).

Four main factors will influence the strength of a non-cemented granular material: original density or packing, mineralogy, grain size, and degree of diagenetic alteration. The relationship between these factors is complex. The first three factors will determine in part the amount of diagenetic alteration which takes place.

The influence of mineralogy on strength has been demonstrated by comparison of the McMurray and Grand Rapids Formations. The Grand Rapids Formation contains quartz grains together with weaker feldspar grains as opposed to the almost totally quartzose McMurray Formation. The consequence of this is a greater curvature of the failure envelope in the Grand Rapids Formation, which results from shearing of the weaker feldspar grains along cleavage planes.

The influences of grain size and diagenetic alteration on strength are difficult to separate, as the grain size has a strong influence on the amount of diagenetic alteration which takes place. From analysis of the strength envelopes obtained for various grain sizes and gradations for the two formations studied, it appears that a smaller grain size will increase the amount of diagenesis which takes place, and thus the strength increase will be greater, provided the environmental conditions are equal (stress, temperature, pH and fluid flow).

An approximate classification system for degree of diagenetic alteration has been presented based on the porosity reduction which a material has undergone. This system is applicable to locked sands with no cementitious cohesion. In a cemented material, the classification system would apply to the minus-cement porosity, as it is a measure of failure envelope curvature and fabric cohesion.

Bibliography

Atkinson, B.K., and Rutter, E.H., 1975. "Pressure solution or indentation?", comment and reply, Geology 3, pp. 477-478.

Barton, M.E., 1974. "Soft sandstones: geotechnical properties and sensitivity to moisture changes", Proc. Seond Int. Congress of the Int. Assoc. of Eng. Geol., Sao Paulo, Vol. 1, Theme IV, Paper 7, 6 pp.

Bathurst, R.G.C., 1958. "Diagenetic fabrics in some British Dinantian Limestones", Liverpool and Manchester Geol. Jour., No. 2, pp. 11-36.

Beard, D.C., and Weyl, P.K., 1973. "Influence of texture on porosity and permeability of unconsolidated sand", Amer. Assoc. Petrol. Geol. Bulletin, Vol. 57, Part 1, pp. 349-369.

Becker, G.F., and Day, A.L., 1916. "Note on the linear force of growing crystals", Jour. Geol., Vol. 24, pp. 313-333.

Carozzi, A.V., 1960. "Microscopic sedimentary petrography", John Wiley and Sons Inc., New York, 485 pp.

Carrigy, M.A., 1959. "General geology of the McMurray area, Part III, Geology of the McMurray Formation", Res. Coun. of Alta. Geol. Div. Memoir 1, Edmonton, Alberta, 130 pp.

Carrigy, M.A., 1967. "The physical and chemical nature of a typical tarsand: bulk properties and behaviour", Proc. 7th World Petrol. Congress, Mexico City, Vol. 3, Tar Sands Section, pp. 573-581.

Carrigy, M.A., 1973. "Mesozoic geology of the Fort McMurray area", Guide to the Athabasca Oil Sands Area, ed. M.A. Carrigy and J.W. Kramers, Alberta Res. Info. Series 65, Edmonton, Alberta, pp. 79-101.

Cayeux, L., 1929. "Les roches sedimentaires de France - roche siliceuses", Mem. Carte Geol. det. France, Paris, Imprimerie Nationale, 774 pp.

Cecil, C.B. and Heald, M.T., 1971. "Experimental investigation of the effects of grain coatings on quartz growth", Jour. Sed. Petrology, Vol. 41, pp. 582-584.

Dapples, E.C., 1959. "The behaviour of silica in diagenesis", Proc. Soc. Econ. Paleontologists and Mineralogists, Spec. Publ. 7, pp. 36-54.

Dapples, E.C., 1962. "Stages of diagenesis in the development of sandstones", Bulletin of the Geol. Soc. of America, Vol. 73, pp. 913-934.

Davis, S.W., 1964. "Silica in streams and ground water", Amer. Jour. Sci., Vol. 262, pp. 870-890.

de Boer, R.B., 1977a. "Pressure solution: theory and experiments", Tectonophysics (Special Issue: Fabrics, Microstructures, and Microtectonics), Vol. 39, pp. 287-301.

de Boer, R.B., 1977b. "On the thermodynamics of pressure solution - interaction between chemical and mechanical forces", Geochim. Coscochim. Acta, 41, pp. 249-256.

de Boer, R.B., Nagtegaal, P.J.C., and Duyvis, E.H., 1977. "Pressure solution experiments on quartz sand", Geochim. Cosmochim. Acta, 41, pp. 257-264.

Dunnington, H.V., 1967. "Aspects of diagenesis and shape change in stylolitic limestone reservoirs", Proc. 7th World Petrol. Congress, Mexico City, Vol. 2, pp. 339-352.

Durney, D.W., 1972. "Solution transfer, and important geological deformation mechanism", Nature, London, 235, pp. 315-317.

Durney, D.W., 1976. "Pressure solution and crystalline deformation", Phil. Trans. Royal Soc. of London, A283, pp. 229-240.

Dusseault, M.B., 1977. "The geotechnical characteristics of the Athabasca Oil Sands", unpublished Ph. D. Thesis, University of Alberta, Edmonton, Alberta.

Dusseault, M.B., and Morgenstern, N.R., 1979. "Locked sands", Quarterly Jour. Eng. Geol., London, Vol. 12, pp. 117-131.

Ernst, W.G., and Blatt, H., 1964. "Experimental study of quartz overgrowths and synthetic quartzites", Jour. Geol., Vol. 72, pp. 461-470.

Every, R.L., Wade, W.H., and Hackerman, N., 1961. "Free energy of adsorption. I: The influence of substrate structures in the SiO_2-H_2O, SiO_2-n-hexane and SiO_2CH_3OH systems", Jour. Phys. Chem., 65, pp. 25-29.

Fraser, H.J., 1935. "Experimental study of the porosity and permeability of clastic sediments", Jour. Geol., Vol. 43, pp. 910-1010.

Fuchtbauer, H., 1967, "Influence of different types of diagenesis on sandstone porosity", Proc. 7th World Petrol. Congress, Mexico City, Vol. 2, pp. 353-369.

Fuchtbauer, H., 1972. "Interstitial waters and silica in sediments", in "Diagenesis of arenaceous deposits", National Conf. on Earth Sciences, pp. 203-286.

Fuchtbauer, H., 1974. "Some problems of diagenesis in sandstones", Bulletin Centre Recherche Pau, Vol. 8, pp. 391-403.

Ginsburg, L., and Lucas, G., 1949. "Presence de quartzites elastiques dans les gres armoricains metamorphiques de Berrien (Finistere)", Acad. Sci. Paris Comptes rendus, Vol. 228, pp. 1657-1658.

Graton, L.C., and Fraser, H.J., 1935. "Systematic packing of spheres", Jour. Geol., Vol. 43, pp. 785-909.

Hawkins, P.J., 1978. "Relationship between diagenesis, porosity reduction, and oil emplacement in late Carboniferous sandstone reservoirs, Bothamsell Oilfield, E. Midlands", Jour. Geol. Soc. of London, Vol. 135, Part 1, pp. 7-24.

Heald, M.T., 1955. "Stylolites in sandstones", Jour. Geol., Vol. 63, pp. 101-114.

Heald, M.T., 1956. "Cementation of Simpson and St. Peter Sandstones in parts of Oklahoma, Arkansas, and Missouri", Jour. Geol., Vol. 64, pp. 16-30.

Heald, M.T., and Larese, R.E., 1974. "Influence of coatings on quartz cementation", Jour. Sed. Petrology, Vol. 44, No. 4, pp. 1269-1274.

Heald, M.T., and Renton, J.J., 1966. "Experimental study of sandstone cementation", Jour. Sed. Petrology, Vol. 36, No. 4, pp. 977-991.

Kenichi, M., 1968. "Free energy of adsorption of water vapor on quartz powder", Nippon Kagaku Zasshi, 89, pp. 346-349.

Kennedy, G.C., 1950. "A portion of the system silica-water", Econ. Geol., Vol. 45, pp. 629-653.

Kramers, J.W., 1974. "Geology of the Wabasca A Oil Sands Deposit (Grand Rapids Formation)", Can. Soc. Petrol. Geol., Mem. 3, "Oil Sands, Fuel of the Future?", ed. L.V. Hills, Calgary, Alberta, pp. 68-83.

Krauskopf, K.B., 1959. "The geochemistry of silica in sedimentary environments", Proc. Soc. Econ. Paleontologists and Mineralogists, Spec. Publ. 7, pp. 4-19.

Krinsley, D.H., and Donahue, J., 1968. "Environmental interpretation of sand grain surface features by electron microscopy", Geol. Soc. of America Bulletin, Vol. 79, pp. 743-748.

Krinsley, D.H., and Doornkamp, J., 1973. "Atlas of quartz sand surface textures", Cambridge University Press, Cambridge, 91 pp.

Krinsley, D.H., and Margolis, S., 1968. "A study of quartz sand grain surface textures with the S.E.M.", Trans. New York Acad. Sci. (Section of Geological Sciences), Vol. 31, pp. 457-477.

Ladanyi, B., and Archambault, G., 1969. "Simulation of shear behaviour of a jointed rock mass", 11th Symp. on Rock Mech., ASCE, Berkeley, pp. 105-125.

Larsen, G., and Chilingar, G.V., (eds.), 1967. "Diagenesis in sediments", Developments in Sedimentology No. 8, Elsevier, Amterdam, 551 pp.

Lerbekmo, J.F., and Platt, R.L., 1962. "Promotion of pressure solution of silica in sandstones", Jour. Sed. Petrology, Vol. 32, No. 3, pp. 514-519.

Margolis, S.V., 1968. "Electron microscopy of chemical solution and mechanical abrasion features on quartz sand grains", Sedimentary Geol., Vol. 2, pp. 243-256.

Maxwell, J.C., 1964. "Influence of depth, temperature, and age on porosity of quartzose sandstone", Amer. Assoc. Petrol. Geol. Bulletin, Vol. 48, pp. 697-709.

Milligan, M.F., 1976. "Model studies for a friable sandstone", unpublished M.Sc. Thesis, University of Alberta, Edmonton, Alberta.

Mizutani, S., 1970. "Silica minerals in the early stage of diagenesis", Sedimentology, Vol. 15, pp. 419-436.

Mossop, G.D., 1978. "Geological controls on reservoir heterogeneity - Athabasca Oil Sands", Proc. Sem. on Underground Excavation in Oil Sands, Dept. of Civil Eng., University of Alberta, Edmonton, Alberta, Paper No. 1.

Novelli, L., and Mattavelli, L., 1967. "Diagenetic phenomena in sandstones of the 'Collesano' Formation (Sicily)", (in Italian), Rend. Soc. Mineral. Ital. 23, pp. 333-350.

Okamoto, G., Okura, T., and Goto, K., 1957. "Properties of silica in water", Geochim. Cosmochim. Acta, Vol. 12, pp. 123-132.

Paterson, M.S., 1973. "Non-hydrostatic thermodynamics and its geologic implications", Reviews of Geophysics and Space Physics, Vol. 11, pp. 355-389.

Patton, F.D., 1966. "Multiple modes of shear failure in rocks", Proc. 1st Int. Congress of the Int. Soc. of Rock Mech., Lisbon, Vol. 1, pp. 509-513.

Pettijohn, F.J., Potter, P.E., and Siever, R., 1972. "Sand and sandstone", Springer-Verlag, New York, 618 pp.

Phillip, W., Drong, H.J., Fuchtbauer, H., Haddenhorst, H.G., and Jankowsky, W., 1963. "The history of migration in the Gifhorn trough (NW Germany)", Proc. 6th World Petrol. Congress, Frankfurt, Sec. I, Paper 19, PD 2, pp. 457-481.

Pittman, E.D., 1972. "Diagenesis of quartz in sandstones as revealed by scanning electron microscopy", Jour. Sed. Petrology, Vol. 42, No. 3, pp. 507-519.

Renton, J.H., Heald, M.T., and Cecil, C.B., 1969. "Experimental investigation of pressure solution of quartz", Jour. Sed. Petrology, Vol. 39, No. 3, pp. 1107-1117.

Rittenhouse, G., 1971. "Pore space reduction by solution and cementation", Bulletin Amer. Soc. Petrol. Geol., Vol. 55, pp. 80-91.

Rosengren, K.J., and Jaeger, J.C., 1968. "The mechanical properties of an interlocked low-porosity aggregate", Geotechnique, Vol. 18(3), pp. 317-326.

Rowe, P.W., 1962. "The stress-dilatency relation for static equilibrium of an assembly of particles in contact", Proc. Royal Soc. of London, A269, pp. 500-527.

Rutter, E.H., 1976. "The kinetics of rock deformation by pressure solution", Phil. Trans. Royal Soc. of London, A283, pp. 203-219.

Rutter, E.H., 1978. "Discussion on pressure solution", Jour. Geol. Soc. of London, Vol. 135 Part 1, p. 135.

Selley, R.C., 1978. "Porosity gradients in North Sea oil-bearing sandstones", Jour. Geol. Soc. of London, Vol. 135, Part 1, pp. 119-132.

Sellwood, B.W., and Parker, A., 1978. "Observations on diagenesis in North Sea reservoir sandstones", disc. cont., Jour. Geol. Soc. of London, Vol. 135, Part 1, pp. 133-135.

Sibley, D.F., and Blatt, H., 1976. "Intergranular pressure solution and cementation of the Tuscarora Orthoquartzite", Jour. Sed. Petrology, Vol. 46, pp. 881-896.

Siever, R., 1957. "The silica budget in the sedimentary cycle", Amer. Mineralogist, Vol. 42, pp. 821-841.

Siever, R., 1959. "Petrology and geochemistry of silica cementation in some Pennsylvania sandstones", Soc. Econ. Paleontologists and Mineralogists, Spec. Publ. 7, pp. 55-79.

Siever, R., 1962. "Silica solubility, 0°-200°C, and the diagenesis of siliceous sediments", Jour. Geol., Vol. 70, No. 2, pp. 127-150.

Skempton, A.W., and Bishop, A.W., 1950. "The measurement of the shear strength of soils", Geotechnique, Vol. 2, No. 2, pp. 90-108.

Sloss, L.L., and Feray, D.E., 1948. "Microstylolites in sandstone", Jour. Sed. Petrology, Vol. 18, pp. 3-13.

Sprunt, E.S., and Nur, A., 1976. "The reduction of porosity by pressure solution: experimental verification", Geology, Vol. 4, pp. 463-466.

Taber, S., 1916. "The growth of crystals under external pressure", Amer. Jour. Sci., Vol. 41 (191), pp. 532-556.

Taylor, J.M., 1950. "Pore space reduction in sandstones", Bulletin Amer. Assoc. Petrol. Geol., Vol. 34, pp. 701-716.

Taylor, J.C.M., 1978a. "Control of diagenesis by depositional environment within a fluvial sandstone sequence in the northern North Sea Basin", Jour. Geol. Soc. of London, Vol. 135, Part 1, pp. 83-91.

Taylor, J.C.M., 1978b. "Discussion on pressure solution", Jour. Geol. Soc. of London, Vol. 135, Part 1, pp. 134-135.

Thomson, A., 1959. "Pressure solution and porosity", Proc. Soc. Econ. Paleontologists and Mineralogists, Spec. Publ. 7, pp.92-109.

Trurnit, P., 1967. "Pressure solution phenomena in detrital rocks", Sedimentary Geol., Vol. 2, pp. 89-114.

Vesic, A.S., and Clough, G.W., 1968. "Behaviour of granular materials under high stresses", ASCE, Jour. Soil Mech. and Found. Div., 94(SM3), pp. 661-688.

Waugh, B., 1970. "Formation of quartz overgrowths in the Penrith sandstone (lower Permian) of northwest England as revealed by scanning electron microscopy", Sedimentology, Vol. 14, pp. 309-320.

Weyl, P.K., 1959. "Pressure solution and the force of crystallization - a phenomenological theory", Jour. Geophysical Research, Vol. 64, No. 11, pp. 2001-2025.

APPENDIX A LIST OF SYMBOLS

Symbol	Units	Definition
γ_{sat}	g/cm^3	saturated density
γ_{bulk}	g/cm^3	bulk density
γ_{dry}	g/cm^3	dry density
w	%	water content
n	%	porosity = volume of voids/total volume
e	-	void ratio = volume of voids/volume of solids
e_{max}	-	maximum void ratio at which soil can be placed
e_{min}	-	minimum void ratio to which material can be compacted (dry compaction)
I_D	%	density index = $\frac{e_{max} - e}{e_{max} - e_{min}}$
D_{60}	mm	60% of soil weight is finer than diameter D_{60}
D_{50}	mm	50% of soil weight is finer than diameter D_{50}
D_{10}	mm	10% of soil weight is finer than diameter D_{10}
C_u	-	coefficient of uniformity = D_{60}/D_{10}
m_v	kPa^{-1}	coefficient of compressibility
a_v	kPa^{-1}	modulus of compressibility, slope of void ratio vs. stress curve
σ_N	kPa	normal stress on soil in direct shear test
τ_p	kPa	peak shearing stress on soil in direct shear test
τ_r	kPa	residual shearing stress on soil in direct shear test
τ_f	kPa	the portion of τ_p above τ_r which results from shearing of grains
τ_d	kPa	the portion of τ_p above τ_r which results from dilatency

Symbol	Units	Definition
$\tan^{-1}(\tau_p/\sigma_N)$	°	secant angle of peak shearing resistance
$\tan^{-1}(\tau_r/\sigma_N)$	°	secant angle of residual shearing resistance
ε_f	cm	displacement at failure
ΔV_f	%/cm	dilatency rate at failure
a	-	correlation parameter for shear strength $\tau_p = a\ \sigma_N{}^b$
b	-	correlation parameter for shear strength $\tau_p = a\ \sigma_N{}^b$

APPENDIX B SAMPLE PREPARATION AND TEST METHODS

B.1 Direct Shear Tests

As discussed above, oil-free samples of McMurray and Grand Rapids Formations were obtained from river valley outcrops in the Fort McMurray area. These specimens were cut from the outcrop face and placed in plastic bags. They were then wrapped in fiberglass tape which provided an all-round confining pressure. The samples were extremely delicate, and this confining pressure was required to keep them intact.

The direct shear test specimens were trimmed from the block samples into a circular brass cutting ring with a bevelled edge. The cutting ring used for samples tested at a normal stress level of 2000 kPa and below was 6.35 cm in diameter and 2.54 cm high, whereas the ring used for specimens tested at higher stresses was 5.08 cm in diameter and 3.0 cm high. The top of the block sample was levelled and the cutting ring was then placed on top. The sand surrounding the cutting edge was carefully trimmed away and the ring pushed down over the sand until approximately 5 to 10 mm of sand protruded above the top of the ring (Figure B.1). The top and bottom of the shear specimen were then levelled off with a straight edge, and the sample was extruded into a circular shear box the same diameter as the cutting ring.

The tests were conducted in a standard direct shear testing appartus, with normal load applied to the sample by use of a hanger and lever arm. A high-capacity direct shear frame was used for the tests conducted above a normal stress level of 2000 kPa. As the samples had very low moisture content, the tests were conducted on unsaturated specimens.

Evaluation of the residual strength of the test specimens was carried out for samples of Grand Rapids Formation, and for samples of McMurray Formation above a normal stress level of 2000 kPa. Five or six residual cycles were run in addition to the peak cycle.

The tests were conducted using a rate of horizontal displacement of .00083 mm/sec for the peak cycle. Residual cycles were conducted at a rate of .0033 mm/sec except for the final cycle, which was slowed to .00083 mm/sec.

Measurements of shear stress, horizontal displacement, and vertical displacement were recorded during each test. These measurements were recorded by an automatic data aquisition system. Plots of shear stress vs. horizontal displacement and vertical displacement vs. horizontal displacement were constructed for all tests. A Mohr-Coulomb envelope has been drawn for each set of test data on the five main sample groups.

The density of the samples was measured in the direct shear cutting ring. Moisture content analysis was performed on the trimmings from each direct shear sample. The density measured by this method is lower than the actual value. This is due to the inaccuracy involved in the sample trimming. Although the specimens are intact and of high quality, small gaps created by the plucking of sand grains from the structure will exist next to the cutting ring.

This lowers the measured density value. The inaccuracy of the sample trimming increases with increased grain size, as larger grains must be removed and larger gaps will be created. The density value in thus lowered by the greatest amount in the samples of coarse-grained McMurray Formation due to the presence of pebbles two to three mm in diameter. This error will not have a large effect on the shear strength of the samples, and the measured value of shear strength will always be lowered by this error.

B.2 Compressibility Tests

Standard one-dimensional or oedometric compressibility tests were conducted on the oil-free samples of McMurray and Grand Rapids Formations. The tests were conducted over a stress range of 3 to 16 MPa. A dead loading frame with lever arm was used to apply stress to the sample.

The samples were trimmed into a circular brass cutting ring 5.08 cm in diameter by 3.0 cm high in the same manner as for the direct shear tests (Figure B.1). The samples were then extruded into the consolidometer. Stress was applied in a vertical direction, with a condition of no lateral yield. As discussed above, some error was involved in the sample trimming. This error will be most important in coarse-grained materials. The error will cause the measured value of compressibility to be higher than the actual value.

An LVDT was used to measure displacement of the sample and a load cell was used to measure the applied stress. The vertical LVDT was mounted on the loading ram of the apparatus, thus no reading could be taken until the initial load of 3 MPa (weight of lever arm and pan) was seated. Thus the exact void ratio under the initial loading increment could not be measured. As a result of this, the modulus of compressibility a_v was calculated and not the coefficient of compressibility m_v. The value a_v is the slope of the void ratio vs. stress curve. The two values are related as follows:

$$a_v=(1+e_o)m_v$$

where e_o is the initial void ratio.

Plots of void ratio vs. stress have been constructed for each test, using the assumption that the void ratio under zero stress is equal to that under the initial loading increment of 3 MPa.

B.3 Grain Size Distribution

The grain size distribution of each of the five main sample groups was analyzed. The samples were washed through a no. 200 sieve (0.074 mm diameter) and oven-dried. The material was then sieved to determine the grain size distribution. Standard ASTM procedure was followed, except that all available sieve sizes were used in the analysis. The parameters D_{10}, D_{50}, D_{60}, and c_u were calculated for each test conducted.

In addition to analysis of the original samples, the grain size distribution of the direct shear test samples after shearing was analyzed to evaluate the extent of grain crushing during shear.

B.4 Density Tests

The density of the five main test materials was measured by air-drying an intact sample of approximately 100 grams and carefully weighing it in a wire mesh basket. The specimen was then immersed in hot carnuba wax which was allowed to penetrate into the pores. Because the wax was used at high temperature, when the sample was removed from the container all the excess wax ran off the sides and through the wire mesh. The sample was thus completely sealed and the original volume was maintained. The volume was then measured by mercury displacement.

A minimum of four specimens were tested for each sample group. Three trials of volume measurement by mercury displacement were performed for each specimen. The results are tabulated as saturated density with a range of measurement error.

Two main errors are associated with this procedure. Firstly, the actual weight of the sample may be slightly less than the measured value, as occasional grains of sand are lost during wax immersion. This loss was observed to be very small. Secondly, the actual volume may be slightly less than the measured volume due to the presence of a thin coating of wax on the outside of the sample. Again, this coating was observed to be very thin, and its influence is probably negligible. The first error, loss of sand grains, will tend to give a measured density higher than the actual value, whereas the second error, the wax coating, will tend to give a density value lower than reality. Thus these two errors will tend to compensate.

B.5 Density Index Tests

The density index (formerly relative density) of each of the five main test materials was evaluated using the ASTM dry procedure. For the minimum density measurement, the dry disaggregated material was poured through a funnel with a 1.9 mm diameter neck into a standard Proctor mold. The top of the mold was removed and the material was screed off with a straight edge. The soil was then weighed and the density was calculated.

The same method of soil placement was used for the maximum density determination, except that the was material was compacted by five minutes of vibration at maximum amplitude on a vibrating table with a 25 pound surcharge weight applied to the soil. Three trials of maximum and minimum density were performed for each sample type.

A higher value could have been obtained for the maximum density by using the wet compaction method. However, the interest was in comparison of the samples and in illustrating the influence of diagenetic alteration on porosity and density.

The density index I_D was calculated as follows:

$$I_D = \frac{e_{max} - e}{e_{max} - e_{min}}$$

where e_{max} is the maximum void ratio, e_{min} is the minimum void ratio, and e is the *in situ* void ratio.

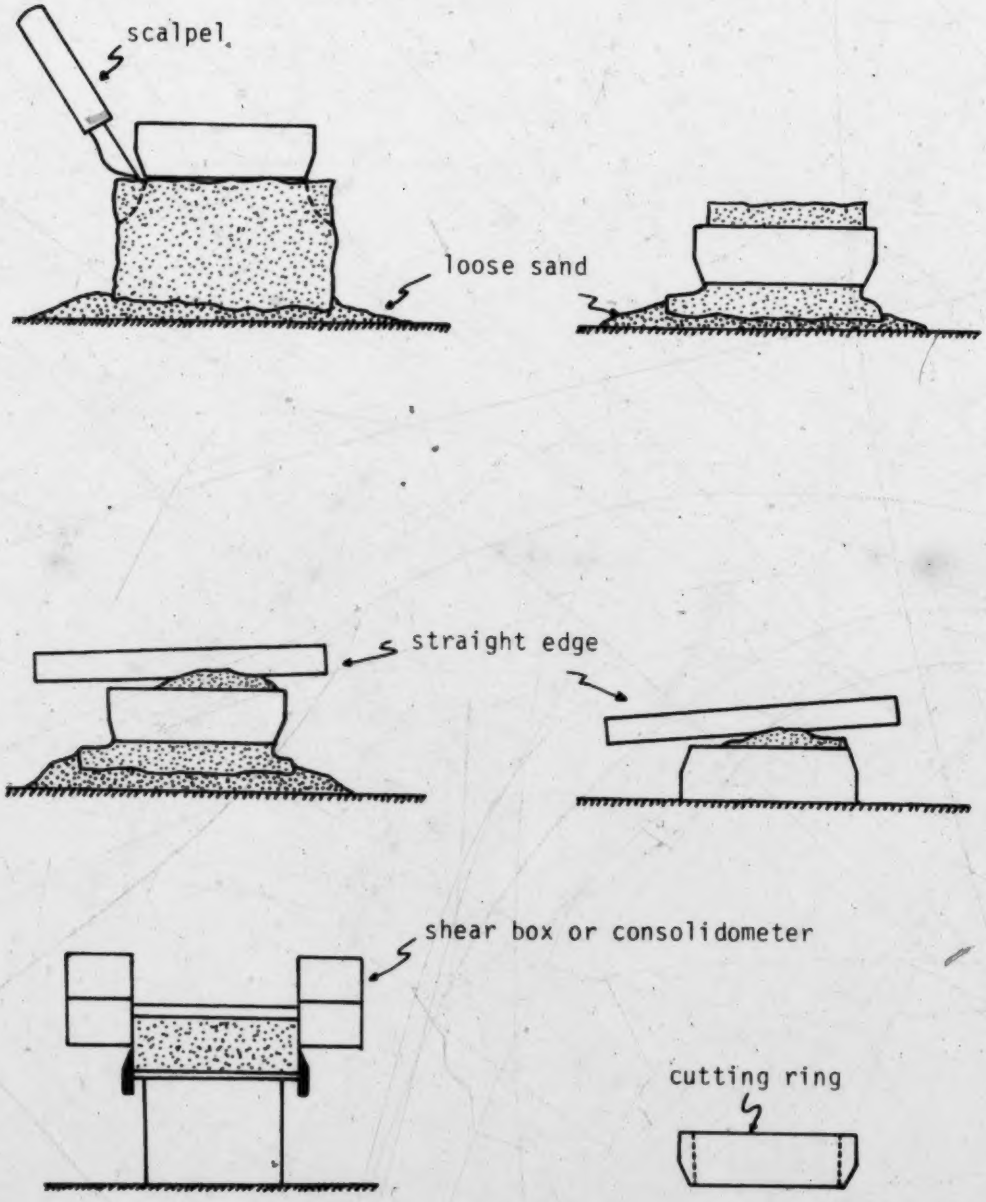
scalpel
loose sand
straight edge
shear box or consolidometer
cutting ring

Figure B.1: Method of sample trimming for direct shear and consolidation test specimens.

APPENDIX C TEST RESULTS

C.1 Direct Shear Test Results

Complete results for all direct shear tests conducted are presented herein. Section C.1.1 contains summary tables of the direct shear test results for all five major sample groups. Section C.1.2 contains plots of shear stress vs. normal stress, secant angle of shearing resistance vs. normal stress, and dilatency rate at failure vs. normal stress for each sample group.

Results of individual tests are presented in section C.1.3. Plots of shear stress vs. horizontal displacement and vertical displacement vs. horizontal displacement are included for all tests conducted, together with the grain size distribution curves after shearing.

In each section, the data for the materials is presented in the following order: fine-, medium-, and coarse-grained McMurray Formation, Grand Rapids Formation A, and Grand Rapids Formation C.

C.1.1 Summary Tables of Direct Shear Test Results

Table C.1: Direct shear test data summary for fine-grained McMurray Formation

Sample	σ_N (kPa)	τ_p (kPa)	$\tan^{-1}(\tau_p/\sigma_N)$ (o)	τ_r (kPa)	$\tan^{-1}(\tau_r/\sigma_N)$ (o)	ε_f (cm)	$\Delta\dot{V}_f$ (%/cm)	γ_{bulk}[1] (g/cm^3)	γ_{sat}[1] (g/cm^3)	γ_{dry}[1] (g/cm^3)	w (%)
FG-1-79	100	130.2	52.5	—	—	0.177	13.7	1.79	2.03	1.66	7.7
FG-2-79	250	305.6	50.7	—	—	0.185	9.9	1.71	2.01	1.62	5.3
FG-3-79	400	382.2	43.7	—	—	0.165	6.3	1.79	2.04	1.67	6.8
FG-4-79	700	659.7	43.3	—	—	0.182	6.3	1.71	2.01	1.63	5.3
FG-5-79	1000	1040.0	46.1	—	—	0.185	6.8	1.85	2.07	1.72	7.8
FG-6-79	2000	1770.3	41.5	1300	33.0	0.283	8.2	1.73	2.02	1.64	5.0
FG-7-79	3000	2553.4	40.4	1994	33.6	0.301	2.8	1.74	2.04	1.66	4.8
FG-8-79	4000	2946.1	36.4	2383	30.8	0.230	2.6	1.70	2.01	1.62	5.3
FG-9-79	5000	3698.7	36.5	2869	29.9	0.170	2.6	1.71	2.01	1.63	5.1

1. Densities were measured in the direct shear cutting ring, thus the measured value is less than the actual value.

Table C.2: Direct shear test data summary for medium-grained McMurray Formation

Summary	σ_N (kPa)	τ_p (kPa)	$\tan^{-1}(\tau_p/\sigma_N)$ (o)	τ_r (kPa)	$\tan^{-1}(\tau_r/\sigma_N)$ (o)	ϵ_f (cm)	$\Delta\dot{V}_f$ (%/cm)	γ_{bulk}^{1} (g/cm^3)	γ_{sat}^{1} (g/cm^3)	γ_{dry}^{1} (g/cm^3)	w (%)
MG-1-78	116	141.6	50.6	—	—	0.155	13.8	—	—	—	—
MG-2-78	242	255.6	46.5	—	—	0.183	7.7	1.57	1.97	1.55	1.3
MG-3-78	400	340.5	40.4	—	—	0.184	6.0	—	—	—	1.1
MG-4-78	700	511.6	36.1	—	—	0.332	4.1	1.61	1.99	1.59	1.4
MG-5-78	1000	719.0	35.7	—	—	0.308	4.0	1.64	2.01	1.62	1.4
MG-6-79	2000	1543.1	37.7	1220	31.4	0.241	6.5	1.67	2.03	1.63	1.3
MG-7-79	3000	2040.3	34.2	1958[2]	33.1[2]	0.167	1.5	1.65	2.03	1.65	0.1
MG-8-79-1	4000	2136.3	28.1	2103[2]	27.7[2]	0.422	-0.5	1.57	1.96	1.54	1.6
MG-8-79-2	4000	2193.5	28.7	2193[2]	28.7[2]	0.493	-0.3	1.66	2.01	1.62	2.3
MG-9-79	5000	2811.1	29.3	2784[2]	29.1[2]	0.415	-0.7	1.62	1.99	1.59	1.9

1. Densities were measured in the direct shear cutting ring, thus the measured value is less than the actual value.

2. These values are an upper bound estimate of residual as the shear stress increased with each successive residual cycle.

Table C.3: Direct shear test data summary for coarse-grained McMurray Formation

Summary	σ_N (kPa)	τ_p (kPa)	$\tan^{-1}(\tau_p/\sigma_N)$ (o)	τ_r (kPa)	$\tan^{-1}(\tau_r/\sigma_N)$ (o)	c_f (cm)	$\Delta\dot{V}_f$ (%/cm)	γ_{bulk}^1 (g/cm^3)	γ_{sat}^1 (g/cm^3)	γ_{dry}^1 (g/cm^3)	w (%)
CG-1-79	100	151.5	56.6	—	—	0.199	15.8	1.81	2.12	1.79	0.9
CG-2-79	250	288.9	49.1	—	—	0.277	9.2	1.79	2.10	1.77	1.1
CG-3-79	400	498.1	51.2	—	—	0.265	9.0	1.86	2.15	1.85	0.6
CG-4-79	700	645.7	42.7	—	—	0.296	5.8	1.75	2.08	1.73	1.1
CG-5-79	1000	873.9	41.2	—	—	0.272	—	1.73	2.06	1.71	1.1
CG-6-79	2000	1443.4	35.8	1290	32.8	0.432	2.2	1.80	2.12	1.79	0.7
CG-7-79-1	3000	2520.5	40.0	2335^2	37.9^2	0.298	2.8	1.79	2.08	1.74	2.8
CG-7-79-2	3000	2350.3	38.1	2350^2	38.1^2	0.578	0.8	1.79	2.08	1.74	2.8
CG-8-79	4000	2565.5	32.7	2565^2	32.7^2	0.537	0.7	1.75	2.06	1.70	2.7
CG-9-79	5000	3404.5	34.3	3404^2	34.3^2	0.595	0.6	1.81	2.10	1.77	2.5

1. Densities were measured in the direct shear cutting ring, thus the measured value is less than the actual value.

2. These values are an upper bound estimate of residual as the shear stress increased with each successive residual cycle.

Table C.4: Direct shear test data summary for Grand Rapids Formation A

Sample	σ_N (kPa)	τ_p (kPa)	$\tan^{-1}(\tau_p/\sigma_N)$ (o)	τ_r (kPa)	$\tan^{-1}(\tau_r/\sigma_N)$ (o)	ϵ_f (cm)	$\Delta\dot{V}_f$ (%/cm)	γ_{bulk}[1] (g/cm^3)	γ_{sat}[1] (g/cm^3)	γ_{dry}[1] (g/cm^3)	w (%)
GRA-1-79	100	162.9	58.5	—	—	0.123	19.7	1.72	2.03	1.64	4.8
GRA-2-79	250	285.6	48.8	171	34.4	0.175	15.9	1.69	2.00	1.60	5.2
GRA-3-79	400	571.7	55.0	260	33.0	0.161	14.7	1.71	2.02	1.63	4.9
GRA-4-79	700	759.1	47.3	450	32.7	0.174	13.0	1.70	2.00	1.61	5.7
GRA-5-79	1000	929.1	42.9	600	31.0	0.177	—	1.69	2.00	1.60	5.3
GRA-6-79	2000	1558.8	37.9	1335[2]	33.7[2]	0.239	5.7	1.73	2.02	1.63	5.9
GRA-7-79	3000	2399.0	38.6	1824[2]	31.3[2]	0.136	3.0	1.70	2.02	1.63	4.6
GRA-8-79	4000	2839.1	35.4	2602[2]	33.0[2]	0.315	0.7	1.68	2.00	1.59	5.3
GRA-9-79	5000	3055.5	31.4	2930[2]	30.4[2]	0.323	-0.6	1.66	1.99	1.58	4.7

1. Densities were measured in the direct shear cutting ring, thus the measured value is less than the actual value.

2. These values are an upper bound estimate of residual as the shear stress increased with each successive residual cycle.

Table C.5: Direct shear test data summary for Grand Rapids Formation C

Sample	σ_N (kPa)	τ_p (kPa)	$\tan^{-1}(\tau_p/\sigma_N)$ (o)	τ_r (kPa)	$\tan^{-1}(\tau_r/\sigma_N)$ (o)	ε_f (cm)	$\Delta\dot{V}_f$ (%/cm)	γ_{bulk}[1] (g/cm^3)	γ_{sat}[1] (g/cm^3)	γ_{dry}[1] (g/cm^3)	w (%)
GRO-0-79	50	85.1	59.6	—	—	0.163	15.8	1.84	1.98	1.55	18.9
GRC-1-79	100	280.0	70.4	90	42.0	0.096	24.8	1.88	2.02	1.61	16.9
GRC-2-79	250	401.7	58.1	190	37.2	0.094	18.1	1.82	2.01	1.61	13.5
GRC-3-79	400	647.3	58.3	287	35.7	0.110	22.8	1.89	2.00	1.59	18.7
GRC-4-79	700	655.0	43.1	525	36.9	0.179	4.5	1.87	2.00	1.59	18.1
GRC-5-79	1000	911.2	42.4	728	36.1	0.210	3.7	1.87	2.03	1.63	14.9
GRC-6-79	2000	1450.5	36.0	1300[2]	33.0[2]	0.231	1.6	1.79	1.99	1.58	13.6
GRC-7-79-1	3000	1594.0	28.0	1447[2]	35.7[2]	0.177	-0.4	1.90	2.01	1.60	18.8
GRC-7-79-2	3000	1829.9	31.4	1727[2]	29.9[2]	0.340	-0.5	1.87	1.98	1.56	20.0
GRC-8-79	4000	2265.2	29.5	2189[2]	28.7[2]	0.357	-2.0	1.87	1.98	1.56	20.0
GRC-9-79	5000	2355.2	25.2	2355[2]	25.2[2]	0.587	-3.9	1.90	2.01	1.60	18.8

1. Densities were measured in the direct shear cutting ring, thus the measured value is less than the actual value.

2. These values are an upper bound estimate of residual as the shear stress increased with each successive residual cycle.

C.1.2 Summary Plots of Direct Shear Test Results

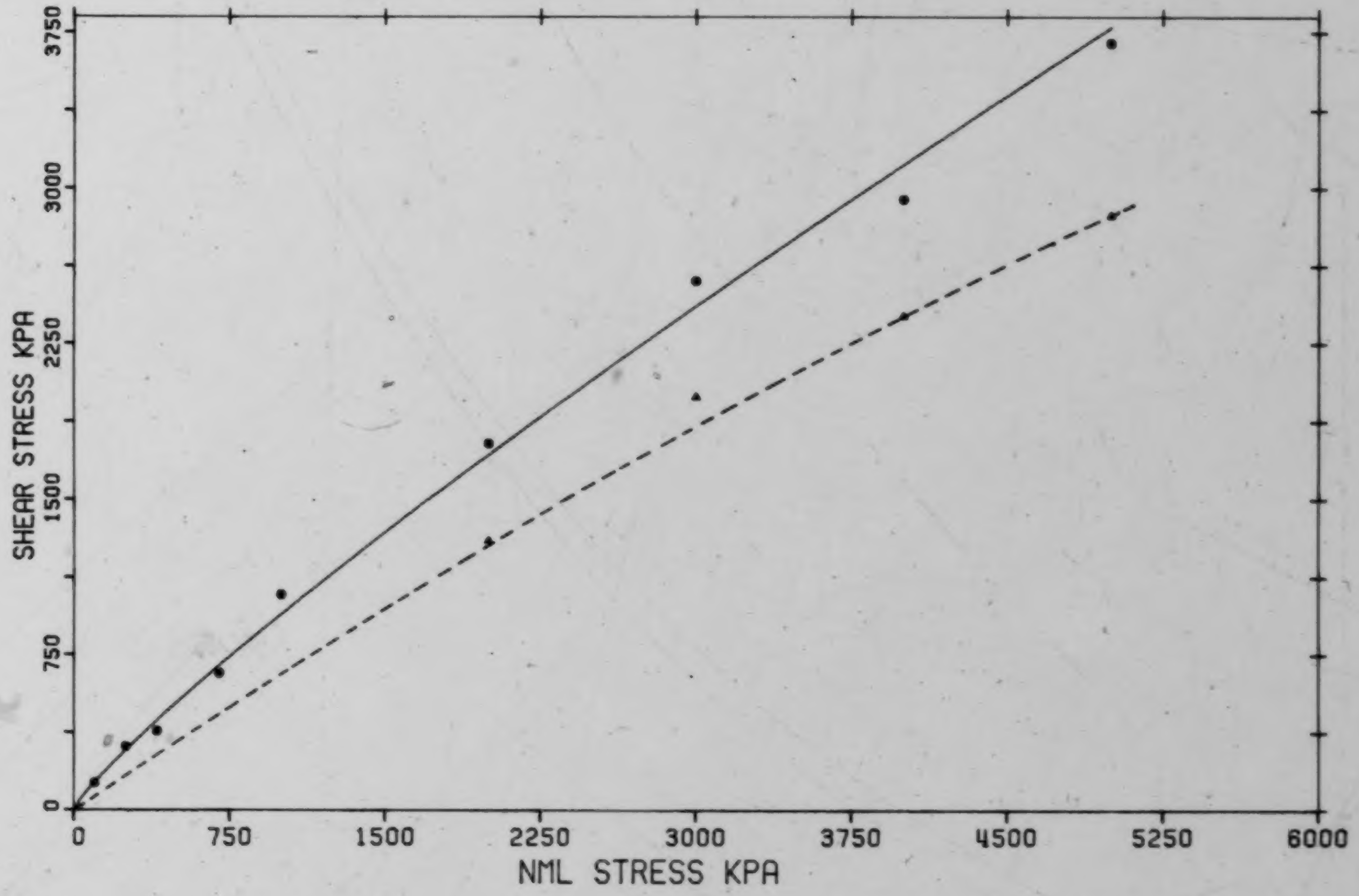

FG MCMURRAY FORMATION SHEAR VS NORMAL STRESS

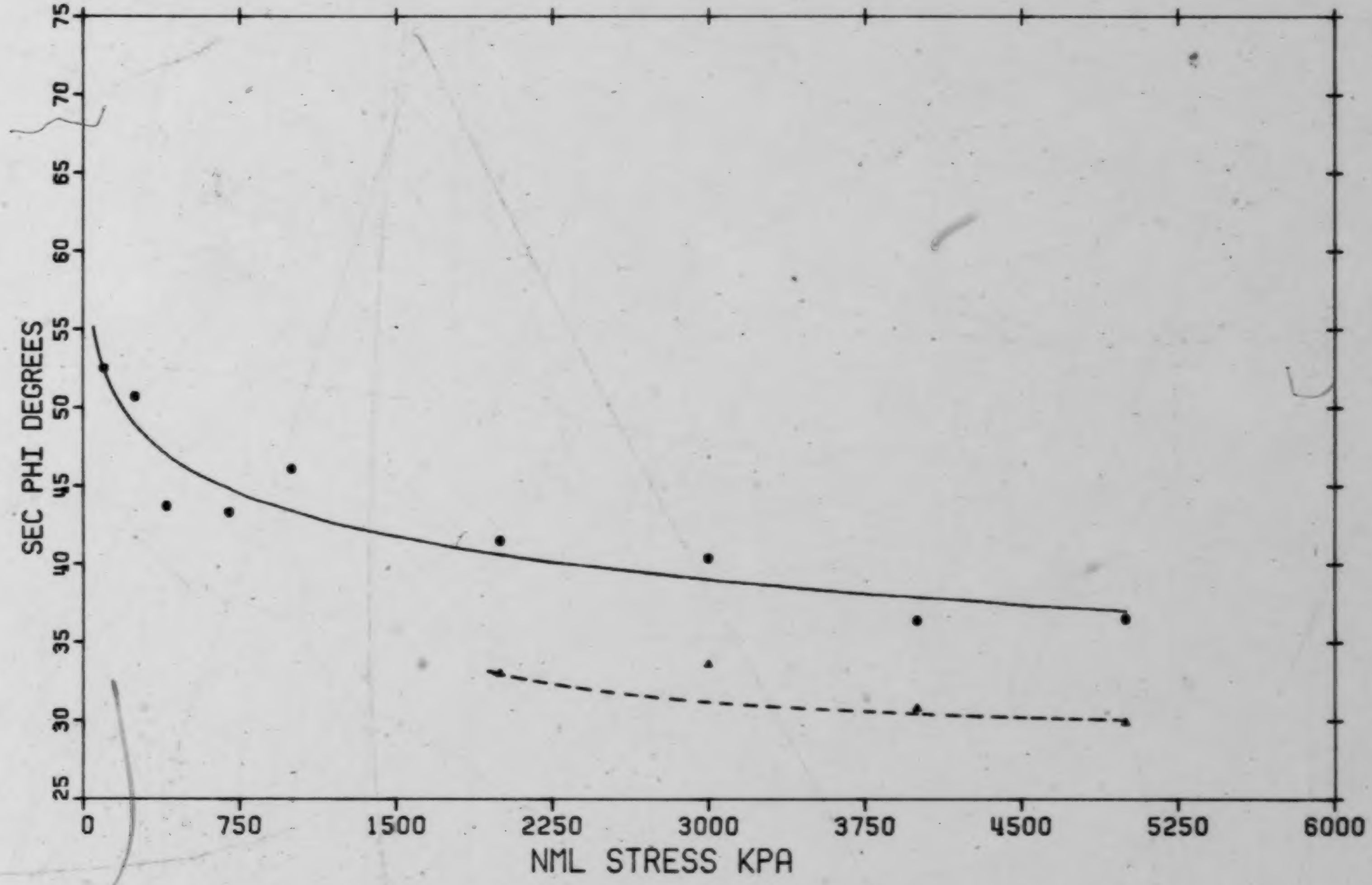

FG MCMURRAY FORMATION PHI VS NORMAL STRESS

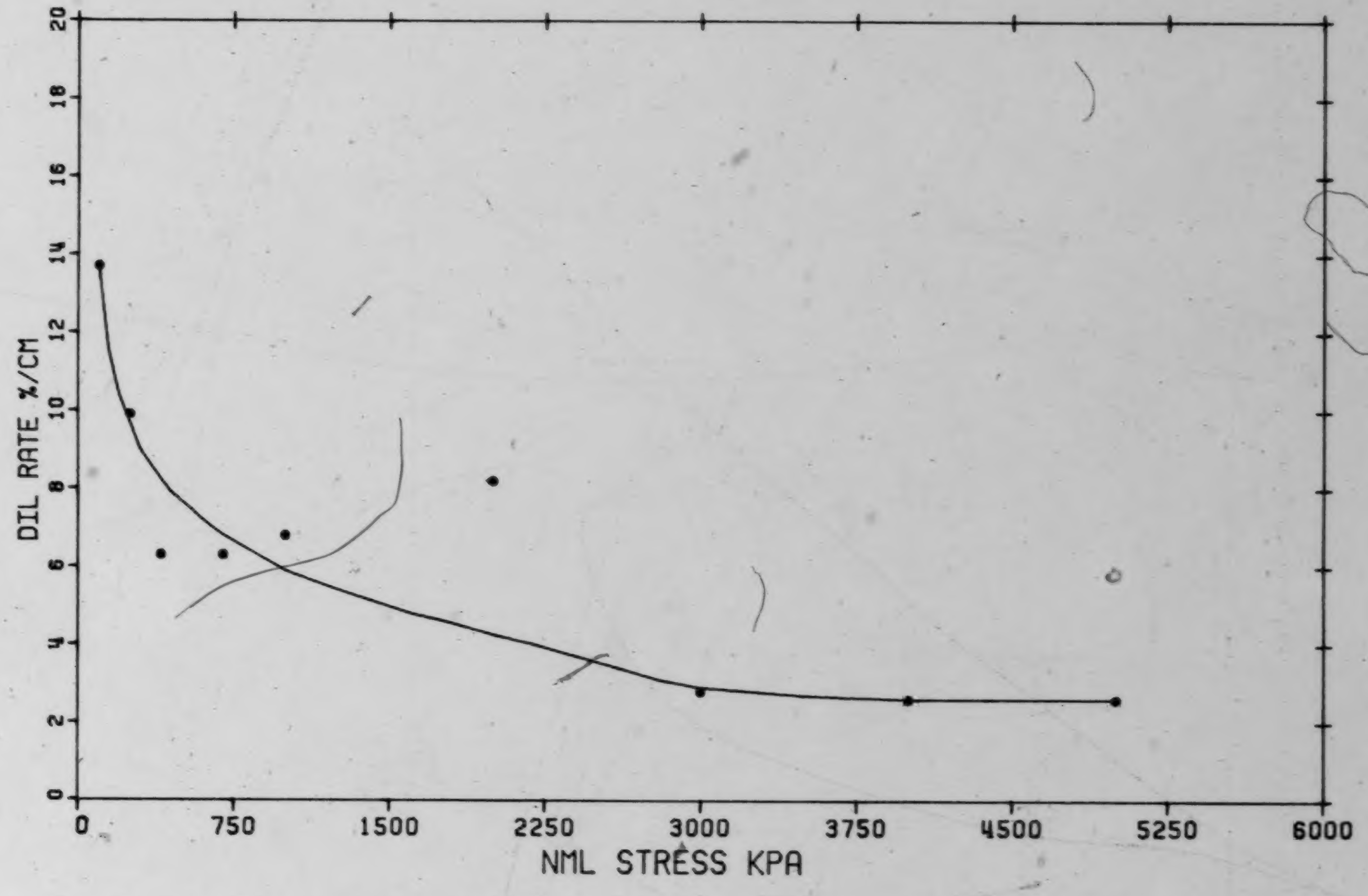

FG MCMURRAY FMN DILATENCY RATE VS NORMAL STRESS

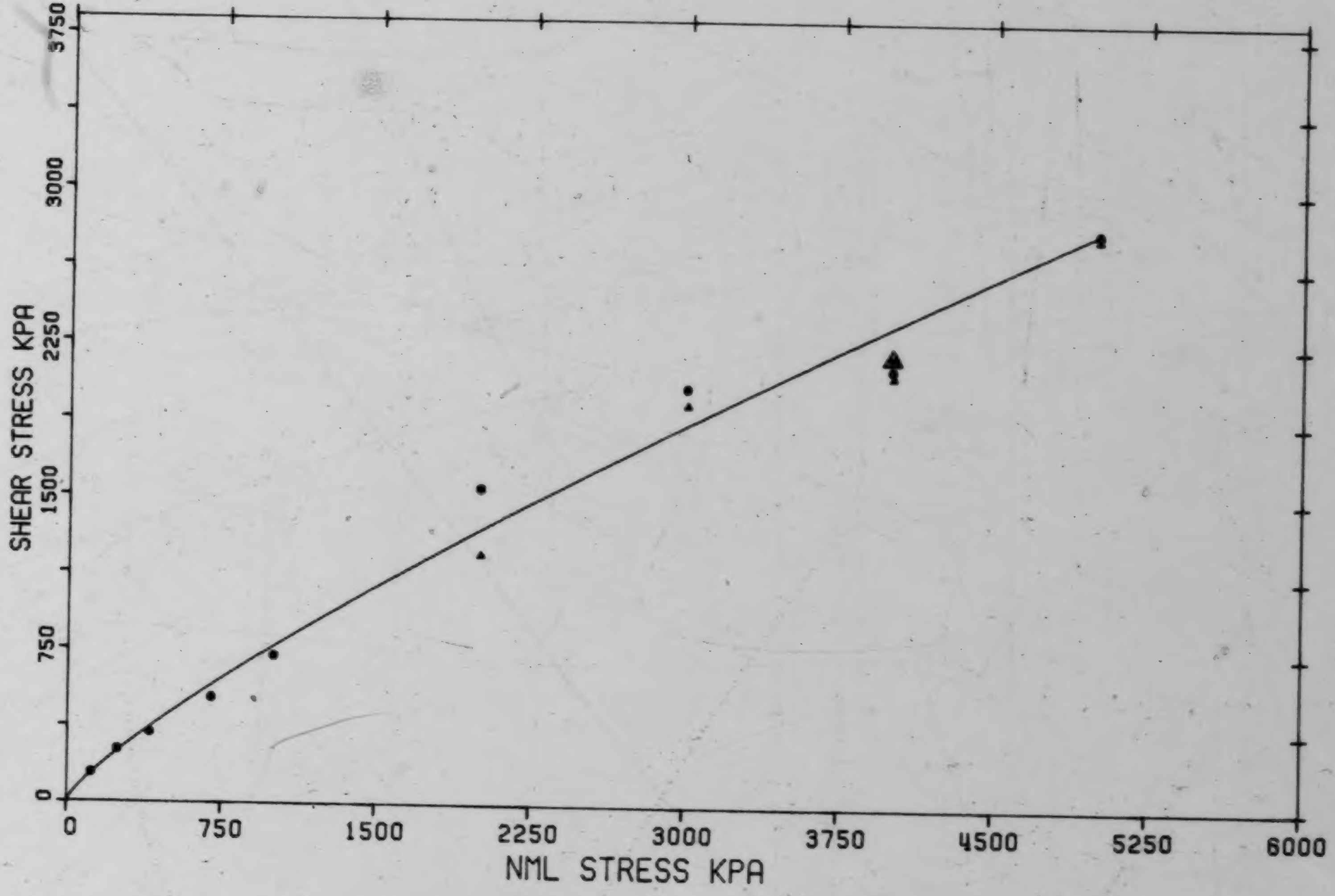

MG MCMURRAY FORMATION SHEAR VS NORMAL STRESS

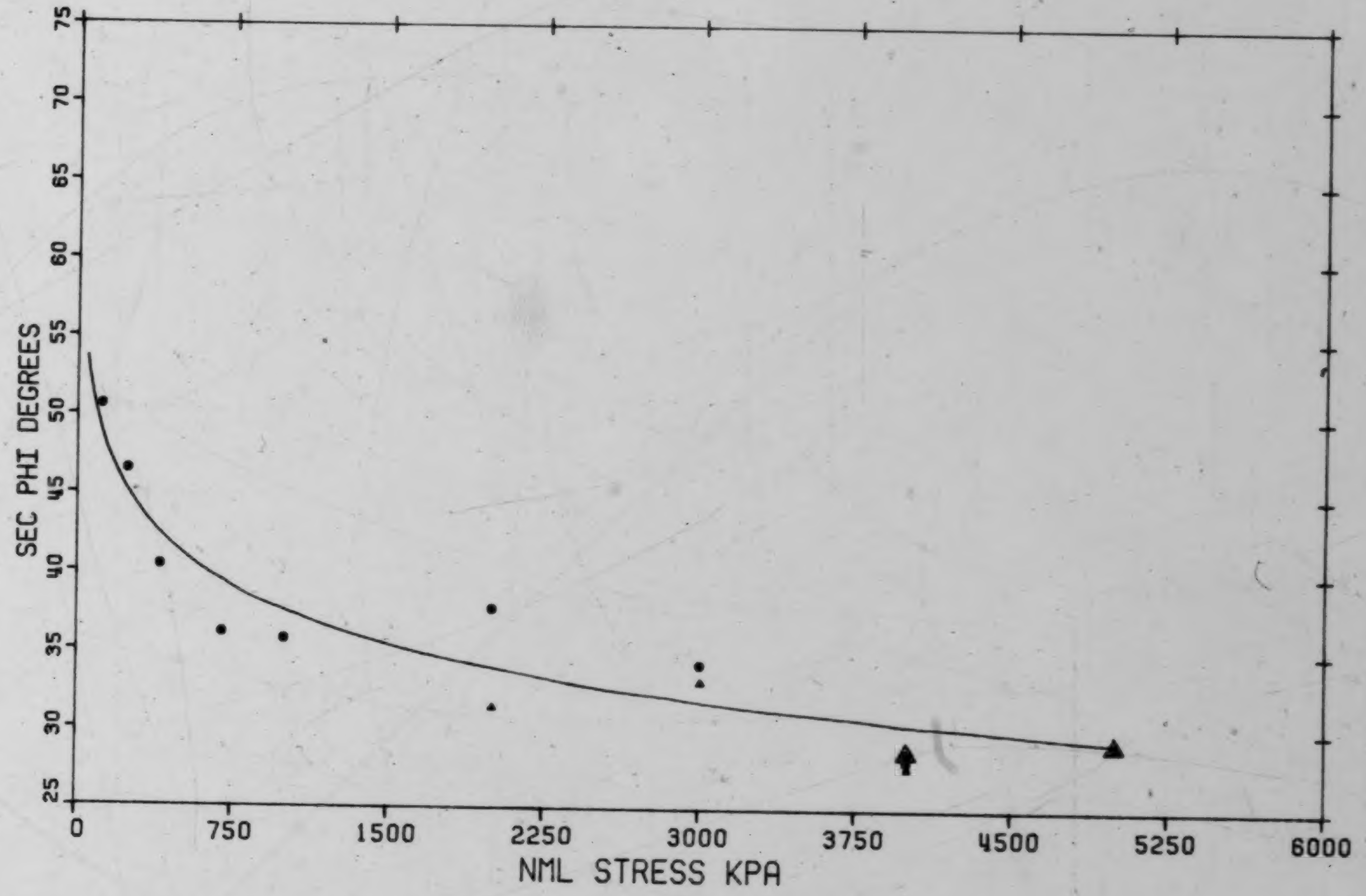

MG MCMURRAY FORMATION PHI VS NORMAL STRESS

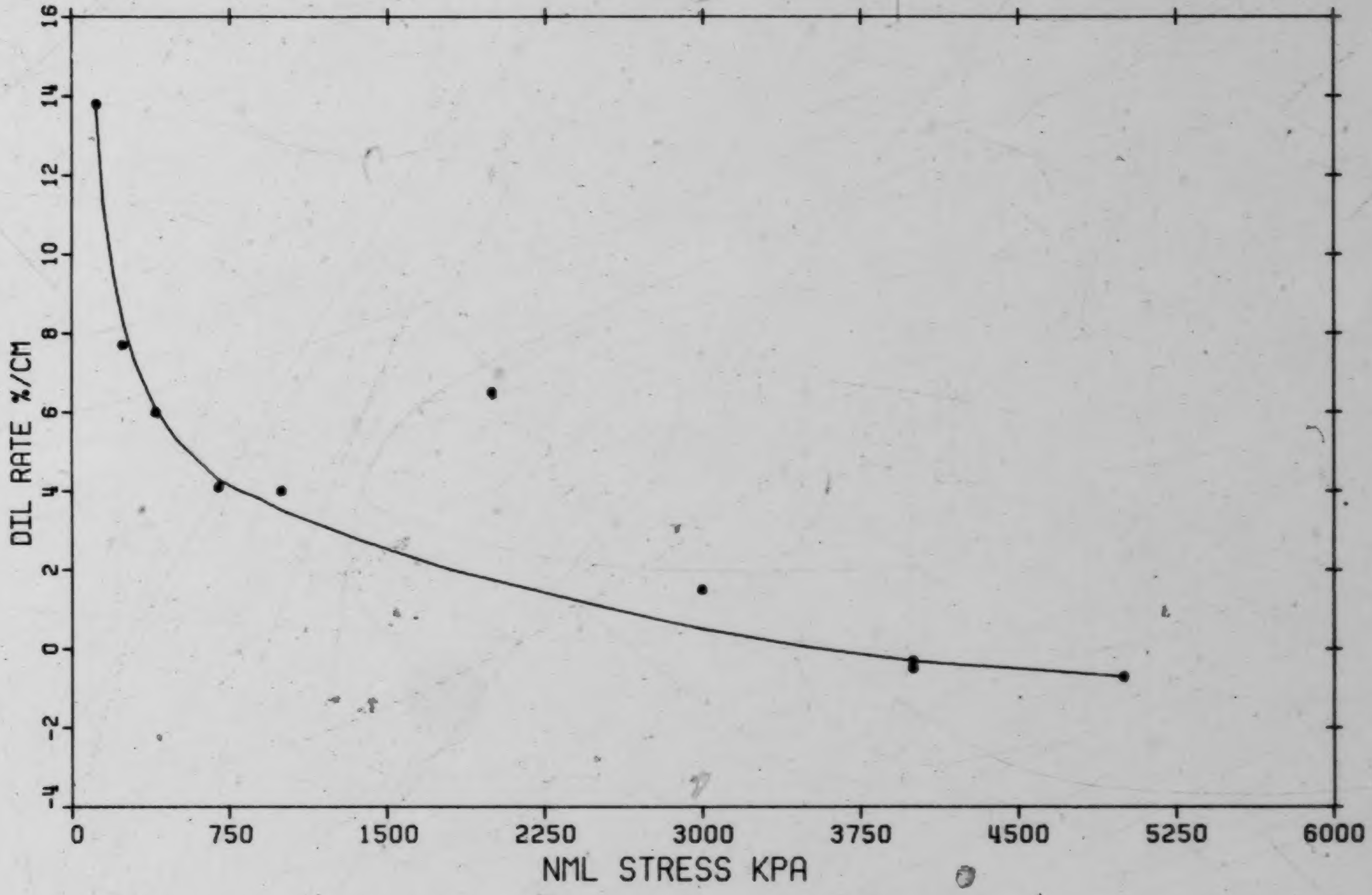

MG MCMURRAY FMN DILATENCY RATE VS NORMAL STRESS

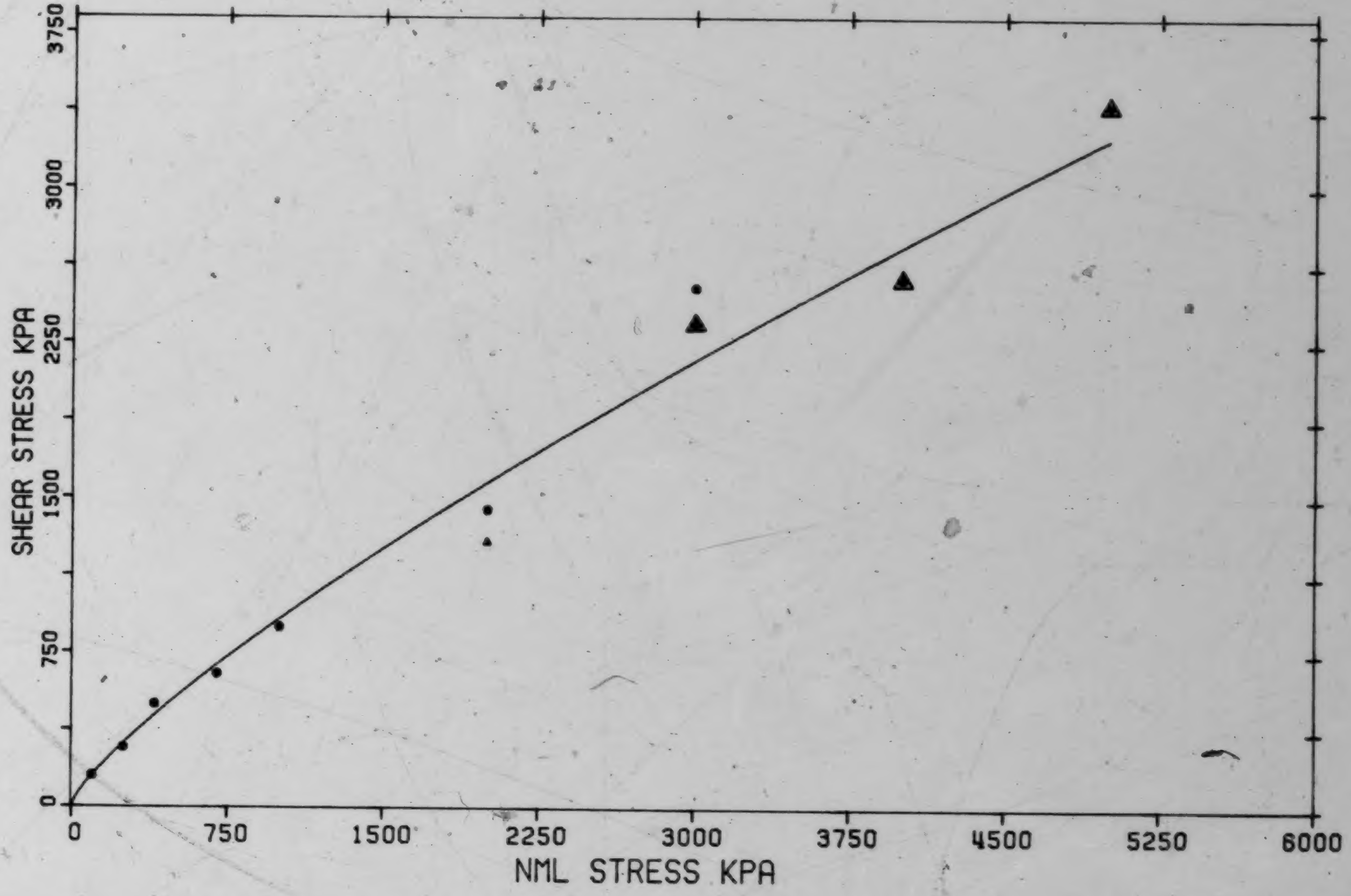

CG MCMURRAY FORMATION SHEAR VS NORMAL STRESS

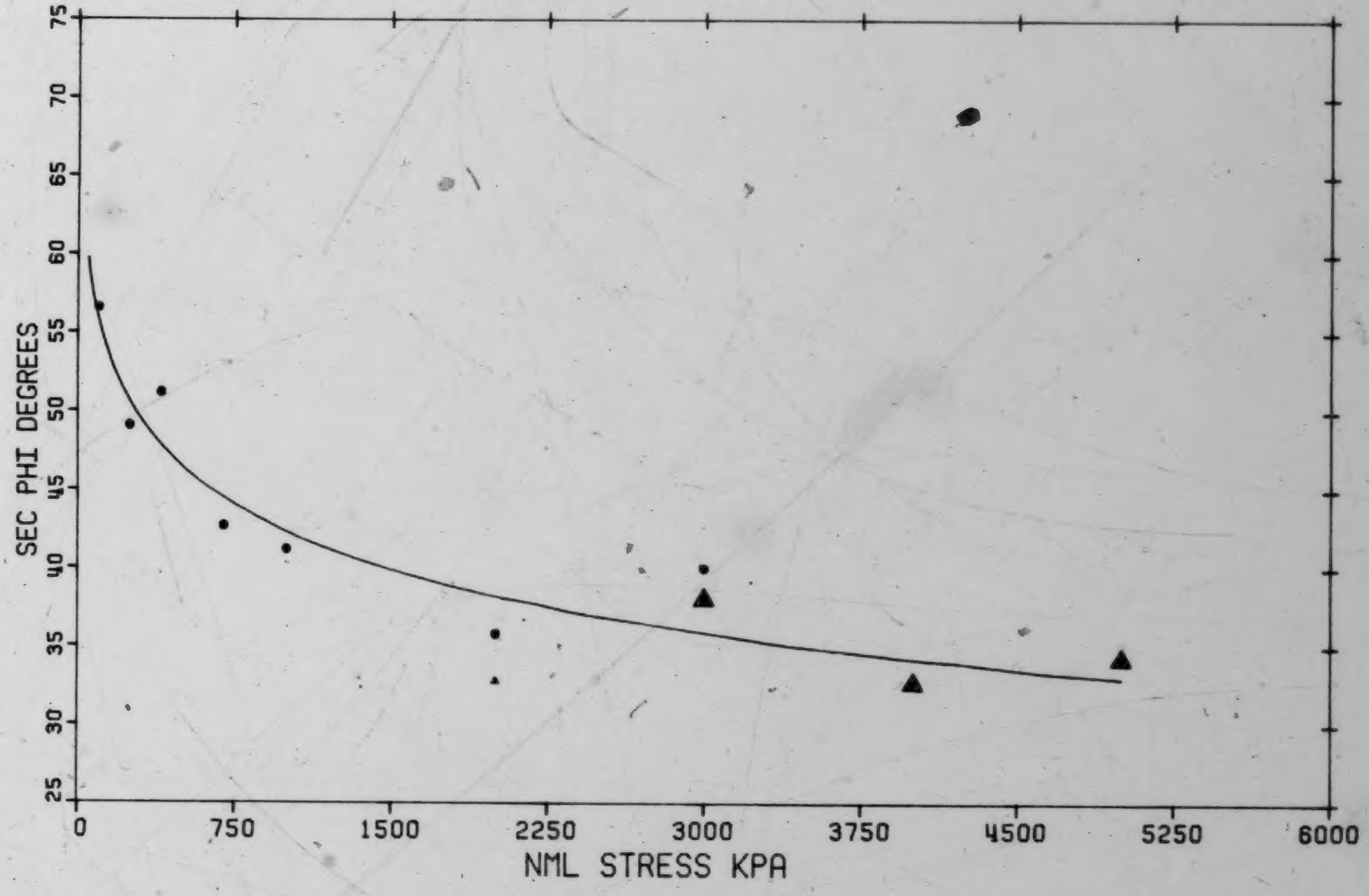

CG MCMURRAY FORMATION PHI VS NORMAL STRESS

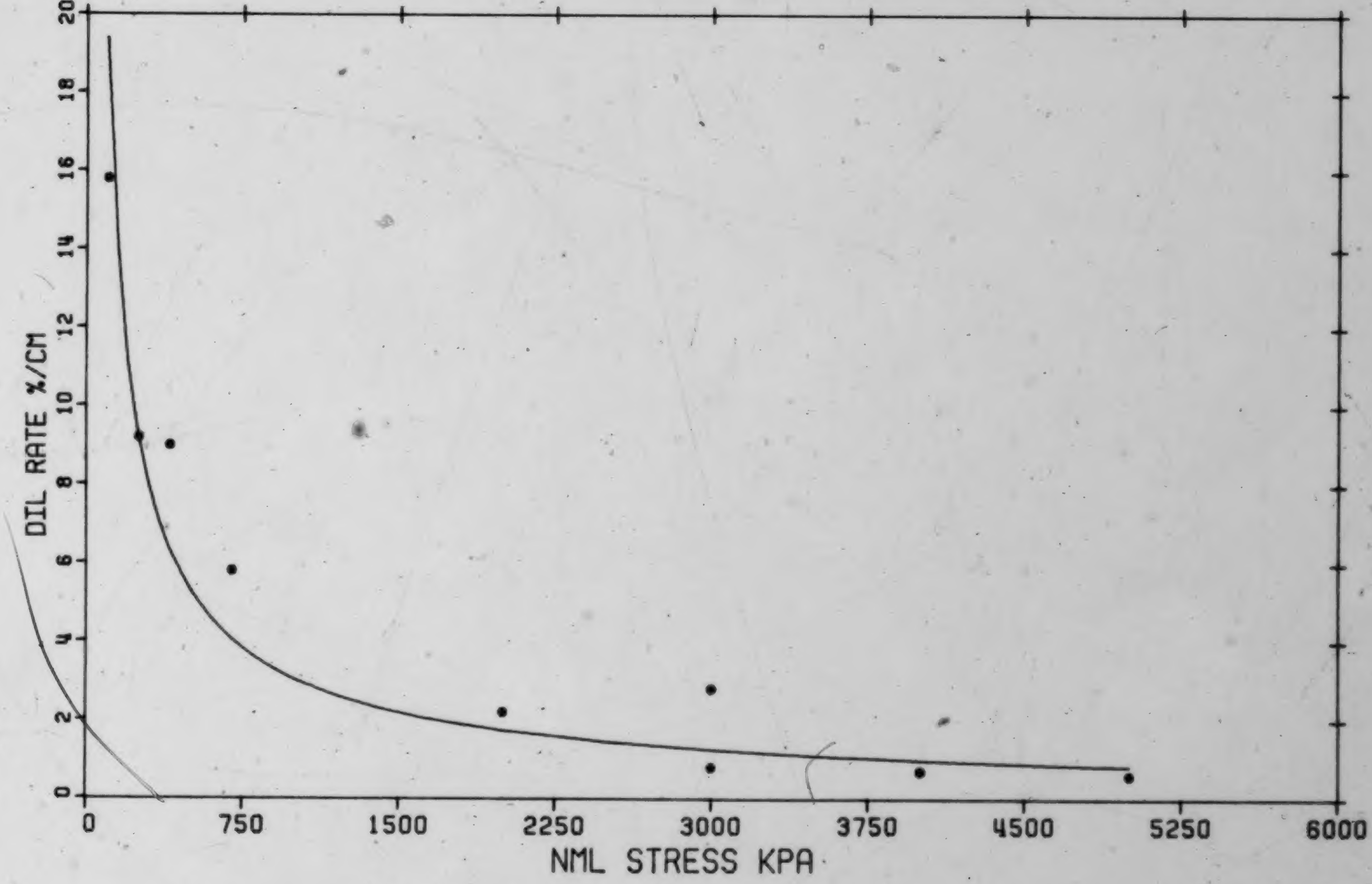

CG MCMURRAY FMN DILATENCY RATE VS NORMAL STRESS

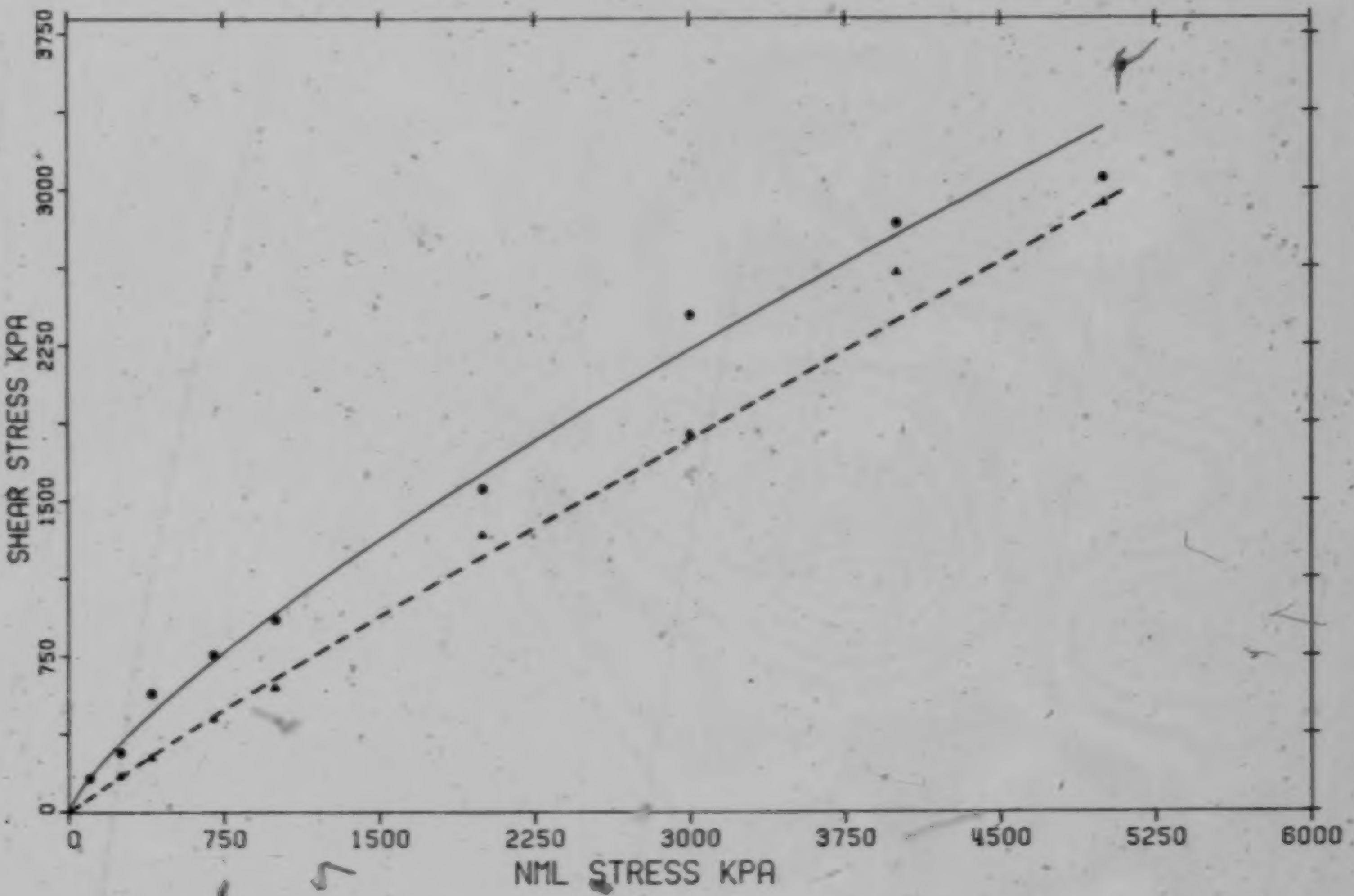

GRAND RAPIDS FORMATION A SHEAR VS NORMAL STRESS

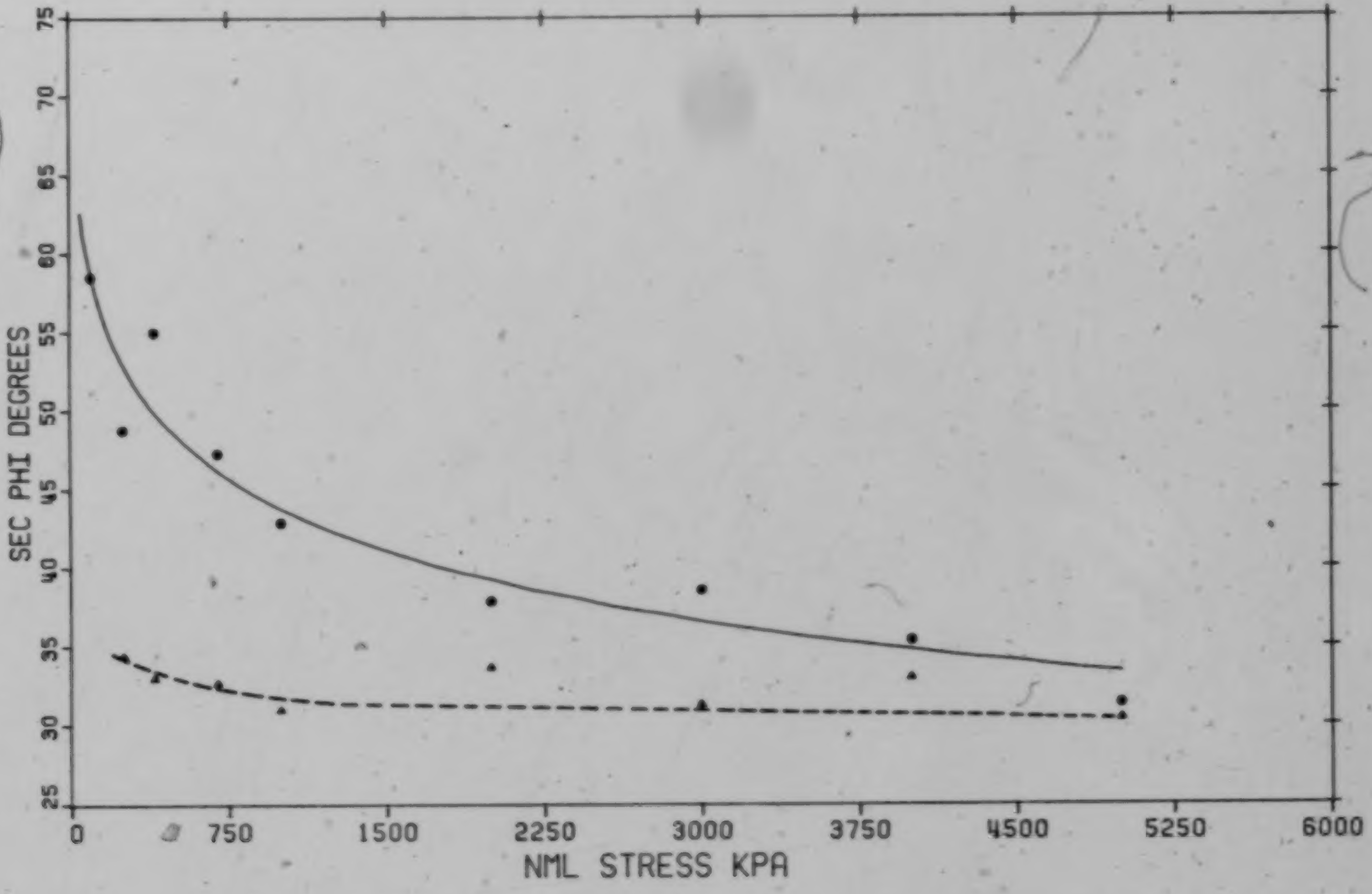

GRAND RAPIDS FORMATION A PHI VS NORMAL STRESS

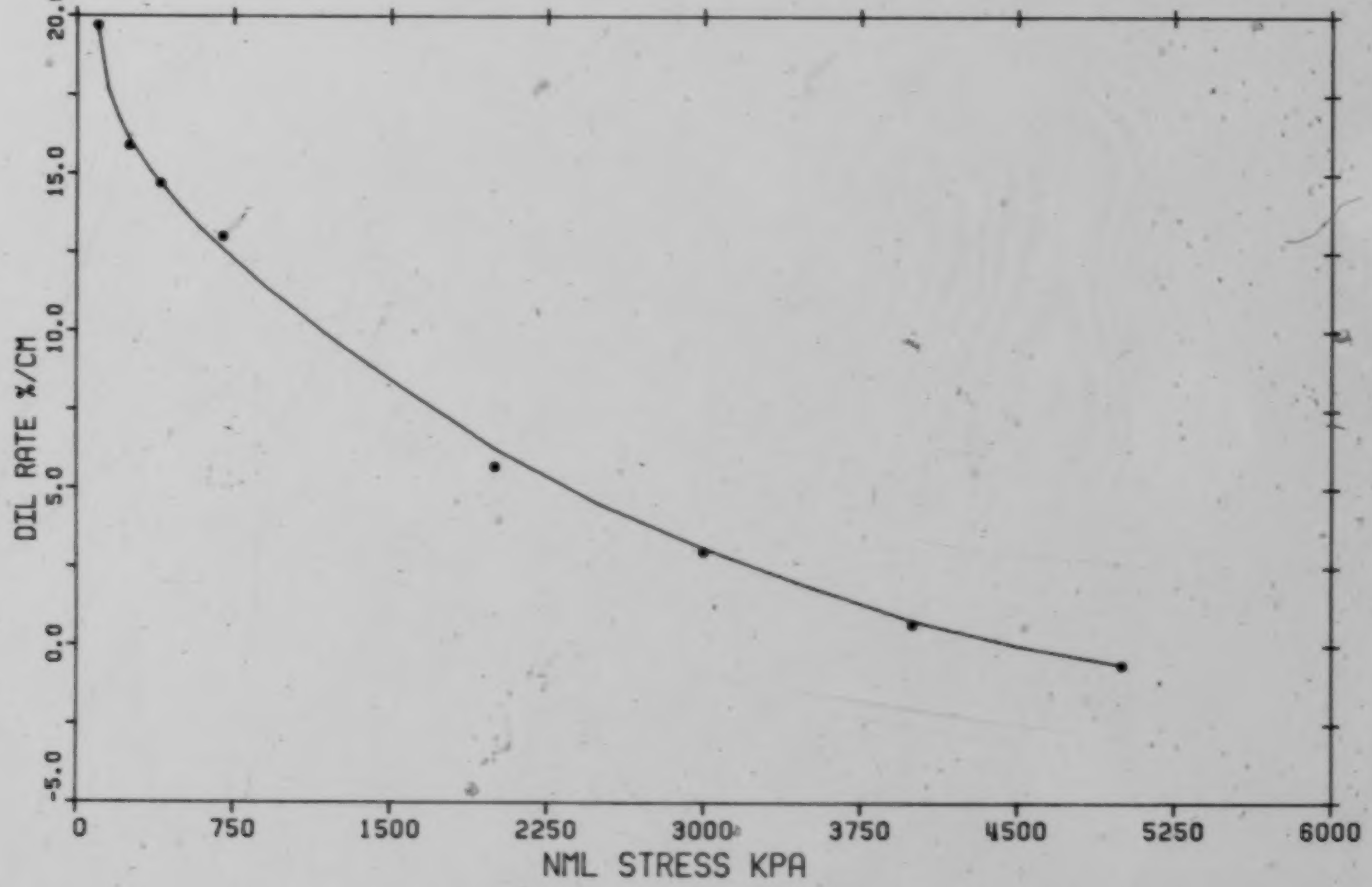

GRAND RAPIDS FMN A DILATENCY RATE VS NML STRESS

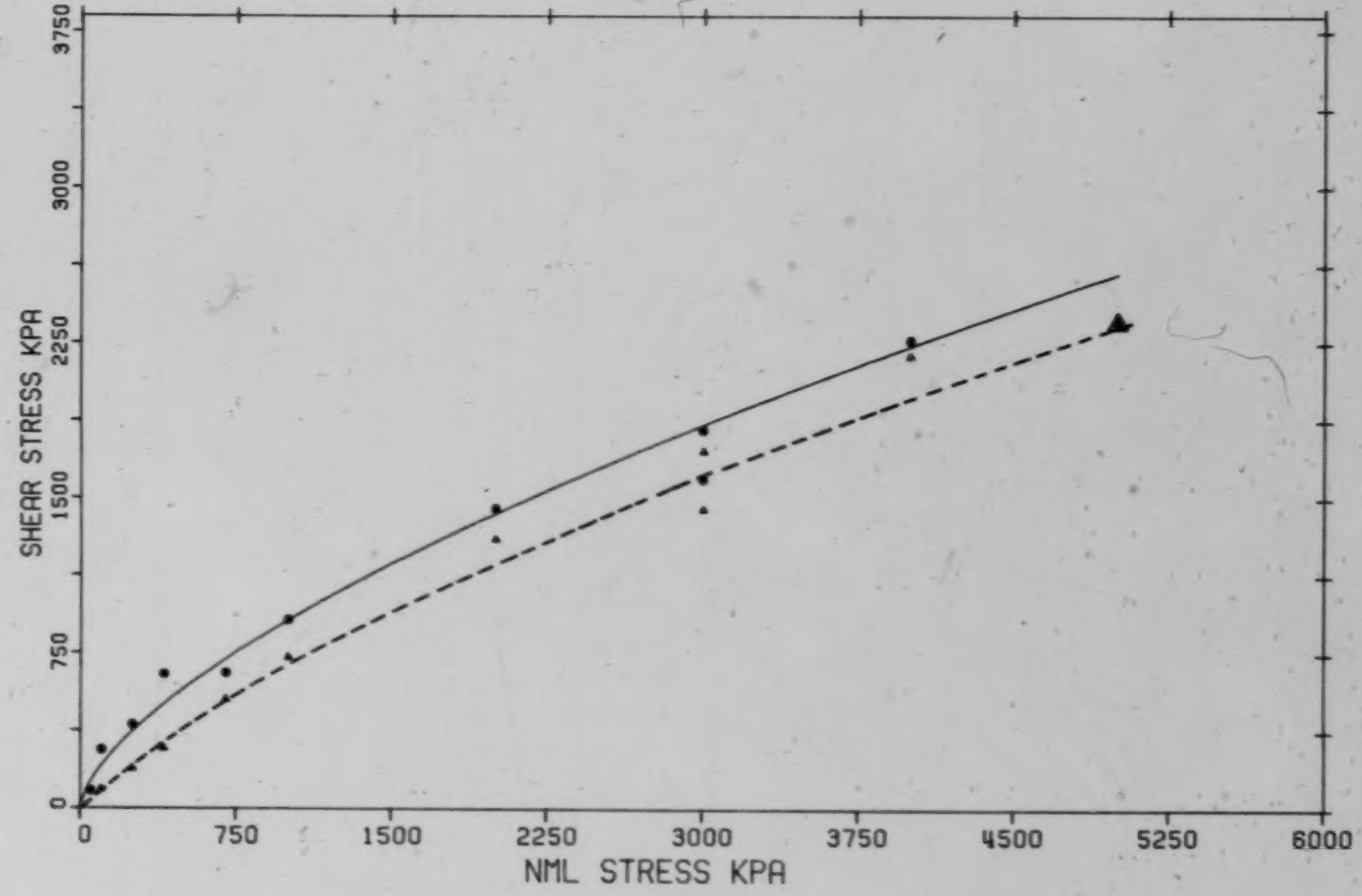

GRAND RAPIDS FORMATION C SHEAR VS NORMAL STRESS

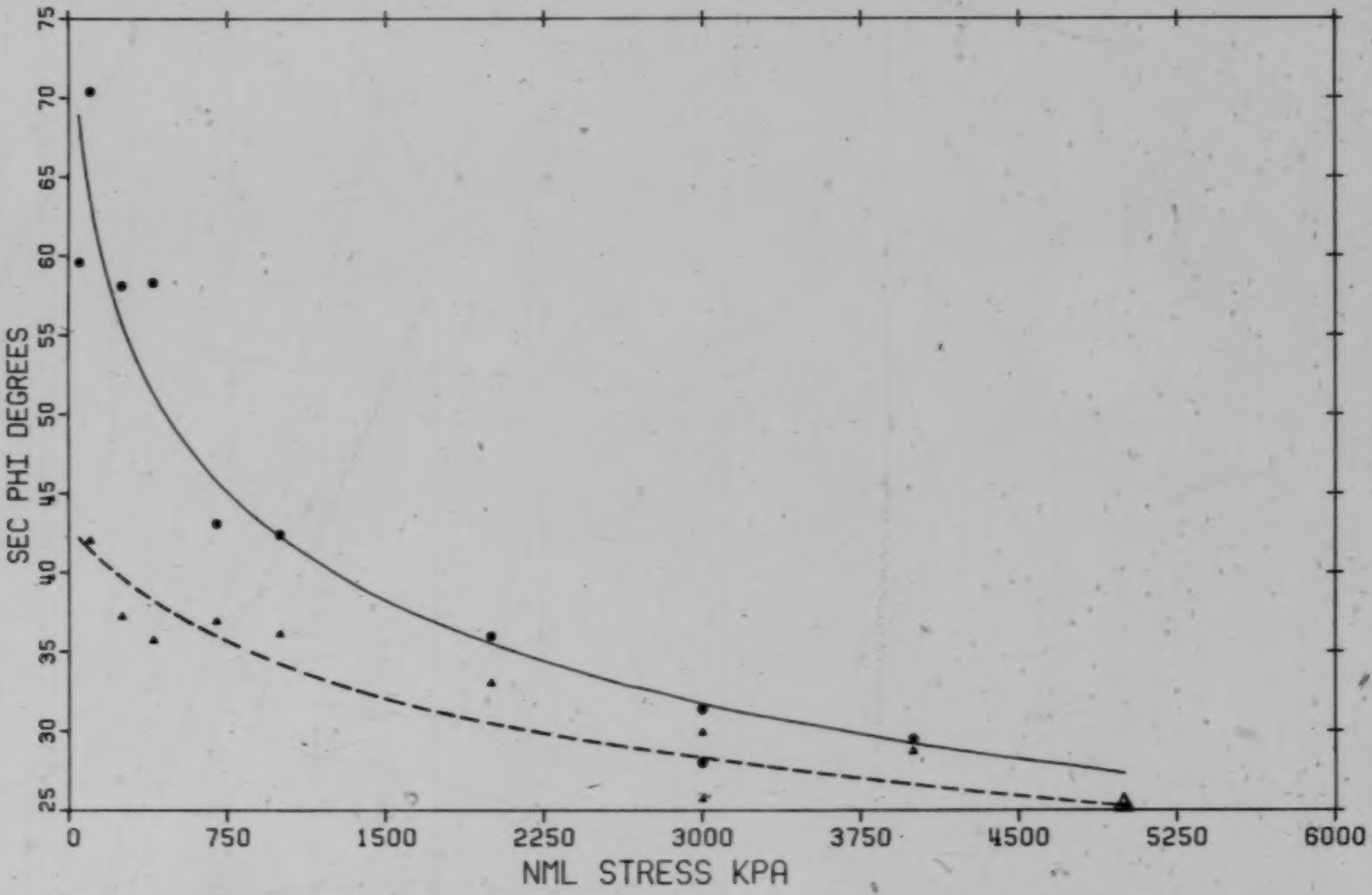

GRAND RAPIDS FORMATION C PHI VS NORMAL STRESS

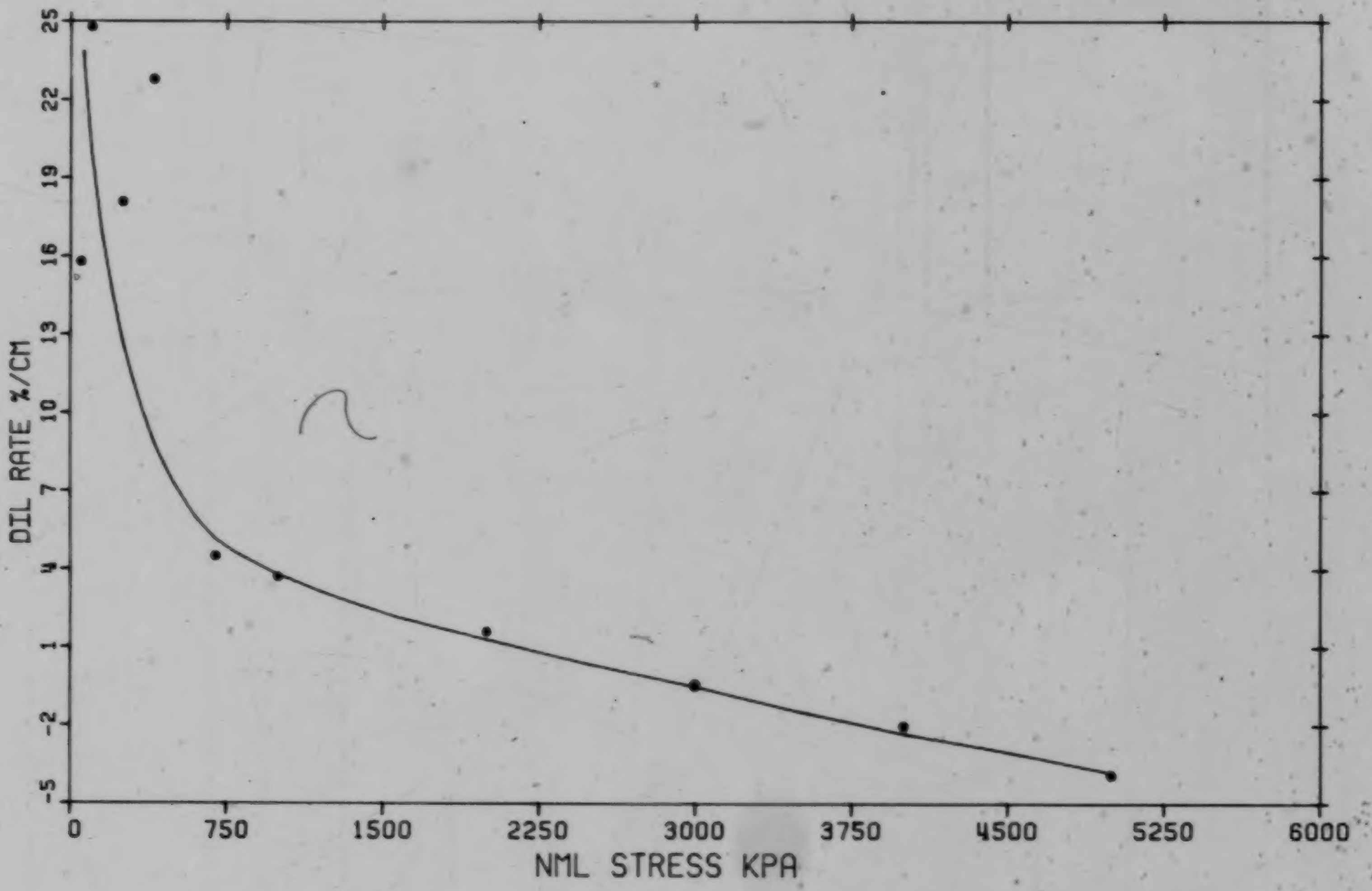

GRAND RAPIDS FMN C DILATENCY RATE VS NML STRESS

C.1.3 Plots for Individual Direct Shear Tests

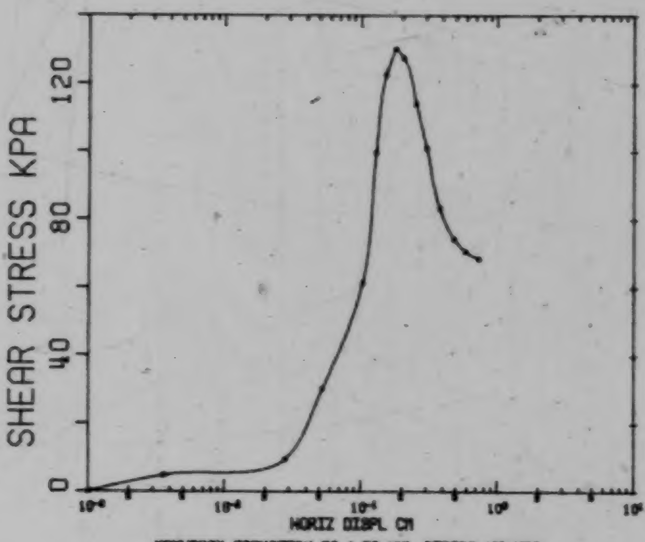

MCMURRAY FORMATION FG-1-78 NML STRESS=100 KPA

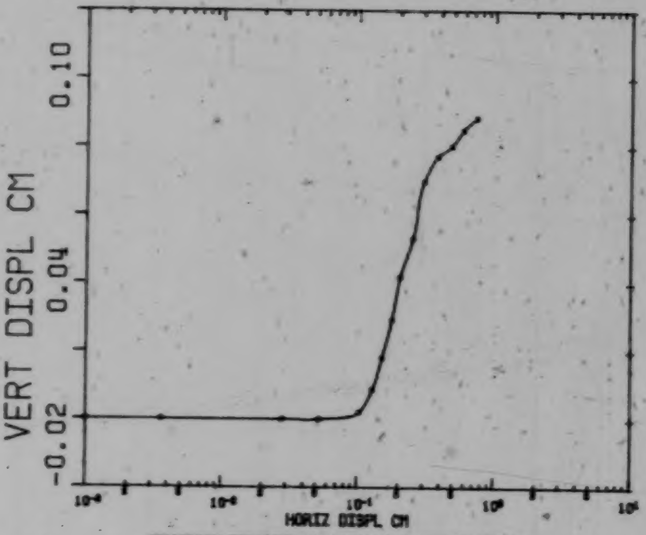

MCMURRAY FORMATION FG-1-78 NML STRESS=100 KPA

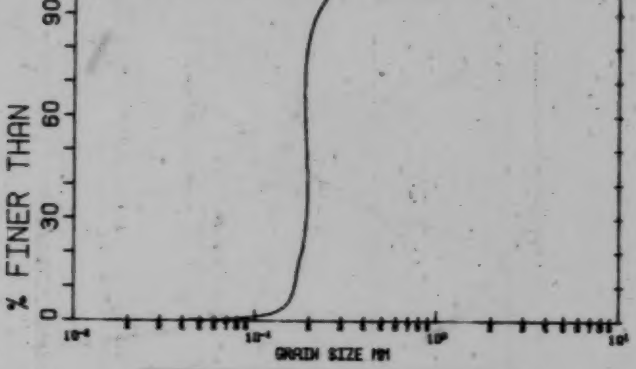

MCMURRAY FORMATION FG-1-78 NML STRESS=100 KPA

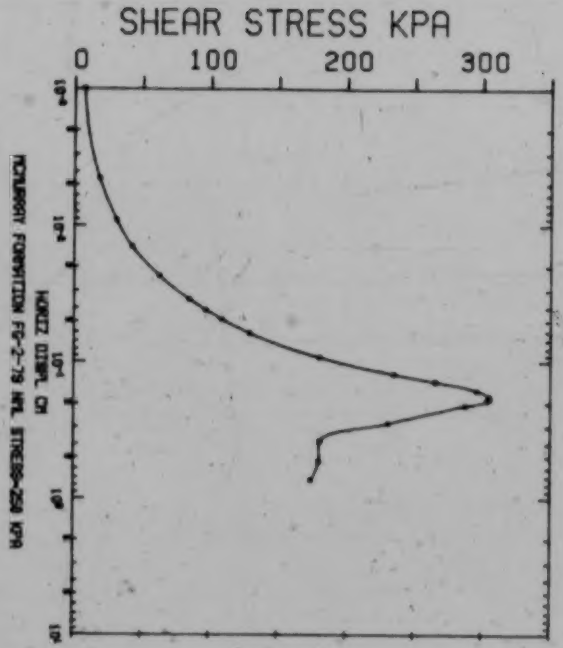
SHEAR STRESS KPA
0
100
200
300
HORIZ DISPL CM
MCMURRAY FORMATION FG-2-79 NML STRESS=258 KPA

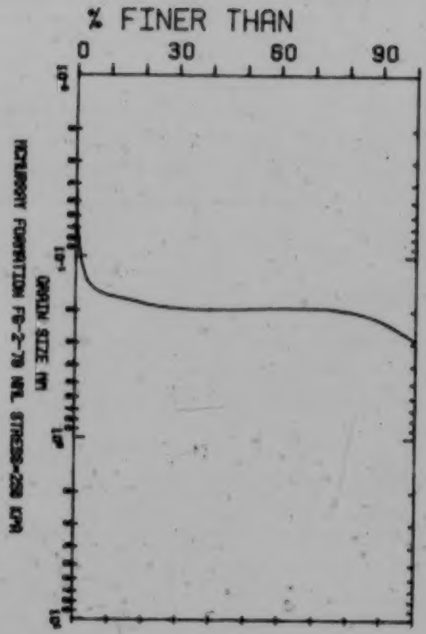
% FINER THAN
0
30
60
90
GRAIN SIZE MM
MCMURRAY FORMATION FG-2-79 NML STRESS=258 KPA

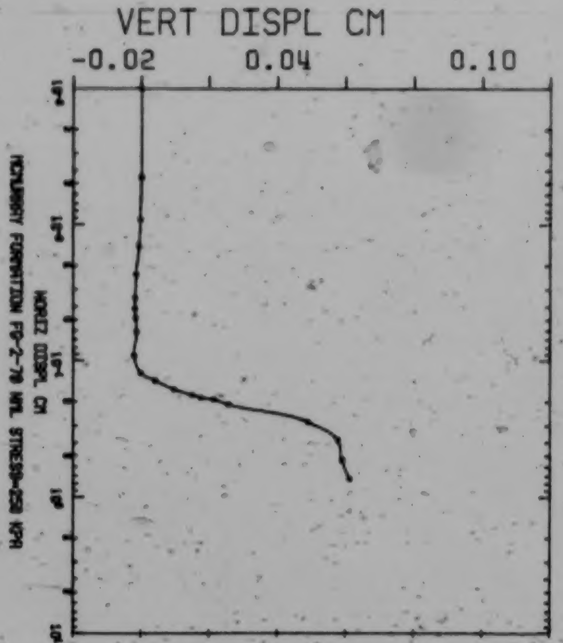
VERT DISPL CM
-0.02
0.04
0.10
HORIZ DISPL CM
MCMURRAY FORMATION FG-2-79 NML STRESS=258 KPA

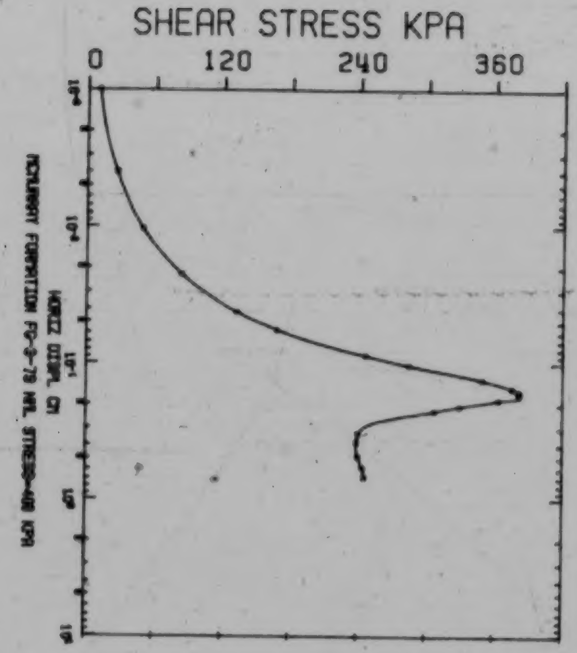
SHEAR STRESS KPA
0
120
240
360
HORIZ DISPL CM
MCMURRAY FORMATION FO-8-79 NML STRESS=400 KPA

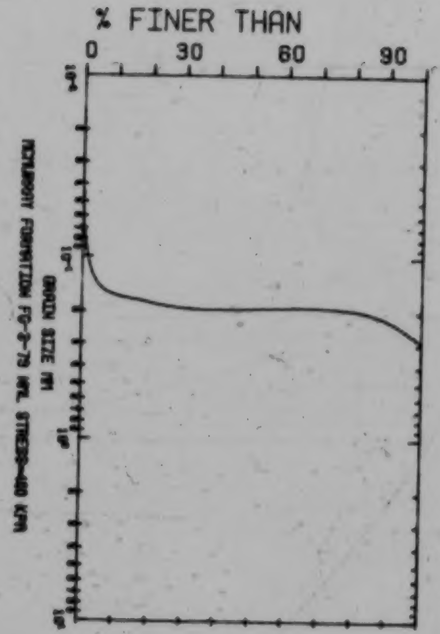
% FINER THAN
0
30
60
90
GRAIN SIZE MM
MCMURRAY FORMATION FO-8-79 NML STRESS=400 KPA

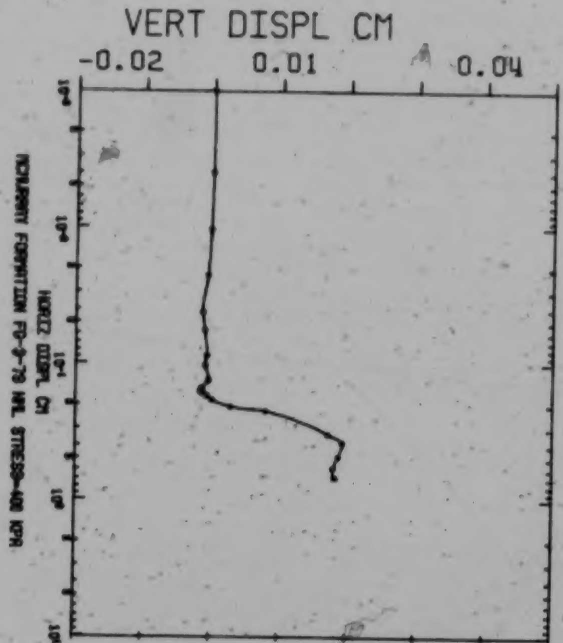
VERT DISPL CM
-0.02
0.01
0.04
HORIZ DISPL CM
MCMURRAY FORMATION FO-8-79 NML STRESS=400 KPA

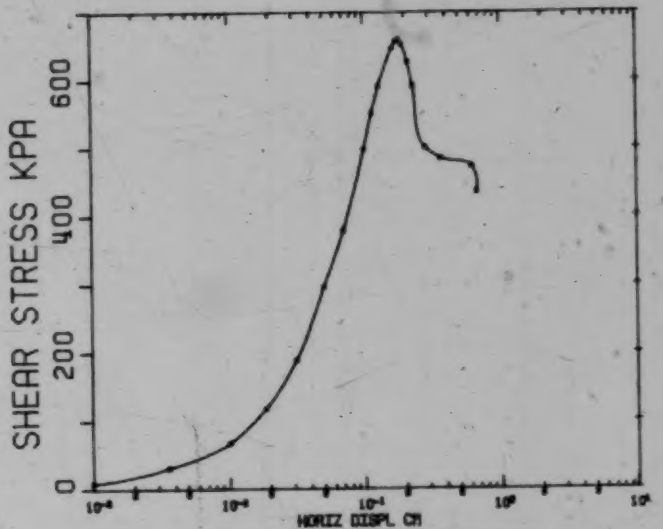

MCMURRAY FORMATION FG-4-79 NML STRESS=700 KPA

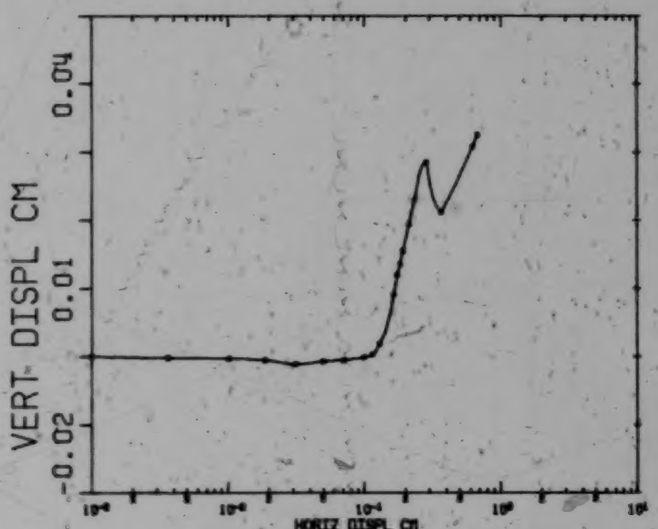

MCMURRAY FORMATION FG-4-79 NML STRESS=700 KPA

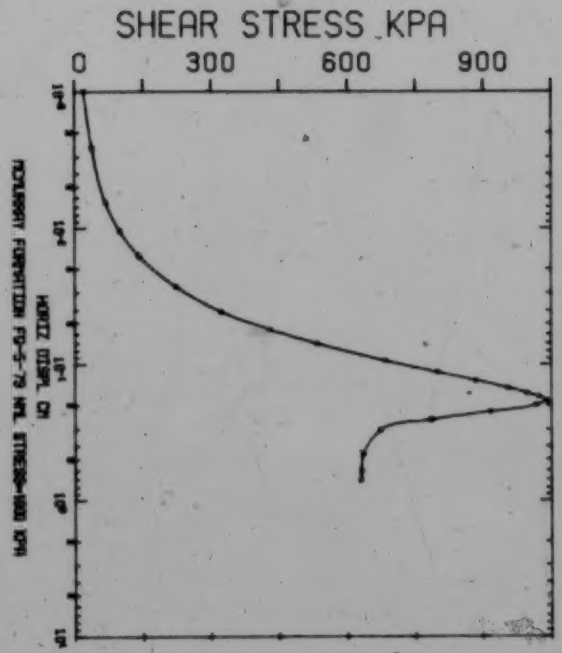
SHEAR STRESS KPA
0
300
600
900
10^{-3}
10^{-2}
10^{-1}
10^{0}
10^{1}
HORIZ DISPL CM
MCMURRAY FORMATION FO-5-79 NTL STRESS=1000 KPA

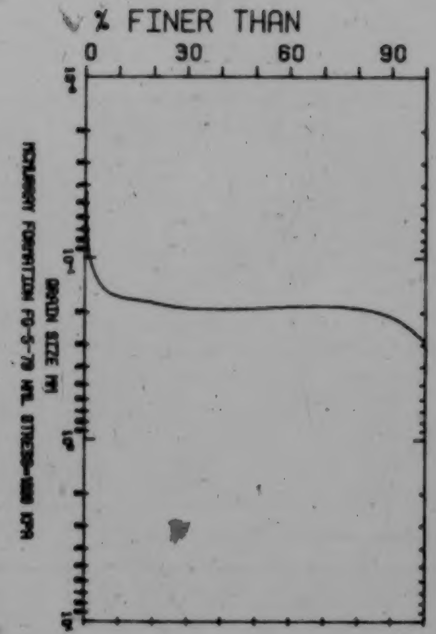
% FINER THAN
0
30
60
90
10^{-2}
10^{-1}
10^{0}
10^{1}
GRAIN SIZE MM
MCMURRAY FORMATION FO-5-79 NTL STRESS=1000 KPA

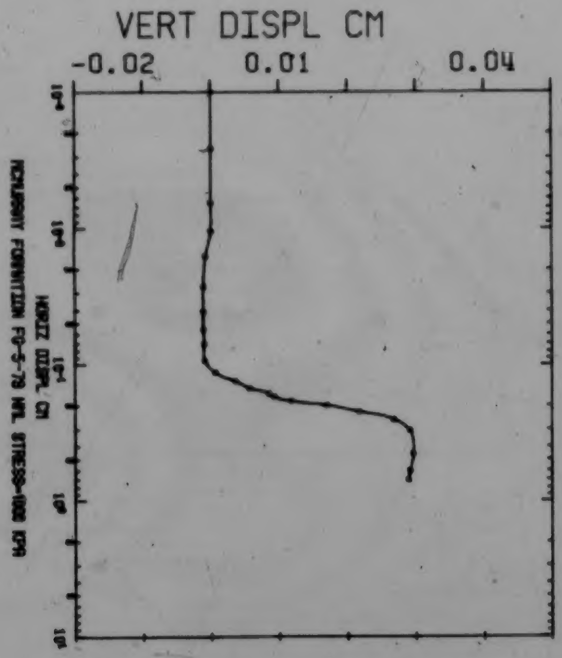
VERT DISPL CM
-0.02
0.01
0.04
10^{-3}
10^{-2}
10^{-1}
10^{0}
10^{1}
HORIZ DISPL CM
MCMURRAY FORMATION FO-5-79 NTL STRESS=1000 KPA

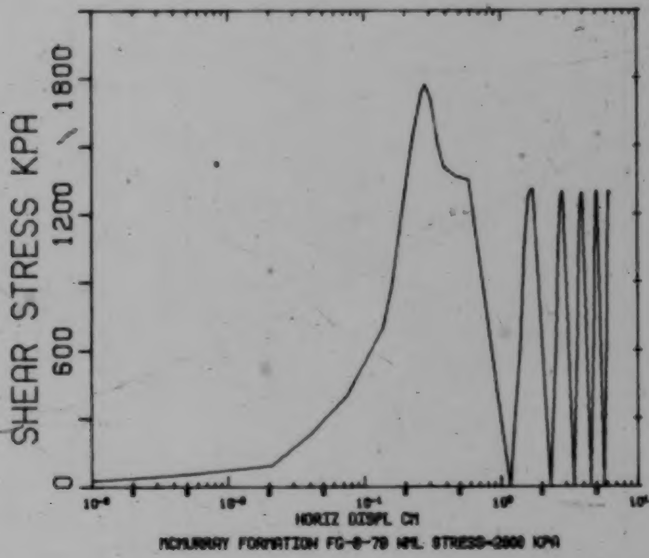
SHEAR STRESS KPA
0
600
1200
1800
10^-3
10^-2
10^-1
10^0
10^1
HORIZ DISPL CM
MCMURRAY FORMATION FG-8-78 NML STRESS=2000 KPA

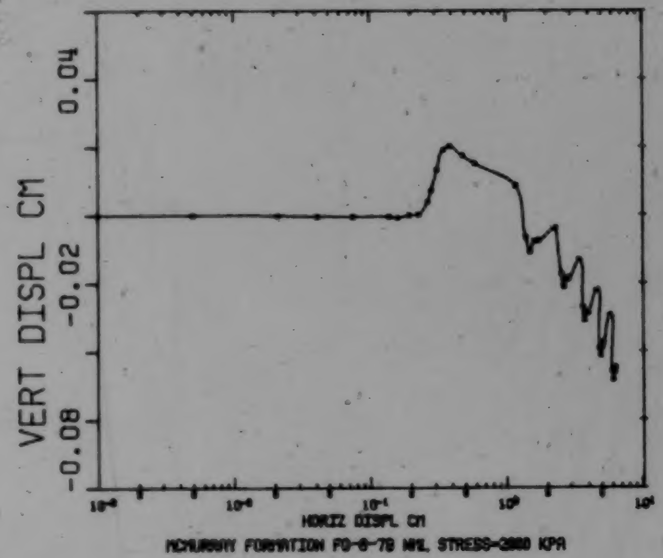
VERT DISPL CM
-0.08
-0.02
0.04
10^-3
10^-2
10^-1
10^0
10^1
HORIZ DISPL CM
MCMURRAY FORMATION FG-8-78 NML STRESS=2000 KPA

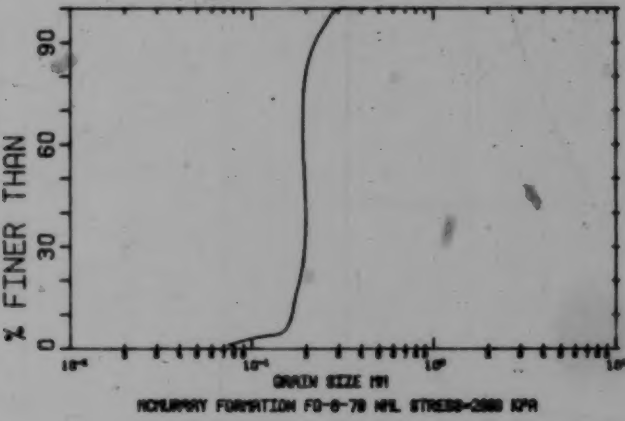
% FINER THAN
0
30
60
90
10^-2
10^-1
10^0
10^1
GRAIN SIZE MM
MCMURRAY FORMATION FG-8-78 NML STRESS=2000 KPA

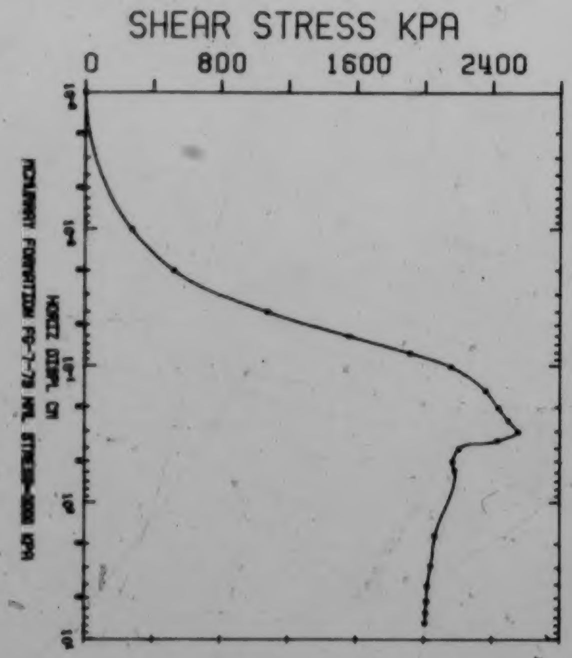
SHEAR STRESS KPA
0
800
1600
2400
HORIZ DISPL CM
MONUMENT FORMATION FO-7-78 NML STRESS=3000 KPA

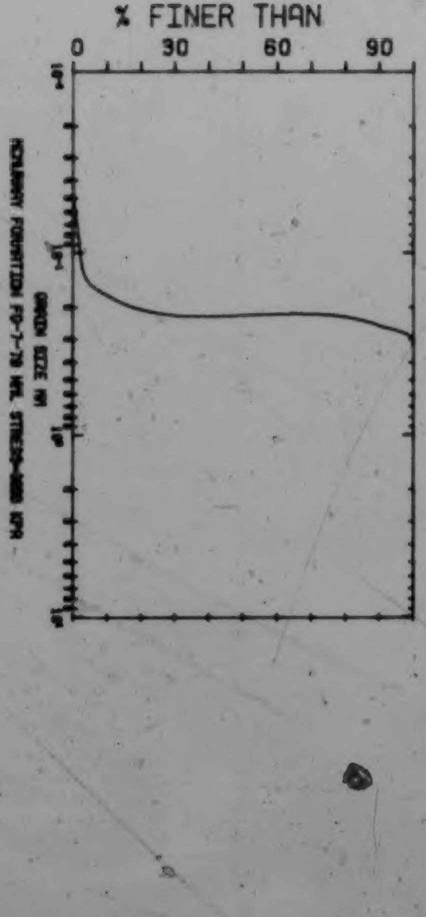
% FINER THAN
0
30
60
90
GRAIN SIZE MM
MONUMENT FORMATION FO-7-78 NML STRESS=3000 KPA

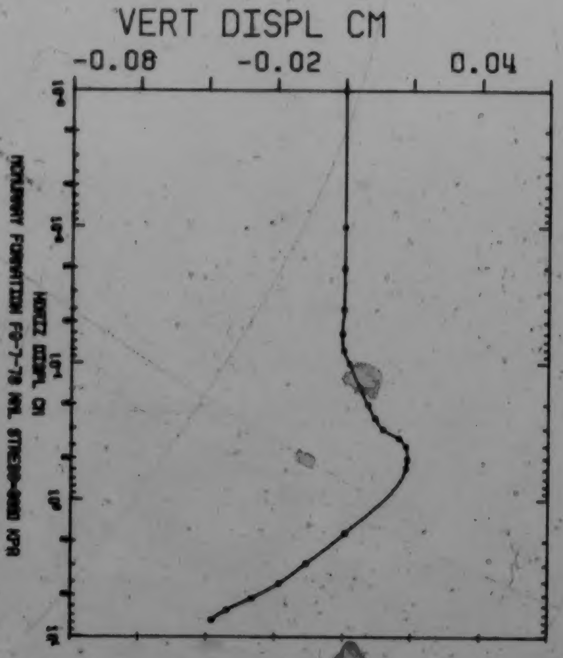
VERT DISPL CM
-0.08
-0.02
0.04
HORIZ DISPL CM
MONUMENT FORMATION FO-7-78 NML STRESS=3000 KPA

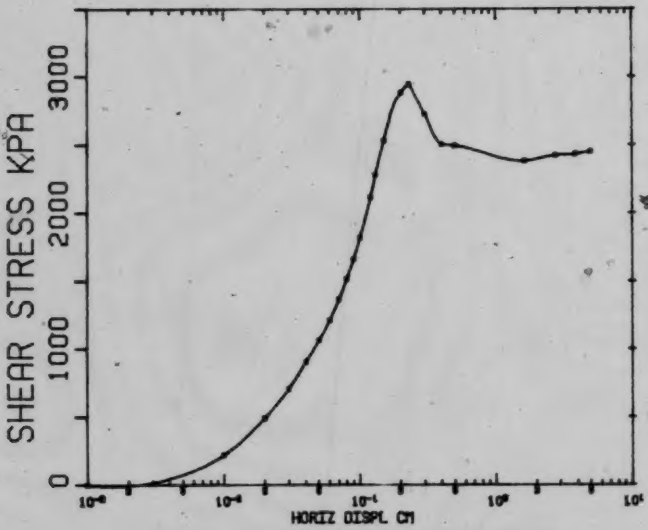

MCMURRAY FORMATION FG-8-79 NML STRESS=4000 KPA

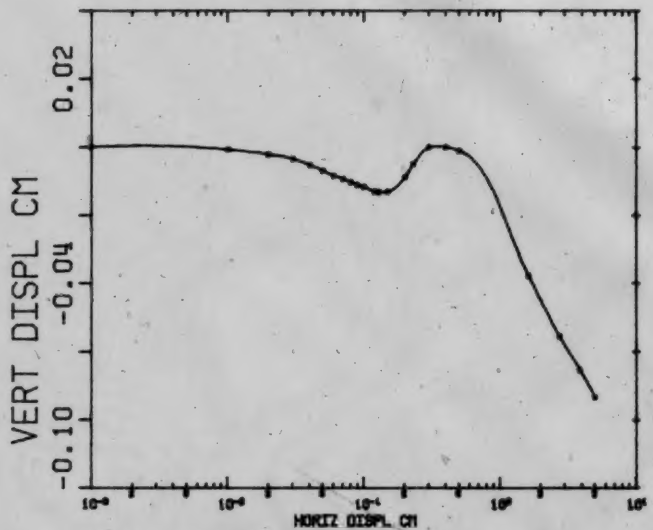

MCMURRAY FORMATION FG-8-79 NML STRESS=4000 KPA

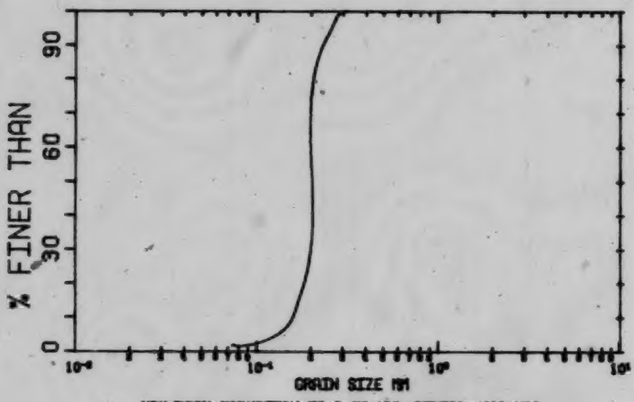

MCMURRAY FORMATION FG-8-79 NML STRESS=4000 KPA

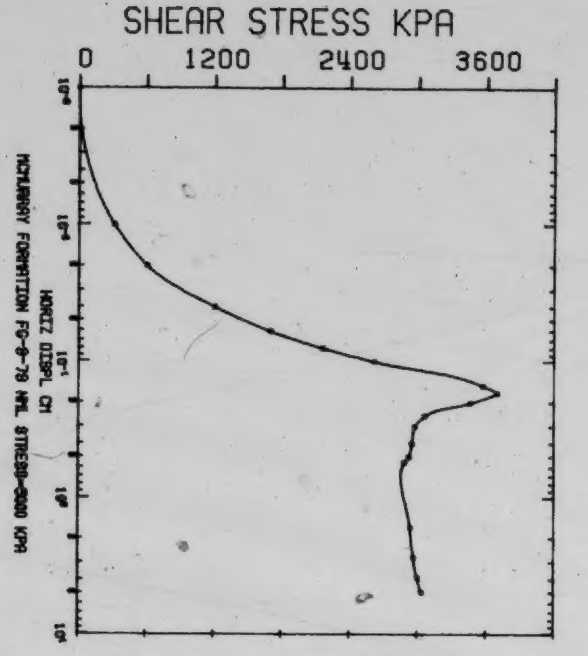
SHEAR STRESS KPA
0
1200
2400
3600
HORIZ DISPL CM
MCMURRAY FORMATION FO-8-78 NML STRESS=5000 KPA

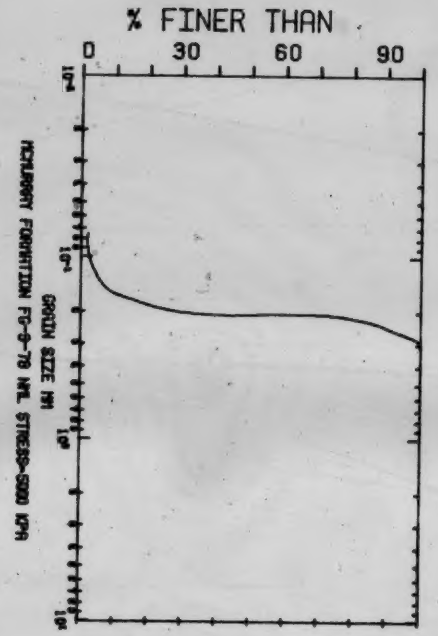
% FINER THAN
0
30
60
90
GRAIN SIZE MM
MCMURRAY FORMATION FO-8-78 NML STRESS=5000 KPA

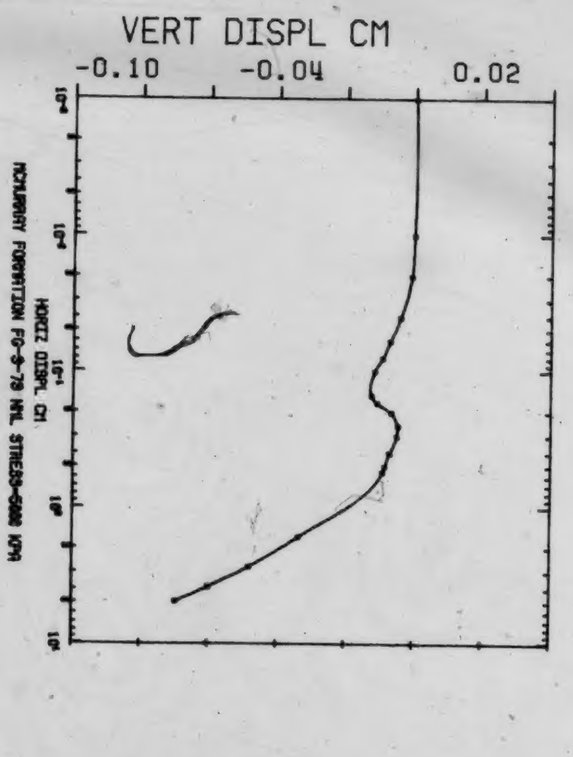
VERT DISPL CM
-0.10
-0.04
0.02
HORIZ DISPL CM
MCMURRAY FORMATION FO-8-78 NML STRESS=5000 KPA

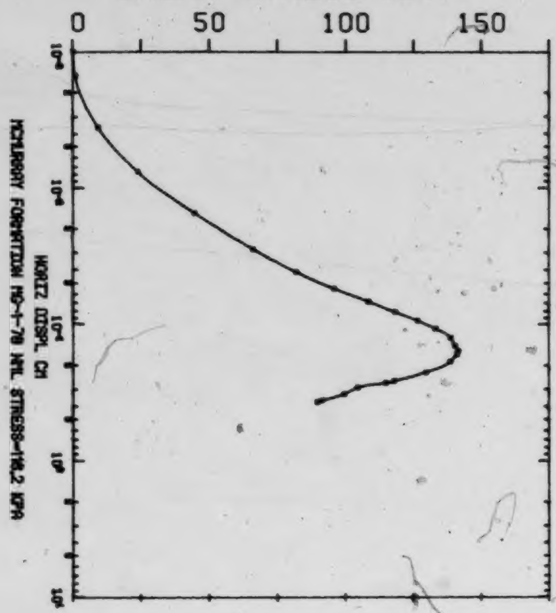
SHEAR STRESS KPA
0
50
100
150
10⁻³
10⁻²
10⁻¹
10⁰
10¹
HORIZ DISPL CM
MCMURRAY FORMATION MO-1-70 NML STRESS=118.2 KPA

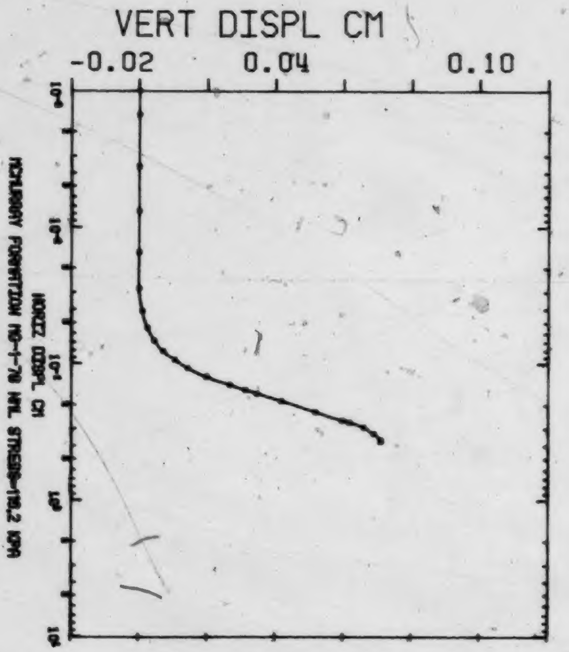
VERT DISPL CM
-0.02
0.04
0.10
10⁻³
10⁻²
10⁻¹
10⁰
10¹
HORIZ DISPL CM
MCMURRAY FORMATION MO-1-70 NML STRESS=118.2 KPA

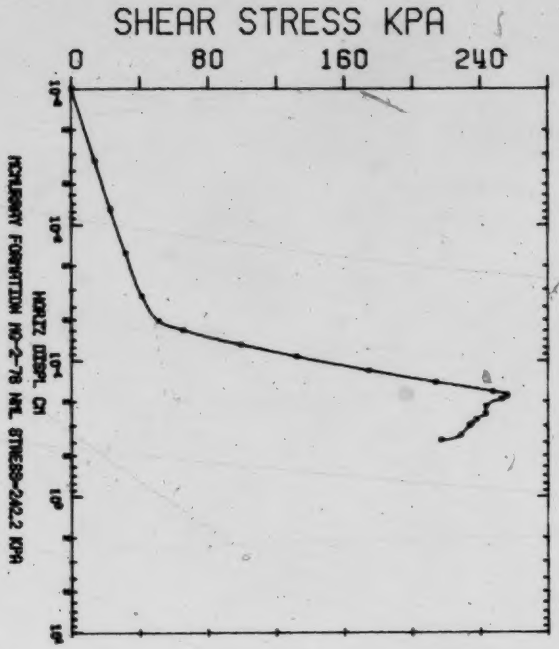
SHEAR STRESS KPA
0
80
160
240
HORIZ DISPL CM
MCMURRAY FORMATION HO-2-78 NML STRESS=242.2 KPA

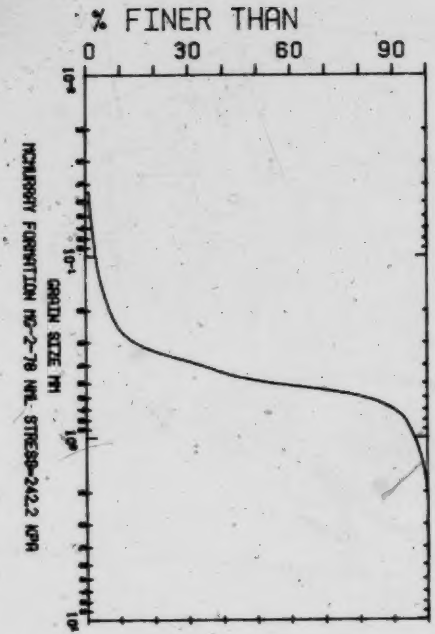
% FINER THAN
0
30
60
90
GRAIN SIZE MM
MCMURRAY FORMATION HO-2-78 NML STRESS=242.2 KPA

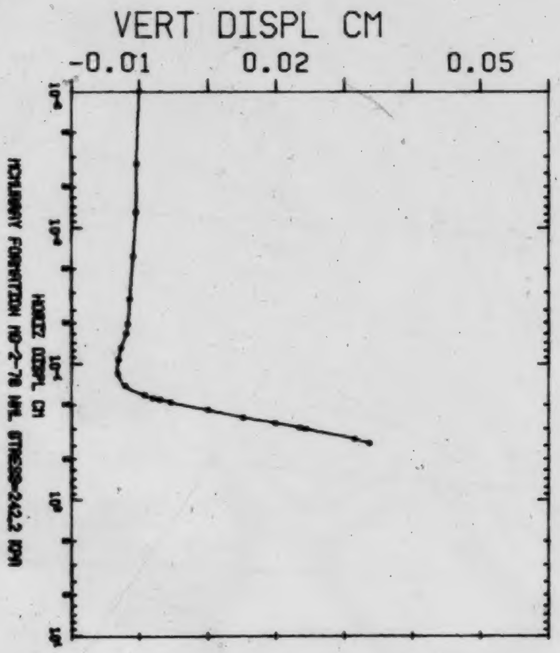
VERT DISPL CM
-0.01
0.02
0.05
HORIZ DISPL CM
MCMURRAY FORMATION HO-2-78 NML STRESS=242.2 KPA

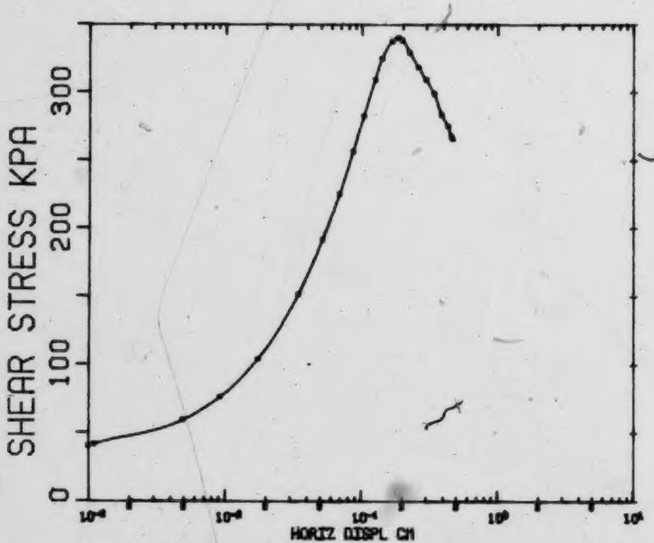

MCMURRAY FORMATION MG-3-78 NML STRESS=400 KPA

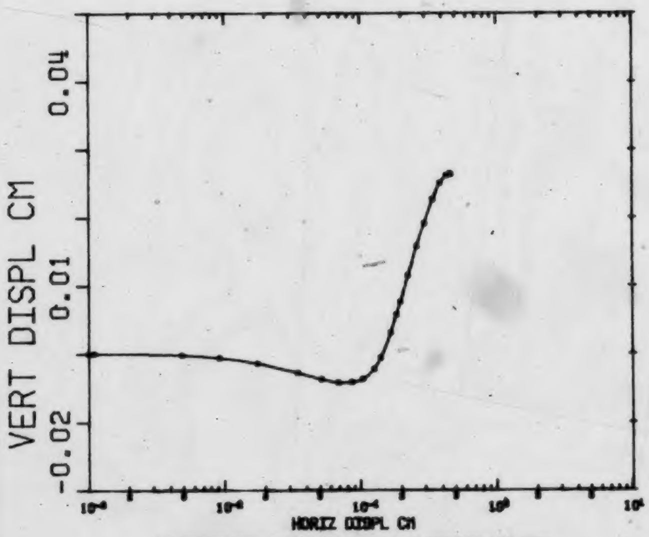

MCMURRAY FORMATION MG-3-78 NML STRESS=400 KPA

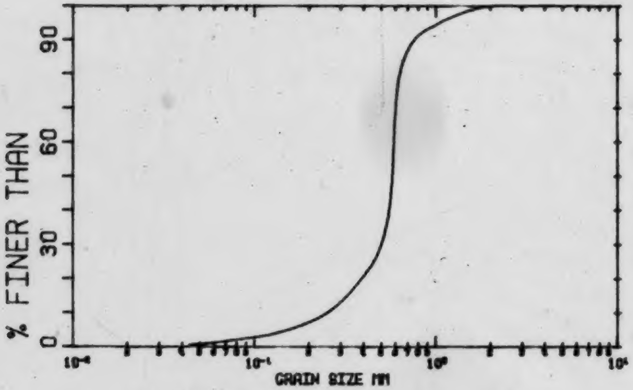

MCMURRAY FORMATION MG-3-78 NML STRESS=400 KPA

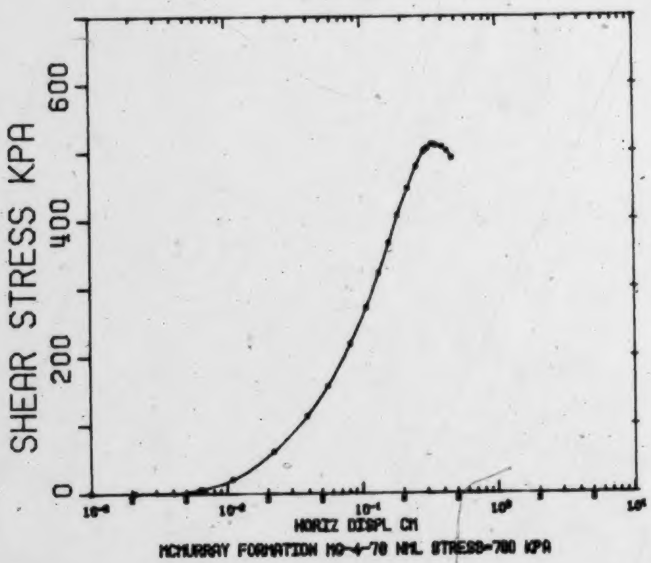
SHEAR STRESS KPA
0
200
400
600
10^{-3}
10^{-2}
10^{-1}
10^{0}
10^{1}
HORIZ DISPL CM
MCMURRAY FORMATION MG-4-78 NML STRESS=700 KPA

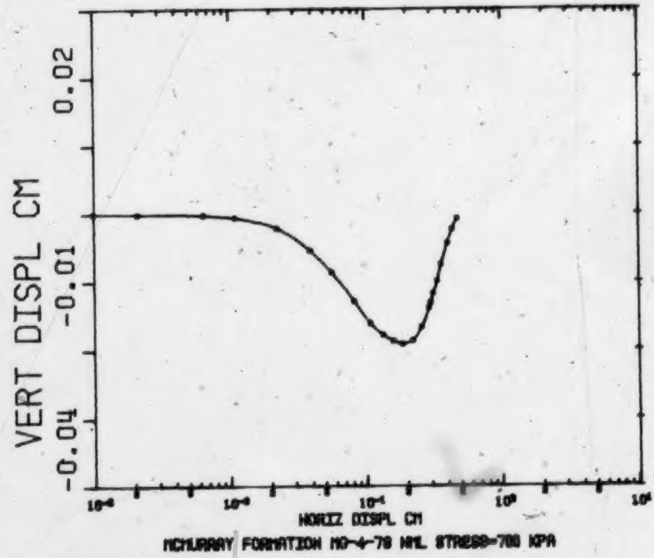
VERT DISPL CM
-0.04
-0.01
0.02
10^{-3}
10^{-2}
10^{-1}
10^{0}
10^{1}
HORIZ DISPL CM
MCMURRAY FORMATION MG-4-78 NML STRESS=700 KPA

6

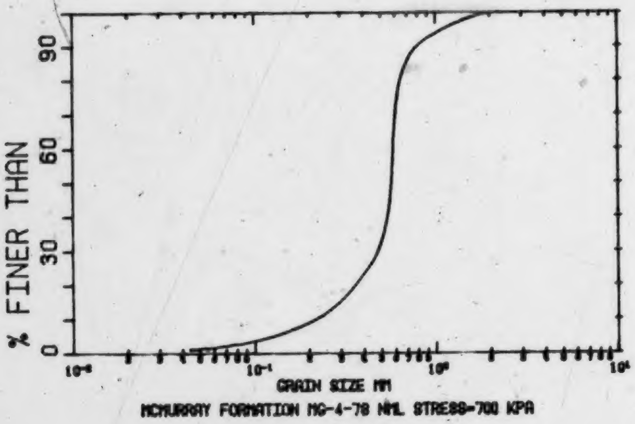
% FINER THAN
0
30
60
90
10^{-2}
10^{-1}
10^{0}
10^{1}
GRAIN SIZE MM
MCMURRAY FORMATION MG-4-78 NML STRESS=700 KPA

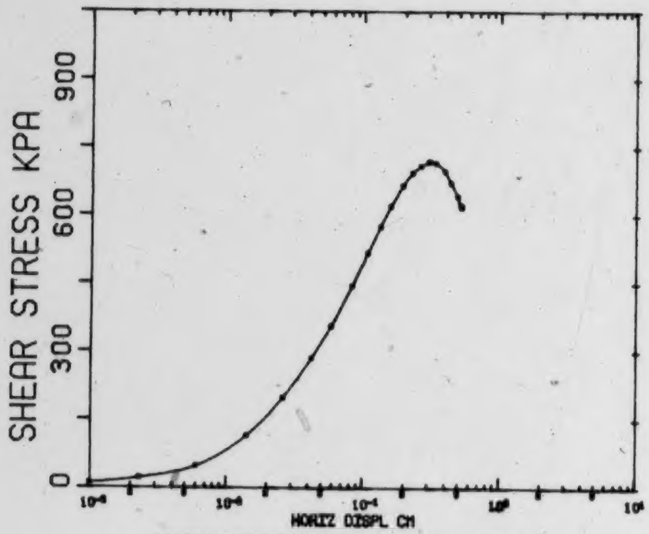

MCMURRAY FORMATION MG-5-78 NML STRESS=1000 KPA

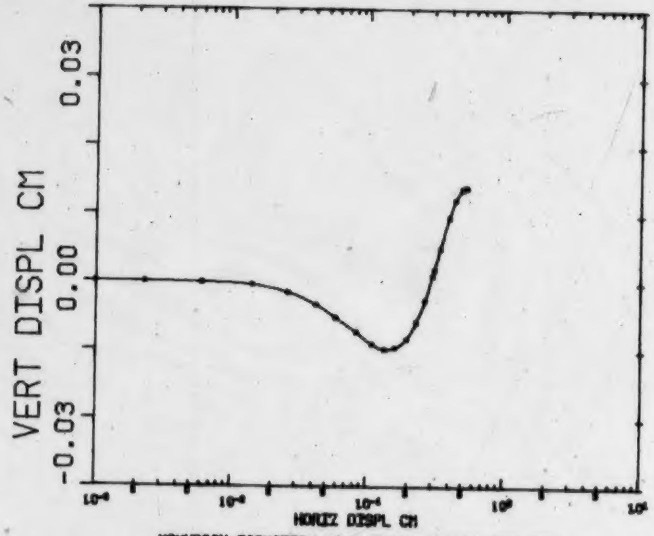

MCMURRAY FORMATION MG-5-78 NML STRESS=1000 KPA

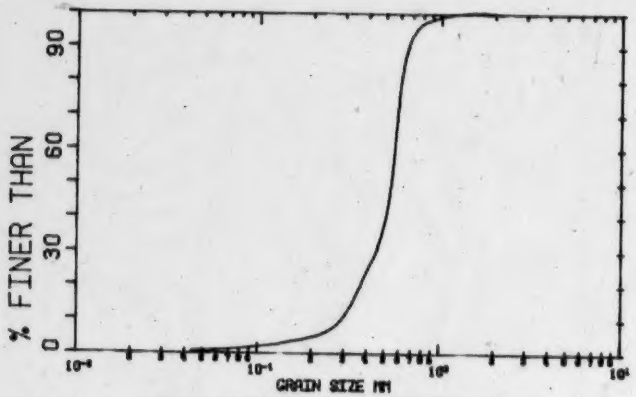

MCMURRAY FORMATION MG-5-78 NML STRESS=1000 KPA

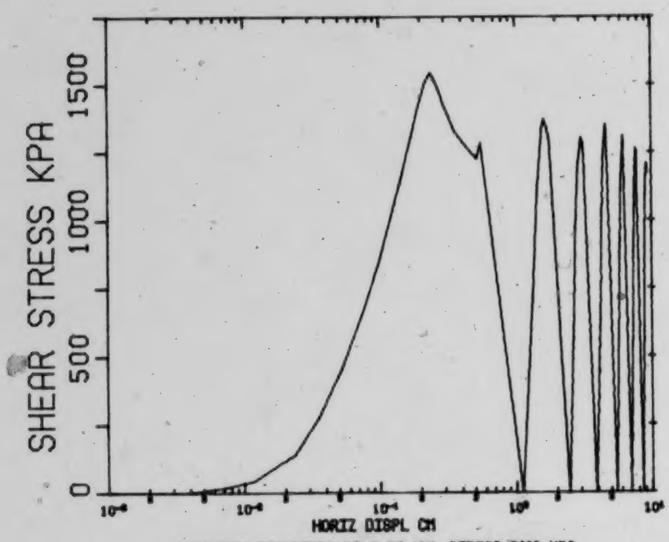

MCMURRAY FORMATION MG-8-78 NML STRESS=2000 KPA

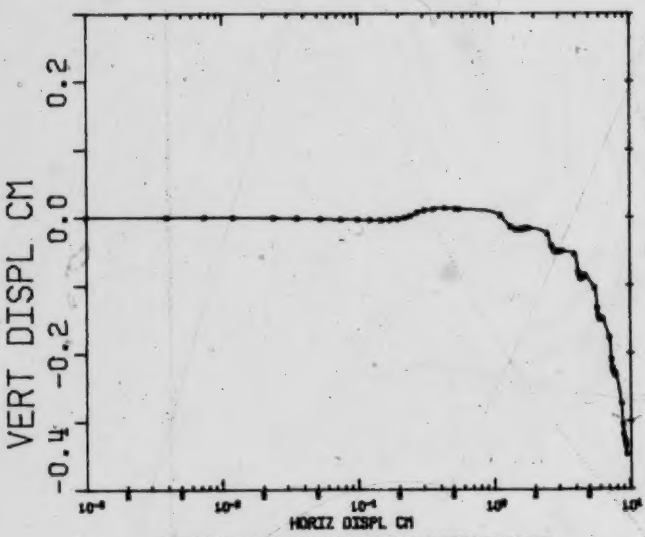

MCMURRAY FORMATION MG-8-78 NML STRESS=2000 KPA

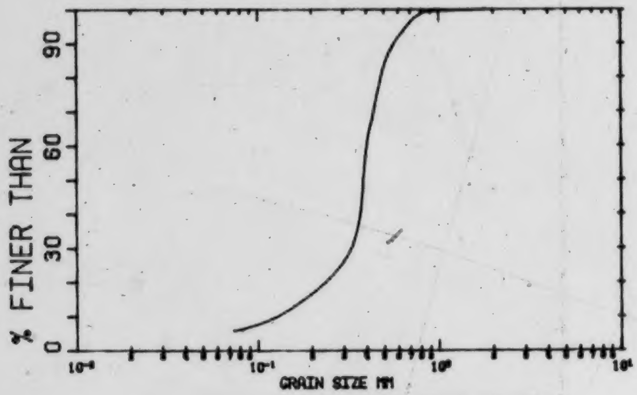

MCMURRAY FORMATION MG-8-78 NML STRESS=2000 KPA

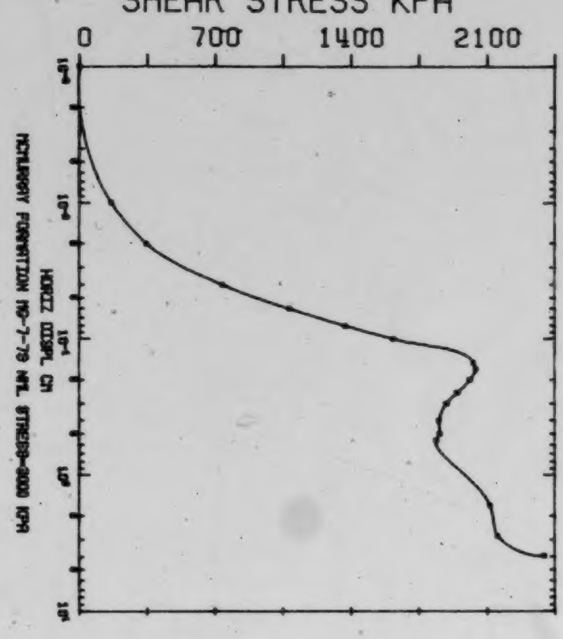
SHEAR STRESS KPA
0
700
1400
2100
10^{-3}
10^{-2}
10^{-1}
10^{0}
10^{1}
HORIZ DISPL CM
MCMURRAY FORMATION MO-7-79 NML STRESS=8000 KPA

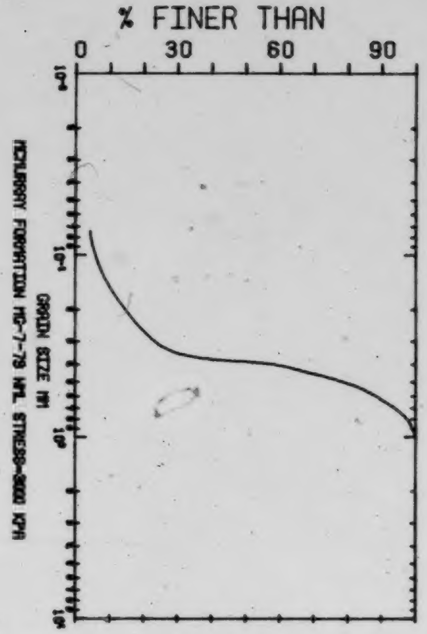
% FINER THAN
0
30
60
90
10^{-2}
10^{-1}
10^{0}
10^{1}
GRAIN SIZE MM
MCMURRAY FORMATION MO-7-79 NML STRESS=8000 KPA

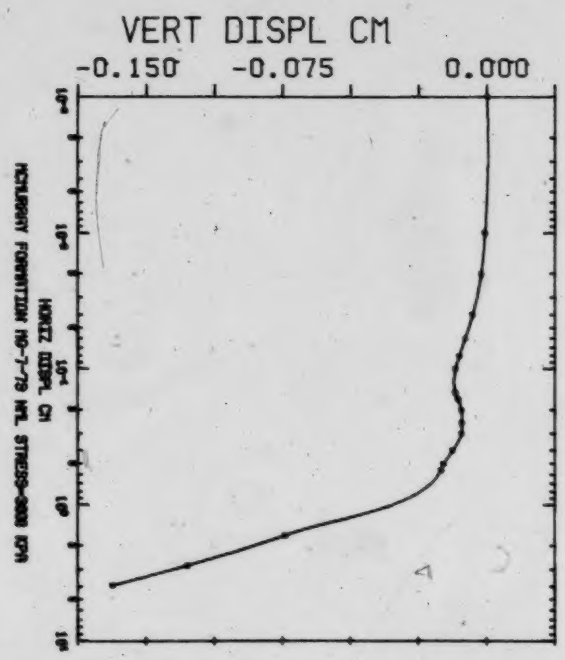
VERT DISPL CM
-0.150
-0.075
0.000
10^{-3}
10^{-2}
10^{-1}
10^{0}
10^{1}
HORIZ DISPL CM
MCMURRAY FORMATION MO-7-79 NML STRESS=8000 KPA

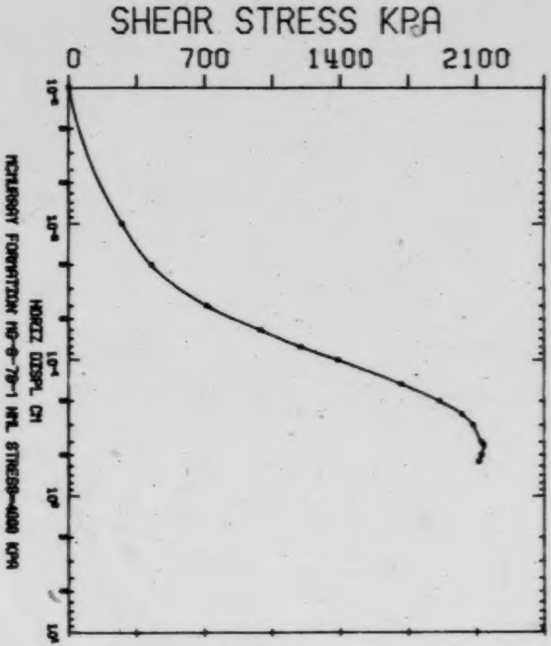
SHEAR STRESS KPA
0
700
1400
2100
10⁻³
10⁻²
10⁻¹
10⁰
10¹
HORIZ DISPL CM
MCMURRAY FORMATION NO-8-78-1 NML STRESS=4000 KPA

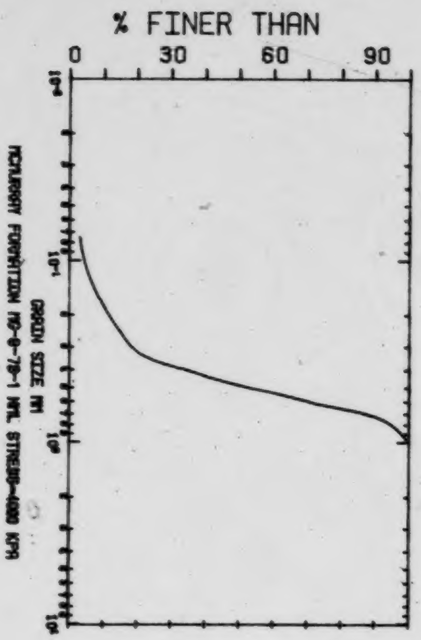
% FINER THAN
0
30
60
90
10⁻²
10⁻¹
10⁰
10¹
GRAIN SIZE MM
MCMURRAY FORMATION NO-8-78-1 NML STRESS=4000 KPA

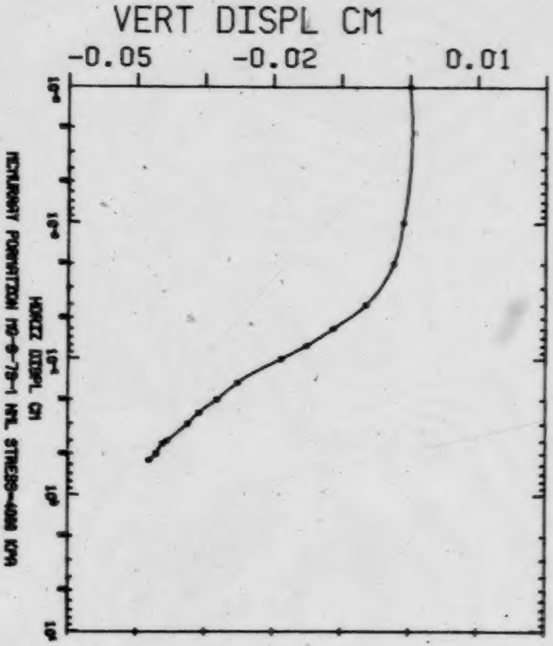
VERT DISPL CM
-0.05
-0.02
0.01
10⁻³
10⁻²
10⁻¹
10⁰
10¹
HORIZ DISPL CM
MCMURRAY FORMATION NO-8-78-1 NML STRESS=4000 KPA

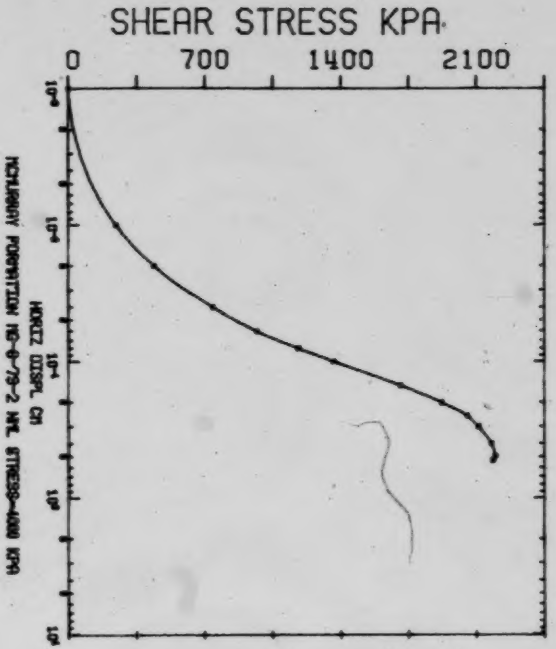
SHEAR STRESS KPA
0
700
1400
2100
HORIZ DISPL CM
MCMURRAY FORMATION HO-8-78-2 NML STRESS=4000 KPA

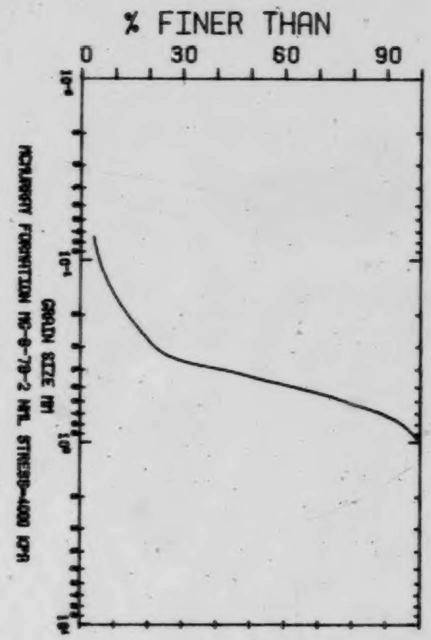
% FINER THAN
0
30
60
90
GRAIN SIZE MM
MCMURRAY FORMATION HO-8-78-2 NML STRESS=4000 KPA

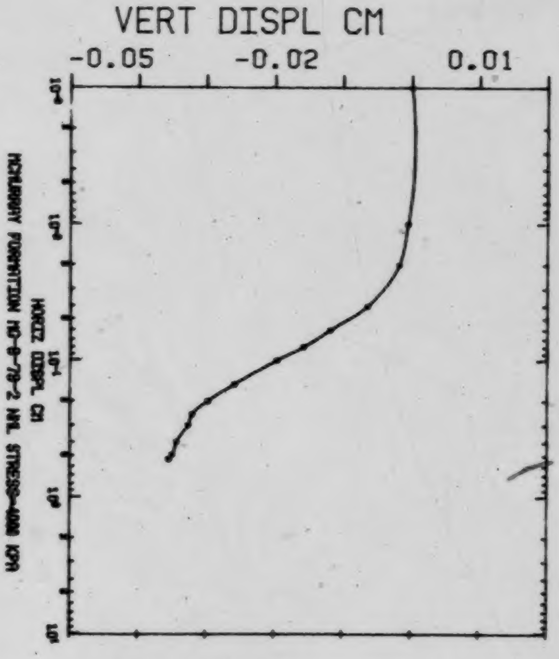
VERT DISPL CM
-0.05
-0.02
0.01
HORIZ DISPL CM
MCMURRAY FORMATION HO-8-78-2 NML STRESS=4000 KPA

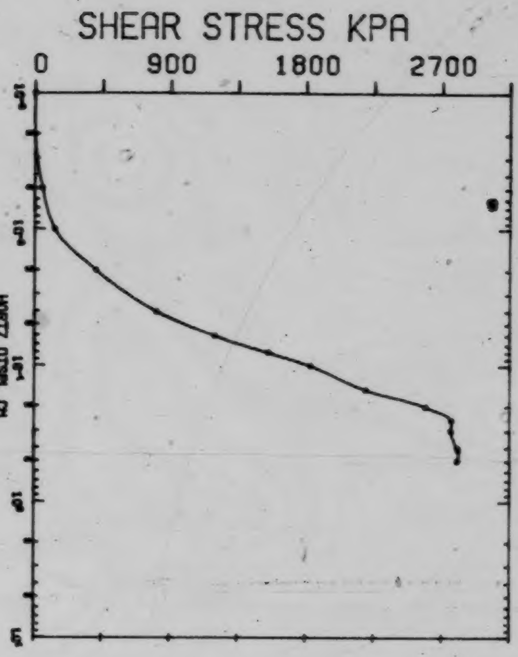
SHEAR STRESS KPA
0
900
1800
2700
10⁻³
10⁻²
10⁻¹
10⁰
10¹
HORIZ DISPL CM
MCMURRAY FORMATION MO-9-79 NML STRESS=5000 KPA

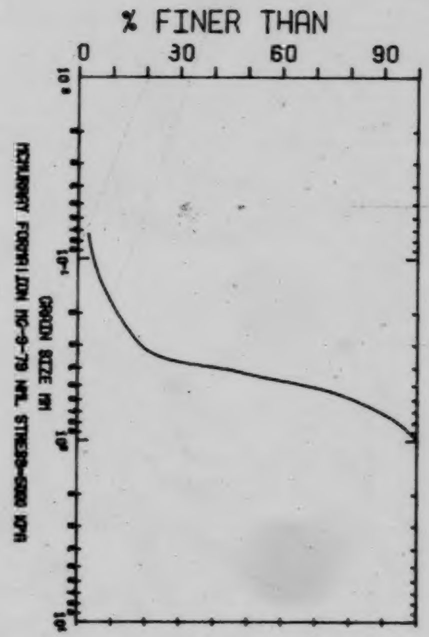
% FINER THAN
0
30
60
90
10⁻²
10⁻¹
10⁰
10¹
GRAIN SIZE MM
MCMURRAY FORMATION MO-9-79 NML STRESS=5000 KPA

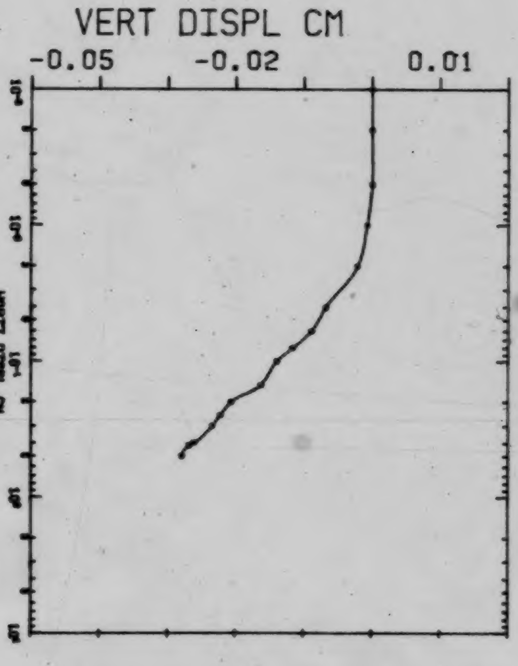
VERT DISPL CM
-0.05
-0.02
0.01
10⁻³
10⁻²
10⁻¹
10⁰
10¹
HORIZ DISPL CM
MCMURRAY FORMATION MO-9-79 NML STRESS=5000 KPA

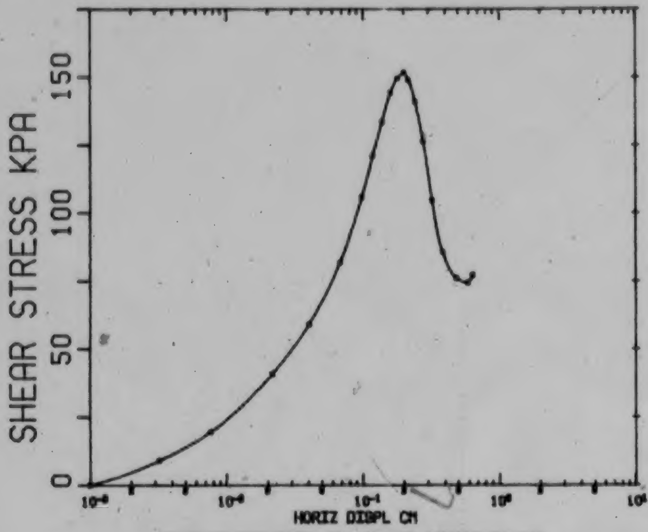

MCMURRAY FORMATION CG-1-79 NML STRESS=100 KPA

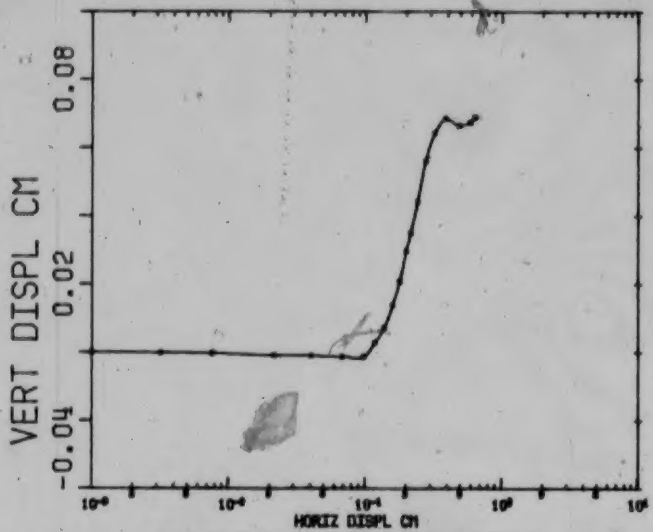

MCMURRAY FORMATION CG-1-79 NML STRESS=100 KPA

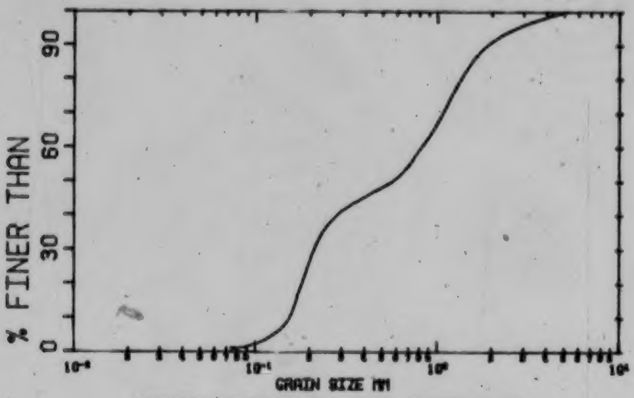

MCMURRAY FORMATION CG-1-79 NML STRESS=100 KPA

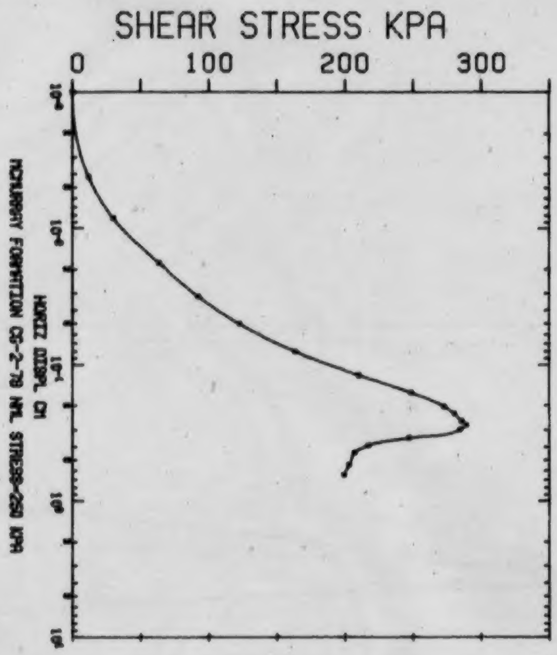
SHEAR STRESS KPA
0
100
200
300
HORIZ DISPL CM
MCMURRAY FORMATION C8-2-79 NML STRESS=250 KPA

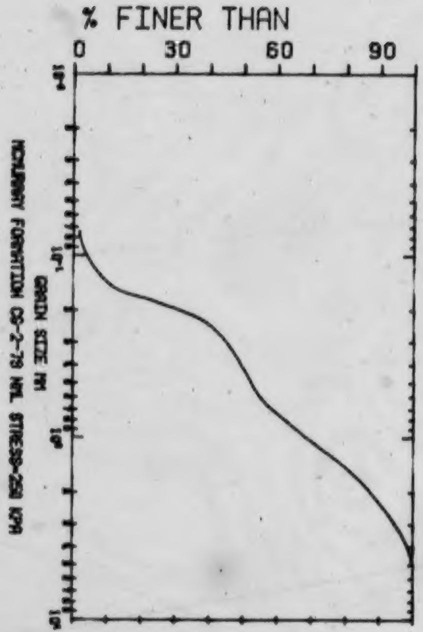
% FINER THAN
0
30
60
90
GRAIN SIZE MM
MCMURRAY FORMATION C8-2-79 NML STRESS=250 KPA

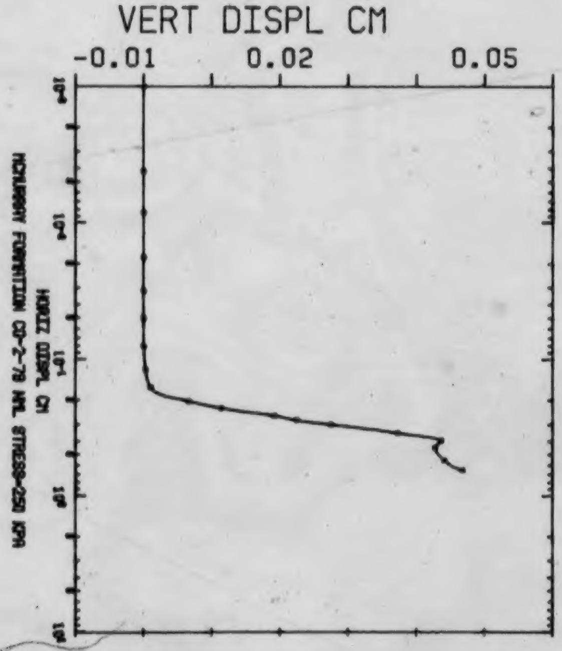
VERT DISPL CM
-0.01
0.02
0.05
HORIZ DISPL CM
MCMURRAY FORMATION C8-2-79 NML STRESS=250 KPA

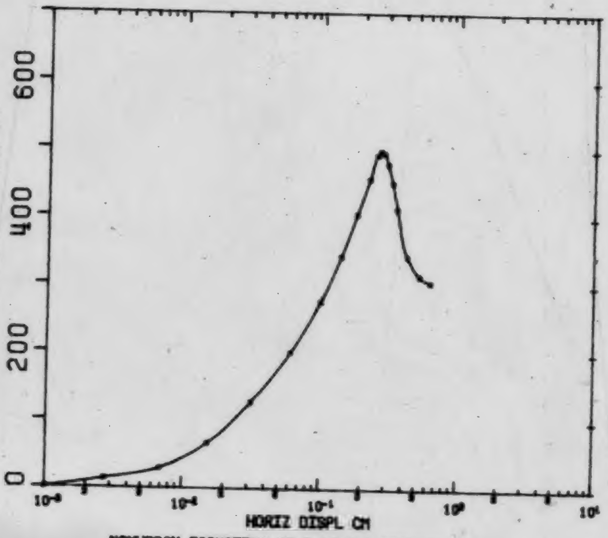

MCMURRAY FORMATION CG-3-79 NML STRESS=400 KPA

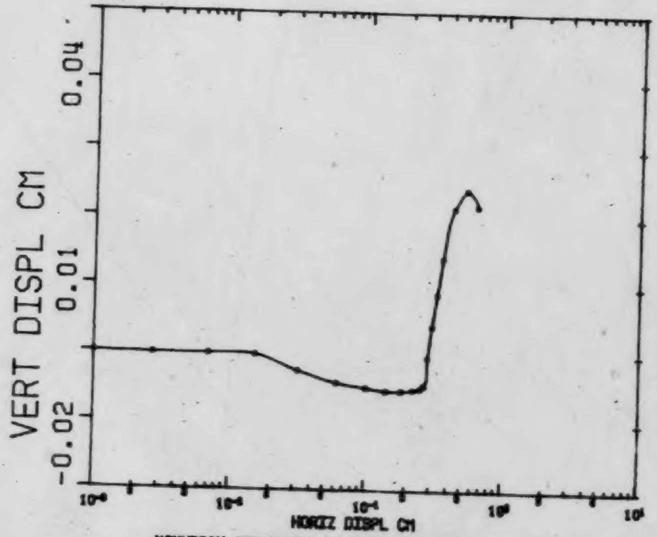

MCMURRAY FORMATION CG-3-79 NML STRESS=400 KPA

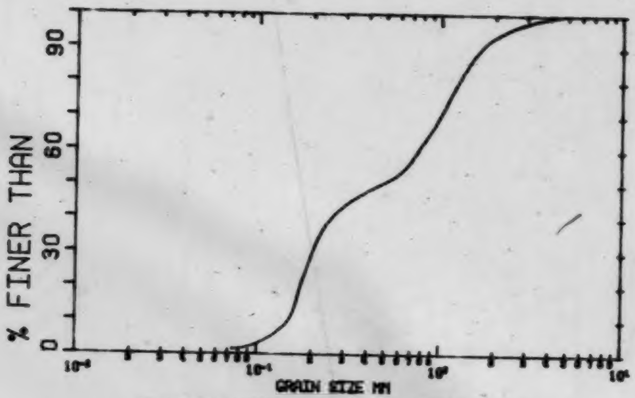

MCMURRAY FORMATION CG-3-79 NML STRESS=400 KPA

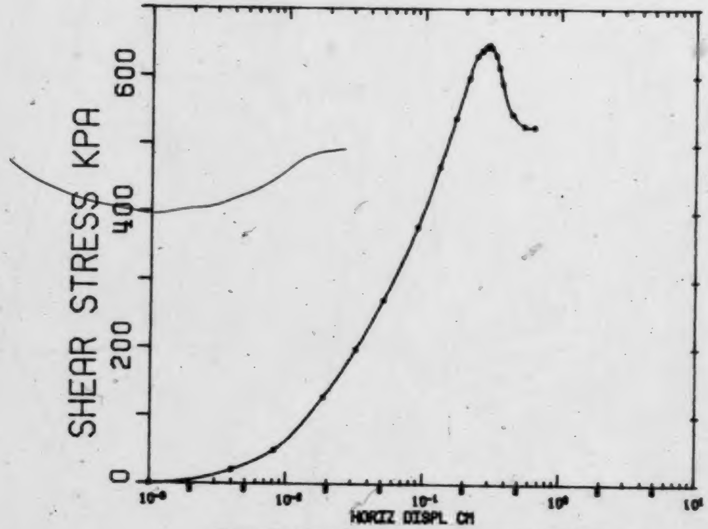

MCMURRAY FORMATION CG-4-78 NML STRESS=700 KPA

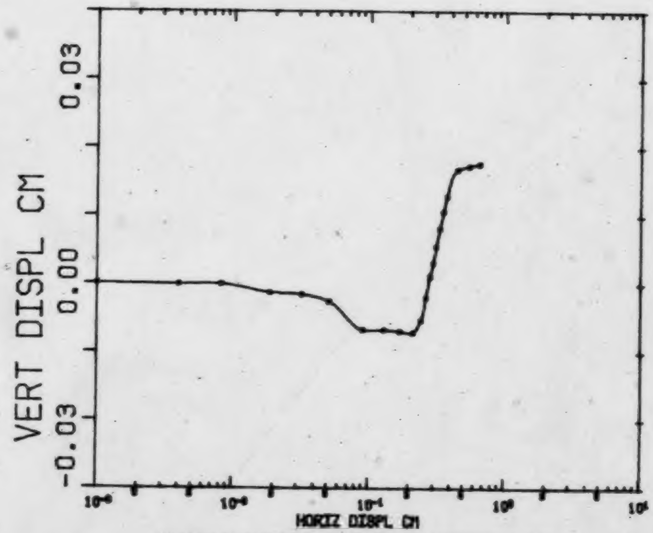

MCMURRAY FORMATION CG-4-78 NML STRESS=700 KPA

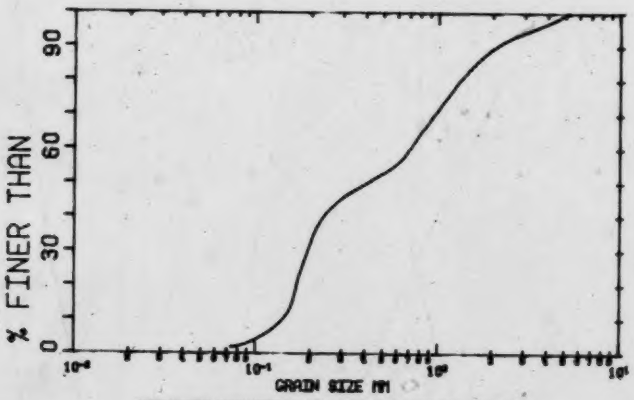

MCMURRAY FORMATION CG-4-79 NML STRESS=700 KPA

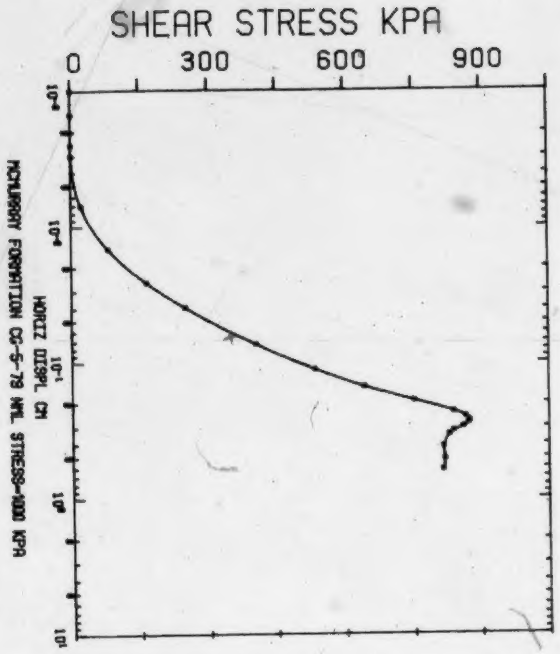
SHEAR STRESS KPA
0
300
600
900
HORIZ DISPL CM
MCMURRAY FORMATION C2-5-79 NML STRESS=1000 KPA

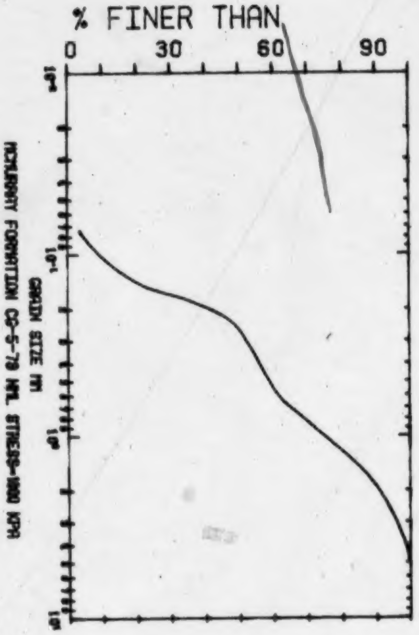
% FINER THAN
0
30
60
90
GRAIN SIZE MM
MCMURRAY FORMATION C2-5-79 NML STRESS=1000 KPA

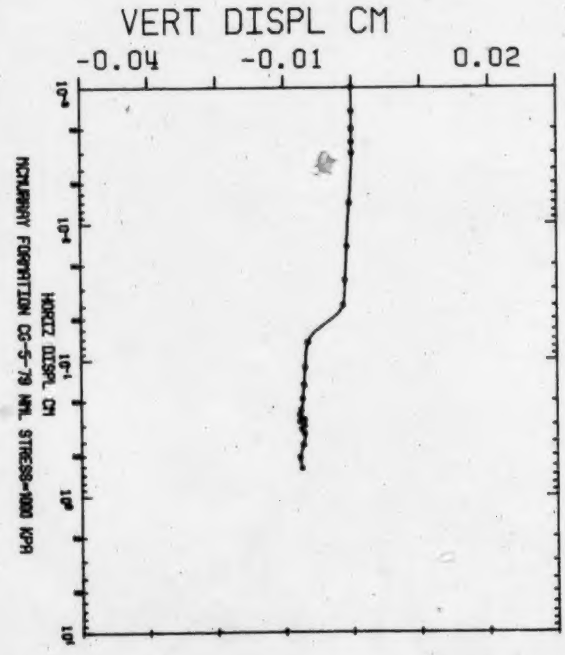
VERT DISPL CM
-0.04
-0.01
0.02
HORIZ DISPL CM
MCMURRAY FORMATION C2-5-79 NML STRESS=1000 KPA

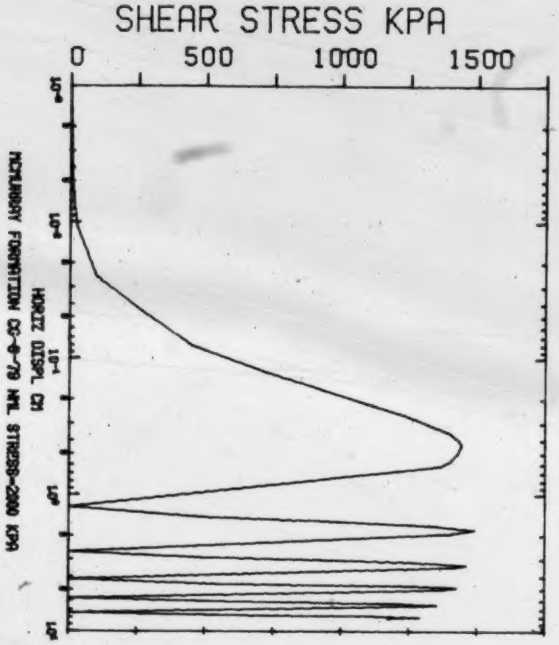
SHEAR STRESS KPA
0
500
1000
1500
HORIZ DISPL CM
MCMURRAY FORMATION CD-8-79 NML STRESS=2000 KPA

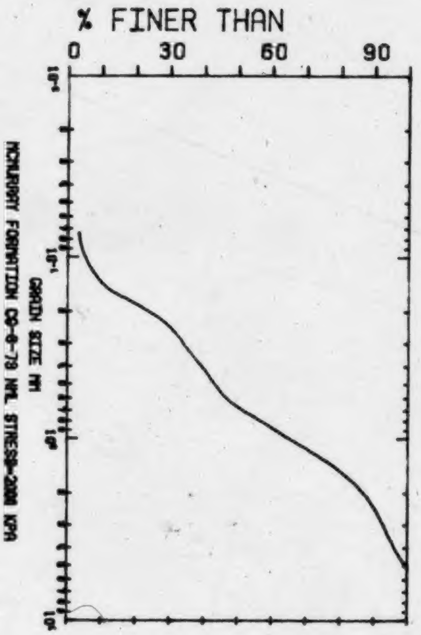
% FINER THAN
0
30
60
90
GRAIN SIZE MM
MCMURRAY FORMATION CD-8-79 NML STRESS=2000 KPA

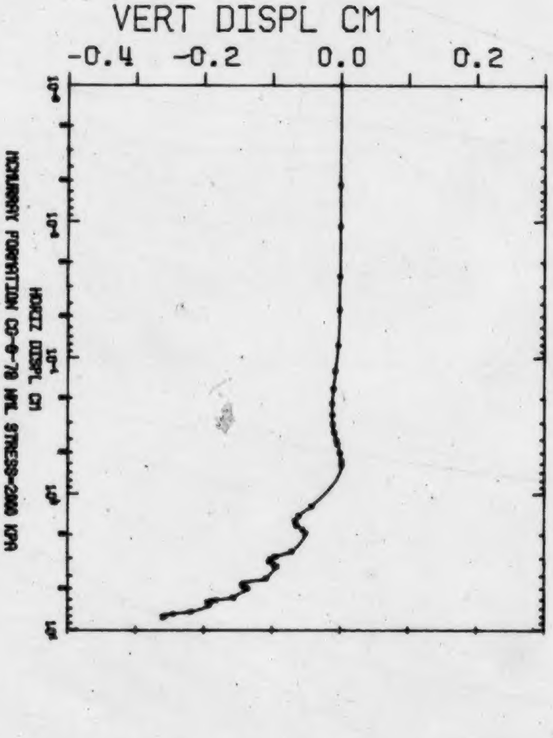
VERT DISPL CM
-0.4
-0.2
0.0
0.2
HORIZ DISPL CM
MCMURRAY FORMATION CD-8-79 NML STRESS=2000 KPA

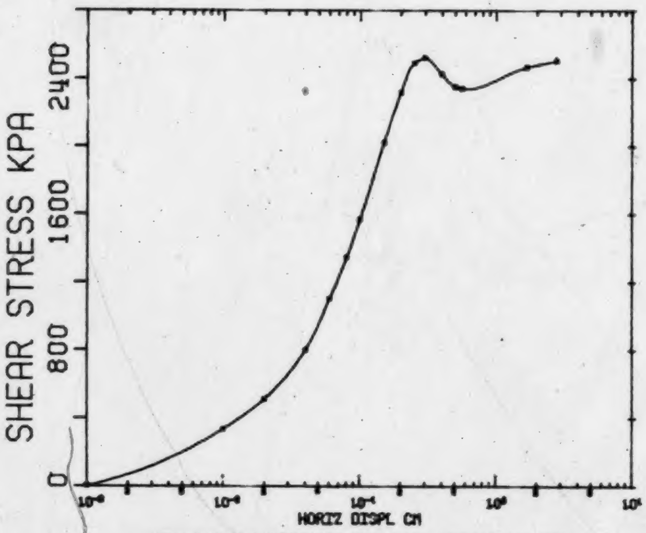

MCMURRAY FORMATION CG-7-79-1 NML STRESS=3000 KPA

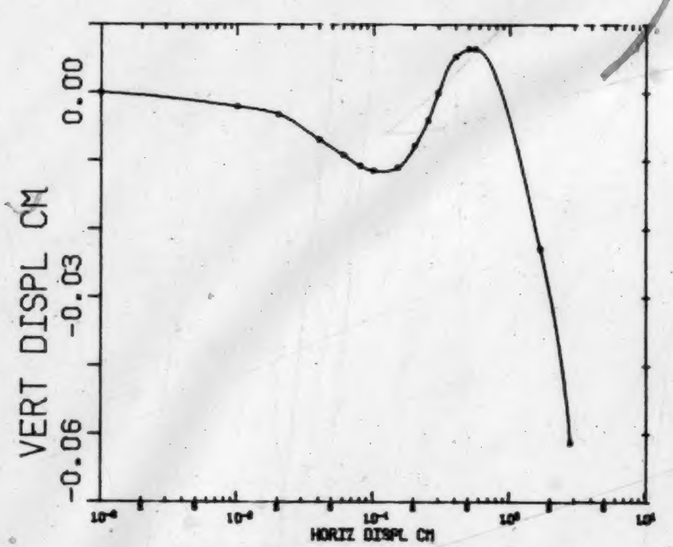

MCMURRAY FORMATION CG-7-79-4 NML STRESS=3000 KPA

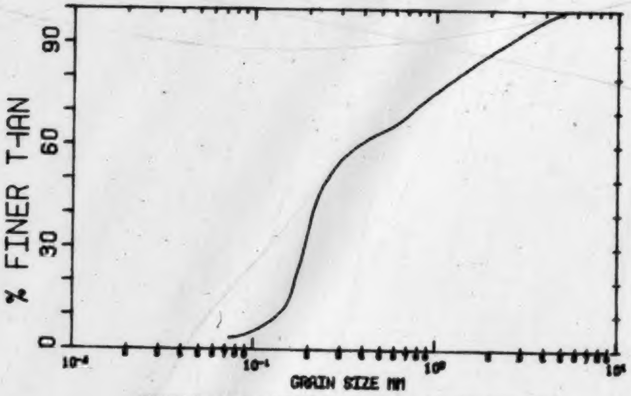

MCMURRAY FORMATION CG-7-79-1 NML STRESS=3000 KPA

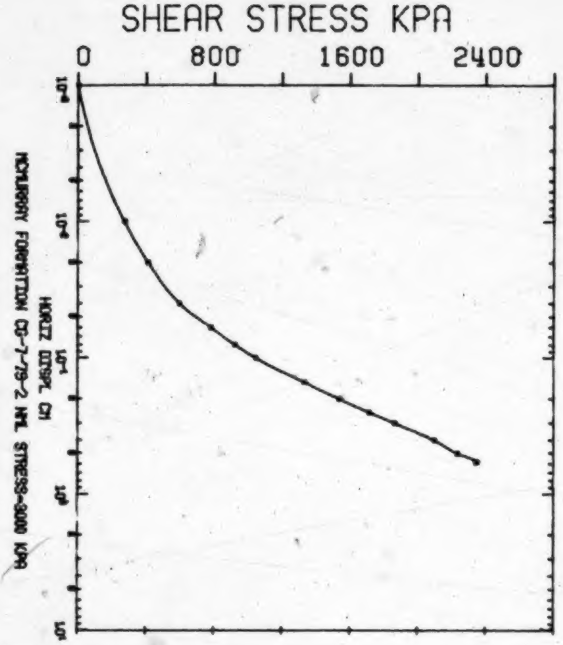
SHEAR STRESS KPA
0
800
1600
2400
10⁻³
10⁻²
10⁻¹
10⁰
10¹
HORIZ DISPL CM
MCMURRAY FORMATION CG-7-79-2 NML STRESS=3000 KPA

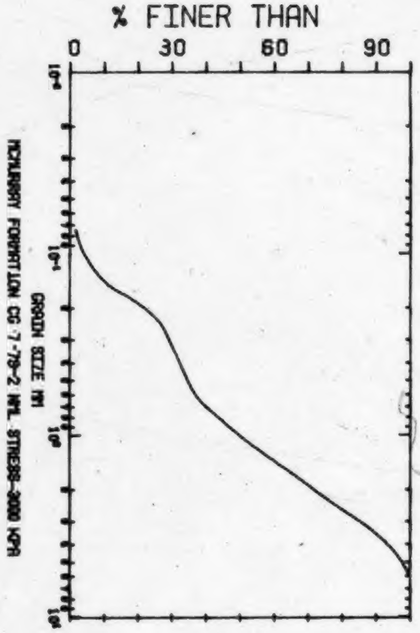
% FINER THAN
0
30
60
90
10⁻²
10⁻¹
10⁰
10¹
GRAIN SIZE MM
MCMURRAY FORMATION CG-7-79-2 NML STRESS=3000 KPA

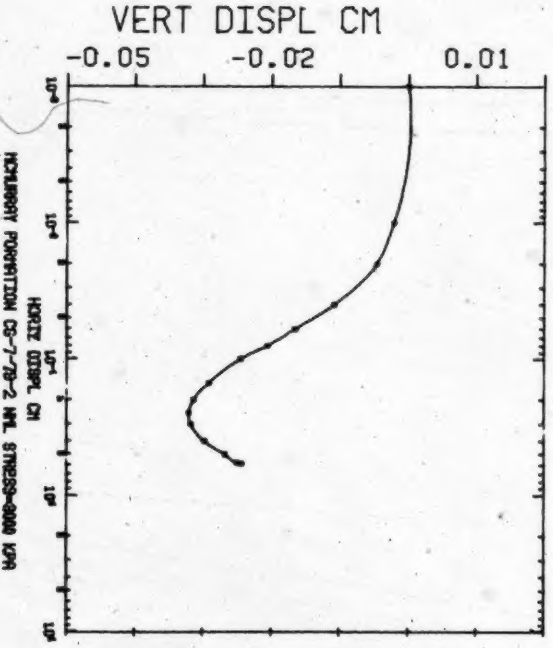
VERT DISPL CM
-0.05
-0.02
0.01
10⁻³
10⁻²
10⁻¹
10⁰
10¹
HORIZ DISPL CM
MCMURRAY FORMATION CG-7-79-2 NML STRESS=3000 KPA

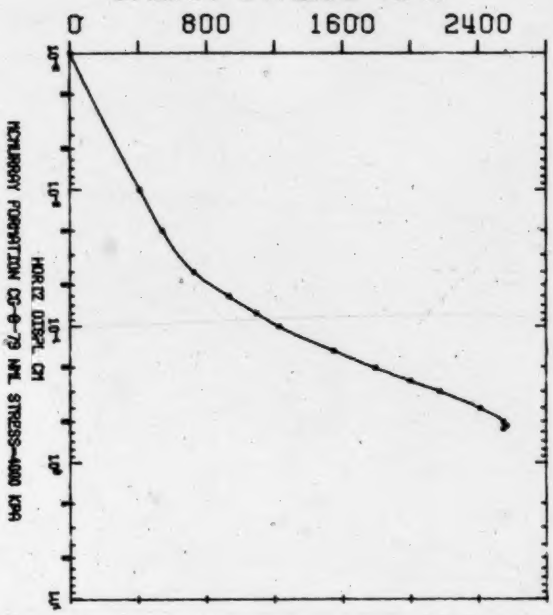
SHEAR STRESS KPA
0
800
1600
2400
HORIZ DISPL CM
MCMURRAY FORMATION CG-8-79 NML STRESS=4000 KPA

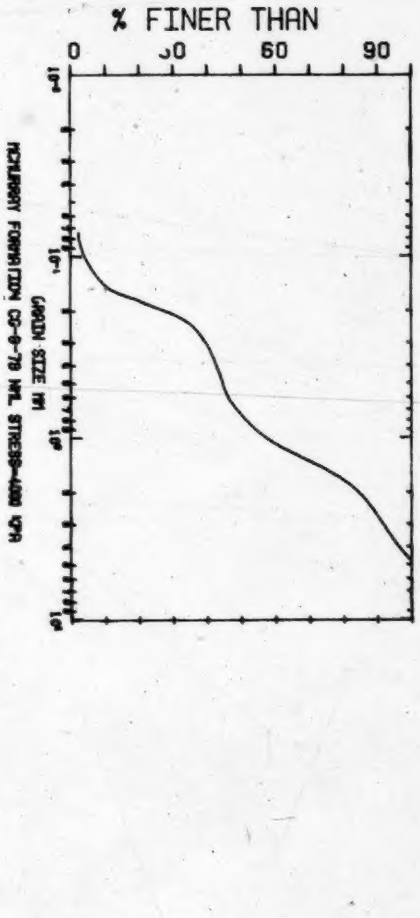
% FINER THAN
0
30
60
90
GRAIN SIZE MM
MCMURRAY FORMATION CG-8-79 NML STRESS=4000 KPA

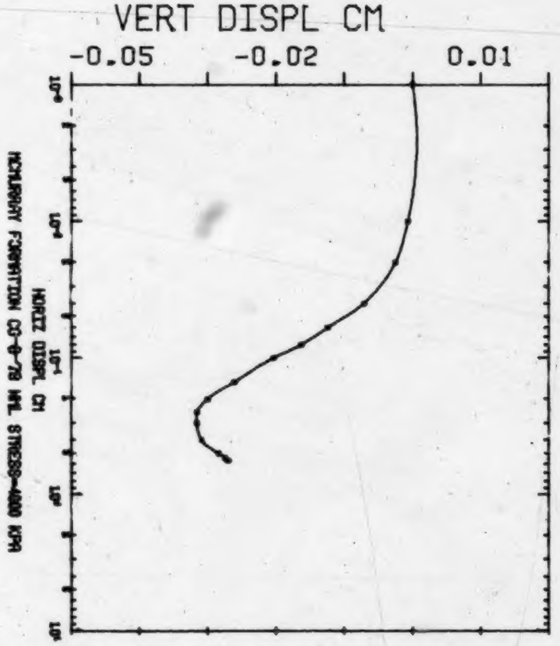
VERT DISPL CM
-0.05
-0.02
0.01
HORIZ DISPL CM
MCMURRAY FORMATION CG-8-79 NML STRESS=4000 KPA

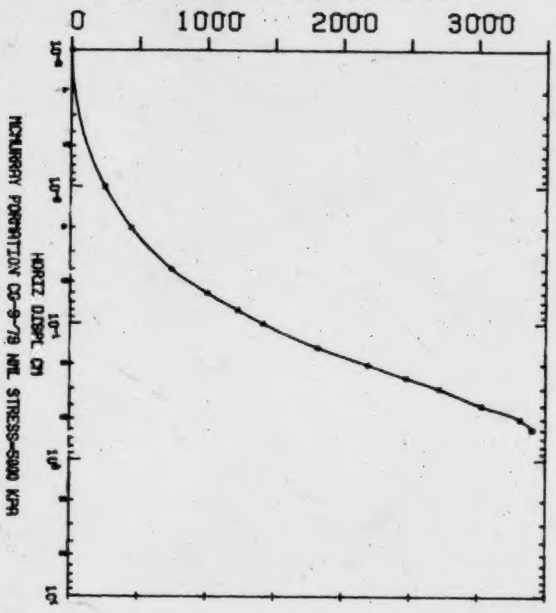
SHEAR STRESS KPA
0
1000
2000
3000
HORIZ DISPL CM
MCMURRAY FORMATION CG-9-79 NML STRESS=5000 KPA

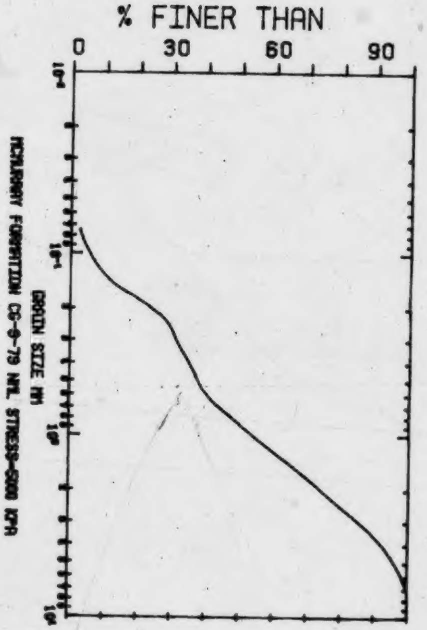
% FINER THAN
0
30
60
90
GRAIN SIZE MM
MCMURRAY FORMATION CG-9-79 NML STRESS=5000 KPA

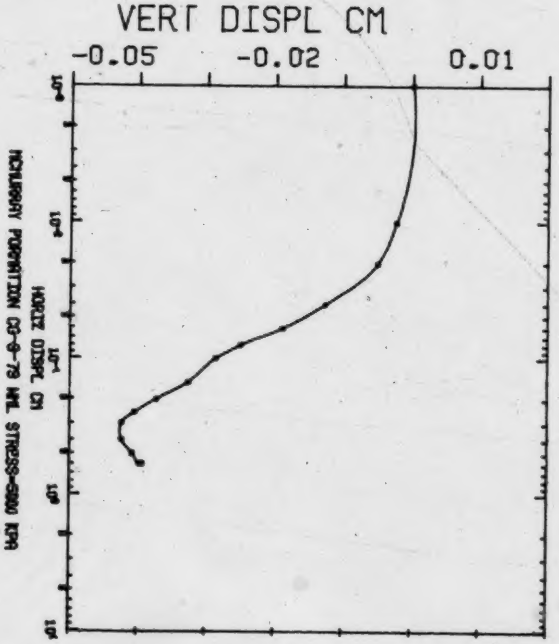
VERT DISPL CM
-0.05
-0.02
0.01
HORIZ DISPL CM
MCMURRAY FORMATION CG-9-79 NML STRESS=5000 KPA

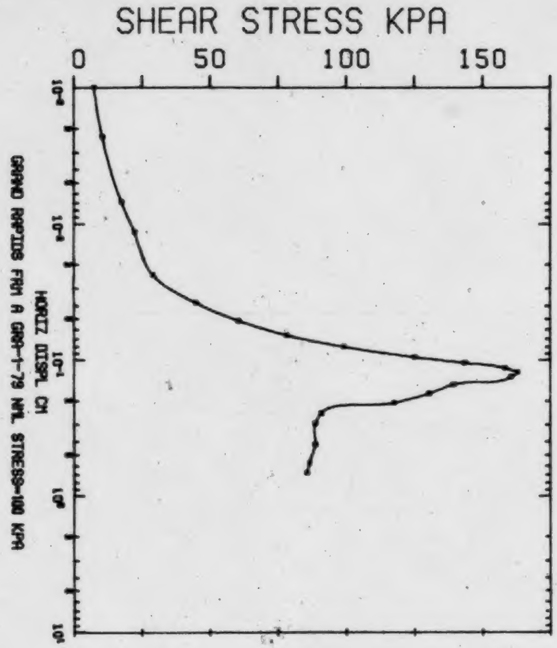
SHEAR STRESS KPA
0
50
100
150
10^-3
10^-2
10^-1
10^0
10^1
HORIZ DISPL CM
GRAND RAPIDS FRM A GRR-1-79 NML STRESS=100 KPA

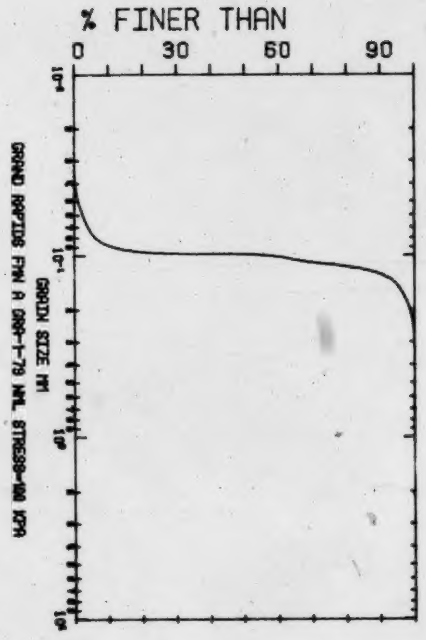
% FINER THAN
0
30
60
90
10^-2
10^-1
10^0
10^1
GRAIN SIZE MM
GRAND RAPIDS FRM A GRR-1-79 NML STRESS=100 KPA

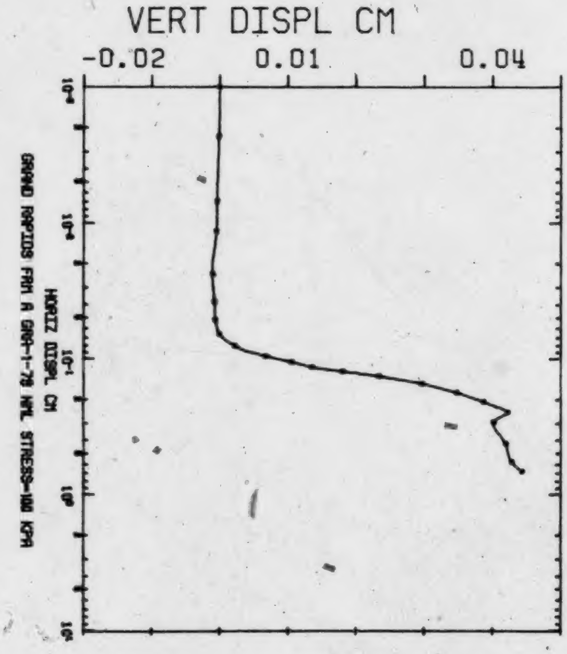
VERT DISPL CM
-0.02
0.01
0.04
10^-3
10^-2
10^-1
10^0
10^1
HORIZ DISPL CM
GRAND RAPIDS FRM A GRR-1-79 NML STRESS=100 KPA

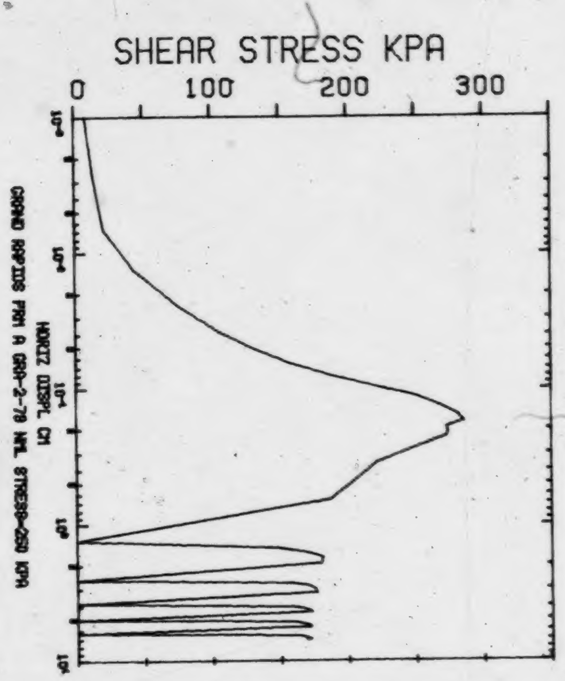
SHEAR STRESS KPA
0
100
200
300
10^{-3}
10^{-2}
10^{-1}
10^{0}
10^{1}
HORIZ DISPL CM
GRAND RAPIDS FRM A GRP-2-78 NML STRESS=250 KPA

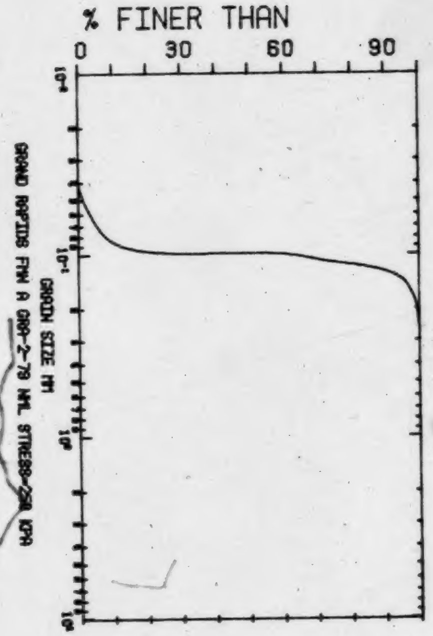
% FINER THAN
0
30
60
90
10^{-2}
10^{-1}
10^{0}
10^{1}
GRAIN SIZE MM
GRAND RAPIDS FRM A GRP-2-78 NML STRESS=250 KPA

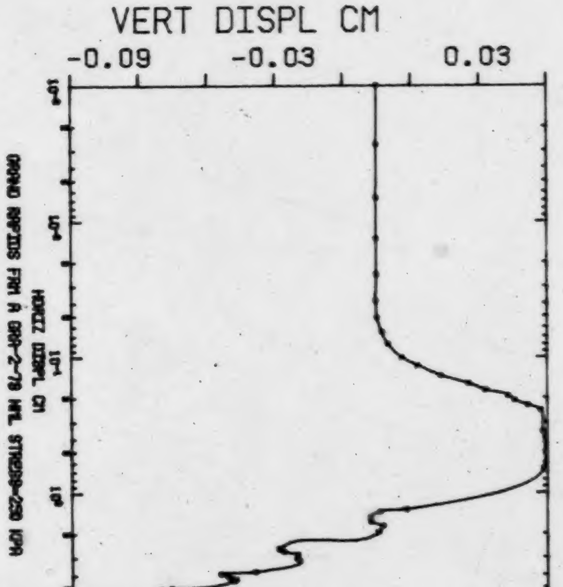
VERT DISPL CM
-0.09
-0.03
0.03
10^{-3}
10^{-2}
10^{-1}
10^{0}
10^{1}
HORIZ DISPL CM
GRAND RAPIDS FRM A GRP-2-78 NML STRESS=250 KPA

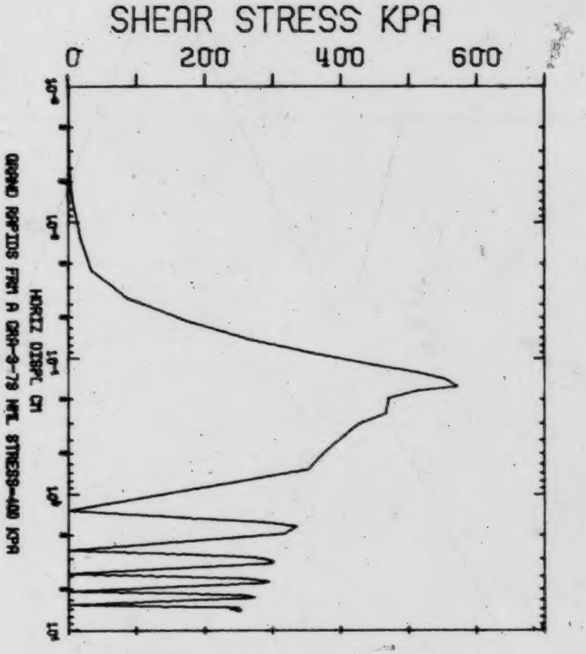
SHEAR STRESS KPA
0
200
400
600
HORIZ DISPL CM
GRAND RAPIDS FMN A GRR-9-79 NML STRESS=400 KPA

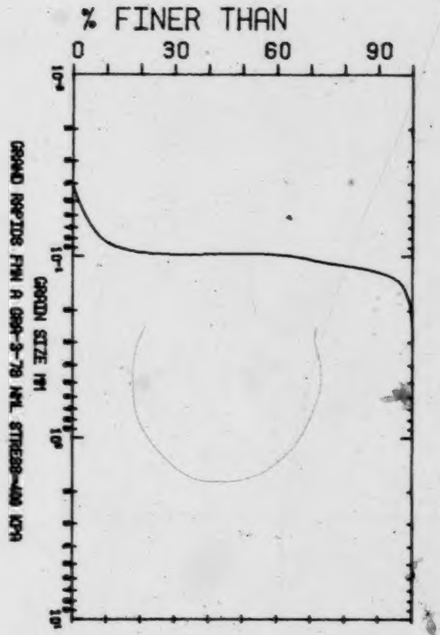
% FINER THAN
0
30
60
90
GRAIN SIZE MM
GRAND RAPIDS FMN A GRR-9-79 NML STRESS=400 KPA

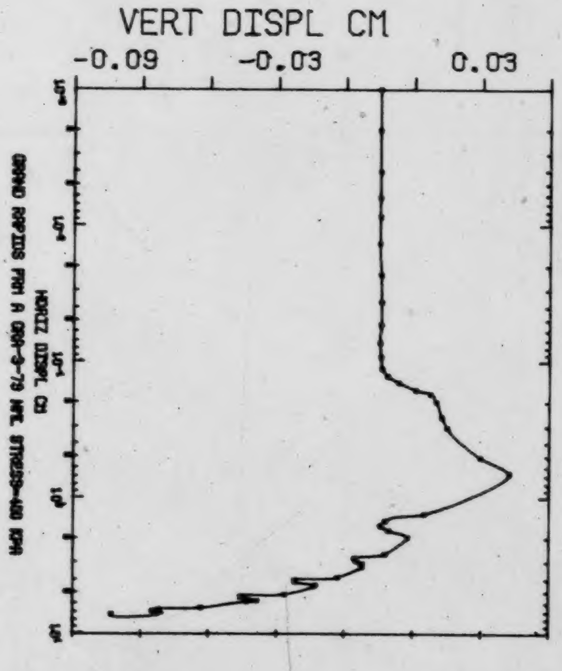
VERT DISPL CM
-0.09
-0.03
0.03
HORIZ DISPL CM
GRAND RAPIDS FMN A GRR-9-79 NML STRESS=400 KPA

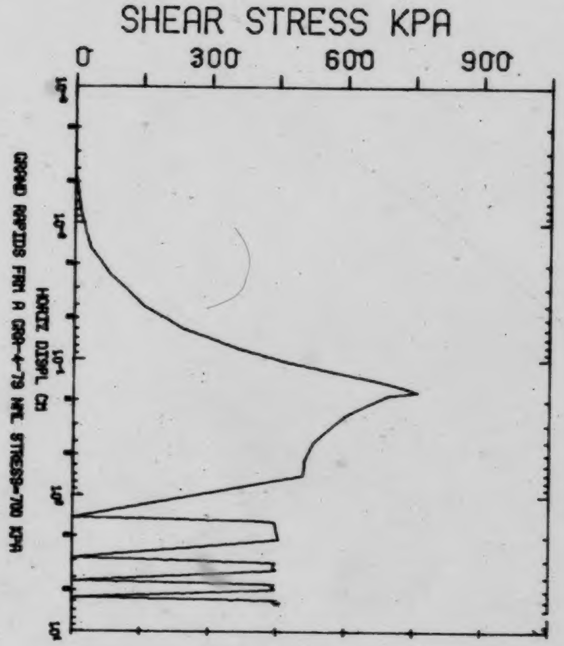
SHEAR STRESS KPA
0
300
600
900
10^-3
10^-2
10^-1
10^0
10^1
HORIZ DISPL CM
GRAND RAPIDS FRM A GRR-4-79 NML STRESS=700 KPA

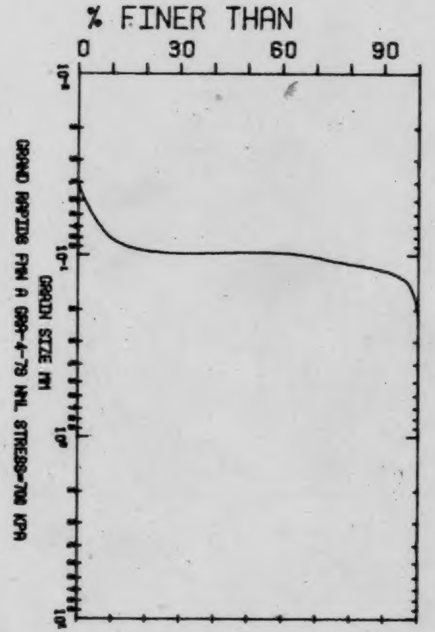
% FINER THAN
0
30
60
90
10^-2
10^-1
10^0
10^1
GRAIN SIZE MM
GRAND RAPIDS FRM A GRR-4-79 NML STRESS=700 KPA

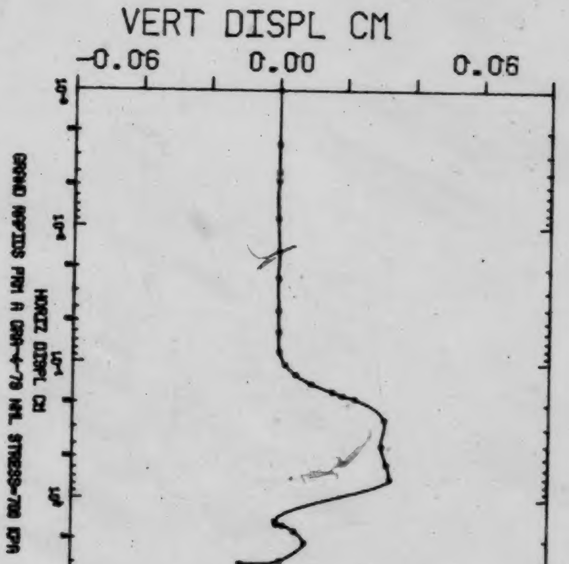
VERT DISPL CM
-0.06
0.00
0.06
10^-3
10^-2
10^-1
10^0
10^1
HORIZ DISPL CM
GRAND RAPIDS FRM A GRR-4-79 NML STRESS=700 KPA

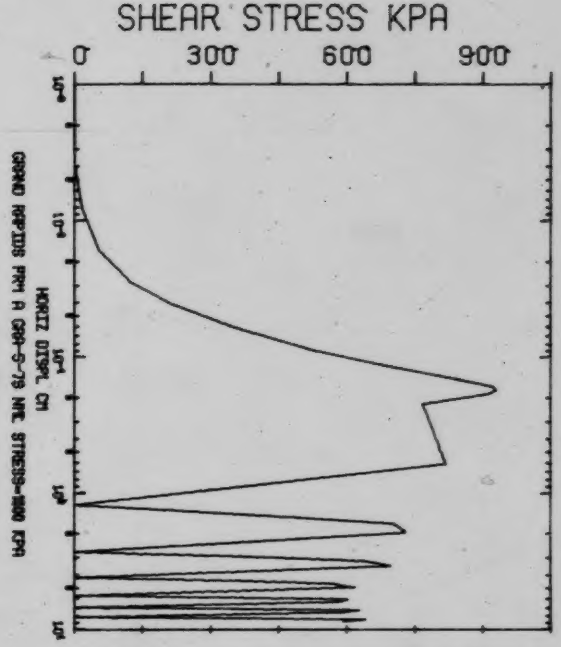
SHEAR STRESS KPA
0
300
600
900
10^{-3}
10^{-2}
10^{-1}
10^{0}
10^{1}
HORIZ DISPL CM
GRAND RAPIDS FRM A GRA-6-79 NML STRESS=1000 KPA

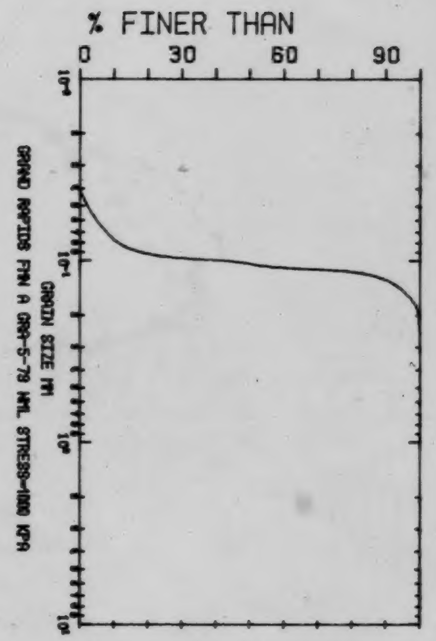
% FINER THAN
0
30
60
90
10^{-2}
10^{-1}
10^{0}
10^{1}
GRAIN SIZE MM
GRAND RAPIDS FMN A GRA-6-79 NML STRESS=1000 KPA

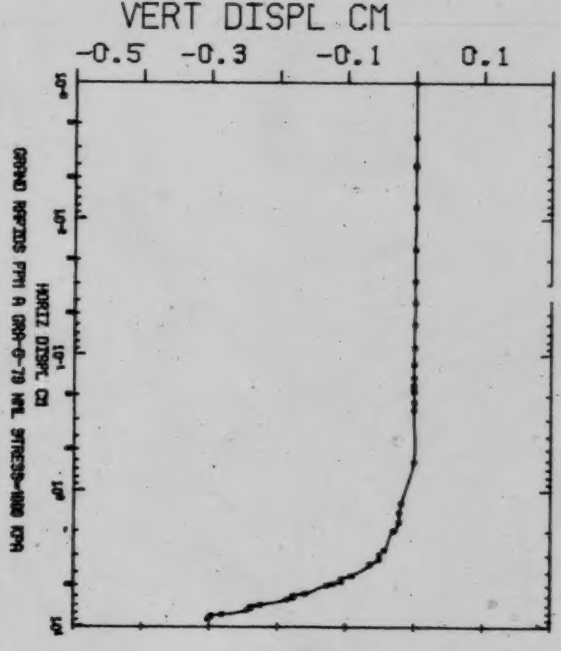
VERT DISPL CM
-0.5
-0.3
-0.1
0.1
10^{-3}
10^{-2}
10^{-1}
10^{0}
10^{1}
HORIZ DISPL CM
GRAND RAPIDS FMN A GRA-6-79 NML STRESS=1000 KPA

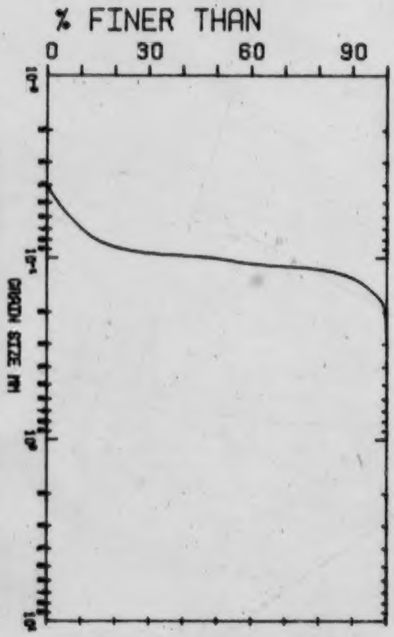
% FINER THAN
0
30
60
90
10^{-2}
10^{-1}
10^{0}
10^{1}
GRAIN SIZE MM
GRAND RAPIDS FRM A GRR-8-79 NML STRESS=2000 KPA

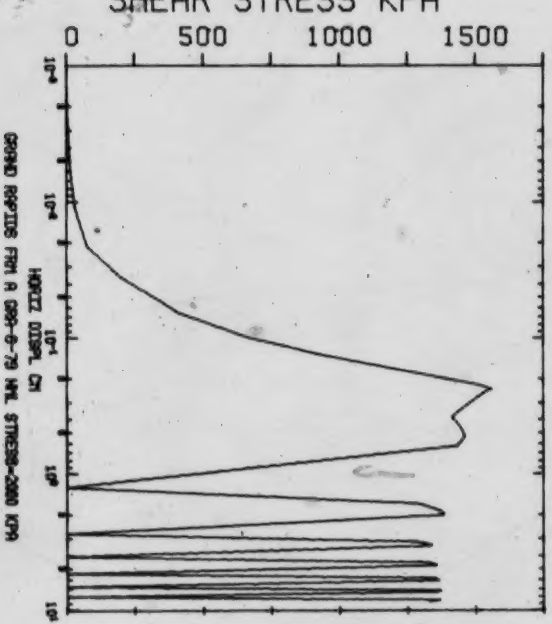
SHEAR STRESS KPA
0
500
1000
1500
10^{-3}
10^{-2}
10^{-1}
10^{0}
10^{1}
HORIZ DISPL CM
GRAND RAPIDS FRM A GRR-8-79 NML STRESS=2000 KPA

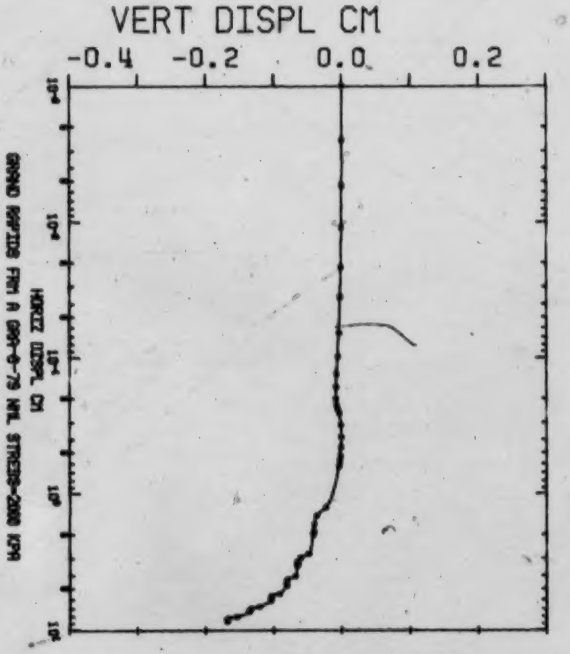
VERT DISPL CM
-0.4
-0.2
0.0
0.2
10^{-3}
10^{-2}
10^{-1}
10^{0}
10^{1}
HORIZ DISPL CM
GRAND RAPIDS FRM A GRR-8-79 NML STRESS=2000 KPA

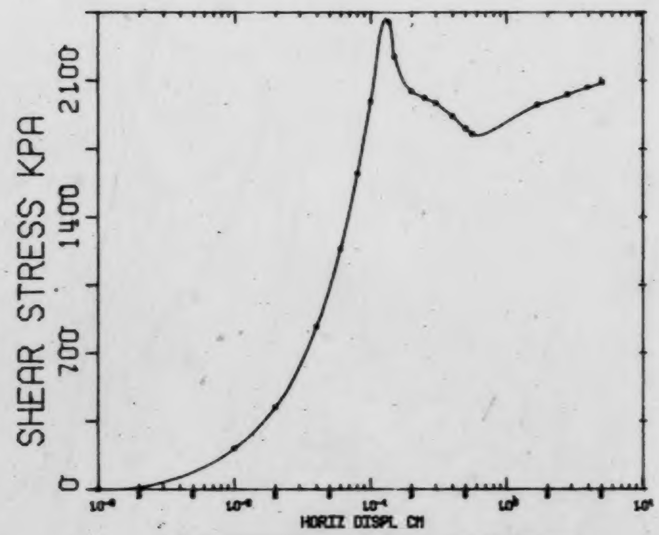

GRAND RAPIDS FMN A GRA-7-79 NML STRESS=3000 KPA

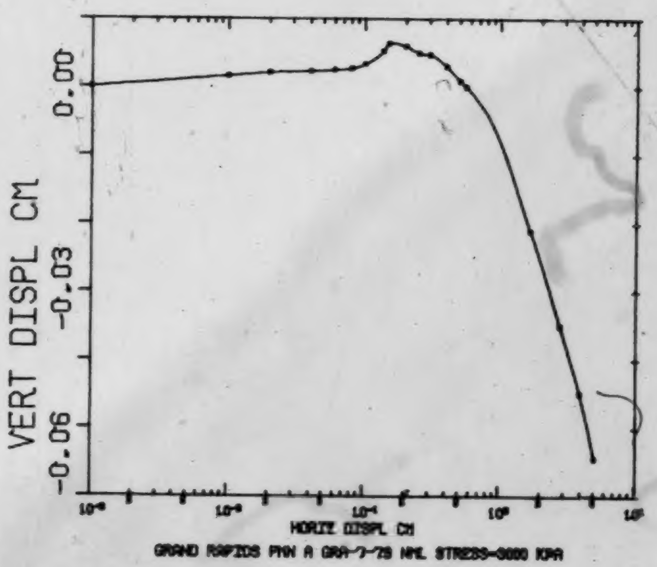

GRAND RAPIDS FMN A GRA-7-79 NML STRESS=3000 KPA

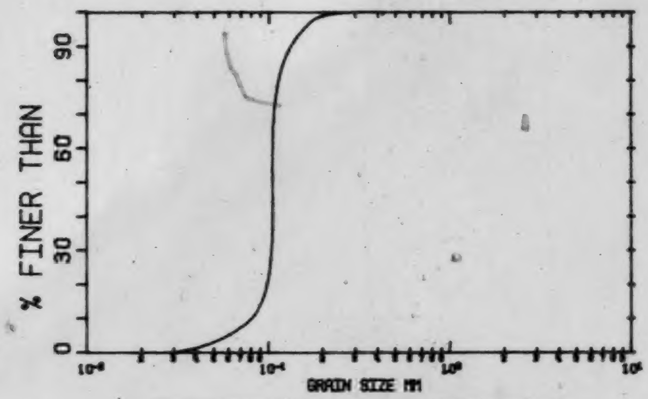

GRAND RAPIDS FMN A GRA-7-79 NML STRESS=3000 KPA

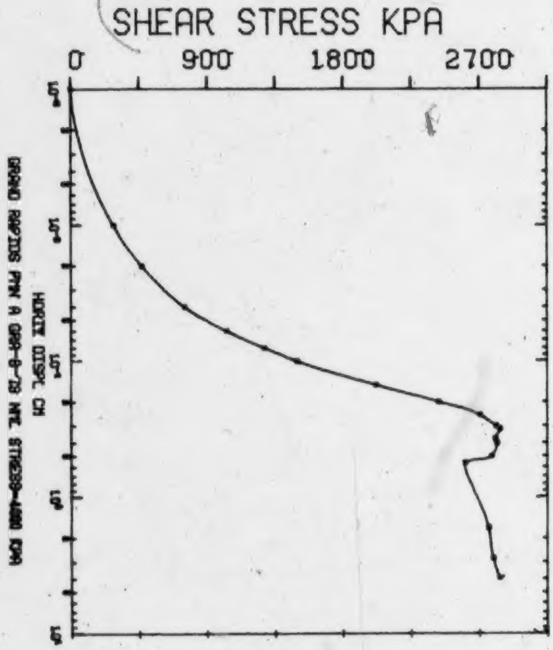
SHEAR STRESS KPA
0
900
1800
2700
HORIZ DISPL CM
GRAND RAPIDS FMN A GRA-8-79 NML STRESS=4000 KPA

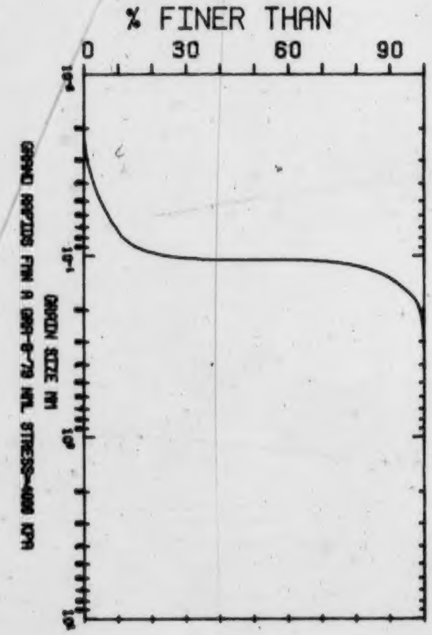
% FINER THAN
0
30
60
90
GRAIN SIZE MM
GRAND RAPIDS FMN A GRA-8-79 NML STRESS=4000 KPA

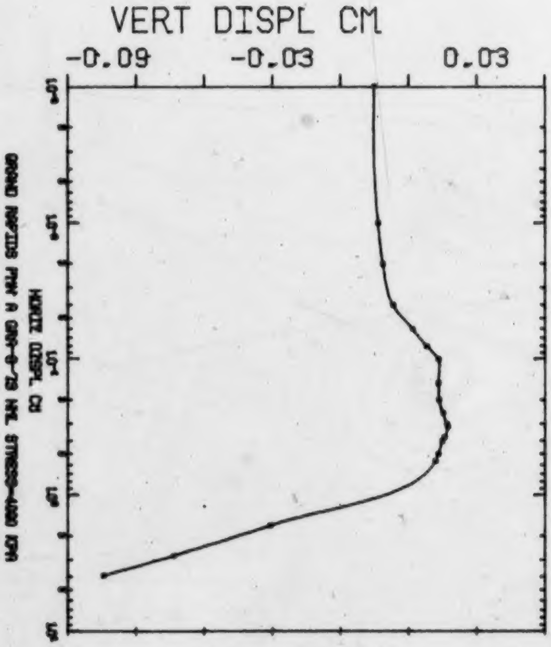
VERT DISPL CM
-0.09
-0.03
0.03
HORIZ DISPL CM
GRAND RAPIDS FMN A GRA-8-79 NML STRESS=4000 KPA

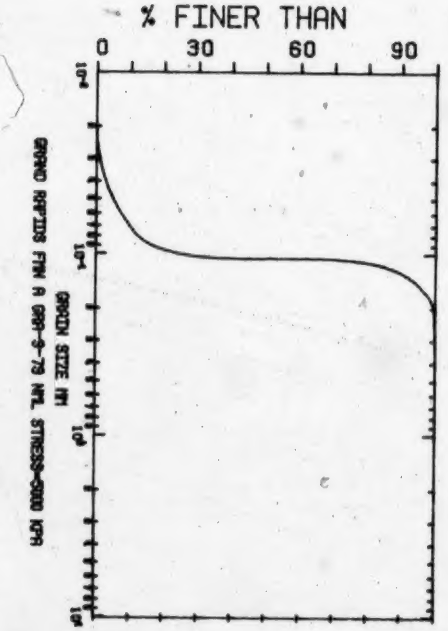
% FINER THAN
0
30
60
90
GRAIN SIZE MM
GRAND RAPIDS FMN A GRR-9-79 NML STRESS=5000 KPA

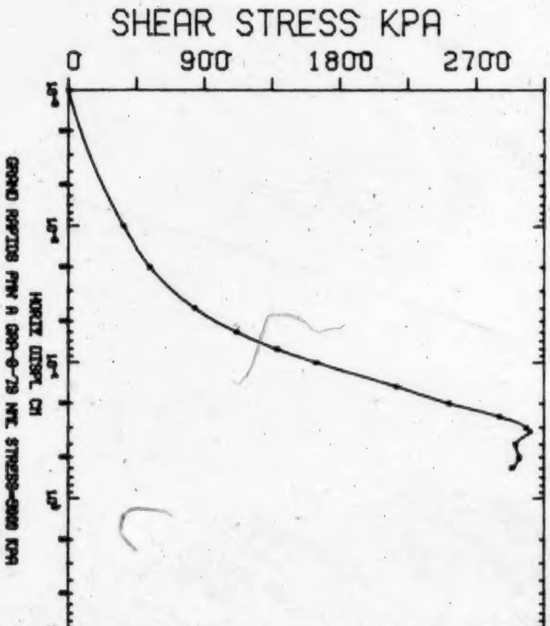
SHEAR STRESS KPA
0
900
1800
2700
HORIZ DISPL CM
GRAND RAPIDS FMN A GRR-9-79 NML STRESS=5000 KPA

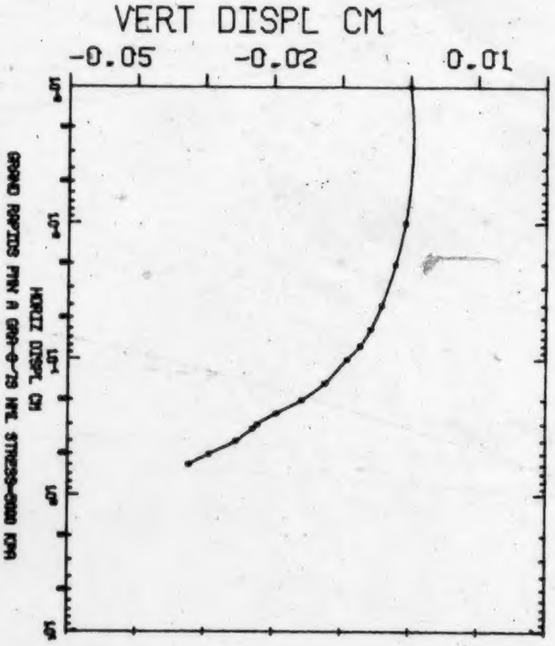
VERT DISPL CM
-0.05
-0.02
0.01
HORIZ DISPL CM
GRAND RAPIDS FMN A GRR-9-79 NML STRESS=5000 KPA

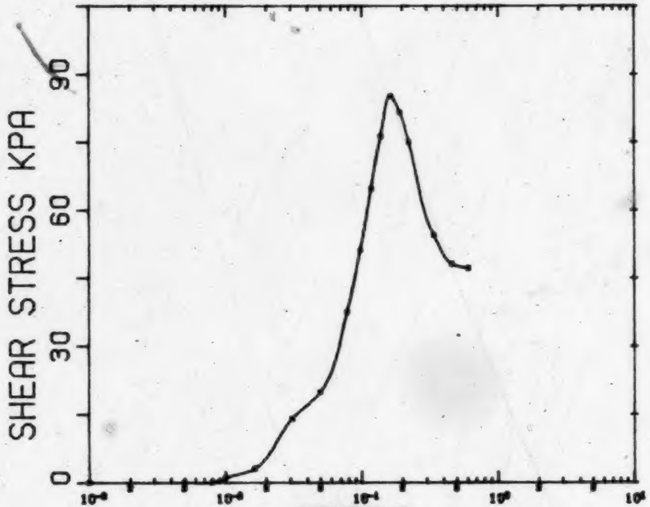

GRAND RAPIDS FMN C GRC-0-79 NML STRESS=50 KPA

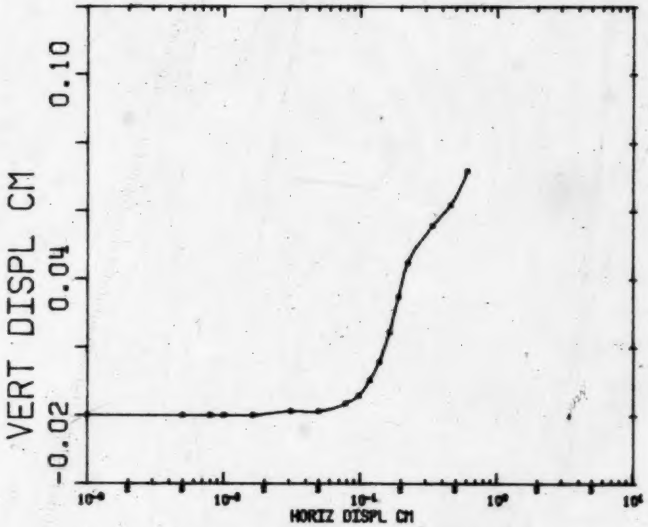

GRAND RAPIDS FMN C GRC-0-79 NML STRESS=50 KPA

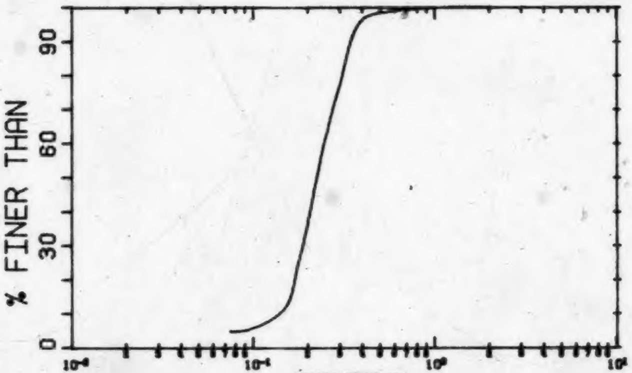

GRAND RAPIDS FMN C GRC-0-79 NML STRESS=50 KPA

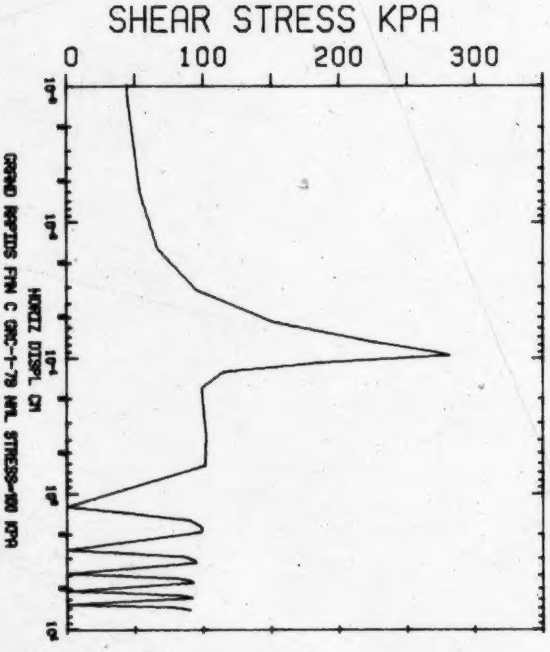

GRAND RAPIDS FMN C GRC-1-79 NML STRESS=100 KPA

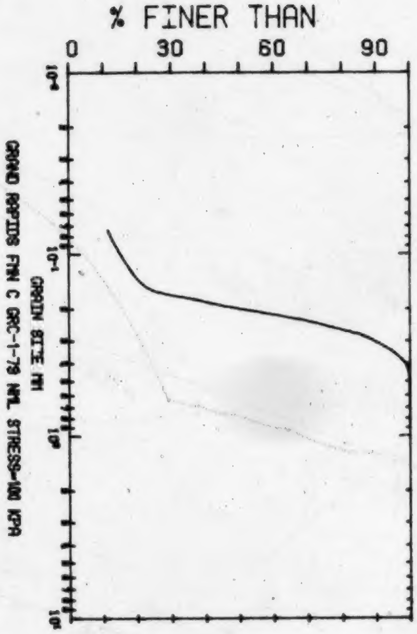

GRAND RAPIDS FMN C GRC-1-79 NML STRESS=100 KPA

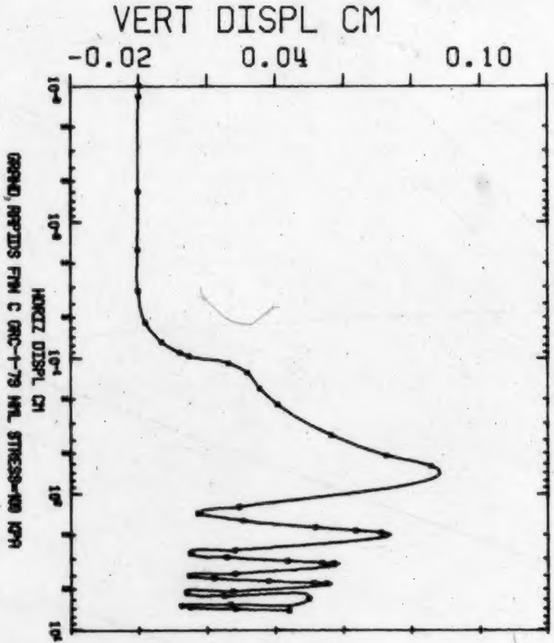

GRAND,RAPIDS FMN C GRC-1-79 NML STRESS=100 KPA

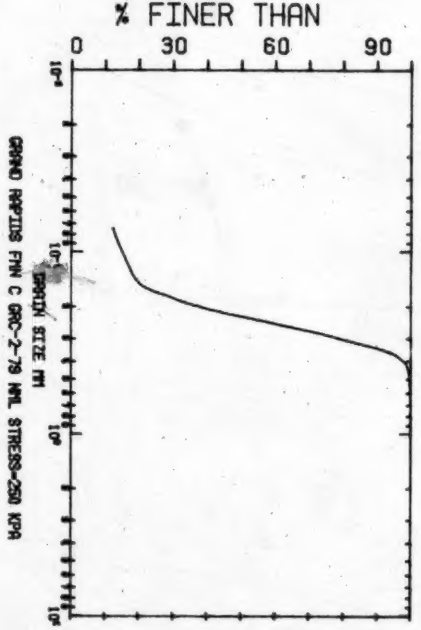
% FINER THAN
0
30
60
90
GRAIN SIZE MM
GRAND RAPIDS FMN C GRC-2-79 NML STRESS=250 KPA

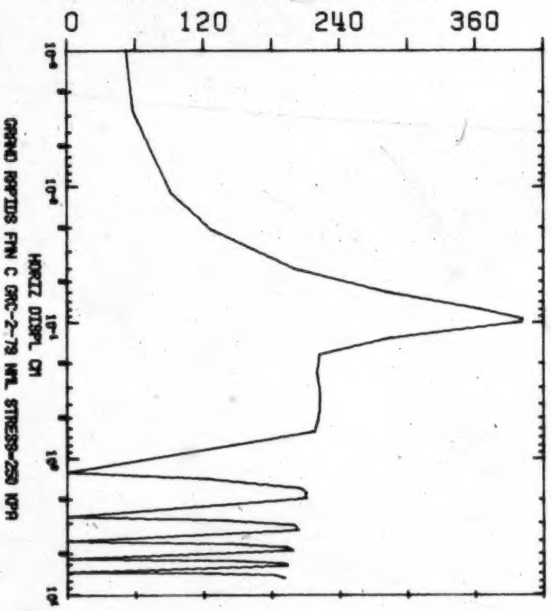
SHEAR STRESS KPA
0
120
240
360
HORIZ DISPL CM
GRAND RAPIDS FMN C GRC-2-79 NML STRESS=250 KPA

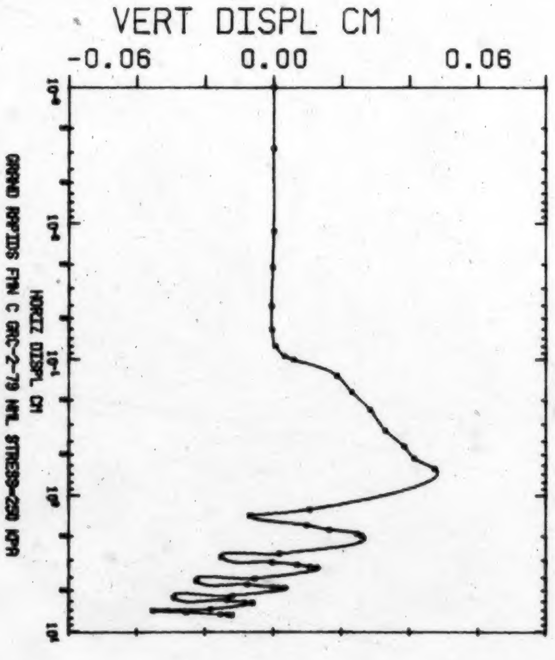
VERT DISPL CM
-0.06
0.00
0.06
HORIZ DISPL CM
GRAND RAPIDS FMN C GRC-2-79 NML STRESS=250 KPA

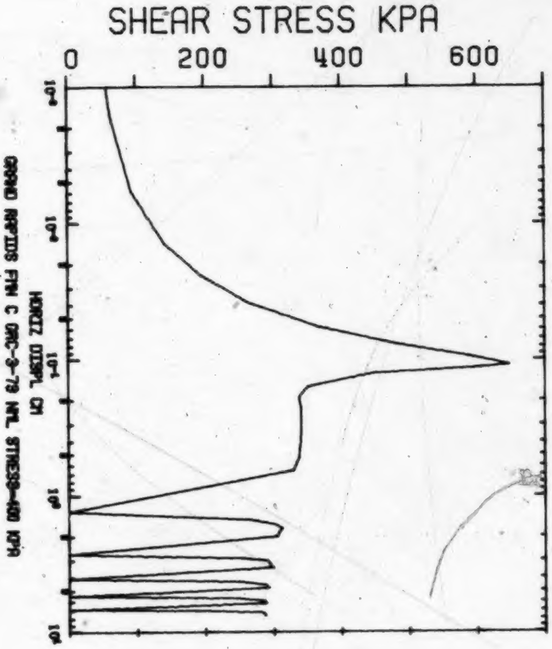
SHEAR STRESS KPA
0
200
400
600
10⁻³
10⁻²
10⁻¹
10⁰
10¹
HORIZ DISPL CM
GRAND RAPIDS FMN C ORC-3-79 NML STRESS=400 KPA

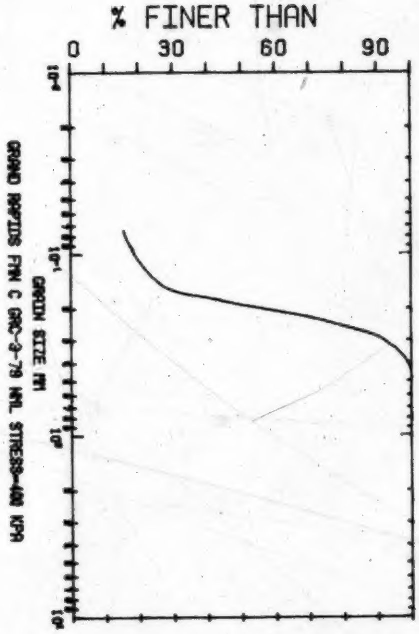
% FINER THAN
0
30
60
90
10⁻²
10⁻¹
10⁰
10¹
GRAIN SIZE MM
GRAND RAPIDS FMN C ORC-3-79 NML STRESS=400 KPA

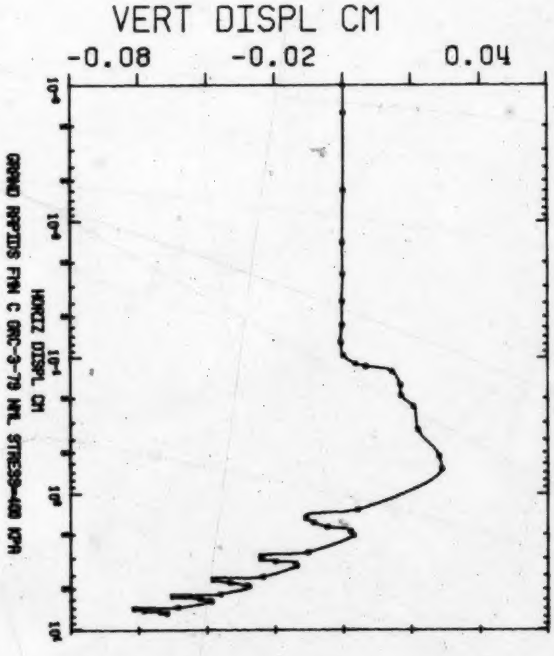
VERT DISPL CM
-0.08
-0.02
0.04
10⁻³
10⁻²
10⁻¹
10⁰
10¹
HORIZ DISPL CM
GRAND RAPIDS FMN C ORC-3-79 NML STRESS=400 KPA

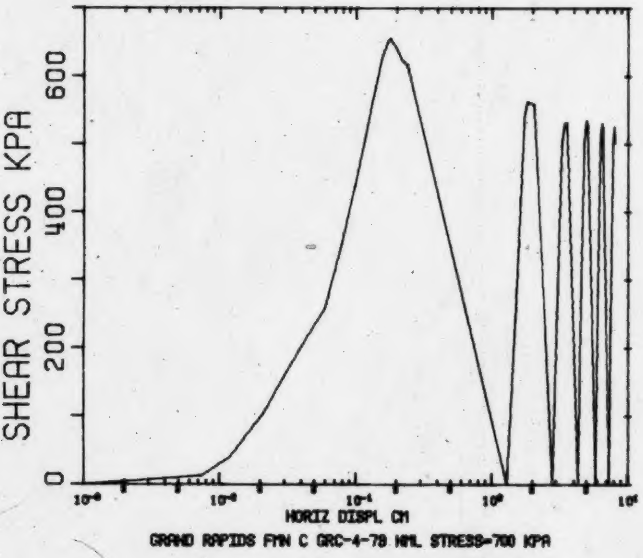
SHEAR STRESS KPA
0
200
400
600
10^-3
10^-2
10^-1
10^0
10^1
HORIZ DISPL CM
GRAND RAPIDS FMN C GRC-4-79 NML STRESS=700 KPA

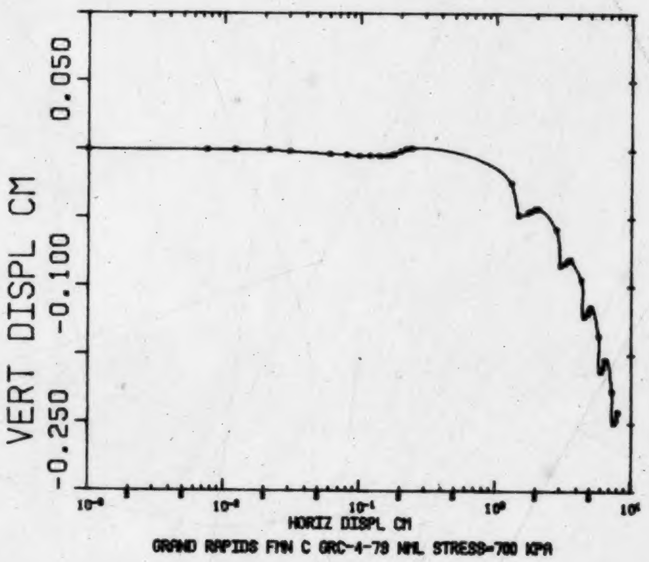
VERT DISPL CM
-0.250
-0.100
0.050
10^-3
10^-2
10^-1
10^0
10^1
HORIZ DISPL CM
GRAND RAPIDS FMN C GRC-4-79 NML STRESS=700 KPA

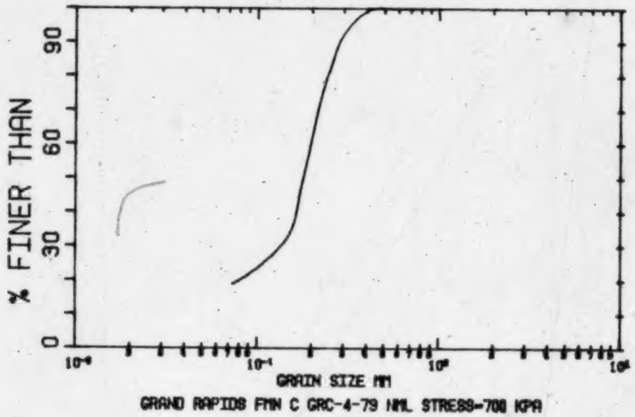
% FINER THAN
0
30
60
90
10^-2
10^-1
10^0
10^1
GRAIN SIZE MM
GRAND RAPIDS FMN C GRC-4-79 NML STRESS=700 KPA

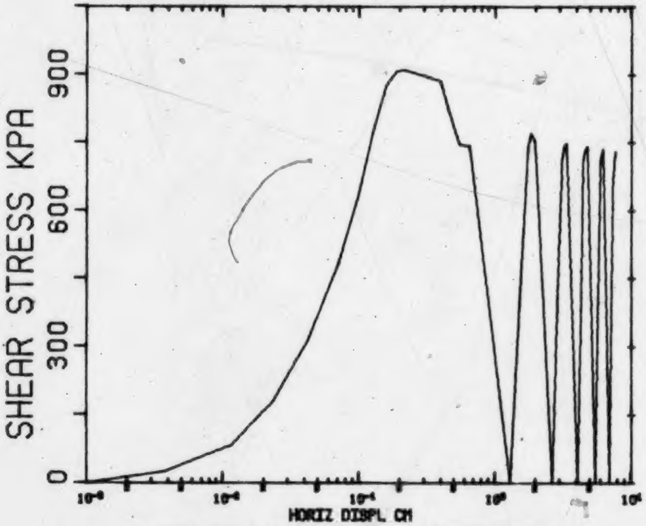

GRAND RAPIDS FMN C GRC-5-79 NML STRESS=1000 KPA

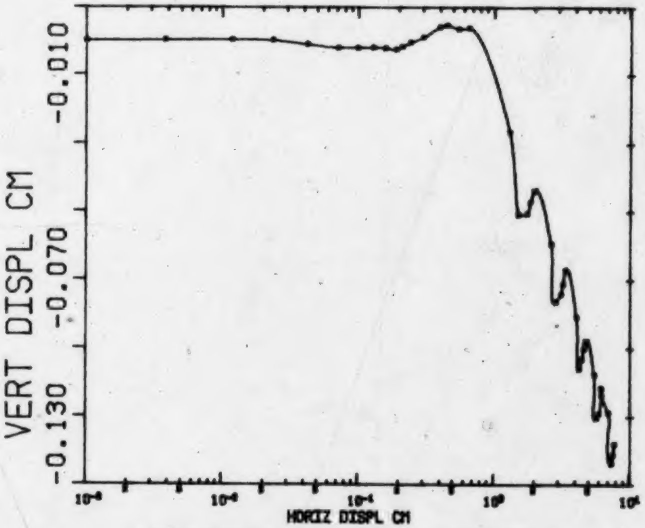

GRAND RAPIDS FMN C GRC-5-79 NML STRESS=1000 KPA

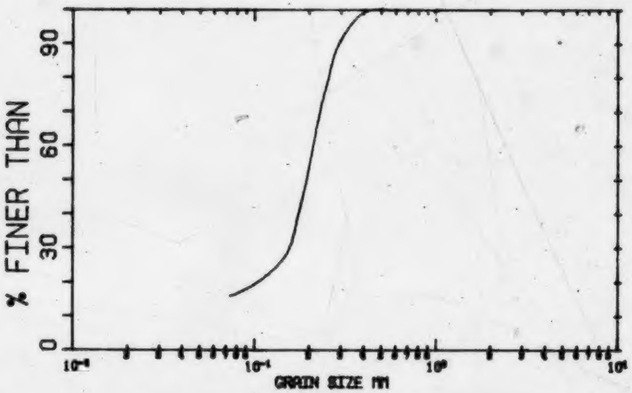

GRAND RAPIDS FMN C GRC-5-79 NML STRESS=1000 KPA

S

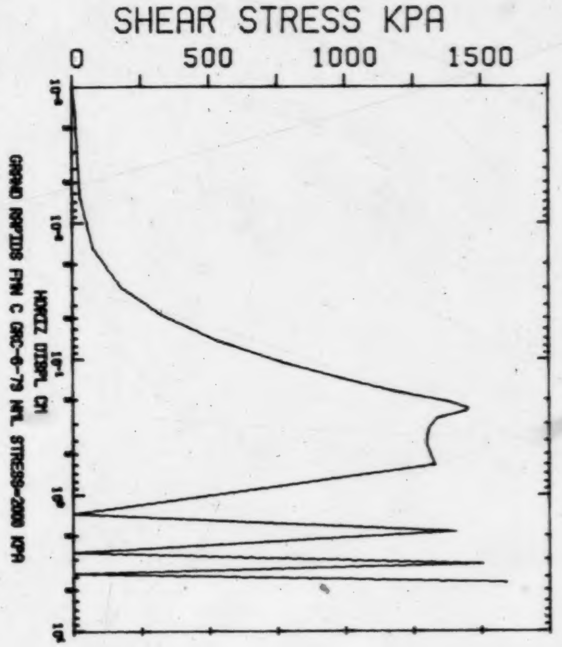
SHEAR STRESS KPA
0
500
1000
1500
HORIZ DISPL CM
GRAND RAPIDS FMN C GRC-6-79 NML STRESS=2000 KPA

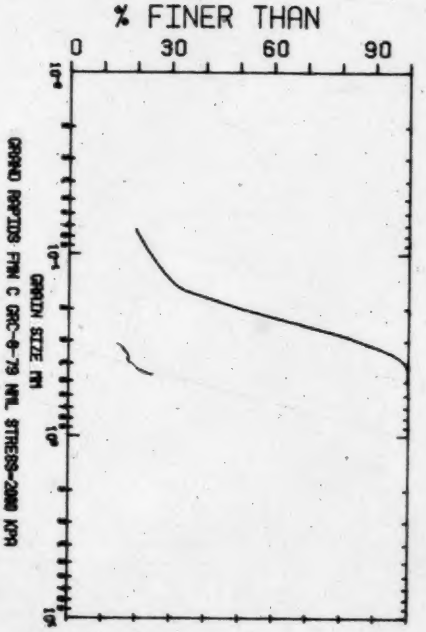
% FINER THAN
0
30
60
90
GRAIN SIZE MM
GRAND RAPIDS FMN C GRC-6-79 NML STRESS=2000 KPA

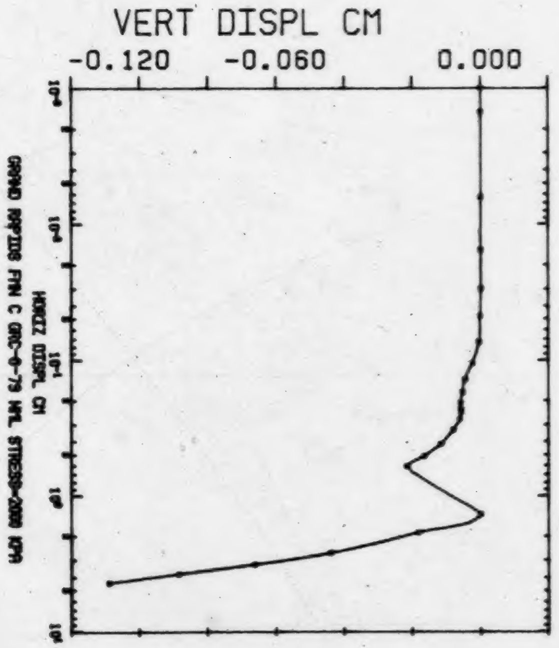
VERT DISPL CM
-0.120
-0.060
0.000
HORIZ DISPL CM
GRAND RAPIDS FMN C GRC-6-79 NML STRESS=2000 KPA

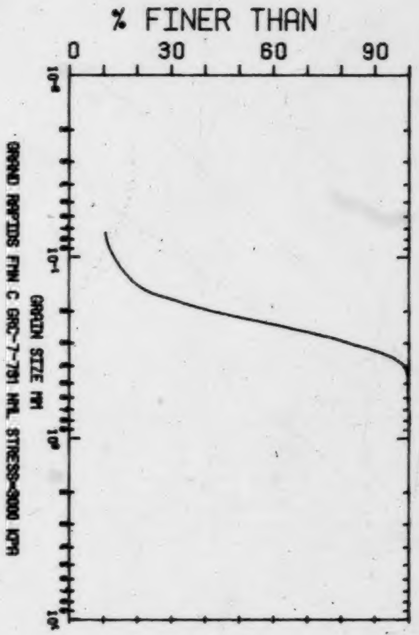
% FINER THAN
0
30
60
90
10^{-2}
10^{-1}
10^{0}
10^{1}
GRAIN SIZE MM
GRAND RAPIDS FMN C GRC-7-781 NRL STRESS=8000 KPA

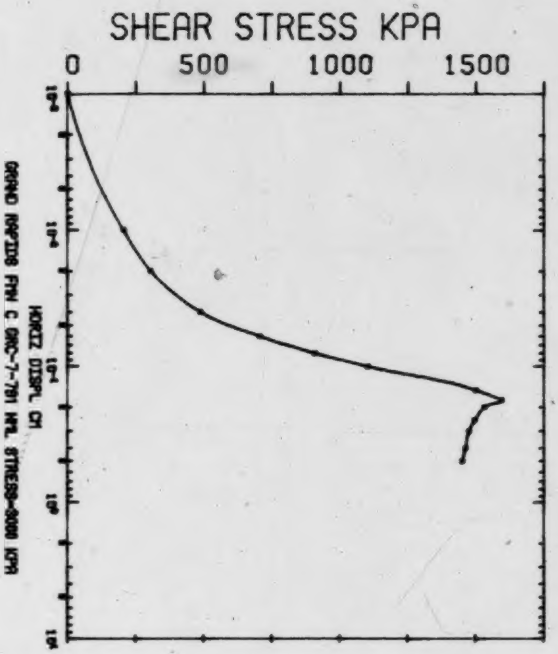
SHEAR STRESS KPA
0
500
1000
1500
10^{-3}
10^{-2}
10^{-1}
10^{0}
10^{1}
HORIZ DISPL CM
GRAND RAPIDS FMN C GRC-7-781 NRL STRESS=8000 KPA

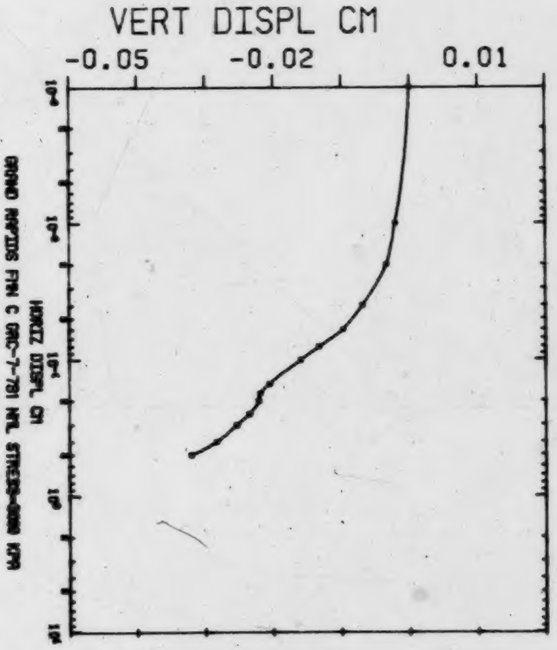
VERT DISPL CM
-0.05
-0.02
0.01
10^{-3}
10^{-2}
10^{-1}
10^{0}
10^{1}
HORIZ DISPL CM
GRAND RAPIDS FMN C GRC-7-781 NRL STRESS=8000 KPA

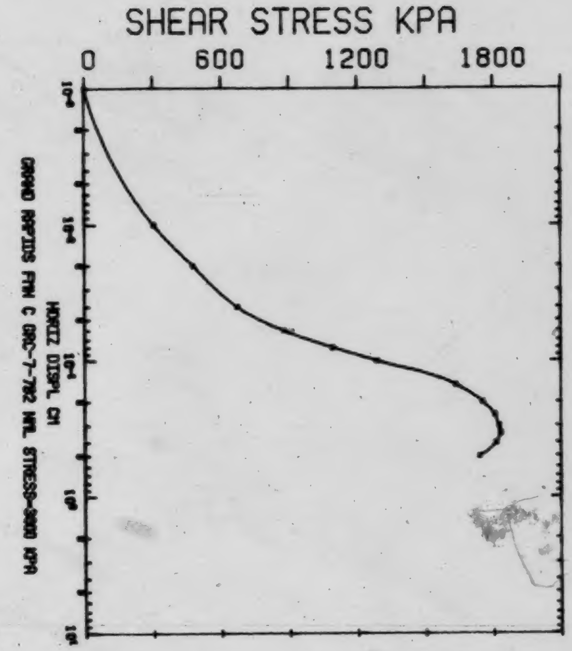
SHEAR STRESS KPA
0
600
1200
1800
HORIZ DISPL CM
GRAND RAPIDS FMN C ORC-7-782 NML STRESS=3000 KPA

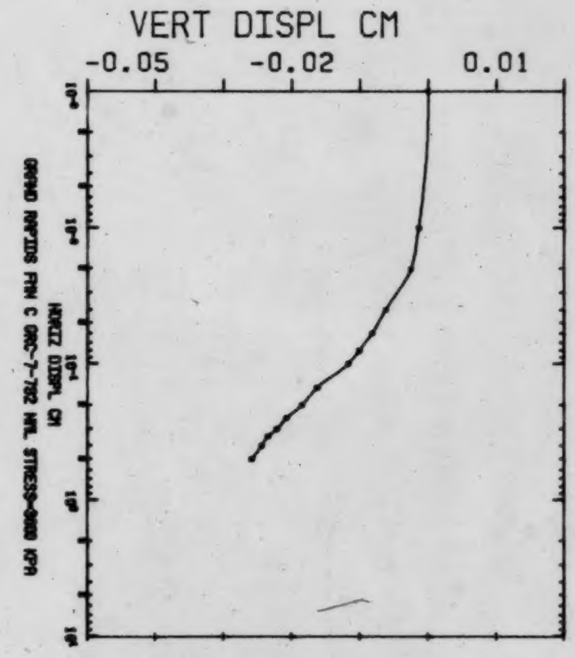
VERT DISPL CM
-0.05
-0.02
0.01
HORIZ DISPL CM
GRAND RAPIDS FMN C ORC-7-782 NML STRESS=3000 KPA

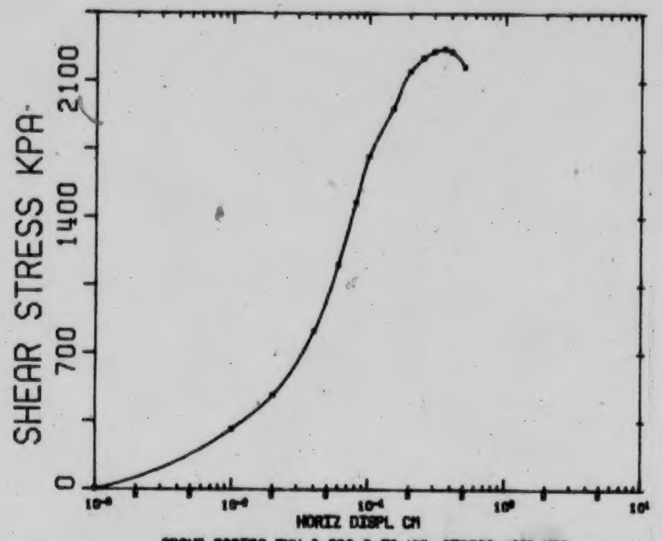

GRAND RAPIDS FMN C GRC-8-79 NML STRESS=4000 KPA

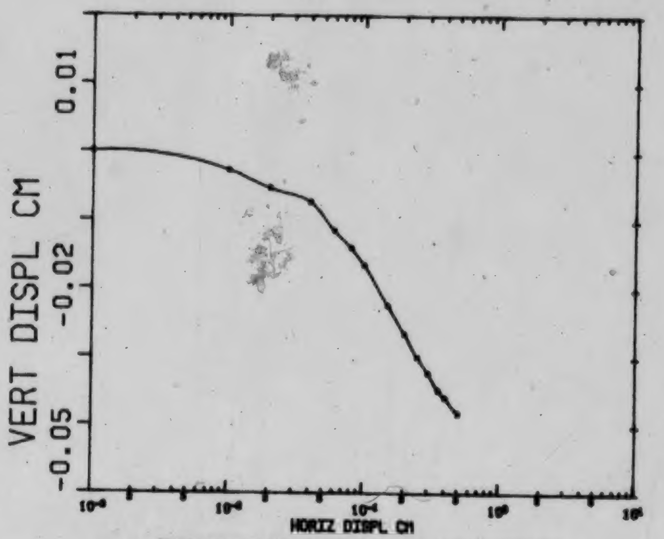

GRAND RAPIDS FMN C GRC-8-79 NML STRESS=4000 KPA

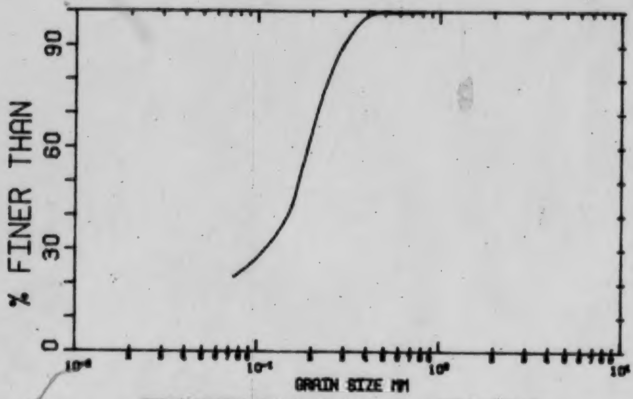

GRAND RAPIDS FMN C GRC-8-79 NML STRESS=4000 KPA

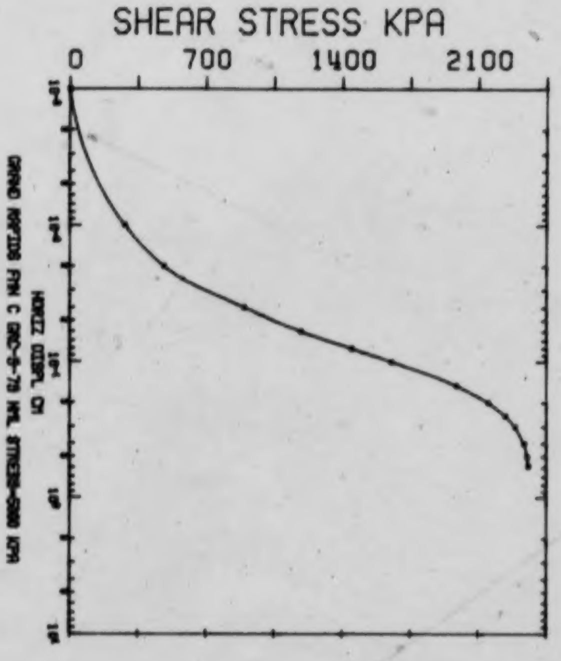
SHEAR STRESS KPA
0
700
1400
2100
HORIZ DISPL CM
GRAND RAPIDS FMN C DEC-8-79 NML STRESS=5000 KPA

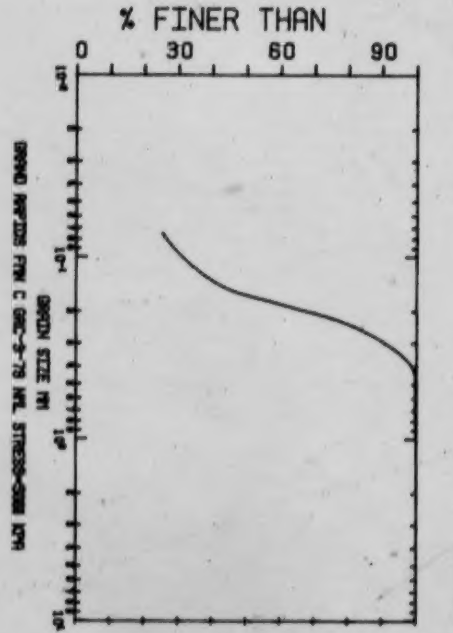
% FINER THAN
0
30
60
90
GRAIN SIZE MM
GRAND RAPIDS FMN C DEC-8-79 NML STRESS=5000 KPA

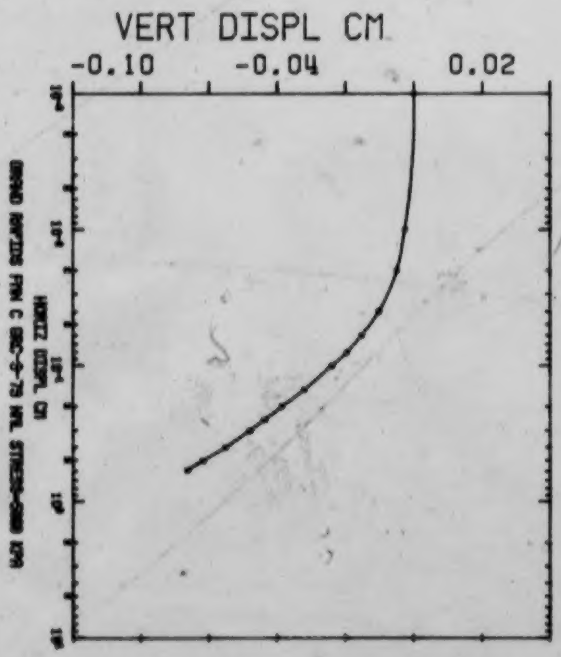
VERT DISPL CM
-0.10
-0.04
0.02
HORIZ DISPL CM
GRAND RAPIDS FMN C DEC-8-79 NML STRESS=5000 KPA

C.2 Compressibility Test Results

The results of oedometer tests conducted on the five main sample groups are presented here. Plots of void ratio vs. stress are given for each tests.

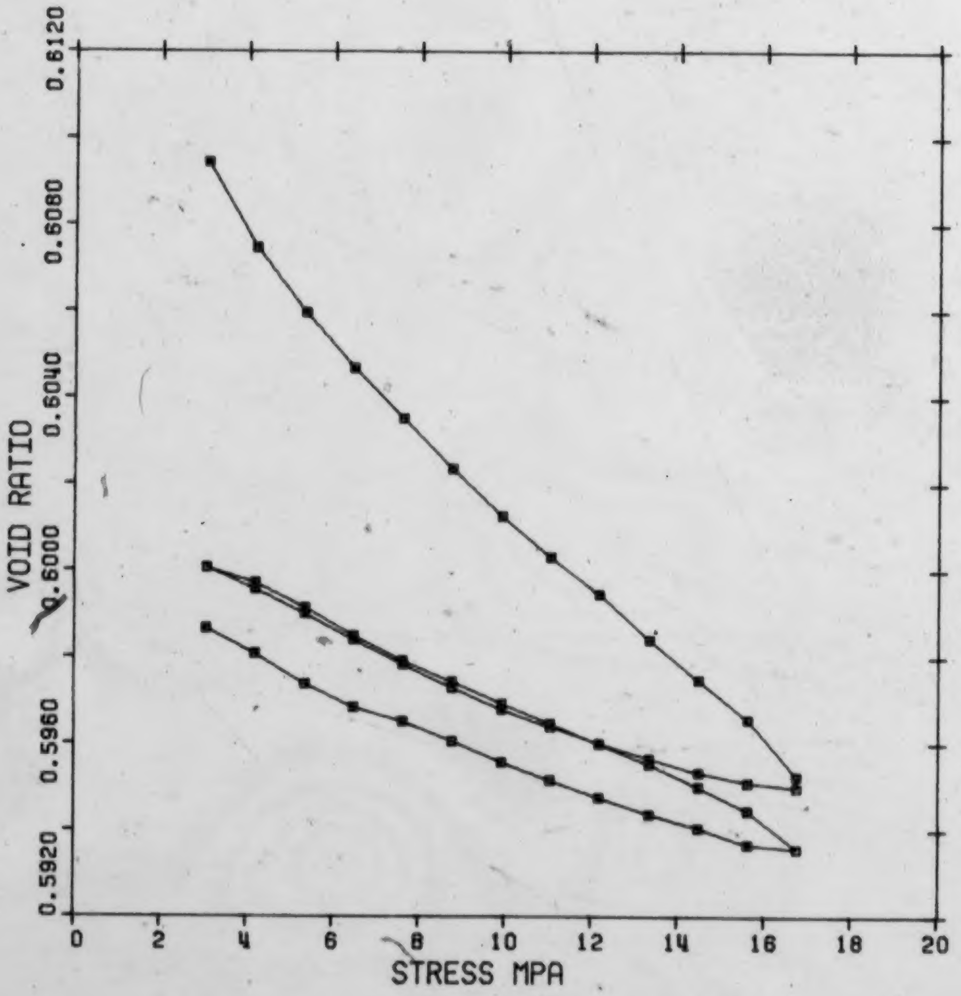

MCMURRAY FORMATION FG-C1-79 COMPRESSIBILITY

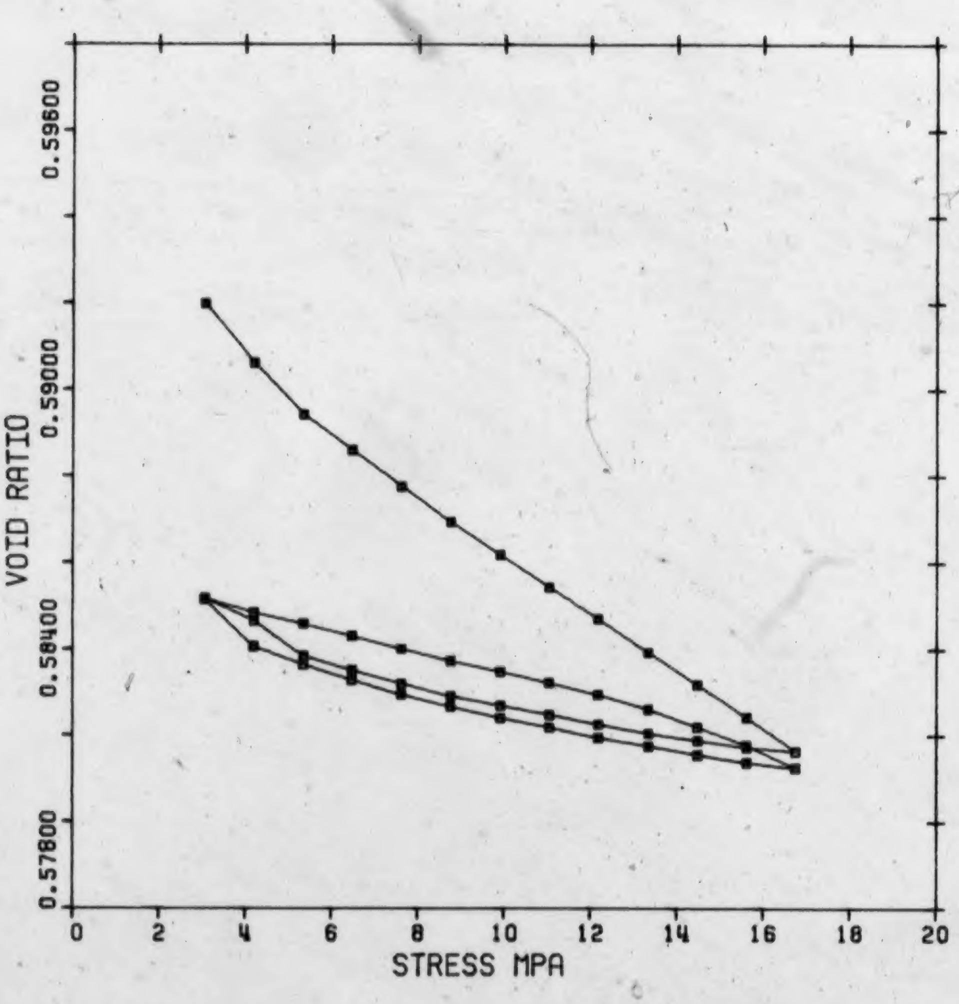

MCMURRAY FORMATION FG-C2-79 COMPRESSIBILITY

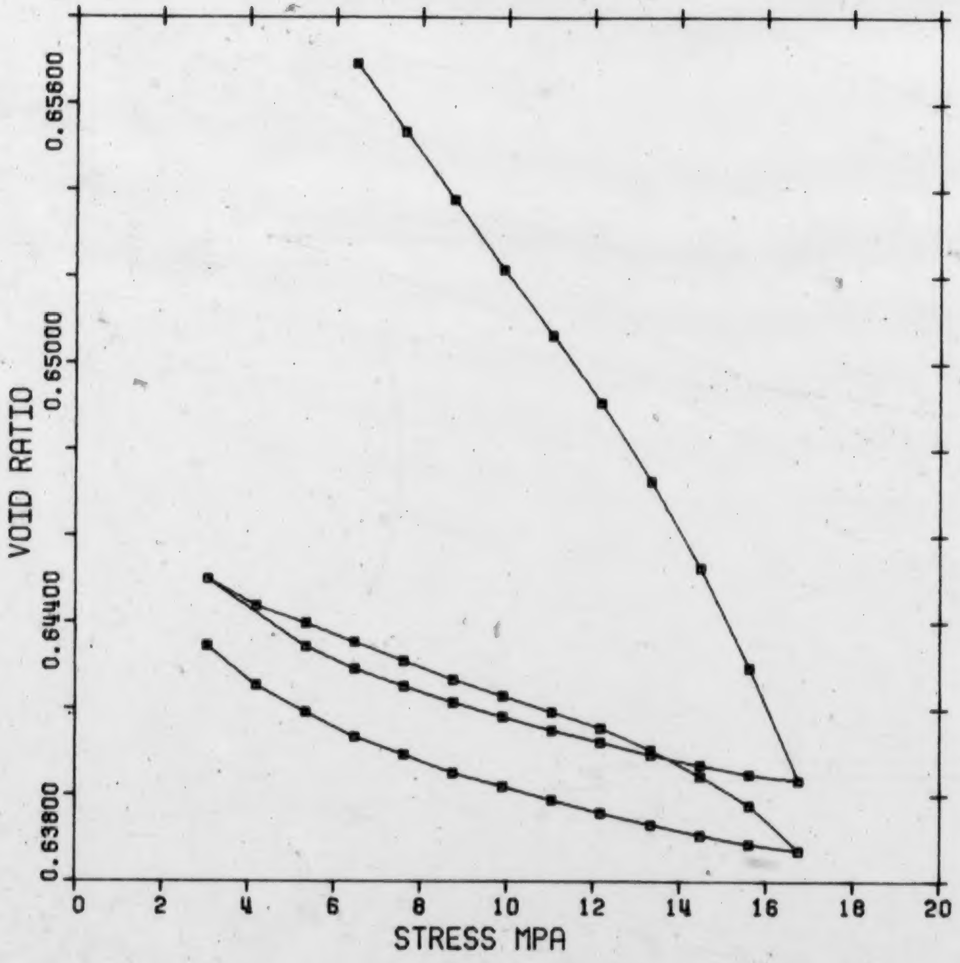

MCMURRAY FORMATION MG-C1-79 COMPRESSIBILITY

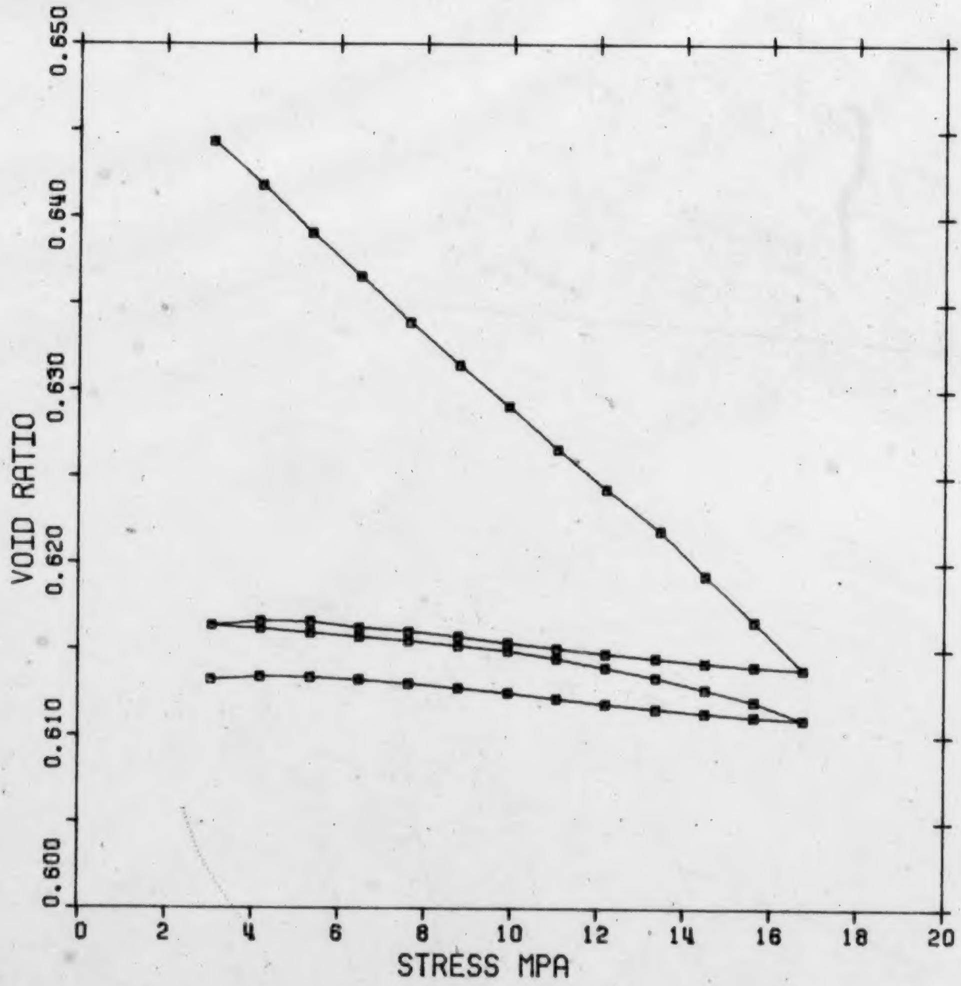

MCMURRAY FORMATION MG-C2-79 COMPRESSIBILITY

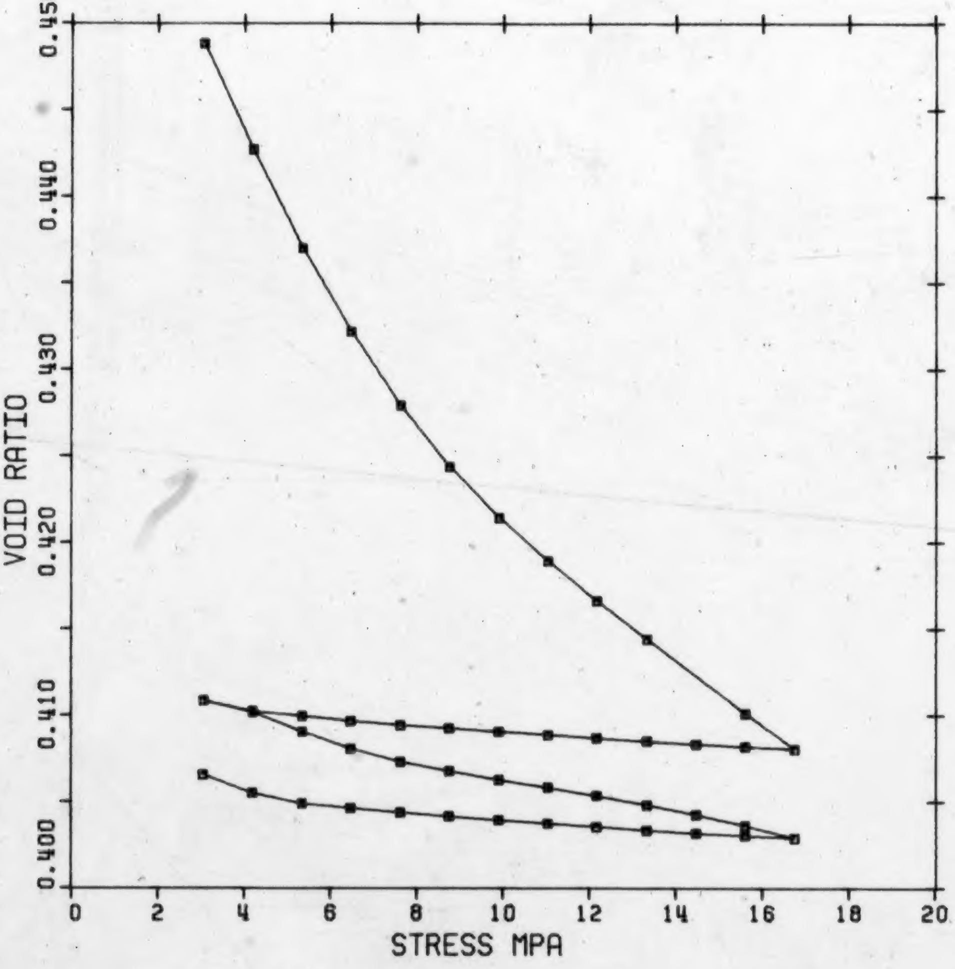

MCMURRAY FORMATION CG-C1-79 COMPRESSIBILITY

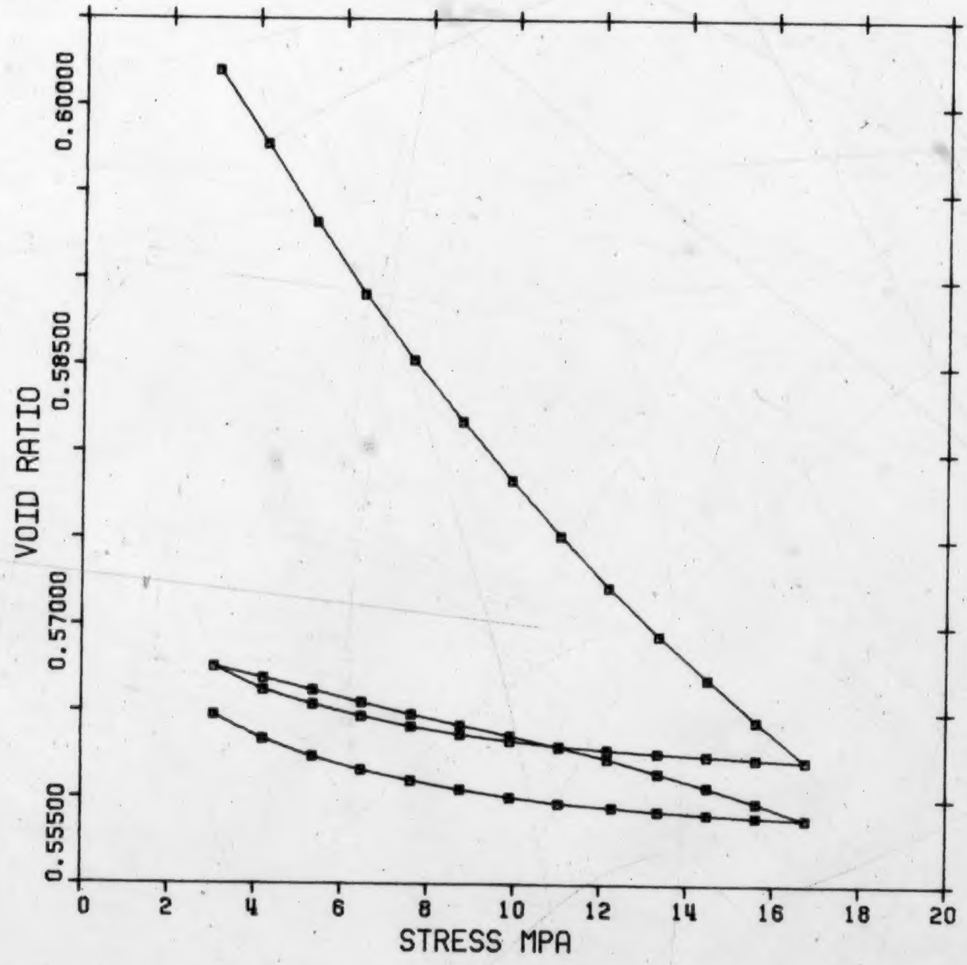

MCMURRAY FORMATION CG-C2-79 COMPRESSIBILITY

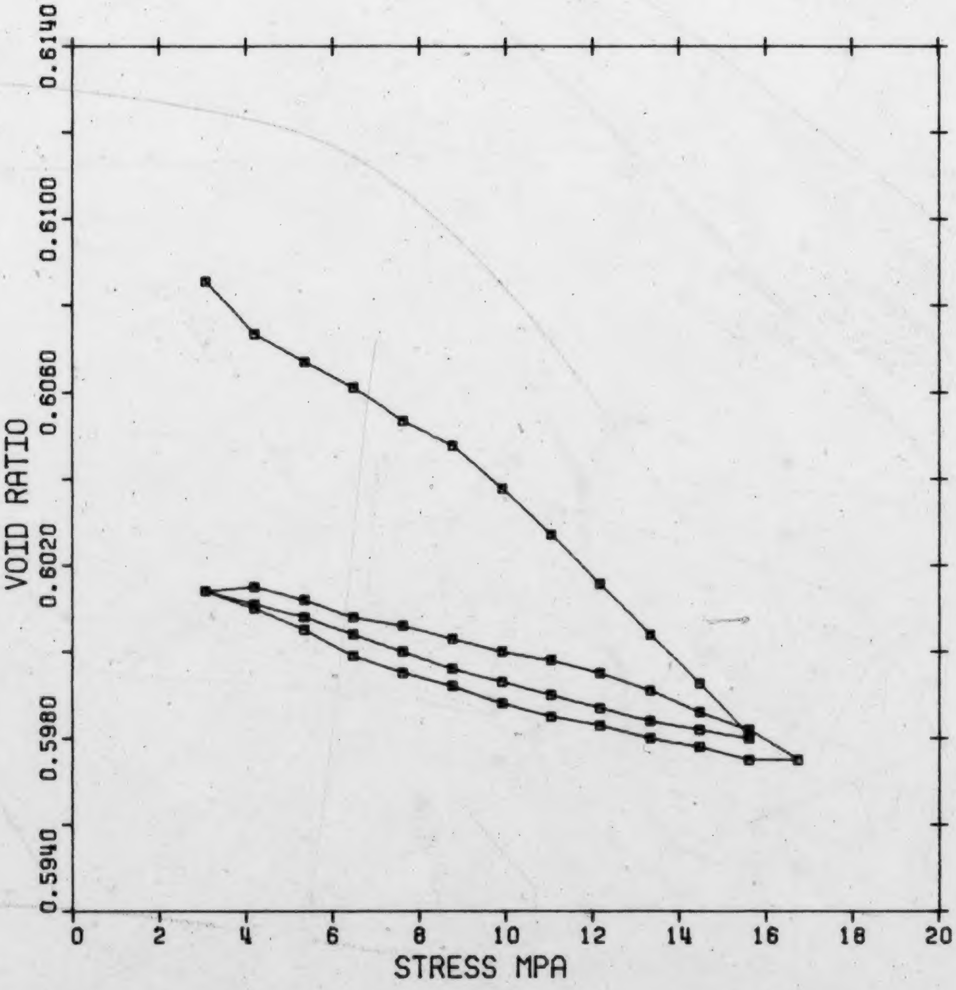

GRAND RAPIDS FMN A GRA-C1-79 COMPRESSIBILITY

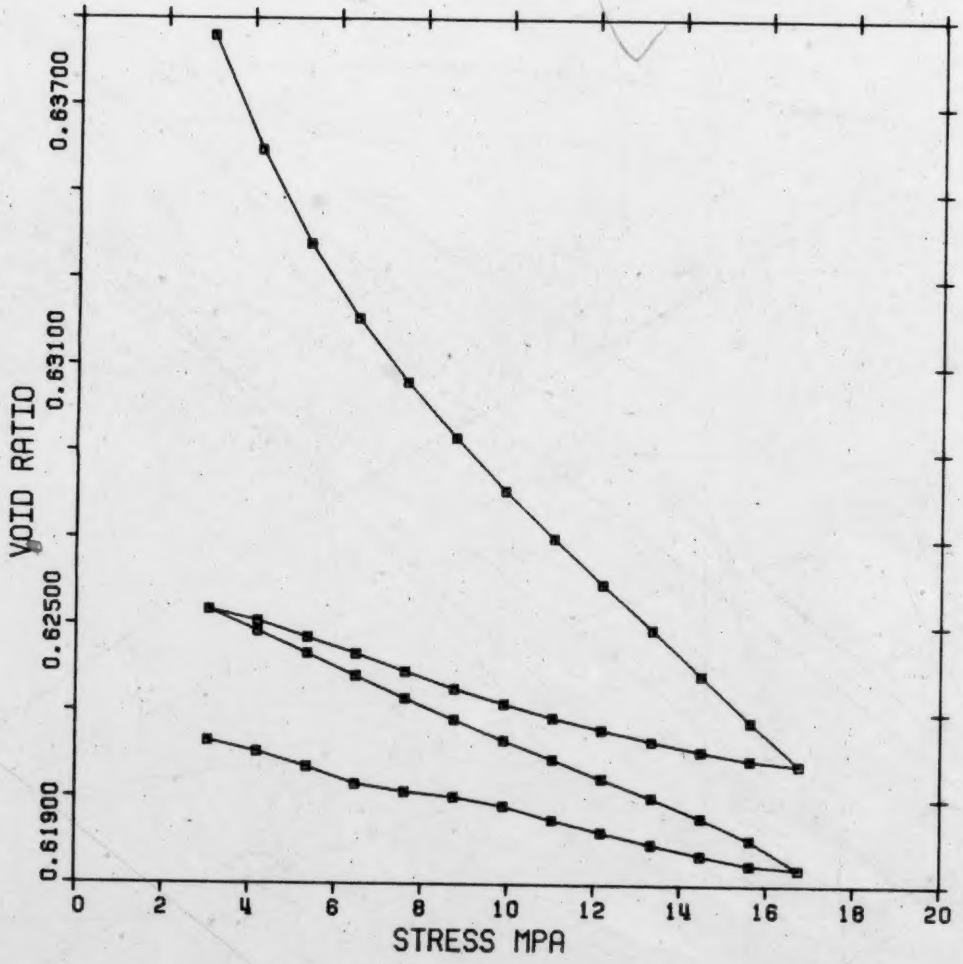

GRAND RAPIDS FMN A GRA-C2-79 COMPRESSIBILITY

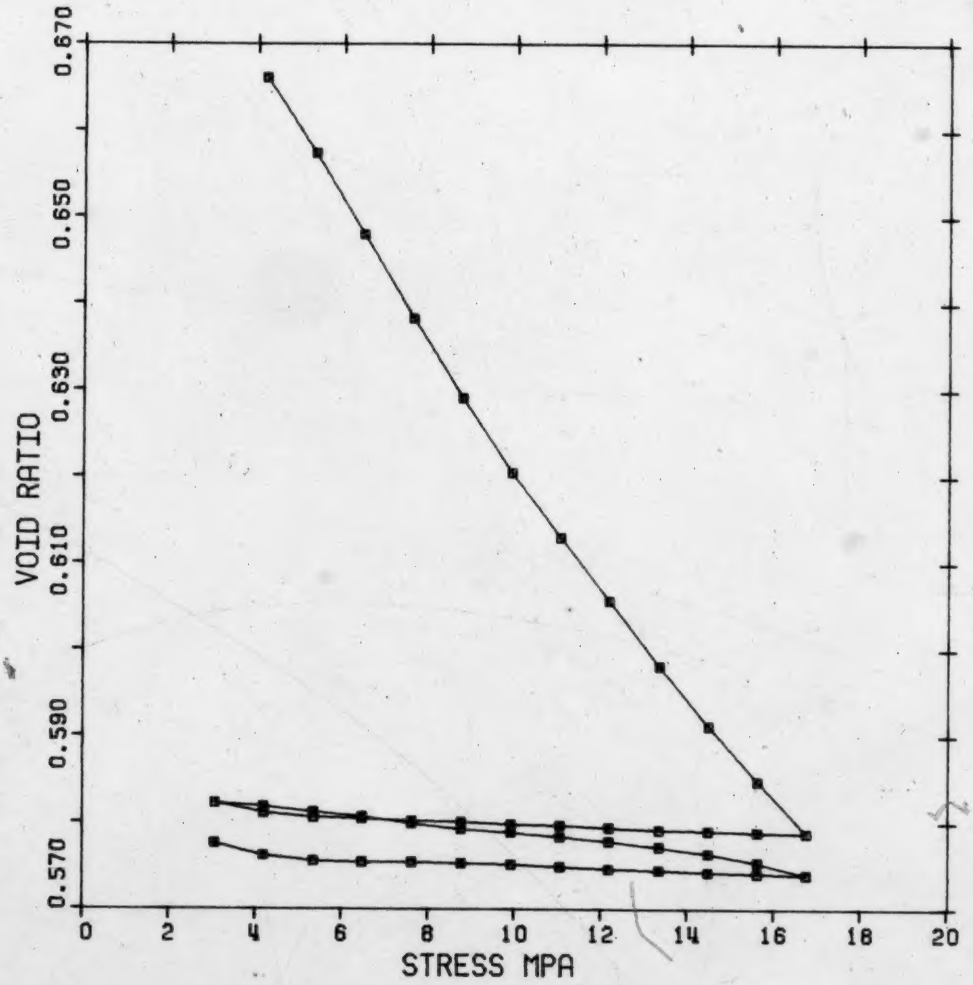

GRAND RAPIDS FMN C GRC-C2-79 COMPRESSIBILITY

C.3 Grain Size Analysis

The grain size distribution curves for the original (unsheared) samples are presented in section C.3.1. Summary tables for the grain size analysis on sheared samples are given in section C.3.2. The grain size curves for the sheared samples are presented with the shear test data in section C.1.3.

C.3.1 Grain Size Distribution Curves for Original Samples

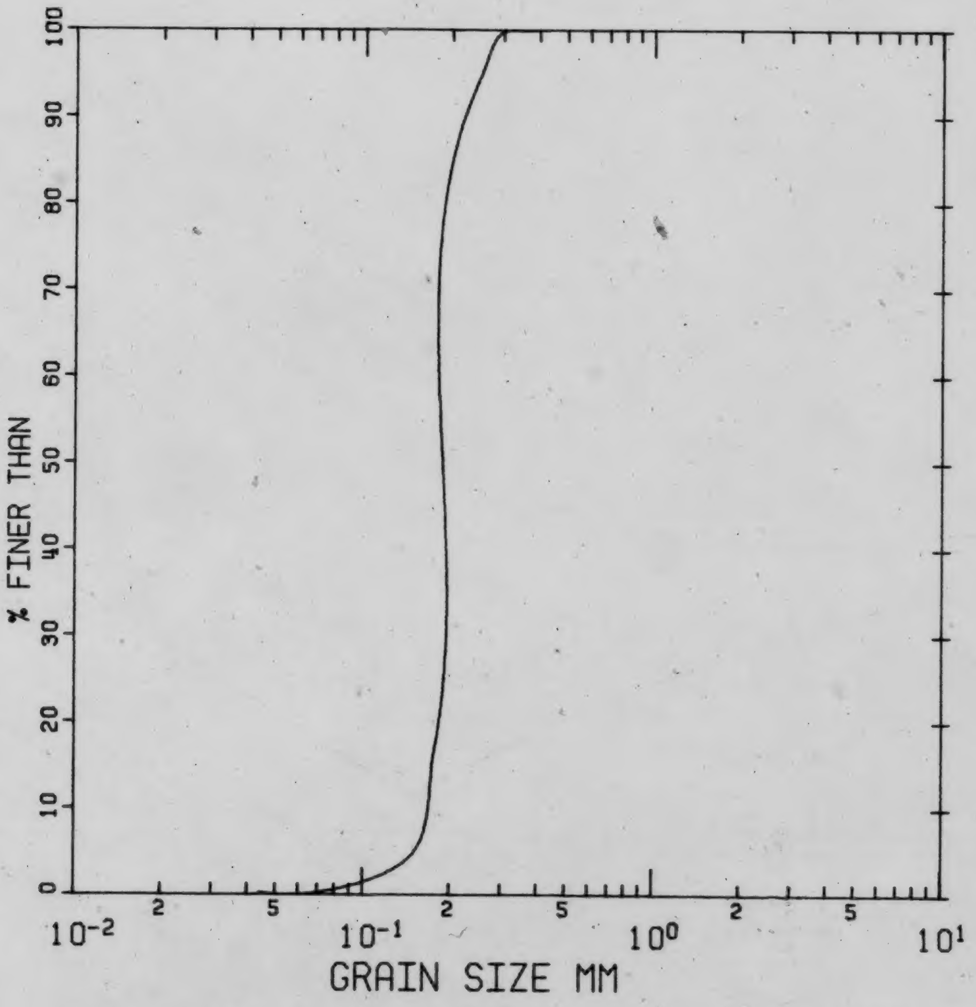

FG MCMURRAY FORMATION ORIGINAL SAMPLE

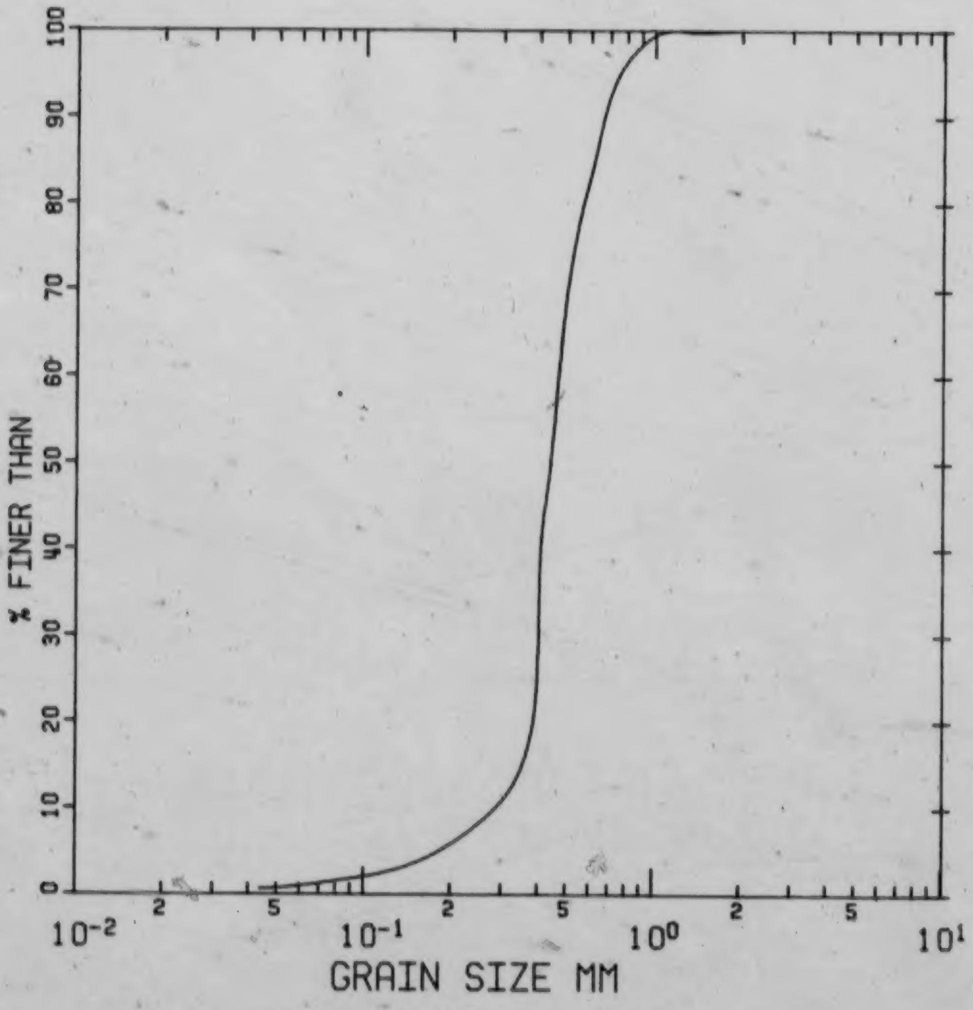

MG MCMURRAY FORMATION ORIGINAL SAMPLE

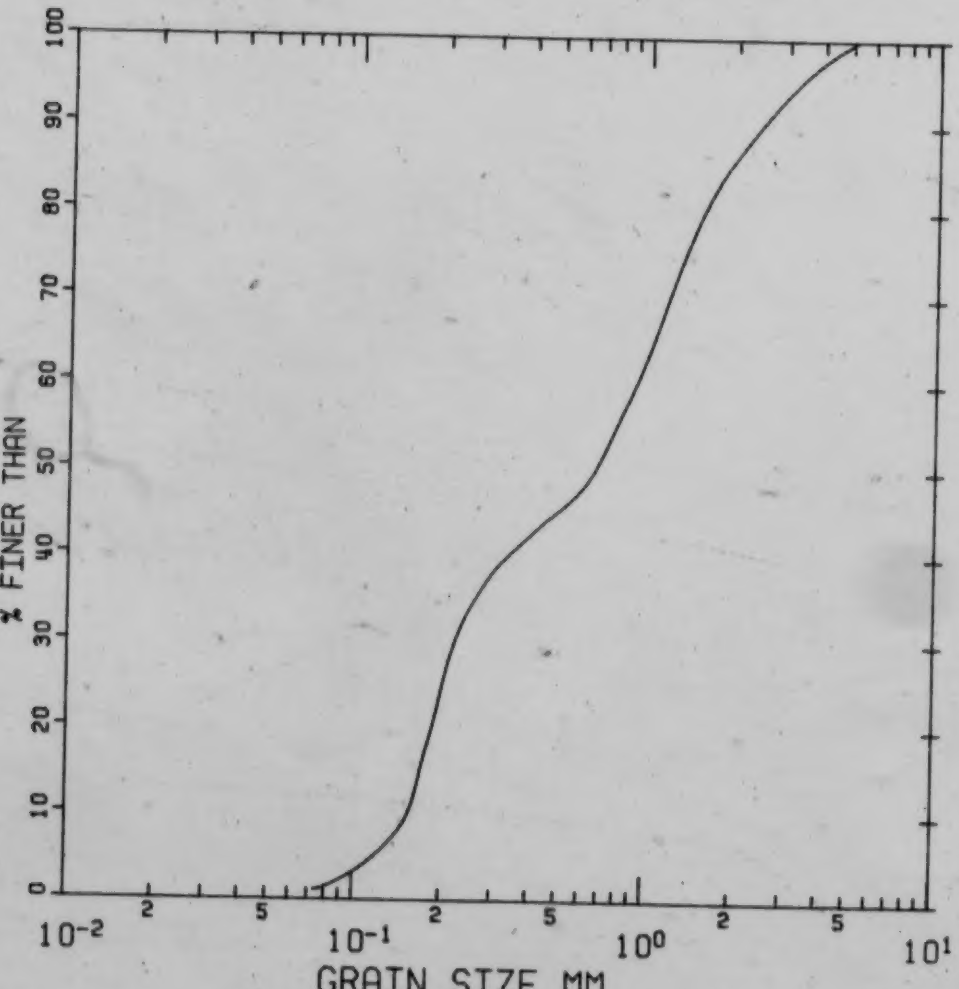

CG MCMURRAY FORMATION ORIGINAL SAMPLE

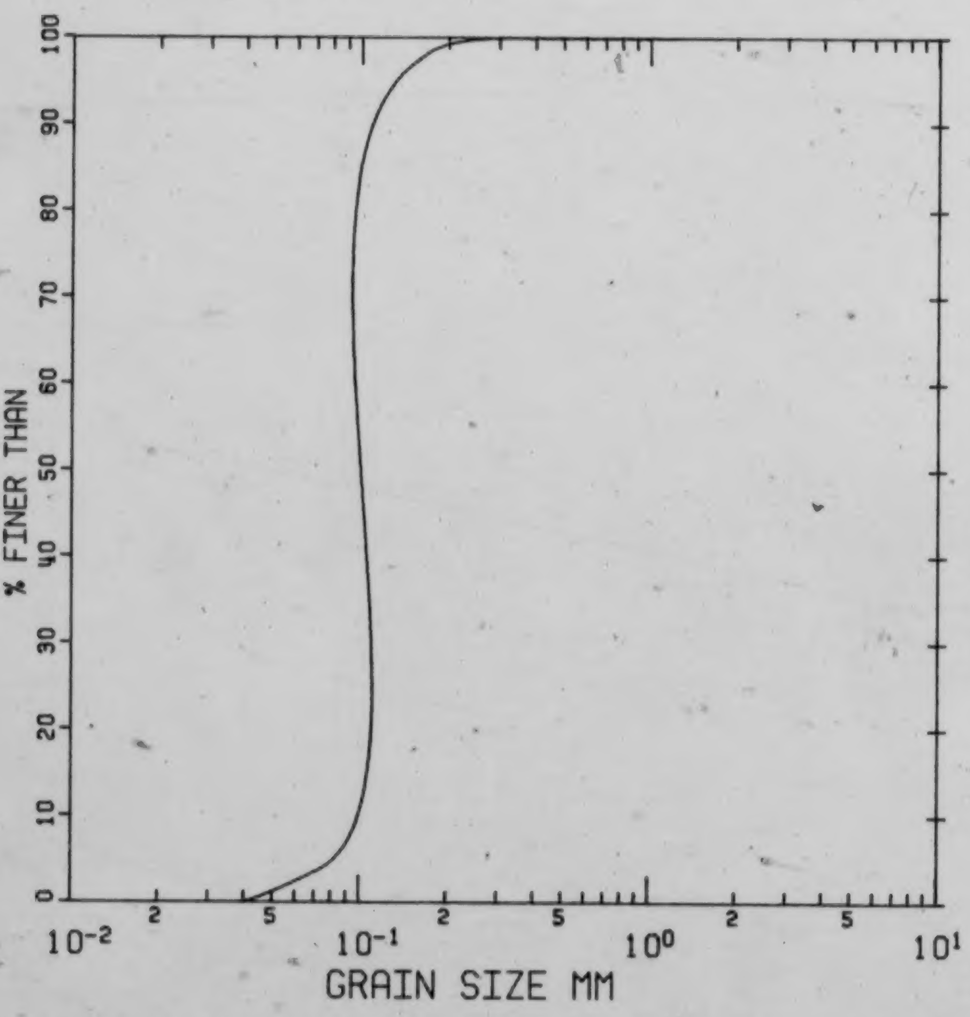

GRAND RAPIDS FORMATION A ORIGINAL SAMPLE

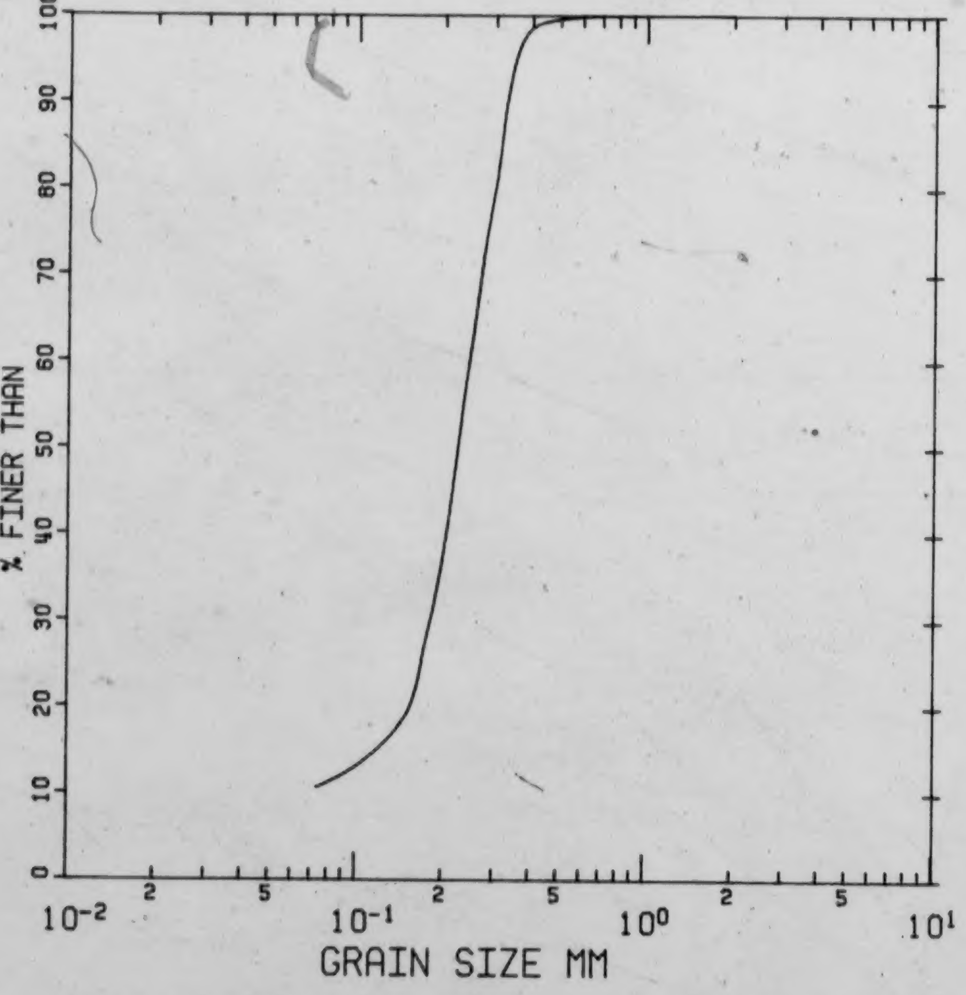

GRAND RAPIDS FORMATION C ORIGINAL SAMPLE

C.3.2 Data Summary for Analysis of Sheared Samples

Table C.6: Grain size data for sheared samples of fine-grained McMurray Formation.

Sample	Normal Stress (kPa)	D_{60} (mm)	D_{50} (mm)	D_{10} (mm)	$c_u = \frac{D_{60}}{D_{10}}$	% passing no. 200 sieve
FG-1-79	100	0.210	0.200	0.160	1.31	0.5
FG-2-79	250	0.210	0.200	0.160	1.31	0.5
FG-3-79	400	0.210	0.200	0.160	1.31	0.6
FG-5-79	1000	0.210	0.195	0.160	1.31	0.7
FG-6-79	2000	0.210	0.205	0.160	1.31	1.2
FG-7-79	3000	0.230	0.210	0.170	1.35	1.5
FG-8-79	4000	0.210	0.200	0.170	1.24	1.9
FG-9-79	5000	0.215	0.205	0.165	1.30	2.0

Table C.7: Grain size data for sheared samples of medium-grained McMurray Formation.

Sample	Normal Stress (kPa)	D_{60} (mm)	D_{50} (mm)	D_{10} (mm)	$c_u = \frac{D_{60}}{D_{10}}$	% passing no. 200 sieve
MG-2-78	242	0.500	0.460	0.260	1.92	1.9
MG-3-78	400	0.550	0.540	0.260	2.12	1.8
MG-4-78	700	0.540	0.505	0.220	2.45	2.3
MG-5-78	1000	0.550	0.520	0.290	1.90	1.2
MG-6-79	2000	0.410	0.380	0.120	3.42	5.9
MG-7-79	3000	0.400	0.380	0.150	2.67	4.2
MG-8-79-1	4000	0.530	0.480	0.177	2.99	3.0
MG-8-79-2	4000	0.480	0.430	0.150	3.20	3.8
MG-9-79	5000	0.480	0.430	0.177	2.71	3.0

Table C.8: Grain size data for sheared samples of coarse-grained McMurray Formation.

Sample	Normal Stress (kPa)	D_{60} (mm)	D_{50} (mm)	D_{10} (mm)	$c_u = \frac{D_{60}}{D_{10}}$	% passing no. 200 sieve
CG-1-79	100	0.800	0.560	0.150	5.33	1.0
CG-2-79	250	0.720	0.420	0.140	5.14	1.7
CG-3-79	400	0.740	0.470	0.150	4.93	1.4
CG-4-79	700	0.670	0.420	0.140	4.79	1.7
CG-5-79	1000	0.520	0.260	0.100	5.20	3.6
CG-6-79	2000	0.850	0.650	0.130	6.54	3.2
CG-7-79-1	3000	0.380	0.250	0.130	2.92	3.4
CG-7-79-2	3000	1.200	0.970	0.130	9.23	1.7
CG-8-79	4000	1.000	0.750	0.140	7.14	2.3
CG-9-79	5000	1.200	0.870	0.130	9.23	2.5

Table C.9: Grain size data for sheared samples of Grand Rapids Formation A.

Sample	Normal Stress (kPa)	D_{60} (mm)	D_{50} (mm)	D_{10} (mm)	$c_u = \frac{D_{60}}{D_{10}}$	% passing no. 200 sieve
GRA-1-79	100	0.099	0.096	0.076	1.30	5.0
GRA-2-79	250	0.098	0.095	0.076	1.29	6.6
GRA-3-79	400	0.094	0.090	0.074	1.27	6.7
GRA-4-79	700	0.095	0.091	0.074	1.28	7.6
GRA-5-79	1000	0.110	0.098	0.074	1.49	9.0
GRA-6-79	2000	0.110	0.098	0.070	1.57	11.8
GRA-7-79	3000	0.115	0.100	0.075	1.53	8.1
GRA-8-79	4000	0.115	0.105	0.073	1.58	10.2
GRA-9-79	5000	0.110	0.100	0.073	1.51	10.8

Table C.10: Grain size data for sheared samples of Grand Rapids Formation C.

Sample	Normal Stress (kPa)	D_{60} (mm)	D_{50} (mm)	D_{10} (mm)	$c_u = \frac{D_{60}}{D_{10}}$	% passing no. 200 sieve
GRC-1-79	100	0.215	0.195	0.060	3.58	11.5
GRC-2-79	250	0.250	0.230	0.050	5.00	12.3
GRC-3-79	400	0.205	0.190	0.040	5.13	15.5
GRC-4-79	700	0.190	0.180	0.040	4.75	19.0
GRC-5-79	1000	0.210	0.190	0.046	4.57	15.8
GRC-6-79	2000	0.210	0.190	0.035	6.00	19.7
GRC-7-79-1	3000	0.240	0.210	0.070	3.43	10.5
GRC-8-79	4000	0.190	0.165	-	-	21.9
GRC-9-79	5000	0.180	0.160	-	-	25.3
GRC-0-79	50	0.245	0.220	0.145	1.69	4.8